MODELLING AND OPTIMISATION OF HEAT EXCHANGER INTEGRATED IN FAN COIL UNIT

By:
Miftah Omar Altwieb

A THESIS SUBMITTED IN PARTIAL FULFILMENT OF THE REQUIREMENTS FOR THE DEGREE OF DOCTOR OF PHILOSOPHY AT THE UNIVERSITY OF HUDDERSFIELD

School of Computing and Engineering
University of Huddersfield
UK

January 2018

DEDICATION

This Thesis is dedicated to the memory of my beloved father

Mr. Omar Altwieb

ABSTRACT

The Fan Coil Unit (FCU) is an integral part of heating, ventilation and air conditioning systems used in residential and commercial buildings. One main component of this device is a multi-tube and fin heat exchanger. Improvement of thermal performance in such heat exchangers is vital for improved performance of FCU. Performance improvements in the FCUs are mainly limited by available technology, manufacturing capabilities and overall cost effectiveness of the design. Better thermal performance usually comes at a cost of higher pressure drop or more expensive materials and manufacturing costs.

In this thesis, a global framework for design and optimisation was developed taking into account overall costs of design, manufacturing and operation. Full 3D CFD models of multi-tube and fins heat exchanger were developed to investigate complex and non-uniform flow on water and air sides of the device. The CFD models were developed to enable local heat transfer analysis within the FCU.

Experimental setup to evaluate performance of the heat exchanger has been designed and built. Different configurations of heat exchanger were tested experimentally and numerically, including the baseline configuration, so called plain fins. More efficient design of louvre fins and and fins with vortex generating mechanism (perforation in the fin surfaces) were also investigated. Best thermal performance was found to be for the perforated louvre fins.

CFD model was validated against experimental results and obtained data was used to create a novel semi-analytical prediction model for Fanning friction factor (f) and Colburn factor (j). Appropriate costs calculation model was also developed and employed for total costs estimation of the FCU over the period of 15 years.

The framework proposed in this thesis for optimised design and development strategy of heat exchangers resulted in development of a novel design which offers significant improvements in comparison to the current design.

This new optimised design of the heat exchanger (with perforation in louvre fins) increased thermal performance by additional 10% while the total costs increased by only 6%.

DECLARATION

- The author of this thesis (including any appendices and/or schedules to this thesis) owns any copyright in it (the ―Copyright‖) and he has given The University of Huddersfield the right to use such Copyright for any administrative, promotional, educational and/or teaching purposes.
- Copies of this thesis, either in full or in extracts, may be made only in accordance with the regulations of the University Library. Details of these regulations may be obtained from the Librarian. This page must form part of any such copies made.
- The ownership of any patents, designs, trademarks and any and all other intellectual property rights except for the Copyright (the ―Intellectual Property Rights‖) and any reproductions of copyright works, for example graphs and tables (―Reproductions‖), which may be described in this thesis, may not be owned by the author and may be owned by third parties. Such Intellectual Property Rights and Reproductions cannot and must not be made available for use without the prior written permission of the owner(s) of the relevant Intellectual Property Rights and/or Reproductions.

ACKNOWLEDGEMENTS

Firstly, I am thankful and grateful to the Almighty Allah, the most merciful and beneficent, for the good health and wellbeing that were necessary to finish this thesis and for giving me the opportunity and strength to do my research.

Secondly, I owe my deepest gratitude to my supervisor, **Prof. Rakesh Mishra**, who has fully supported me throughout my long journey to do my research and to write this thesis. I would like to acknowledge the considerable amount of help and support provided by my co-supervisor **Dr. Krzysztof Kubiak** to finalise this thesis.

Thirdly, I would like to express my gratitude to TEV-Limited Brighouse-UK for their support in carrying out this research particularly to Darren Davison and James Carr-Smith.

Last but not the least, I wish to thank **my wife and my family (here and in my country)**, for their devoted care, quiet sacrifices, and indispensable role as a wife and mother during the previous years of my study.

Table of Contents

List of Figures

List of Tables

NOMENCLATURE

A_1	Heat transfer surface areas for hot fluid	m^2
A_2	Heat transfer surface areas for could fluid	m^2
A_w	Heat transfer area of the wall	m^2
A_c	Flow cross sectional area	m^2
A_o	Total surface area	m^2
A_f	Fins total surface area	m^2
A_b	Base area	m^2
A_t	Total heat transfer surface area of the heat exchanger	m^2
Cp_1, Cp_w	Specific heats for the hot fluid	J/kg K
Cp_2,Cp_a	Specific heats for the cold fluid	J/kg K
C_{min}	Product of mass and specific heat of the fluid which has a lower thermal capacity rate	kJ/sec K
C_{max}	Product of mass and specific heat of the fluid which has a higher thermal capacity rate	kJ/sec K
C^*	Heat capacity rate ratio	
C_f	Skin friction coefficient	
C_{Total}	Total cost	£
$C_{Capital}$	Capital cost	£
$C_{Operating}$	Operating cost	£
$C_{Material}$	Material cost	£
$C_{Manufacturing}$	Manufacturing and installation cost	£
C_{Tubes}	Cost of the tubes	£
C_{fins}	Cost of the tubes	£
$C_{Housing}$	Cost of the housing	£
C_1	Cost of tubes material	£/Kg
C_2	Cost of Aluminium per unit volume	£/mm^3
C_3	Cost for steel sheet per unit volume	£/mm^3
C_{KWhr}	Power cost for 1 kwhr (kilowatt hour)	£
D_h	Hydraulic diameter	m

D_c	Fin collar outside diameter	m
D_{out}	Outer diameter of the tube	m
ESD	Estimated standard deviation	
f	Fanning friction factor	
F_t	Fin thickness	mm
F_p	Fin spacing	m
F_w	Fin width	m
F_H	Fin height	m
h_1, h_h, h_w	Heat transfer coefficient for hot fluid	W /m^2 K
h_2, h_c, h_a	Heat transfer coefficient for cold fluid	W /m^2 K
h_D	Hole diameter	m
h_S	Hole spacing	m
j	Colburn factor	
j/f	Efficiency index	
JF	JF factor optimisation factor	
k_w	Thermal conductivity of the wall material	W/m K
K_I	Abrupt contraction pressure-loss coefficient	
K_e	Abrupt expansion pressure-loss coefficient	
K_a	Thermal conductivity of the fin material	W/m K
t_{Tube}	Tube thickness	m
L_{Tube}	Total length of the tubes	m
L_p	Longitudinal pitch	m
$\dot{m}_1$	Mass flow rate for hot fluid	kg/sec
$\dot{m}_2$	Mass flow rate for cold fluid	kg/sec
MV	Arithmetic means of (n) number of measurements	
Nu	Nusselt number	
n	Number of measurements in the set	
NTU	Number of transfer units	
P_p	Pumping power	W
ΔP	Pressure drop	Pa

P_r	Prandtl number	
$P_{Water-side}$	Pumping powers required to operate the water-side	W
$P_{Air-side}$	Pumping powers required to operate the air-side	W
$\dot{Q}_h$	Heat transfer rate for hot fluid	W
$\dot{Q}_c$	Heat transfer rate for cold fluid	W
$\dot{Q}$	Actual heat transfer rate	W
$\dot{Q}_{max}$	Maximum possible heat transfer rate	W
$\dot{Q}_{avg}$	Average heat transfer rate	W
R_w	Wall thermal resistance	m^2 K
R_e	Reynolds number	
R	Radius of a circular fin which has the same efficiency as the rectangular fin	m
r_o	Outer radius of the tube	m
SU	Standard uncertainty	
SV	The result of the i^{th} measurement (sample value)	
T_{1i},T_{hi}	Hot fluid inlet temperature	K
T_{1o},T_{ho}	Hot fluid outlet temperature	K
T_{2i}, T_{ci}	Cold fluid inlet temperature	K
T_{2o}, T_{co}	Cold fluid outlet temperature	K
ΔT_{lm}	Log mean temperature difference	
ΔT_w	Difference between the inlet and outlet temperature of the water	K
T_p	Transverse pitch	m
t_{op}	Operational hours per year	hr/yr
U	Overall heat transfer coefficient	W/m^2 K
U_T	Frictional velocity	m/sec
$V_{Housing}$	Volume of the steel sheet used to create the housing	mm^3
y^+	Non-dimensional distance from the wall	m
Δy	First layer height in the viscous sublayer of the boundary layer	m

GREEK SYMBOLS

δ_w	Wall thickness	m
ε	Heat exchanger effectiveness	
η_p	Efficiency of the fan or pump	%
η_o	Surface efficiency	%
η_f	Fin efficiency	%
μ	Dynamic Viscosity	Pa sec
ν	Kinematic viscosity	Pa sec
ρ	Fluid density	kg/m^3
ρ_1	Density of air inlet	kg/m^3
ρ_2	Density of air outlet	kg/m^3
ρ_m	Mean density	kg/m^3
σ	Ratio of the minimum flow area to the frontal area	
τ_w	Wall shear stress	Pa

SUBSCRIPTS

1	Hot fluid
2	Cold fluid
a	Air
i	Inlet
avg	Average
c	Cold fluid (Air)
f	Fin
h	Hot fluid (Water)
m	Mean
o	Outlet
p	Pump
w	Water

Chapter 1 **INTRODUCTION**

SUMMARY: A Fan Coil Unit (FCU) is a part of a Heating, Ventilation and Air Conditioning (HVAC) system used in residential, commercial, and industrial buildings. These devices consist of a heating or cooling coil and a fan. This chapter briefly introduces the FCU and its main components. The enhancement techniques to improve the heat transfer have been discussed. Furthermore, this chapter provides the main research aims of this study related to optimisation of heat transfer performance.

1.1 Introduction

Heating, ventilation, and air conditioning (HVAC) system design is a sub-discipline of mechanical engineering. These systems are designed based on the principles of thermodynamics, fluid mechanics, and heat transfer. These days HVAC plays an important role while developing a medium to large industrial and office buildings such as skyscrapers, where safe and healthy building conditions are regulated through management of comfort indicators such as temperature and humidity induction of fresh air from outside if necessary.

A fan coil unit (FCU) is a part of an HVAC system used in residential, commercial, and industrial buildings. These devices consist of a heating or cooling coil and a fan. Typically, a fan coil unit is not connected to the ductwork, and is used to control the temperature in the space where it is installed, or serve multiple spaces. It is controlled either manually using on/off switch or using a thermostat.

Due to their simplicity, fan coil units are more economical to install than ducted or central heating systems with air handling units. However, they can be noisy because the fan is within the same space. There can be in several unit configurations, including horizontal (ceiling mounted) or vertical (floor mounted).

1.2 Operating principle

The basic Fan Coil Unit (FCU) is manufactured using galvanised steel, which consists of a back panel, side panels, spigot panel, fan deck assembly, heat exchanger, drain tray assembly, filter, electrics assembly and access panels. In general, any FCU primary inputs are the flow rate of air, air temperature, the flow rate of liquid and its temperature, whereas heat transfer rate, pressure drop and noise level are the primary outputs that need to be analysed.

The basic operation of FCU uses re-circulated air which is air pulled into the FCU using the fan deck assembly. The heat exchanger has either cold or hot water circulating through the tubes, depending on what is required. The air which is drawn across the heat exchanger is then cooled or heated and expelled through various ducts, which are attached to the spigot panel into the room below which is seen in Figure 1.1. Various sensors and controls systems are used with the FCU to control the temperature in the room.

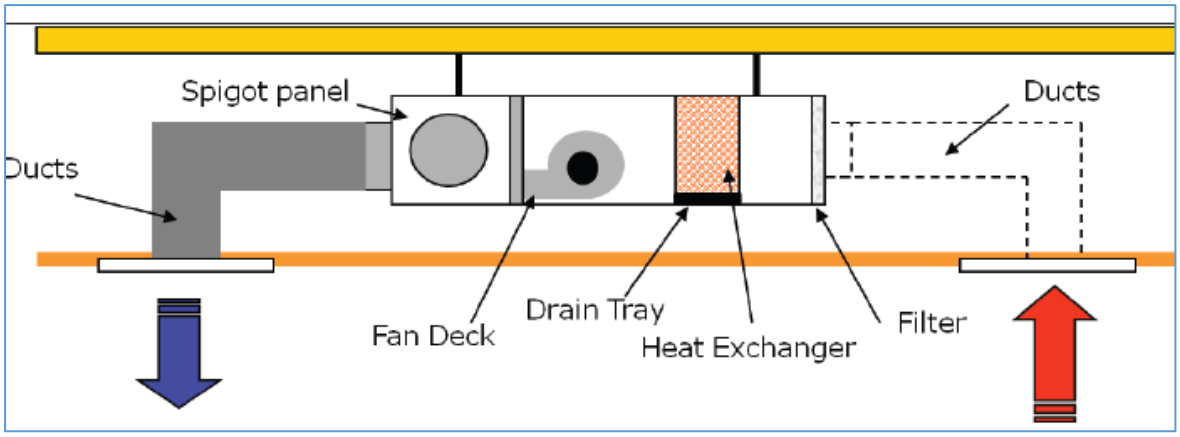

Figure 1.1 Operation of a Fan Coil Unit [1]

A centrifugal fan draws the air across the heat exchanger which will have either cold or hot water through the copper tubes; this is then expelled into the room as seen in Figure 1.2.

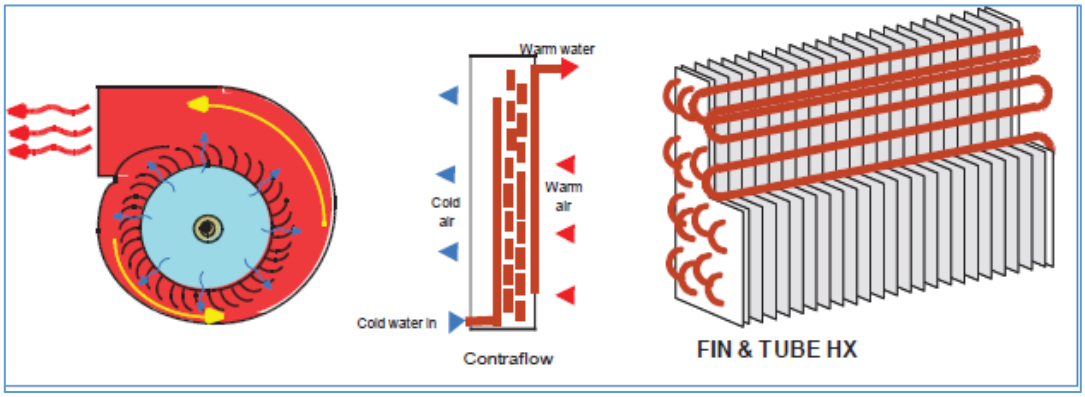

Figure 1.2 Fan operation [2]

1.3 Heat Exchangers

As described in the previous section, heat exchanger represents the main part of the FCU. It can be defined as a device that is used to transfer thermal energy (enthalpy) between two or more fluids, between a solid surface and a fluid, or between solid particulates and a fluid, at different temperatures and in thermal contact. In heat exchangers, there are usually no external heat and work interactions. Typical applications involve heating or cooling of a fluid stream and evaporation or condensation of single or multicomponent fluid streams. In a few heat exchangers, the fluids exchanging heat are in direct contact. In most heat exchangers, heat transfer between fluids takes place through a separating wall or into and out of a wall in a transient manner. In many heat exchangers, the fluids are separated by a heat transfer surface, and ideally, they do not mix or leak. They are used in many applications, such as in heating, ventilation and air conditioning systems (HVAC), power generation and manufacturing

system. The term heat exchanger is generally used to describe a variety of heat transfer equipment such as condensers, evaporators, economisers and radiators. A detailed information about the heat exchanger analysis under different operating conditions will be discussed in the next chapter.

1.4 Fan Motors

In order to circulate the required air, a fan motor is installed within the FCU. These motors can be either AC or electronically commutated DC (ECDC) motor. Both the motors are capable of rotating with variable speed. However, AC motors need an additional multi tap transformer to vary its speed. The new ERP (energy rated product) directive has forced many companies to design new ECDC fan motors which are compliant with the ERP directive and can produce huge savings on energy bills but come at a higher price. The new ECDC fan motors are up to 57% more efficient than the AC fan motor, the AC fan uses 118watts of power input compared to only 75watts on the ECDC fan and has 0.75 of specific fan power compared to only 0.31 on the ECDC. They run cooler due to a lower energy input, have a reduced maintenance and lower lifetime costs. Table 1-1 Comparisons between AC and DC fan motor [1] shows the comparison between AC and DC motors.

Table 1-1 Comparisons between AC and DC fan motor [1]

	Airflow	Volts	Input Power (W)	Specific Fan Power (W/(l/s))	Consumption 12h per day (kWh)	
AC Speed 6	180	210	118	0.66	1.416	
DC Speed 6	180	230	71	0.4	0.852	40% Improvement
AC Speed 3	135	170	78	0.58	0.936	
DC Speed 3	135	230	35	0.26	0.42	55% Improvement
AC Speed 1	55	90	45	0.82	0.54	
DC Speed 1	55	230	10	0.18	0.12	78% Improvement

1.5 Insulation

Providing adequate cooling & heating and low noise levels are the two most important parameters that consumers expect from any FCU. The noise levels can be reduced by applying

an acoustic insulation to certain areas of the FCU. However, this will increase the total cost of the FCU [3].

1.6 Heat Transfer Enhancement Techniques

In recent years, development of energy efficient heat exchangers has become a concern for many researchers and experts as the cost of energy and material has increased significantly[4], [5].

Enhanced surfaces transfer more heat than a standard surface, a reduction in weight of the heat exchanger for a given heat duty and pressure drop and a decrease in the pumping power for a given size and heat duty are the main benefits of enhancement device. In general, enhancement or augmentation techniques are classified into active and passive techniques. In addition, a combination of both active and passive techniques may be used for the aim of additional improvement in the thermo-hydraulic performance of a heat exchanger. The following sections include more details about these techniques.

1.9.1 Active Techniques

These techniques require external power to cause the expected flow improvement and modification in the rate of heat transfer. Using external forces such as mechanical aids, electric field, surface or fluid vibration and electrohydrodynamic fields are examples of these techniques.

1.9.2 Passive Techniques

Generally, these techniques use surface or geometrical modifications to the flow channel by employing inserts or additional devices. The main result of that is a higher heat transfer coefficients, and it also may lead to increase in the pressure drop [6]. The passive techniques require no direct application of external power. These techniques include extended or rough surfaces (where the effective heat transfer area is increased) , fluid or gas additives, swirl flow devices, surface tension devices, etc.[2],[7]

1.7 Motivation

In many engineering applications, process of transferring heat between two mediums at different temperatures in a direct contact or separated by a solid wall occurs in a device called heat exchanger. This function of exchanging the heat can also be found in a variety of relevant equipment such as condensers, evaporators, economisers, FCU and radiators. They are all commonly known as heat exchangers. Thermal performance of the heat exchanger depends on

a variety of factors including materials, used medium like water or air, device configuration, water flow and air flow etc… Increase of thermal performance can provide significant cost savings during both manufacturing and operation of the device. Optimisation of the heat exchangers itself as well as cost saving, and faster design and development processes are often referred to as heat transfer augmentation, enhancement or intensification. Main gains in thermal performance are usually achieved by increase in convective heat transfer by reduced thermal resistance. However, better thermal performance usually is coming at a cost of increased pressure drop across the heat exchanger and therefore increased energy requirement during operation. This could be partially compensated for by smaller designs and overall device miniaturisation of the heat exchanger unit. Therefore, design and development of new type of heat exchangers is often an act of balancing competing requirements and different objectives at different stages of the design process. More in-depth analysis is required to access in a unified manner fluid side flow, air- side flow performance, materials, manufacturing costs, operational and maintenance costs and energy efficiency.

In the process of designing or predicting the performance of a heat exchanger is necessary to link the total heat transfer rate to various process variables. These variables include; heat exchanger geometry, flow arrangements, materials and design configurations such as tube sizes, fins geometry, operating conditions and cost of operation. Furthermore, the experimental and numerical analysis of the heat exchanger under steady condition cannot be applied on the transient condition; hence, it is vital to conduct separate studies to analyse the performance characteristics of the heat exchanger under this condition.

An optimum design for a heat exchanger has to provide maximum heat transfer rate at low pressure drop. As with high pressure drop in the heat exchanger, a large pump size is required to overcome the flow resistance caused by this pressure drop which may lead to an increase in the cost of the system.

The total duty of a heat exchanger depends on the difference between the inlet and outlet fluid temperatures and the mass flow rate. The total duty for FCU that is 1.43 m long can vary from 2 KW to 5 KW [1] depending on the mass flow rate for the same inlet and outlet fluid temperatures difference.

The primary focus of this study is to analyse the current heat exchanger and propose some design modifications in order to optimise the FCU design in such way that it will take into account whole life cycle of the device including development, manufacturing, and operation.

Therefore, emphasis will be given not only to the thermal performance but also to the cost of manufacturing and operation.

1.8 Research Aims

The main aim of this thesis is to improve thermal performance and minimise the costs of the fan coil unit (FCU) and the specific aims formulated for this research study are described below. Detailed research objectives have been placed in the next section in order to make them easy to find. Three specific research aims can be formulated as follows: -

- Development of a novel approach to analyse the thermal performance of a multi-tube and fin heat exchanger used in the current FCU unit experimentally and numerically under steady state operating condition,
- Development of more efficient design for multi-tube and fin heat exchanger geometry to improve FCU thermal performance,
- To develop a novel performance optimisation model and to apply it to develop more efficient design of fins configuration for the multi-tube heat exchanger used in the current FCU based on multi-objective optimisation and total cost analysis.

1.9 Research objectives

Based on the research aim presented in the previous section, and after conducting a detailed literature review which will be carried out in chapter 2, the following objectives have been allocated to aid the research aims: -

A1. Development of a novel approach to analyse the thermal performance of a multi-tube and fin heat exchanger used in the current FCU unit experimentally and numerically under steady state operating condition:

1.1 To carry out a qualitative and quantitative analyses of the results achieved experimentally and numerically using a novel 3D CFD model for the baseline model,

1.2 To use CFD to predict heat transfer coefficients and local fin efficiency for multi tube and fin heat exchanger,

1.3 To determine the effect of longitudinal pitch, transverse pitch and fin spacing on the thermal performance of multi tubes and fins heat exchanger,

1.4 To develop a semi-empirical prediction model for the Colburn (j) factor and Fanning friction factor (f) for the multi-tube and fin heat exchanger with plain fins.

A2. Development of more efficient design for multi-tube and fin heat exchanger geometry to improve FCU thermal performance:

2.1 To present a novel fin configuration (perforated plain fin) and compare its thermal performance with plain and louvre fins configurations,

2.2 To carry out a comparative numerical study of the airside performance of multi-tube and fin heat exchanger under steady state operating conditions having plain, louvre and perforated louvre fins,

2.3 To develop a combined semi-empirical prediction model for Colburn (j) factor and Fanning friction factor (f) which can be used for different fin configurations,

2.4 To formulate the effect of hole diameter and hole spacing of the perforations on the thermal performance of the multi-tube and fin heat exchanger.

A3. Development of novel performance optimisation model and its application to develop more efficient design of fins configuration for the multi-tube heat exchanger used in the current FCU based on multi-objective optimisation and total cost analysis:

3.1 To propose a time efficient optimisation strategy which take into consideration limited experimental inputs, CFD modelling and optimisation,

3.2 To employ the new optimisation strategy to evaluate the thermal performance of the heat exchanger used in the FCU with combination of plain, perforated and louvre fins arrangements,

3.3 To derive an optimised model for the FCU design based on the heat exchanger performance with the following inputs: fins geometry, fins arrangements and total cost,

3.4 To assess the effectiveness of the proposed optimisation strategy by prototyping and validating the new optimised design.

1.10 Organisation of Thesis

This thesis is organised into seven main chapters. **Chapter 1** presents an introduction to the fan coil unit (FCU), its main components and operating conditions principles. From this introduction, the motivation for carrying out this research has been defined, which identifies the main areas to be reviewed in Chapter 2.

Chapter 2 starts with a background about the analysis of the heat exchanger under different operating conditions. The next part of this chapter presents an overview of current published literature on multi-tubes and fins heat exchangers. This chapter includes a review about the research that has been carried out in the analysis of the thermal performance of the multi-tube and fin heat exchanger used in the current FCU unit experimentally and numerically under steady state operating condition. Moreover, a review of available literature for the design modifications to improve the thermal performance of multi-tube and fin heat exchanger has also been included. The last part of this chapter contains the literature review being carried out on the optimisation techniques for multi-tube and fin heat exchanger. Details of the scope of research have been provided in the form of specific research aims and objectives.

Chapter 3 has been divided into two parts; the first part includes in detail a description of each component that has been used in the experimental facility. The experimental setup has been developed to validate the numerical model for multi-tubes and fins heat exchanger and to evaluate the effect of enhanced heat transfer for the optimum modified model on the thermal performance of the heat exchanger. Additionally, an estimation of the uncertainty of experimental results has been included. The second part provides the fundamentals of Computational Fluid Dynamics (CFD). The CFD modelling for the model of multi-tubes and fins heat exchanger has been included. It covers in detail the implemented meshing technique for the flow domain. Furthermore, this chapter specifies the suitable boundary conditions and solver settings.

In **Chapter 4**, in order to understand the complex flow structure in multi-tube and fin heat exchanger, a detailed qualitative and quantitative analysis of the results achieved numerically and experimentally has been carried out. Furthermore, the effect of various geometric and flow-related parameters on heat transfer and pressure drop characteristics on both air-side and water-

side for the heat exchanger has been investigated. The regression analysis and the corresponding equations for heat transfer and pressure drop characteristics as functions of all relevant parameters have been presented.

Chapter 5 deals with the design modifications to improve the thermal performance of multi-tube and fin heat exchanger. This chapter includes an extensive experimental and numerical studies to compare these design modifications with the baseline model of the heat exchanger.

Chapter 6 presents an optimisation model for multi-tube and fin heat exchanger. Moreover, the cost estimation of FCU integrated with multi-tube and fin heat exchanger has been included. This study includes a comparison between baseline and modified models in order to evaluate the effectiveness of the modifications.

Chapter 7 draws the overall conclusions of the thesis and provides several recommendations for possible future work.

Chapter 2 **HEAT EXCHANGERS ANALYSIS AND LITERATURE REVIEW**

SUMMARY: In the introduction chapter, detailed information regarding the parameters affecting the design of multi-tube and fin heat exchanger has been identified. This chapter provides detailed information about analysing the heat exchanger under different operating conditions followed by an intensive literature review to highlight the knowledge gaps in the existing literature. The literature review has been divided into three main part; I) analysis of performance of a heat exchanger used in the current FCU unit experimentally and numerically under steady state operating condition, II) design modification to enhance thermal performance of the heat exchanger and III) multi-objective optimisation of the new design and cost analysis. Based on this analysis, research objectives aligned with specific research aims have been formulated.

2.1 Heat Exchangers Analysis

In order to analyse the heat exchanger and to determine the amount of heat that will be transferred from one fluid to another, some fundamental assumptions are made as follows [8]:

- Heat exchangers are steady-flow or unsteady-flow devices.
- Thermal properties of all fluids are almost constant.
- Constant overall heat transfer coefficient.
- No heat exchange between the heat exchanger and the surroundings (Adiabatic).
- The fluids are gaining the heat through the solid surfaces.

There are three primary flow arrangements in heat exchangers: counter-flow, parallel-flow, and cross-flow. In the counter-flow exchanger, the fluids enter the exchanger from opposite sides. This is the most efficient design because it transfers the greatest amount of heat. In the parallel-flow version, both the fluids enter from the same end and move parallel to each other as they flow to the other side. For very long systems, the output temperature of both fluids becomes the same. The cross-flow heat exchanger moves the fluids in a perpendicular fashion. Figure 2.1 depicts the temperature profiles and schematics of the double-pipe heat exchanger for parallel-flow and counter-flow.

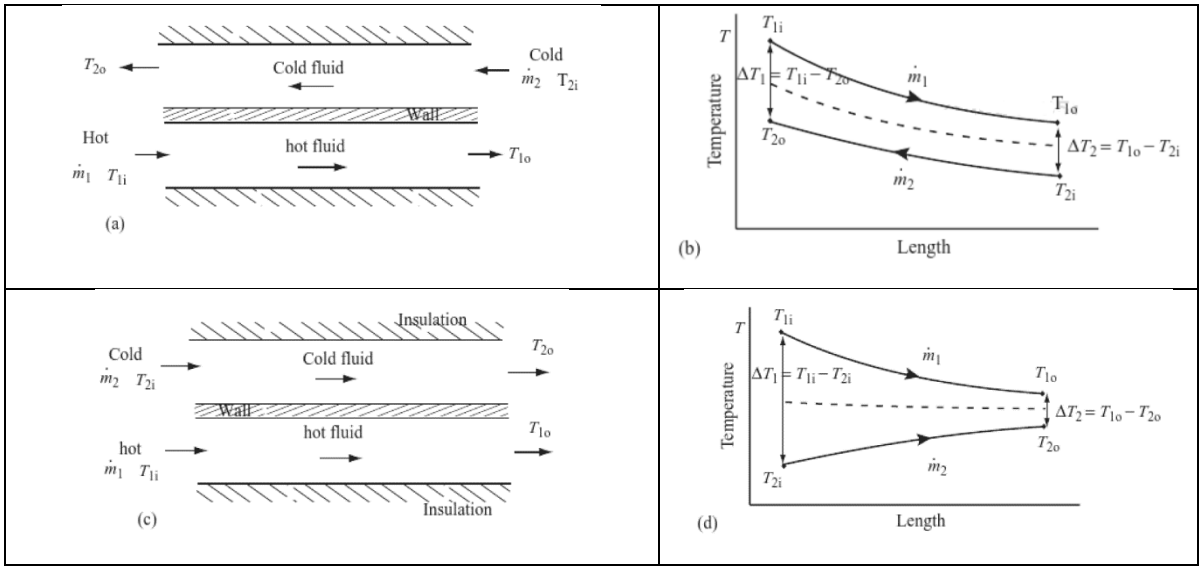

Figure 2.1 the counter flow arrangements: (a) Schematic for counter-flow channels and (b) the temperature distribution. The parallel-flow arrangements: (c) Schematic for parallel-flow channels and (d) the temperature distribution [9]

From the previous assumptions, the first law of thermodynamics can be written as.

$$\dot{Q}_h = \dot{Q}_c \tag{2.1}$$

where the heat transfer rate for hot fluid is $\dot{Q}_h$ and the heat transfer rate for cold fluid is $\dot{Q}_c$, respectively.

$$\dot{Q}_h = \dot{m}_1 Cp_1 (T_{1i} - T_{1o}) \tag{2.2}$$

$$\dot{Q}_c = \dot{m}_2 Cp_2 (T_{2o} - T_{2i}) \tag{2.3}$$

where $\dot{m}_1$ and $\dot{m}_2$ are the mass flow rate for hot and cold fluid, respectively, and Cp_1 and Cp_2 are the specific heats for the hot and cold fluid, respectively.

The overall heat transfer coefficient, heat exchanger effectiveness and the pressure drop within the heat exchanger are the most important parameters in the analysis of the heat exchanger. Therefore, the overall heat transfer coefficient, the heat exchanger effectiveness, basic methods to calculate the thermal effectiveness and the heat exchanger pressure drop will be discussed in the next sections.

2.1.1 Overall Heat Transfer Coefficient

To find an equation for the overall heat transfer coefficient, a thermal circuit across the wall between the hot and cold fluid can be constructed as shown in Figure 2.2.

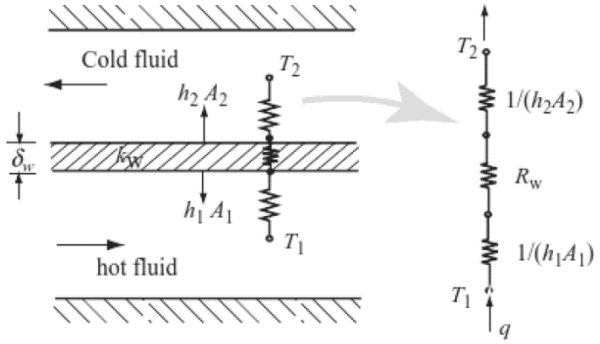

Figure 2.2 Thermal Resistance and Thermal Circuit for a Heat Exchanger [10]

The resistance network around the wall can be expressed in three terms,

- Convective resistance through the hot fluid
- Conductive resistance through the wall
- Convective resistance through the cold fluid

The UA value (the overall conductance) is defined as [9],

$$UA = \frac{1}{\frac{1}{h_1 A_1} + R_w + \frac{1}{h_2 A_2}} \tag{2.4}$$

Where U is the overall heat transfer coefficient, h_1 and h_2 are the heat transfer coefficients for hot and cold fluids, respectively, A_1 and A_2 are the heat transfer surface areas for hot and could fluids, respectively, and R_w is the wall thermal resistance. For flat wall, this resistance equals to:

$$R_w = \frac{\delta_w}{k_w A_w} \tag{2.5}$$

where δ_w is the wall thickness, k_w is the thermal conductivity of the wall material and A_w is the heat transfer area of the wall.

2.1.2 Colburn (j) factor and Fanning friction factor (f)

In order to analyse the thermal performance of the heat exchanger, it is important to compute heat transfer and pressure drop characteristics accurately by using non-dimensional parameters. In the experiments, it is more common to present the heat transfer characteristics using Colburn (j) factor and the pressure drop characteristics using Fanning friction factor (f) as a function of Reynolds number (R_e) [7]. Definitions for these factors have been presented by [7] as follows,

Fanning friction factor is the ratio between wall shear stress and the flow kinetic energy per unit volume.

Colburn factor a modified Stanton number to take into consideration the moderate variations in the Prandtl number (P_r) for a range from 0.5 to 10.0 in turbulent flow.

The Colburn j factor and the friction factor f can be computed from Eq.s (2.6) and (2.7), respectively.

$$j = \frac{h_a}{\rho_a V_{a(max)} C_{pa}} P_r^{\frac{2}{3}} \tag{2.6}$$

$$f = \frac{A_c}{A_o}\frac{\rho_m}{\rho_1}\left[\frac{2\rho_1 \Delta P}{G_c^2} - (K_i + 1 - \sigma^2) - 2\left(\frac{\rho_1}{\rho_2} - 1\right) + (1 - \sigma^2 - K_e)\frac{\rho_1}{\rho_2}\right] \tag{2.7}$$

The Eq. (1.7) has been proposed by Kays and London [11] and the coefficients K_I and K_e are the abrupt contraction pressure-loss coefficient and the abrupt expansion pressure-loss coefficient, respectively. These coefficients are adapted from Figure 2.3 [12].

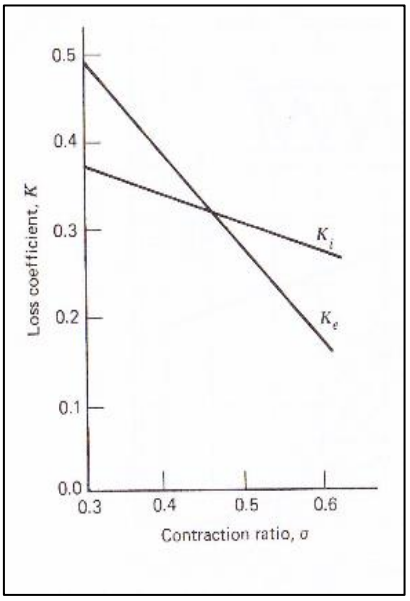

Figure 2.3 Entrance and Exit Pressure Drop Coefficients for Plate-Fin Heat Exchanger [12]

A_c is the flow cross sectional area and σ represents the ratio of the minimum flow area to the frontal area. ρ_1, ρ_2 *and* ρ_m are the density of air inlet, air outlet and mean density, respectively.

2.2 Classification of Heat Exchangers

Heat exchangers classification will be discussed in this section. In general, heat exchangers can be classified according to transfer processes, a number of fluids used in the system, degrees of surface compactness, construction features, flow arrangements, and heat transfer mechanisms [13].

Generally, heat exchangers can be classified into two groups: -

A. According to its construction features

- Double-pipe
- Shell-and-Tube
- Plate heat exchanger (PHE)
- Finned-Tube Heat Exchangers
- Plate-Fin Heat Exchangers

B. According to the fluid used.

- Gas-Liquid
- Liquid-Liquid
- Gas-Gas

2.2.1 The Heat Exchanger Effectiveness

The heat exchanger effectiveness ε is defined as the ratio between the actual heat transfer rates to the maximum possible heat transfer rate, therefore ε can be written as: -

$$\varepsilon = \frac{\dot{Q}}{\dot{Q}_{max}} \tag{2.8}$$

The maximum possible heat transfer rate will occur when the difference in inlet temperature and outlet temperature is the maximum value. Hence, for parallel-flow heat exchanger Eq. 2.8 can be written as follows [9]

$$\varepsilon = \frac{T_{1i} - T_{1o}}{T_{1i} - T_{2i}} \tag{2.9}$$

2.2.2 Basic Methods to Calculate Thermal Effectiveness

There are four basic design methods to calculate the thermal effectiveness of heat exchangers [14]:

1. ε-NTU method
2. LMTD method
3. P-NTU_t method
4. ψ-P method

The fundamentals of the first two methods are discussed next because of their importance in the analysis.

I. ε-NTU method

This method has been proposed by [15]. The method expresses the total heat transfer rate from the hot fluid to the cold fluid in the heat exchanger as:

$$Q = \varepsilon C_{min}(T_{1i} - T_{2i}) \quad (2.10)$$

where, C_{min} denotes to the product of mass and specific heat of the fluid which has a lower thermal capacity rate.

In this method, the effectiveness of the heat exchanger is a function of the number of transfer units (NTU), the heat capacity rate ratio (C^*) and (U) the overall heat transfer coefficient.

Number of transfer units (NTU): is a ratio between the overall conductance and the smaller heat capacity rate.

$$NTU = \frac{UA}{C_{min}} = \frac{1}{C_{min}} \int_A UdA \quad (2.11)$$

Where (U) is the overall heat transfer coefficient ($W/m^2 K$).

Heat capacity rate ratio (C^*) is the ratio between the smaller and larger heat capacity rate for the two fluid streams so that $C^* \leq 1$.

$$C^* = \frac{C_{min}}{C_{max}} = \frac{(mCp)_{min}}{(mCp)_{max}} \quad (2.12)$$

where, (C_{max}) denotes to the product of mass and specific heat of the fluid which has a higher thermal capacity rate.

From equations 2.10 and 2.12

$$\varepsilon = \frac{C_h(T_{hi}-T_{ho})}{C_{min}(T_{hi}-T_{ci})} = \frac{C_c(T_{co}-T_{ci})}{C_{min}(T_{hi}-T_{ci})} \quad (2.13)$$

In general, as the effectiveness of the heat exchanger increases as the NTU increases. However, there are exceptions such that after reaching a maximum value, the effectiveness decreases with increasing NTU.

II. LMTD method

Another way to express the heat transfer rate is [13],

$$Q = UAF\Delta T_{lm} \quad (2.14)$$

where U is the overall heat transfer coefficient, A is heat transfer area, and ΔT_{lm} is the log mean temperature difference, defined as

$$\Delta T_{lm} = \frac{\Delta T_1 - \Delta T_2}{\ln\left(\frac{\Delta T_1}{\Delta T_2}\right)} \quad (2.15)$$

where

$$\Delta T_1 = T_{1i} - T_{2i} \text{ And } \Delta T_2 = T_{1o} - T_{2o} \text{ for parallel flow} \quad (2.16)$$

$$\Delta T_1 = T_{1i} - T_{2o} \text{ And } \Delta T_2 = T_{1o} - T_{2i} \text{ for counter flow} \quad (2.17)$$

F is the correction factor which depends on the flow arrangements. At the install design stages, the value for the correction factor can be assumed as in Table 2-1[16].

Table 2-1 Estimated Values for the Correction Factor [16]

Heat exchanger type	Correction Factor
True counter flow	1.0
Double-pipe heat exchanger in counter flow arrangement	1.0
Shell type of shell and tube heat exchanger	1.0
Cross flow heat exchanger	0.7
TEMA E shell with single pass on both shell side and tube side	0.7

In General, for the design of compact heat exchangers, the ε-NTU method is used. In contrast, for the design of shell and tube heat exchangers, the LMTD method is used [16].

2.2.3 Heat Exchanger Pressure Drop

Pressure drop in a heat exchanger is an important factor; it is vital to consider during the design process. This factor will determine the pumping power or fan work input necessary to keep the continuous of the flow through the heat exchanger. Hence poor design can result in additional cost. Pressure drop calculations are required for both fluid streams, and in most cases flow consists of either two internal streams or an internal and external stream. Pressure drop is affected by a number of factors, namely the type of flow (laminar or turbulent) and the passage geometry.

In general , calculating the pressure drop in a heat exchanger is necessary for many applications for at least two reasons [14]:

1- The pumping power (P_p) is the power required to run the working fluids and this power is related to the heat exchanger pressure drop. Equation 2.18 describes the relationship between the pumping power and the heat exchanger pressure drop for moving devices such as pumps, fans, and blowers.

$$P_p = \frac{\dot{m}\Delta P}{\rho} \tag{2.18}$$

2- At large pressure drop, the heat transfer rate is considerably affected by the saturation temperature change for a condensing/evaporating fluid.

2.3 Transient Behaviour of a Heat Exchanger

Under practical conditions, steady testing is not feasible or practical because the inputs of the heat exchanger are time dependent. Hence, it is very important to analysis the heat exchanger under transient conditions where the inputs and the outputs are dependent on time [17]. Heat exchangers with two working fluids are operating at different states,

- Steady state where the inlet and outlet temperatures of both fluids are constant over time.
- Transient state where one or both fluids is / are having a change in its inlet temperature.

According to [17] the transient inputs can be:

- Step input; where the inlet temperature or flow rate changed suddenly to a new value.
- Frequency input; where the inlet temperature or flow rate changed periodically.
- Impulse input; where the inlet temperature or flow rate changed by an infinite amplitude.

Figure 2.4 illustrates a diagram for these inputs.

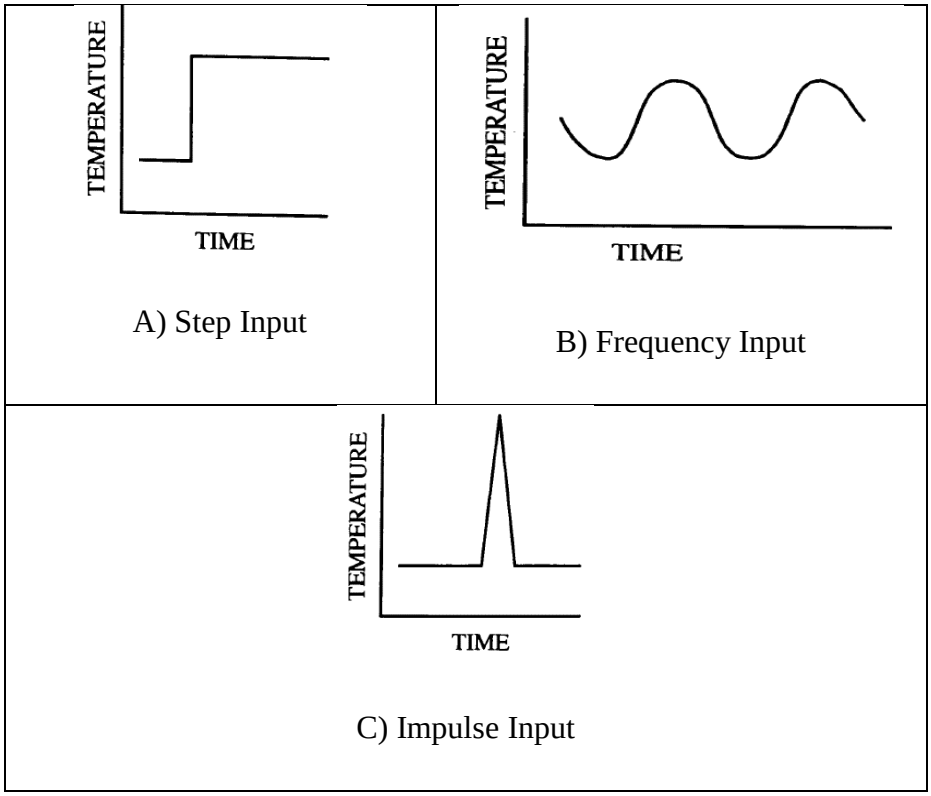

Figure 2.4 Transient Inputs [17]

A mathematical model is proposed by many researches [18],[19],[20],[7] and [21] to express the convective heat transfer between the wall of a heat exchanger and fluid streams at constant velocities. The model consists of three linear partial differential equations. The schematic description of cross flow heat exchanger is shown in Figure 2.5.

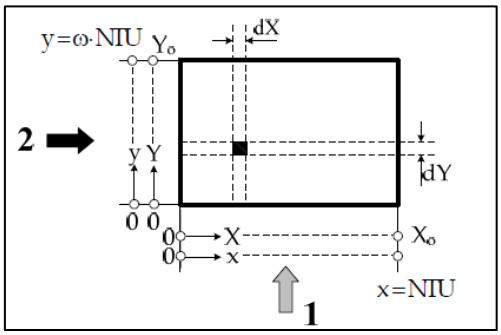

Figure 2.5 Schematic Description of Cross Flow Heat Exchanger[22]

In order to develop a mathematical solution for cross flow heat exchanger model some simplifying assumptions are made. The assumptions are as follows [22]:

- Single phase for both fluids and they are unmixed;
- Adiabatic setup;
- Neglecting the axial conduction in both fluid and walls;
- Constant fluid velocity in each flow path;

- Both fluids are finite-velocity liquids or gases;
- The independence of the heat transfer characteristics and physical properties from temperature, position and time.

Based on the previous simplifying assumptions and by applying the energy equations on both fluids, three simultaneous partial differential equations can be written [22] which are shown below:

$$M_w C_{P_w} \frac{\partial T_w}{\partial t} = (hA)_1 (T_1 - T_w) - (hA)_2 (T_w - T_2) \quad (2.19)$$

$$m_1 C_{P_1} X_0 \left[\frac{\partial T_1}{\partial X} + \frac{1}{u_1}\frac{\partial T_1}{\partial t}\right] = (hA)_1 (T_1 - T_w) \quad (2.20)$$

$$m_2 C_{P_2} Y_0 \left[\frac{\partial T_2}{\partial Y} + \frac{1}{u_2}\frac{\partial T_2}{\partial t}\right] = (hA)_2 (T_w - T_2) \quad (2.21)$$

where,

M_w and Cp_w are the mass and specific heat of the wall of heat exchanger, respectively.

In experiments, the single blow transient testing has been used to obtain the heat transfer characterises of the heat exchanger [23]. The test is based on changing the state of the fluid from steady to a transient condition in a short time by changing the inlets condition.

2.4 Literature Review

Multi-tube and fin type heat exchangers have numerous application areas in the field of thermal engineering. There are several fin shapes such as plain, louvre, convex-louvre, and wavy. Among these designs, plain fin configuration is the most common fin design in heat exchanger applications, due to its simplicity and rigidity. Circular type tubes are the typical geometries used in heat exchangers.

Many studies have been carried out to improve the performance of heat exchangers to meet a certain duty. These studies involve many techniques and can be classified as two major techniques [2],

- Active technique, use external forces, such as electric field, surface vibration.

- Passive technique, use special surface geometries or fluid additives

2.5 Analysis of Performance of a Heat Exchanger Used in the Current FCU Unit Experimentally and Numerically under Steady State Condition

2.5.1 Experimental Studies

Wilson [24] experimentally developed a method to evaluate the convection coefficients in a variety of convective heat transfer processes. The method divided the overall thermal resistance into three major resistances; the internal convection, the tube wall and the external convection. The result of this method is represented graphically in Figure 2.6, where the water-side heat transfer coefficient is a function of water velocity.

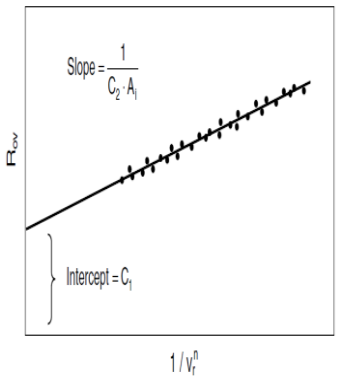

Figure 2.6 Original Wilson Plot [25]

Modifications of Wilson method were carried out by Sieder-Tate [26], Colburn [27] and Dittus-Boelter [28]. These modifications correlate Nusselt number with the Reynolds and Prandtl numbers in conformity with Equation (2.1). In those correlations, the authors assumed the exponents of the Reynolds number (nA) and Prandtl number (mA) for Eq. (2.22).

$$\mathrm{Nu_A} = \mathrm{C_A Re_A^{nA} Pr_A^{mA}} \tag{2.22}$$

where, A is denoted for fluid A, C is constant, m is an exponent of Prandtl number and n is an exponent of Reynolds number.

Wang et al. [29] provided an experimental data, by studying 15 samples with different geometries and a range for Reynolds number from 300 to 7500, on the plain fin and tube heat exchanger having 3/8th (9.52 mm) tube diameter. Furthermore, the effect of fin spacing, the number of tube rows and fin thickness on the heat transfer and friction characteristics are also studied. The results of this study are shown (Figure 2.7) in terms of friction factor and Colburn *j*-factor against Reynolds number. The study showed that there is no effect of the fin thickness

on the heat transfer or friction characteristics. The number of tube rows has negligible effect on the friction factor. Also, for the range of Reynolds number used in this study, it has found that the fin spacing has no effect on the heat transfer characteristics. However, the study does not take in account changing the diameter of the tubes.

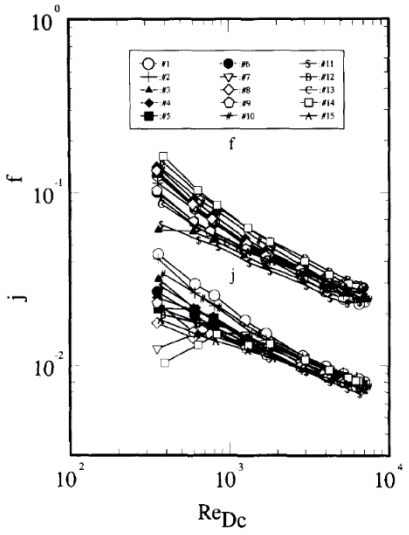

Figure 2.7 Friction Factor and Colburn j-Factor for the Tested Samples [29]

Abu Madi et al. [30] examined the thermal characteristics of the round tube and plate finned heat exchangers. Based on consideration of the heat transfer and fluid flow relations for the heat exchanger surfaces, Abu Madi et al. developed a novel approach for deriving the geometric ratios in the correlation equations. Authors state that the fin type affects the heat transfer and friction factor, whilst the numbers of tube rows have an insignificant effect on the friction factor. The number of tube rows effect was found to be influenced by the fin and tube geometries as well as the Reynolds number. However, authors didn't not mention the number of fin used, as well as the experiments are only limited to four rows of tubes.

Wang et al. [31] studied the airside performance of fin and tube heat exchangers with plain fin configurations. A sum of 18 samples was tested to study the effect of the number of tube rows, fin spacing and tube diameter on the thermal hydraulic characteristics. The author concluded that the fin pitch has a strong effect on the heat transfer characteristics for a range of Reynolds number from 300 to 3000 and for one and two number of tube rows. Moreover, a very small effect of the number of rows on the friction performance has been found and the effect of tube diameter on heat transfer performance are linked to fin pitch.

Halıcı et al. [32] investigate the influence of the number of tube rows on heat, mass and momentum transfer experimentally for flat-plate finned-tube heat exchangers under both wet and dry surface conditions and for a range of Reynolds number between 300 and 2000. Heat exchangers used in this study consist of Aluminium fins and Copper tubes. The number of rows was increased from (1 to 4) for the same geometry of flat-plate finned-tube heat exchangers. It has been found in this study that, the Colburn and friction factors are higher for wet surfaces comparing with dry surfaces.

Wang [33] tested 36 plain fin and tube heat exchangers with a different number of tube rows to examine the heat and mass analogy under dehumidifying process. The study has been carried out for a range for Reynolds number between 250 and 7500. Wang stated that the ratio of $h_{c,o}/h_{d,o}\ C_{p,a}$ is in the range between 0.6 and 1.1 and it is unaffected by any variations of fin spacing at low Reynolds number, as it can be seen from Figure 2.8. where ($h_{c,o}$) is the sensible heat transfer coefficient, ($h_{d,o}$) is the mass transfer coefficient and ($C_{p,a}$) is the heat capacity.

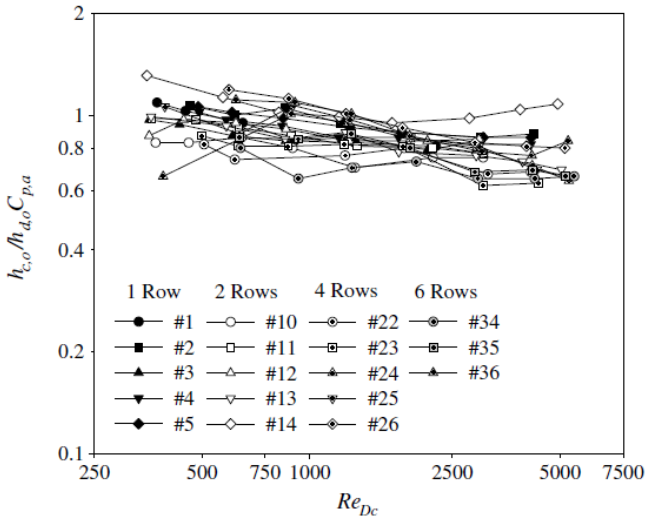

Figure 2.8 Variation of the Value hc,o⁄hd,o Cp,a with Reynolds Number [33]

Taler [34] presented two methods for determining the air-side heat transfer coefficient for a model of two-pass radiator consists of two inline rows of oval tubes with smooth plain fins. Taler developed a correlation for the heat transfer coefficient on the air-side based on the first method which is based on the experimental data. Furthermore, he concluded that the heat transfer coefficients based on the air temperature difference across the heat exchanger obtained from the second method, CFD simulation, are larger because the CFD simulation does not account for the thermal contact conductance between tubes and fins.

Chaudhari et al. [35] studied the effect of finned heat exchanger over a without finned tube heat exchanger on the overall heat transfer coefficient. The study was done experimentally for an automobile radiator. The authors concluded with:

- Experiment setup is a useful tool to analyse a finned tube heat exchanger.
- The overall heat transfer rate for a non-finned tube heat exchanger is less than the finned type.

Taler et al. [36] proposed two modified methods, the first one is to predicate the mean value of thermal contact resistance in plate fin and tube heat exchanger. The second is to find the average heat transfer coefficient for the air flow. Those methods were established based on experimental and CFD simulations data. Taler et al. recommended pre-setting the value of thermal contact resistance between the tube and the fin of the CFD model on the source of the experimental data.

Wang et al.[37] carried out an experimental comparative study of the airside performance of fin and tube heat exchanger having plain, louvre and semi-dimple vortex generator (VG) for a different number of tubes row and different fin spacings. The results of this study indicated that the effect of a number of tubes row on the heat transfer coefficients is small for both louvre and semi-dimple vortex generator fin geometry. Furthermore, the heat transfer coefficients for louvre fin geometry, for a number of tubes row equal to 2 and 4 rows, is about 2-15% higher than those of semi-dimple vortex generator fin geometry.

Song et al. [38] experimentally investigated the effect of fin pitch, tube pitch and two sizes of curved delta winglet vortex generators with different base length on the heat transfer and pressure drop performance of circular tube-fin compact heat exchanger. The study used Colburn factor (j) and friction factor (f) to evaluate the heat transfer and pressure drop characteristics of the heat exchanger, respectively. The results of this study reveal that at low Reynolds number, heat transfer enhancement has been achieved for the smaller vortex generator which locates close to the tube. Furthermore, changing the fin pitch has a strong effect on the friction factor and therefore on the cost of the heat exchanger.

2.5.2 Numerical Studies

A prediction of the heat transfer and fluid flow performance of the heat exchanger is mainly carried out by some extensive experimental studies. However, the capability of the numerical studies has increased which allowed CFD simulations to be used more frequently.

Singh et al. [39] introduced two segment by segment models, resistance model and conduction model, that account for fin conduction for the refrigerant to air heat transfer in fin and tube heat exchanger. The results of this study showed a good agreement with some experiments. However, this study was based on refrigerant to air heat transfer in fin and tube heat exchanger.

Borrajo-Peláez et al. [40] presented 3-D numerical simulations, using CFD, to compare both an air-side and an air/water-side models. The effect of Reynolds number, fin pitch, tube diameter, fin length and thickness on the mechanical and thermal efficiencies was studied. The authors evaluated the model performance by using two non-dimensional parameters; the air side Nusselt number and a friction factor. It was found that the effect of the five parameters over the mechanical and thermal efficiencies can be well reported using these non-dimensional coefficients.

Dong et al. [41] presented an experimental and numerical investigation of friction factor and heat transfer performance for a fully developed turbulent region of air flow in a wavy fin. The investigation was done experimentally and numerically. The results of this investigation indicated that there is a negligible effect on the different wavy fin profiles (Triangular, Sinusoidal and Triangular round corner) on friction factor and heat transfer performance. In addition, the standard *k*-ε model (SST) is the most appropriate mode to simulate the air flow and heat transfer of wavy fin, for a range (1000 – 5500) of Reynolds number.

Lu et al.[42] carried out a numerical study to establish the effect of fin spacing, tube pitch, fin thickness, and tube diameter on thermal performance of a two-row fin and tube heat exchanger. The performance of the heat exchangers is evaluated in terms of the ratio between heat transfer rate and pressure drop ($^{Q}/_{\Delta P}$) and the coefficient of performance (COP). The results of this study indicate that as the longitudinal tube pitch and of transverse tube pitch increases, the ratio ($^{Q}/_{\Delta P}$) increases steadily. However, the ratio ($^{Q}/_{\Delta P}$) diminishes as the tube diameter and fin thickness goes higher. Additionally, an optimum value for the ratio ($^{Q}/_{\Delta P}$) has been achieved at 6–8 fin per inch.

Čarija et al.[43] used CFD to analyses the fluid flow of the air side of a multi-row fin and tube heat exchanger with flat (plain) and louvred fins in a range of Reynolds number, based on fin spacing and air frontal velocities, between 70 and 350. The study reported that at Reynolds number equal to 350, an increase in heat transfer performance of 58% was obtained for louvre fins comparing with flat fins. Furthermore, as the louvre length increases an almost linear

improvement in heat transfer performance can be noticed for a constant Reynolds number, as can be seen in Figure 2.9.

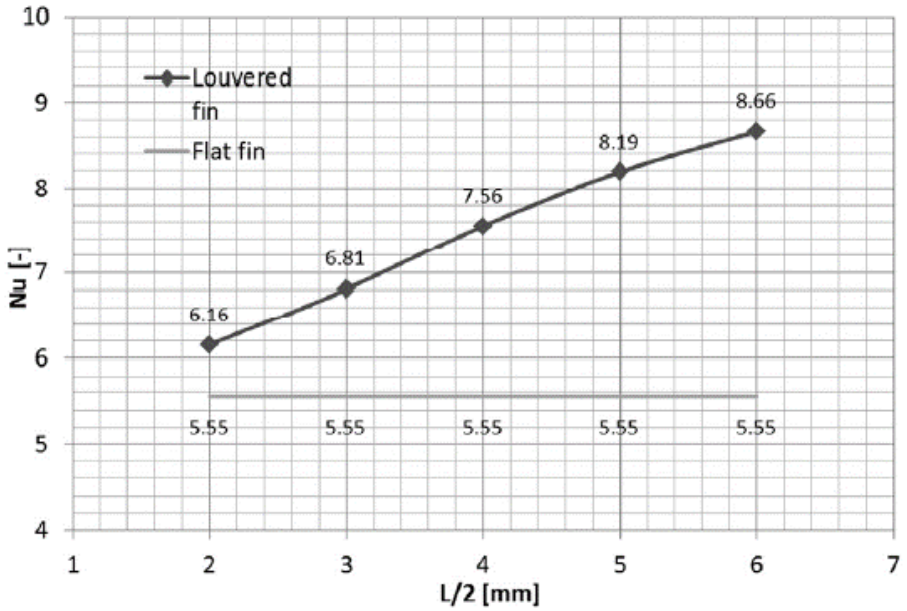

Figure 2.9 Linear Relations between Louver Length and Heat Transfer Performance [43]

Altwieb et al. [44] carried out an experimental and numerical investigation on the response of a multi tube and fin heat exchanger under steady state operating conditions. In these investigations, a novel 3D numerical model with the full geometry of the heat exchanger has been implemented to develop a set of design equations which can be used to predict the heat transfer rate and the pressure drop across the airside.

2.5.3 Summary of Literature Regarding the Analysis the performance of the heat exchanger used in the current FCU unit experimentally and numerically under Steady State Condition

In order to identify the knowledge gaps in the area of analysing the performance of the heat exchanger used in the current FCU unit experimentally and numerically under steady state condition, the literature review has been carried out. Consequently, it can be noticed that the published literature has a limited range of investigation parameters. Furthermore, the literature presented lack certain aspects, such as:

1. Most of the CFD based studies use a computational domain which takes into consideration only a part of the fin,
2. A majority of these studies lack local flow field analysis, such as local fin efficiency, local heat transfer coefficient and temperature distribution of the working fluid and on

fins. The identification of the improvement of these local flow features may improve the performance of the heat exchanger,

3. A majority of the literature seems to be omitting the profiles of the air flow with different velocities in centre and at the edges of the test section. As well as influence of the temperature profile along the water tube.

2.6 Development of more efficient design for multi-tube and fin heat exchanger geometry to improve the FCU thermal performance

In recent years, many studies have been carried out to improve the performance of a multi-tube and fin heat exchanger and therefore to improve the thermal performance of the FCU. The main task behind these studies is to enhance the thermal performance of the heat exchanger with less pressure drop and a reduction in both material weight and cost.

Wang et al. [45] carried out an experimental study on the airside performance of compact slit fin and tube heat exchangers. Authors provided a comparison between the compact slit fin and louvre and plain fin surface using different comparison methods; comparison using Colburn and friction factors, comparison of heat transfer as a function of fluid power and performance comparison with a reference surface. The results of this study showed that:

- A small effect for the number of tube row on the frictional performance for the present compact slit fin geometry.
- The slit breadth represents a major function to improve the heat transfer performance. In contrast, the slit height represents a minor function to improve the heat transfer performance.
- Based on the comparison of the air-side performance between compact slit, louvre and plain fins. It is found that the compact slit and louvre fin are similar in the results.

According to Webb et al [46] and Wang et al [47] extending the fin surface come to be one of the most important means to enhance the heat transfer performance. Moreover, the plain fin is common use because of it is easy to manufacture, simply to assemble and result a lower pressure drop.

Torii et al. [4] presented a novel strategy, delta winglet-type vortex generators, to enhance the heat transfer characterises of fin and tube heat exchanger with circular tubes at low Reynolds number. The thermal performance of this novel fin has been evaluated experimentally. The

configuration of winglet type vortex generator on the fin surface-tube is depicted in Figure 2.10.

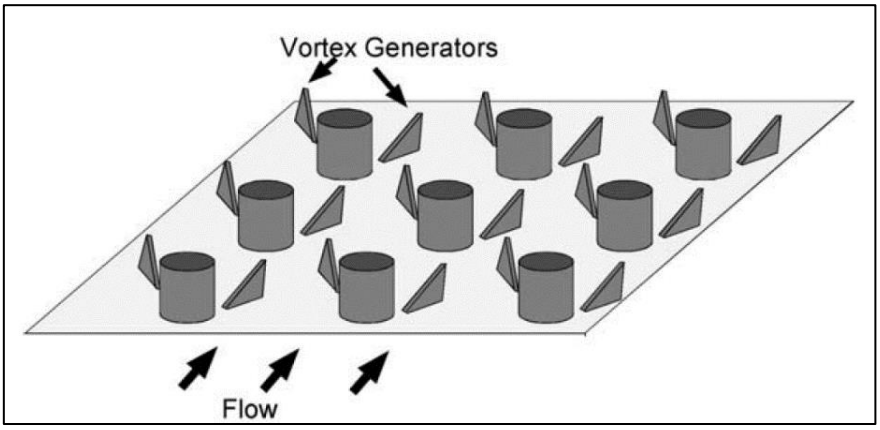

Figure 2.10 Configuration of Winglet Type Vortex Generator on the Fin Surface-Tube [4]

The results of this study revealed that for a staggered tube banks, the heat transfer was improved by 10% to 30% this was accompanied by a decrease of 34% to 55% in the pressure drop, for the Reynolds number ranging from 350 to 2100. Joardar et al. [5] applied the same technique on a compact plain fin and tube heat exchanger. The study was carried out by comparing the overall heat transfer and pressure drop performance of the modified designs; one with a single-row and the other with three-row winglet vortex generators, with a baseline model with no winglet vortex generators, Figure 2.11illustrates the three fins configurations, over a Reynolds number range of $220 \leq Re \geq 960$.

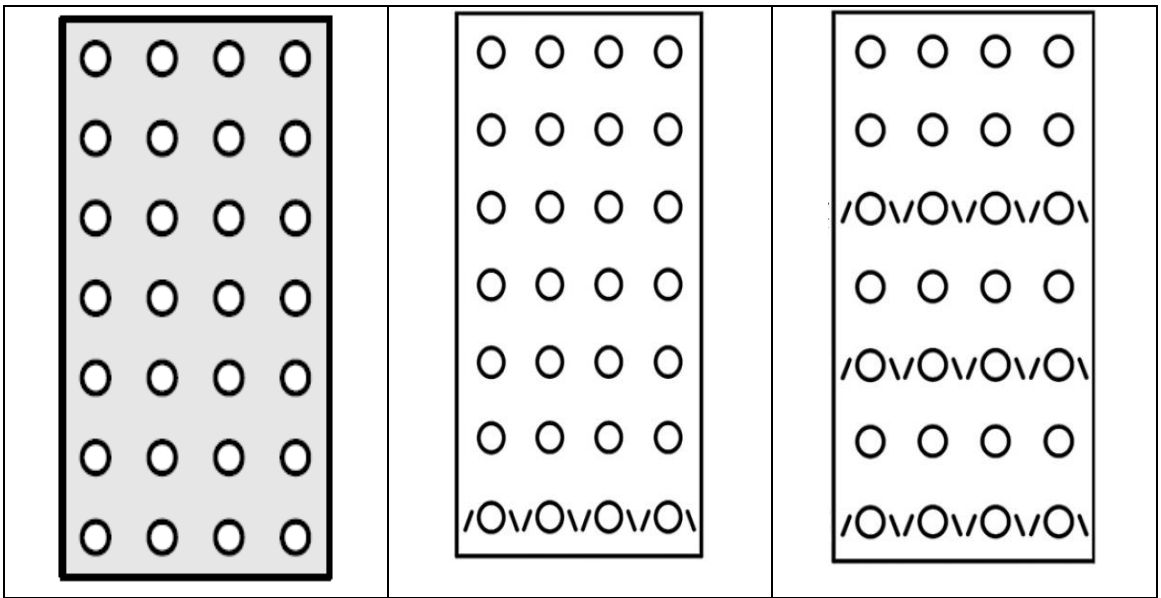

A) Baseline Fin	*B) Single-Row Winglet Vortex Generators Fin*	*C) Three-Row Winglet Vortex Generators Fin*

Figure 2.11 Winglet Vortex Generators Fins Configurations [5]

The results of this study showed that vortex generator technique can significantly enhance the performance of fin-tube heat exchangers where, for the single-row winglet configuration, the air-side heat transfer coefficient increased from 16.5% to 44% and the pressure drop has gone higher by 12%. For the three-row vortex generator configuration, the heat transfer coefficient increases with Reynolds number from 29.9% to 68.8% with a rise of the pressure drop by 26% at Reynolds number = 960 to 87.5% at Reynolds number = 220.

Erek et al. [48] numerically investigated the impacts on heat transfer and pressure drop by changing the fin geometry of a plate fin and tube heat exchanger. The investigation observed that placing the fin tube at downstream region affects heat transfer positively. Another important result of this investigation is that larger heat transfer and pressure drop values are obtained as the fin height is increased, due to the increased heat transfer surface area.

Banerjee et al. [23] numerically studied the effect of having perforations on plain annular fins on the heat transfer and pressure drop characteristics with various locations of the perforations. The numerical study has been carried out for a range of frontal air velocity from 1 m/sec to 5 m/sec and a corresponding range of Reynolds number was between 4000 and 24,000. The study takes into consideration also the effect of the non-uniform fin spacing on the pressure drop. The results of this study indicate that the location of the perforation on fin surfaces significantly affect the performance of this fin and it has recommended having the perforation on the back side of the fin. In addition, it is reported that the pressure drop for non-uniform fin spacing is lower than the uniform fin spacing design.

Liu et al. [49] carried out a numerical investigation to study the effect of the perforation size and number on the air-side (j) factor and heat transfer rates of finned-tube heat exchangers for different fin spacing. The results of the numerical simulations of the perforated fins have been compared with plain fins with the aim to evaluate the heat exchanger performance. It has been found that, by increasing the air-side Reynolds number from 750 to 2350 and for a constant fin spacing, the air-side (j) factor has increased by 3% and 8.1%, respectively. Moreover, perforated fins heat exchanger has a higher air-side (j) factor comparing with plain fins heat exchanger.

2.6.1 Summary of Literature Regarding the Development of more efficient design for multi-tube and fin heat exchanger geometry to improve FCU thermal performance

In the previous section, a literature review regarding the development of new design for multi-tube and fin heat exchanger geometry to improve FCU thermal performance has been carried out. It has noticed that the literature presented above lack certain aspects, such as:

1. The scope of work that is published is very limited on the perforations of plain or louvre fins which represents a passive enhancement technique to improve the thermal performance of the heat exchanger. The influence of perforations on local flow features as well as global performance indicators is a major research gap that needs to be bridged.
2. Majority of equations which have been developed for the design purposes have limited applicability and these do not include all the geometric parameters corresponding to the fins.
3. Most of these studies lack in investigation of parameters such as hole diameter and hole spacing of the perforations. These parameters significantly affect the thermal performance of multi-tube and fin heat exchanger which need to be investigated.

2.7 Multi-objective optimisation of the more efficient design and cost analysis

As discussed in Chapter 1, the heat exchanger is the most important part in the FCU. Therefore, the following section provides a detailed review of the available literature in the field of optimise the design of multi-tube and fin heat exchanger.

Fax et al. [50] has presented the first systematic heat exchanger optimisation methodology in 1957. The methodology applies the Largrangian multipliers method in the optimisation of plate-fin gas turbine heat exchanger based on analytical solutions.

Queipo et al. [51] has combined numerical simulations and the Genetic Algorithm technique (GA) to optimise of electronics cooling. This work is regarded as the first work to use numerical solver in heat exchanger optimisation. In addition, Guessous et al. [52] devolved a simplified framework for shape optimisation of engine cooling system (radiator). The framework combines the GAMBIT® and FLUENT® software with an in-house code. Moreover, Suram et al. [53] optimised the fin shape of the heat exchanger using numerical simulations coupled with graph based evolutionary algorithm.

Mishra et al.[54] and Xie, Sunden et al.[55] used the Genetic Algorithm technique (GA) to design and optimise a compact heat exchangers (CHE). The technique was sufficient to exploit the problem and deal with numerous variables within different constraints. Xie, Sunden et al. carried out a theoretical optimisation design by taking into consideration the minimum total volume or/and total annual cost of the CHE as objective functions in the GA, respectively. The authors concluded that the optimised CHE provides a reduction in both total volume and total cost with or without pressure drop constraints. Furthermore, the presented method can be transferred for use in optimisation design of different types of heat exchangers with different fins configurations such as perforated, slotted and louvered fins. Mishra et al. developed a genetic algorithm based optimisation technique for cross flow plate-fin heat exchangers using offset-strip fins. The aim of the study was to minimise the number of entropy generation units for a specified heat duty under given space restrictions.

Rao et al.[56] carried out a thermodynamic optimisation of a cross flow plate-fin heat exchanger using the particle swarm optimization (PSO) algorithm technique. The authors considered the minimisation of entropy generation units and minimum total volume and/or minimum total cost as objective functions. In their conclusion, the authors mentioned that the PSO technique is simple in concept, has few parameters and easy to put into practice comparing with Genetic Algorithm technique (GA).

Juan et al. [57] optimised a plate fin and tube heat exchanger using the Genetic Algorithm technique (GA). The fin pitch, the transverse and longitudinal tube pitches and the tube diameter were considered as optimization parameters within reasonable constraints, the total rate of heat transfer and the total pressure drop of the air side are considered as two differing objective functions. Results show, in the range of Re = 1200–14000, an increase of the total heat transfer rate of the optimized heat exchanger by about 2.1–9.2% comparing with the original one, the heat transfer coefficient increased by about 8.2–14.7% and the total pressure drop decreased by about 4.4–8%.

Myhren et al. [58] optimised the heat output of a ventilation radiator by proposing a simplified fin configuration model. The model has been used to optimise the spacing between convection fins. The results of this study showed that thermal performance of the ventilation radiator can be enhanced by decreasing the distance between convection fins inside the radiator panels in order to enlarge the area of heat transfer surfaces. This change in the internal geometry could mean a considerable increase in the pressure drop.

Yun et al. [59] carried out an experimental study to analysis the effect of fin pitch, angle of slit pattern, slit length and slit height on the thermal performance of a heat exchanger with slit fins. The authors used a novel dimensionless factor to determine the optimised condition of each parameter from the aforementioned parameters. The factor is named JF factor and it is the larger-the-better. The JF factor can be expressed as,

$$JF = \frac{{}^{j}/_{j_R}}{\left({}^{f}/_{f_R}\right)^{1/3}} \tag{2.23}$$

where, j is Colburn factor which symbolised the heat transfer characteristics and f is Fanning friction factor which symbolised the pressure drop characteristics of the heat exchanger. j_R and f_R are the values of j and f for the reference heat exchanger used in the experimental results.

The work presented by Yun et al. [59] has been followed by MS Kim et al. [60] and Jonghyeok et al.[61] to carry out a multi-objective optimisation and use the JF factor as a single-objective function for the optimisation of a heat exchanger with offset-strip fins and a channel with aligned dimples and protrusions, respectively. However, the above-mentioned research works have been mainly focused on the optimisation based on geometrical parameters and the objective of minimum total cost is not considered as an optimisation objective.

Song et al. [57] employed ANSYS Workbench software, and Fluent to study the heat transfer and pressure drop characteristics of offset strip fins. The authors developed new correlations for j is Colburn factor f is Fanning friction factor for Aluminium plate-fin heat exchanger NB/T 47006-2009. In this study, it has been stated that the traditional empirical formula is not able to cover the general specifications of domestic offset strip fins. Therefore, it is vital to develop more precision correlation using a numerical technique in order to optimise the design of the heat exchanger.

Singh et al. [62] carried out a systematic numerical study on the overall performance and weight reduction of a cross-flow type fin and tube heat exchanger design for a waste heat recovery application. The study aimed to improve the thermal performance and reduce the total cost of the heat exchanger by proposing a new geometric design based on changing a dimensionless design variable named aspect ratio (α) from $\alpha = 0.1$ (triangular profile of the fin) to 1(trapezoidal profile of the fin). However, the numerical model for the heat exchanger used in this study has considered only one-half of the fin.

2.7.1 Summary of Literature Regarding Multi-Objective Optimisation of the more efficient Design and Cost Analysis

In the previous section, the literature review about the optimisation of the heat exchanger has been presented. To the best of author's knowledge, there is limited work that has been carried out on the optimisation process of the heat exchanger, such as:

1. The existing studies do not explain in detail the optimum design procedure of the heat exchanger. Therefore, the development of a reasonable reference framework for the optimum design of the heat exchanger is required.
2. Majority of the presented studies regarding the optimisation of the heat exchanger lack the total costs optimisation.
3. The lack of optimum design procedure (optimisation strategy) of the heat exchanger which take into consideration maximum heat transfer, low pressure drop and least total cost.

For successful completion of the project and achieving all the previous-mentioned aims and objectives, a combination of experimental and numerical investigations have been carried out. The following chapter will provide a detailed explanation of the experimental setup and the numerical method that have been employed in this study.

Chapter 3 **EXPERIMENTAL SETUP AND NUMERICAL MODEL**

SUMMARY: Based on the research objectives that have been presented in the chapter two, this chapter develops various tools for numerical and experimental research which are called collectively framework used in this study. The first part of this chapter provides a detailed description of the experimental setup which has been designed and built at the University of Huddersfield with the cooperation of TEV Ltd, Brighouse-UK. The description includes the equipment used, configuration of the setup, test procedure and the method of estimating the uncertainties in the experiment. The second part deals with the methodology of the CFD modelling for multi-tubes and fins heat exchanger which is used in this study. The methodology includes the governing equations, model geometry, model meshing, and justification of applied boundary conditions.

3.1 Introduction

An experimental setup has been designed and built at the University of Huddersfield with the cooperation of TEV Ltd, Brighouse-UK to perform the experiments of the multi-tubes and fins heat exchanger model. Figure 3.1 shows a schematic diagram of the experimental setup. The main objectives of the experimental work are:

- To validate the numerically predicated results of multi-tubes and fins heat exchanger models with the results obtained from experimental tests.
- To evaluate enhanced heat transfer and pressure drop for the optimum new model on the thermal performance of multi-tubes and fins heat exchanger model as compared to the baseline model that has been mentioned in previous chapter.

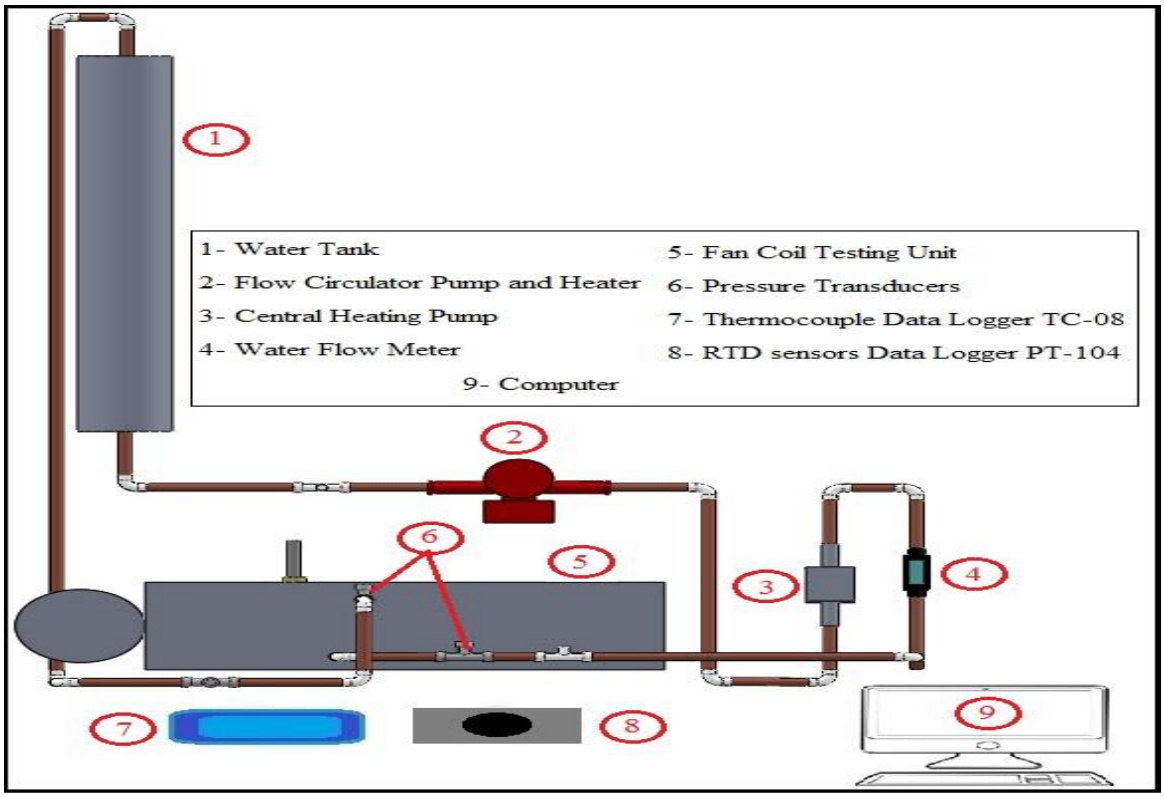

Figure 3.1 Schematic of the Experiment Setup

3.2 Test Rig Components

The setup is mainly composed of a water tank, heater, pump, flow meter, fan coil testing unit, pressure transducers, thermocouples data logger, RTD sensors data logger and a computer. In the following individual elements of this setup have been explained.

3.2.1 Water Tank

4” Pipe was used to store the water required to be circulated through the flow loop. The tank has 5 L volume capacity. In order to minimise the heat loss, the tank has been wrapped using reflector foil which reduces heat loss from the water tank by reflecting heat back into it, as shown in Figure 3.2.

Figure 3.2Water Tank

3.2.2 Flow Circulator Pump and Heater

The heater, shown in Figure 3.3, was used to heat the water up to 60° (C) and 75° (C) [37], [45] using a controller shown in Figure 3.4. The heater has a power rating of 0.9 kW at 230 V.

Figure 3.3Water Heater

Moreover, this heater has the capability to pump water through the flow loop at low flow rates which can be used to analyse the flow through the system in laminar region.

Figure 3.4 Heater's Controller

3.2.3 Central Heating Pump

This standard high-efficiency pump was used to pump water through the flow loop at high flow rates. This pump, shown in Figure 3.5, has a LED display for setting the set point and displaying current consumption (range between 4 to 40W). The pump has a 6 m maximum delivery head.

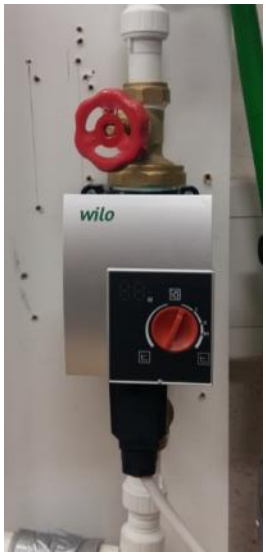

Figure 3.5Water Pump

3.2.4 Water Flow Meter

To measure water flow rate, a Flowmax 44i was used, shown in Figure 3.6. This water flow meter is able to calculate the volume flow of liquids based on the ultrasonic technology. The measuring range for this flow meter is 0.3 to 21 (L/min). The flow meter requires 18 to 30 V DC power supply while the current output is 4-20 mA, a current to voltage converter has been used to connect the flow meter with DAQ. In addition, the flow meter is able to show the actual flow and volume counter on a background lighted display.

Figure 3.6Water Flow Meter

3.2.5 Fan Coil Testing Unit

Figure 3.7 shows a schematic diagram of the fan coil testing unit. The unit is mainly composed of test section (housing), centrifugal fan, heat exchanger and some measuring components. The details of these individual elements will be discussed in following sections.

I. Test Section (Housing)

The testing section was made up from galvanised steel sheet with 2 mm thickness riveted together to form the test section which holds the heat exchanger and fan assembly. The test section is 650 mm long, 165 mm wide and 175 mm high.

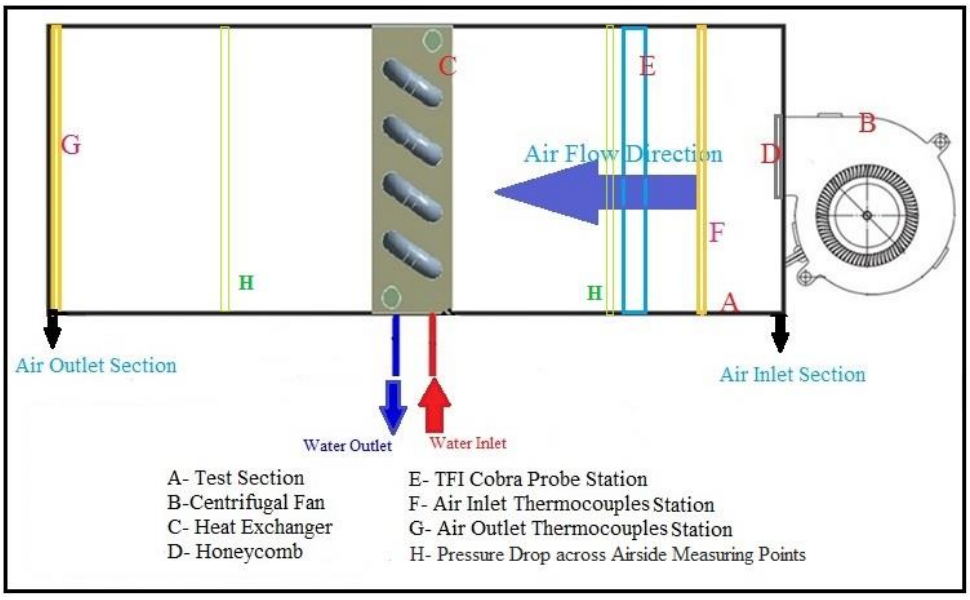

Figure 3.7 Schematic of the Fan Coil Testing Unit

II. Single-Sided Centrifugal Fan with Integrated Electronically Commutated (EC) Motor

In this study, a single-sided centrifugal fan with integrated electronically commutated (EC) motor has been sourced for the purpose of this research. The EC motor has been controlled

using a potentiometer, to control voltage in order vary the speed of motor allowing changing the various air flow rates to pass through test section. The technical specifications of this fan are shown in Table 3-1.

Table 3-1 Single-sided Centrifugal Fan Technical Specification [63]

Description	Value
Voltage	1 ~ 230 VAC
Voltage Range	1 ~ 200-277 VAC
Frequency	50/60 Hz
Power	119 W
Rated current	0.9 A
Speed	2150 rpm
Airflow	610.0 m^3 / hr
Operating temperature range	-25 ... + 30 ° C
Direction of rotation	Clockwise viewed from the rotor facing
Engine type	M3G074-CF
Engine Model	Energy-saving EC motor with integrated electronics
Motor protection / Protection	Built-in anti-lock.
Protection class	IP44
Motor insulation class	B
Bearings	Ball bearing
Material	The rotor galvanized, electronics encased in Aluminum castings.
Impeller	Made from galvanised sheet steel
Mounting position	Free
Electrical connection	Cable 450 mm.
Weight	2.4 kg

III. Heat Exchanger

The model of multi-tube and fin type heat exchanger was used in this study has plain fins shown in Figure 3.8. The heat exchanger consists of two rows of tubes of 9.52 mm diameter, each row

contains 5 tubes, the over length of each tube is 130 mm and they are joined together with 25 mm bend.

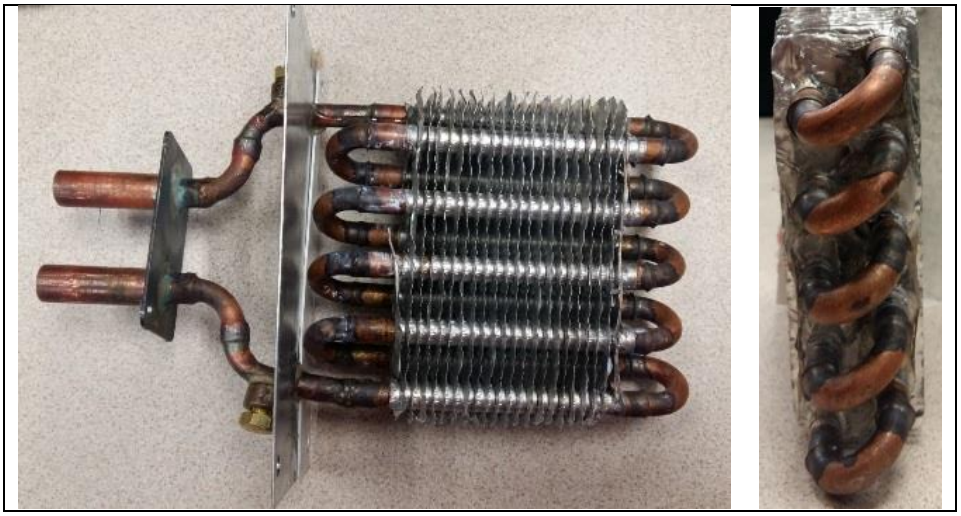

Figure 3.8 Multi-tube and Fin Heat Exchanger with Plain Fins (Baseline Model)

Tubes are made up from Copper with 0.26 mm thickness. The heat exchanger has 21 staggered configuration fins made up from Aluminium with 0.12 mm thickness. Fins are 44 mm wide and 125 mm high and they are placed 4.23mm apart from each other (6 fins per inch). fins are attached to the Tubes by a tight mechanical (press) fit. The detailed dimension of the heat exchanger is shown in Figure 3.9.

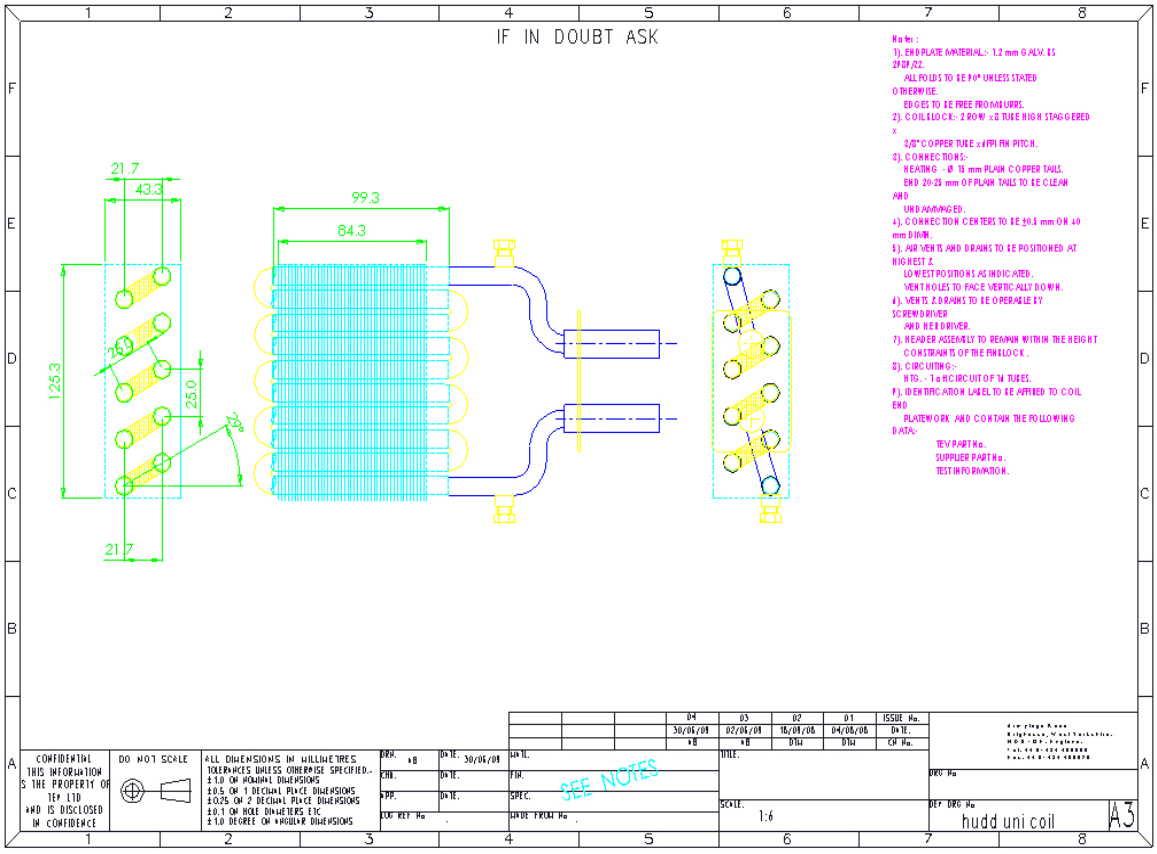

Figure 3.9 Heat Exchanger Dimensions

IV. Flow Straightener (Honeycomb)

In order to suppress the incoming free turbulence flow honeycomb was placed at the outlet of the centrifugal fan.

V. TFI Cobra Probe Station

In this study, the cobra probe was used to measure the air velocity at the inlet of the test section, as shown in Figure 3.10. The cobra probe is a multi-hole pressure probe able to resolve 3-components of velocity and local static pressure in real time. Moreover, the ASHRAE standard 41.2 was adapted to measure the air velocity at 25 points in the inlet section [37, 64]. The details of this process are described in Appendix B.

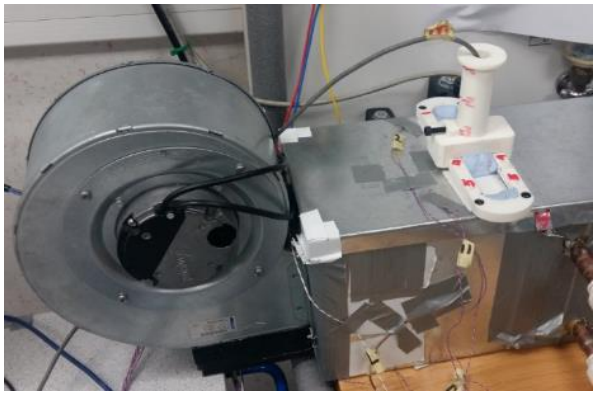

Figure 3.10 TFI Cobra Probe Station

VI. Air Inlet and Outlet Temperature Measuring Stations

The air inlet and outlet temperatures upstream and downstream the testing unit were measured by two measuring stations; each measuring station is composed of seven T-type exposed welded tip thermocouples (Copper / Constantan) [37, 64]. Using seven thermocouples for each side has two advantages; The first is to improve the accuracy by having large signal, and the second is automatic averaging of the air temperature distribution on both inlet and outlet measuring stations. The specifications of thermocouple are shown in Table 3-2.

Table 3-2 T-type Thermocouples Specifications [65]

Description	**Value**
Thermocouple Type	T-type exposed welded tip
Operating range	-75°C to +250°C
Cable Length	2000 mm
Standards Met	ANSI
Typical accuracy	0.5 °C

The data from these thermocouples were recorded then averaged. During testing, these thermocouples were repeatedly checked and calibrated using a standard thermometer. See Appendix A.

VII. Micro-Manometer

The pressure drop across the airside of the heat exchanger was detected by using DPM TT550 micro-manometer, Figure 3.11. The micro-manometer can measure the static pressure in range ± 0.4 to 5000 Pascal.

Figure 3.11 DPM TT550 Micro-Manometer

3.2.6 RTD Sensors

Water inlet and outlet temperatures were measured by Pico technology temperature probes (RTD-PT100) [37]. Table 3-3 provides the technical specification of these sensors. Furthermore, during testing these sensors were repeatedly checked and calibrated using open surface water bath which has a thermometer indicator. See Appendix A.

Table 3-3 RTD Sensors Specifications [66]

Description	**Value**
Sensors Type	PT100
Temperature Measurement Range	-75 to +250°C
Accuracy	±0.15°C at 0°C
Probe Length	120 mm
Probe Diameter	3.3 mm
Cable	2 m PVC

3.2.7 Pressure Transducers

The pressure drop across the waterside of the heat exchanger was detected by using two pressure transducers (IMP - Industrial Pressure Transmitter); one in the water inlet section and

the other is in the outlet. Table 3-4 provides the technical specification of these pressure transducers. Moreover, both sensors have been connected with USB-1616HS series data acquisition which is able to record the voltage readings coming from both sensors and then these voltage readings are converted to a corresponding pressure using a calibration equation.

Table 3-4 Pressure Transducers Specifications [67]

Description	Value
Sensors Type	IMP - Industrial Pressure Transmitter
Pressure Datum	Gauge
Pressure Range	0 to 4 Bar
Output	0 - 10V / 3-wire
Process Connection	G 1/4" male DIN 3852
Operating Temperature	-20° to +80°C
Supply Voltage	13 - 32V DC

3.2.8 Data Loggers

All the data coming through the thermocouples were recorded using Pico thermocouple data logger TC-08 and Pico log data logger software. The data logger has eight channels and two of these data loggers have been used in this test setup. The specifications of the data logger are summarised in Table 3-5.

Table 3-5 Pico Thermocouple Data Logger Specifications [68]

Description	Value
No. of channels	8 miniature thermocouple inputs
Accuracy	±0.2% of reading + 0.5°C
Overload protection	>±30V
Voltage input range	±70mV
Maximum sampling rate	10 readings per second (100ms)
Resolution	20 bits
Output connectors	USB.1 – connector cable supplied

Thermocouple types supported	B, E, J, K, N, R, S, T
Dimensions	85 x 145 x 25mm
Power requirements	Powered from USB port

In addition, a PT-104 Platinum resistance data logger was used to convert the voltage coming through the RTD sensors into corresponding temperatures. Pico log data logger software was used to record these temperatures. Table 3-6 summarised the specifications of the PT-104 data logger.

Table 3-6 PT-104 Platinum Resistance Data Logger specifications [69]

Description	Value
Sensor	PT100, PT1000
Range	–200 to +800 °C
Accuracy (at 23 ±2 °C)	0.01% of reading + 0.015 °C
Number of inputs	4
Converter resolution	24 bits
Conversion time	720 ms per channel
Input connectors	4-pin mini-DIN
Input impedance	>1 MΩ
Output connectors	USB and Ethernet

3.2.9 Computer

A PC has been used to record all the data coming from data acquisition, water flow meter, pressure transducer sensors, cobra probe and data loggers.

3.3 Tests Procedure

In the present study, tests were performed by drawing an air flow over the fins side of the heat exchanger, while circulating hot water through the tubes of the heat exchanger. Two different types of tests have been carried out; steady state and transient tests. The steps below describe how to prepare the experimental setup for testing:

- Fill the tank with water
- Turn on the heater by setting water temperature in the heater controller to 60° C
- Turn on the water pump and adjust it at a certain water flow rate

- Wait some time until the water temperature reach 60°C. In the meantime, connect thermocouples, RTD sensors and pressure transducers with data loggers and data acquisition and connect them with the computer
- After the water temperature reach 60°C, turn on the centrifugal fan at a certain air velocity by using the potentiometer
- Prepare the data logger software
- The water temperature will drop due to the effect of the air blown from fan. Therefore, make sure that the water temperature is in range of 60 ±1 °C (steady state condition) before starting recording the readings
- Start testing

3.4 Estimating Uncertainty

The error in measurement is defined as the difference between its true and measured values. However, this definition is not helpful because it is not easy to know which is the true quantity of these values. Therefore, it is necessary to compute the uncertainty when presenting an experimental results [70]. Generally, the uncertainty of measurement is described as the amount of errors or doubts in taking measurement [71]. These errors or doubts are mainly due to measuring instrument, measuring process, human error (operator skills) and operating condition.

For any set of data, the standard uncertainty (SU) can be calculated using the equation (3.1) [72], [73]:

$$SU = \frac{ESD}{\sqrt{n}} \tag{3.1}$$

where, ESD is the estimated standard deviation and n is the number of measurements in this set.

The estimated standard deviation (ESD) for (n) number of measurements can be expressed mathematically as:

$$ESD = \sqrt{\frac{\sum_{i=1}^{n}(SV-MV)^2}{(n-1)}} \tag{3.2}$$

Where, SV is the result of the i^{th} measurement (sample value) and MV the arithmetic means of (n) number of measurements which can be calculated using the equation below:

$$MV = \frac{1}{n}\sum_{i=1}^{n} SV \quad (3.3)$$

Based on the calculation procedure shown above using the equations Eq. (3.1), (3.2) and (3.3) and the set of data for steady state test 1 (plain fins), the results for calculating the standard uncertainty are shown in Table 3-7 for the thermocouples in inlet and outlet measuring stations, 2 RTD sensors 2 pressure transducers and water flow rate which were used in the experiments.

Table 3-7 Standard Uncertainty Results

Description		Standard Uncertainty Value
Inlet Measuring Station	TC-1	0.003
	TC-2	0.001
	TC-3	0.002
	TC-4	0.001
	TC-5	0.001
	TC-6	0.001
	TC-7	0.001
Outlet Measuring Station	TC-1	0.015
	TC-2	0.012
	TC-3	0.012
	TC-4	0.009
	TC-5	0.007
	TC-6	0.007
	TC-7	0.003
RTD Sensors	Water-IN	0.0052
	Water-OUT	0.0053
Pressure Transducers	Water-IN	0.0002
	Water-OUT	0.0002
Water Flow Rate	Water Flow Rate	0.0003

After a detailed description of the experimental setup by showing the equipment used, test procedure and the method of estimating the uncertainties in the experiment. The next part of this chapter includes the methodology of the CFD modelling for multi-tubes and fins heat exchanger.

3.5 Introduction to CFD

The Computational Fluid Dynamics (CFD) software FLUENT® is used in this study to carry out the simulation to analyse the pressure drop and heat transfer characteristics in multi-tubes and fins heat exchanger. Computer modelling, such as those carried out by CFD software

FLUENT®, has received a lot of attention in recent years and became increasingly popular as an alternative approach to address the problems in the real world. Computer modelling can provide detailed information on fluid flow, heat and mass transfer mechanism. Moreover, numerical methods are much more flexible and less expensive compared to experimental analysis, as it gives an opportunity to test new methods and flexibility to make any modifications before they are executed through experiments.

3.6 CFD Codes

CFD codes are structured around the numerical algorithms that can address the problems of fluid flow. For the aim to provide easy access to their solving power, all commercial CFD packages include sophisticated user interfaces to input problem parameters and to study the results. Thus, all codes contain four main elements [74]. These are:

- Problem Identification
- Pre – Processor
- Solver
- Post – Processor

An overview of CFD modelling is shown in Figure 3.12.

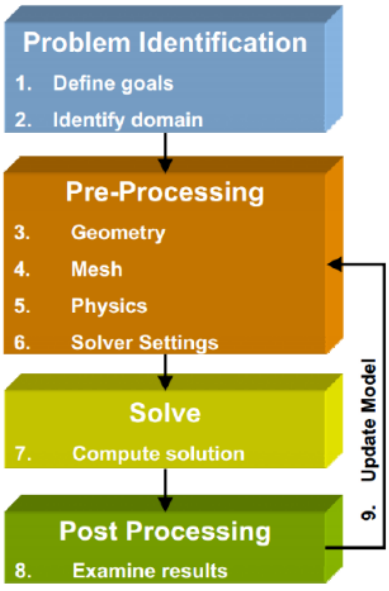

Figure 3.12 Overview of CFD Modelling [75]

3.7 Governing Equations of Fluid flow

The governing equations of fluid flow represent mathematical statements of the conservation laws of Physics:

- The mass of a fluid is conserved.
- The rate of change of momentum equals the sum of the forces on a fluid particle. (Newton's second law)
- The rate of change of energy is equal to the sum of the rate of heat addition to and the rate of work done on a fluid particle. (First law of thermodynamics)

The fluid is regarded as a continuum. For the analysis of fluid flows at macroscopic length scales, the molecular structure of matter and molecular motions may be ignored. The behavior of the fluid is described in terms of macroscopic properties such as velocity, pressure, density and temperature etc. These are averages over suitably large numbers of molecules. A fluid particle or point in a fluid is then the smallest possible element of fluid whose macroscopic properties are not influenced by individual molecules.

3.7.1 Mass Conservation in 3D

For the fluid element, the mass balance equation can be written as follows:

Rate of increase of mass in fluid element = *Net rate of flow of mass into fluid element* (3.4)

There is no any change rate of density for an incompressible fluid. Therefore, the mass conservation equation is:

$$\text{Div } V = 0 \tag{3.5}$$

The Eq. (3.5) describes the net flow of mass out of the element across its boundaries. The above equation in longhand notation can be written as:

$$\frac{\partial u}{\partial x} + \frac{\partial v}{\partial y} + \frac{\partial w}{\partial z} = 0 \tag{3.6}$$

3.7.2 Momentum Equations in 3D

Newton's second law can be expressed as follows,

Rate of increase of Momentum of the fluid particle = *Sum of flow of forces on the fluid particle* (3.7)

Surface forces and the body forces are the two types of flow forces on fluid particles; surface forces include pressure, viscous and gravity forces while body forces include centrifugal and electromagnetic forces. It is a common practice to highlight the contributions due to the surface forces as separate terms in the momentum equations and to include the effects of body forces as source terms.

The x-component of the momentum equation is found by setting the rate of change of x–momentum of the fluid particle equal to the total force in the x – direction on the element due to surface stresses, plus the rate of increase of x – momentum due to sources. The equation is as follows [76]:

$$\rho g_x + \frac{\partial \sigma_{xx}}{\partial x} + \frac{\partial \tau_{yx}}{\partial y} + \frac{\partial \tau_{zx}}{\partial z} = \rho \left(\frac{\partial u}{\partial t} + u \frac{\partial u}{\partial x} + v \frac{\partial u}{\partial y} + w \frac{\partial u}{\partial z} \right) \tag{3.8}$$

Similarly, y and z components of momentum equation are given by:

$$\rho g_y + \frac{\partial \sigma_{xy}}{\partial x} + \frac{\partial \tau_{yy}}{\partial y} + \frac{\partial \tau_{zy}}{\partial z} = \rho \left(\frac{\partial v}{\partial t} + u \frac{\partial v}{\partial x} + v \frac{\partial v}{\partial y} + w \frac{\partial v}{\partial z} \right) \tag{3.9}$$

$$\rho g_z + \frac{\partial \sigma_{xz}}{\partial x} + \frac{\partial \tau_{yz}}{\partial y} + \frac{\partial \tau_{zz}}{\partial z} = \rho \left(\frac{\partial w}{\partial t} + u \frac{\partial w}{\partial x} + v \frac{\partial w}{\partial y} + w \frac{\partial w}{\partial z} \right) \tag{3.10}$$

3.7.3 Energy Equation in 3D

The energy equation is derived from the first law of thermodynamics, it can be written as follows,

Rate of increase of energy of fluid particle = *Net rate of heat added to fluid* + *Net rate of work done on fluid* (3.11)

Conservation of energy of the fluid particle is ensured by equating the rate of change of energy of the fluid particle to the sum of the net rate of work done on the fluid particle, the net rate of heat addition to the fluid and the rate of increase of energy due to sources. The energy equation is [74]:

$$\rho\frac{DE}{Dt} = -\text{div}(pu) + \left[\frac{\partial(u\tau_{xx})}{\partial x} + \frac{\partial(u\tau_{yx})}{\partial y} + \frac{\partial(u\tau_{zx})}{\partial z} + \frac{\partial(v\tau_{xy})}{\partial x} + \frac{\partial(v\tau_{yy})}{\partial y} + \frac{\partial(v\tau_{zy})}{\partial z} + \frac{\partial(w\tau_{xz})}{\partial x} + \frac{\partial(w\tau_{yz})}{\partial y} + \frac{\partial(w\tau_{zz})}{\partial z}\right] + \text{div}(k\,\text{grad}\,T) + S_E \quad (3.12)$$

The energy equation for solid materials which is solved in FLUENT can be written as [77],

$$\frac{\partial(\rho h)}{\partial t} = \nabla.(k\nabla T) + S_h \quad (3.13)$$

Where, the h is the enthalpy which can be expressed as,

$$h = \int_0^T C_p\,dT \quad (3.14)$$

S_h is the enthalpy source. The term $[\nabla.(k\nabla T)]$ represents the conduction (Fourier's Law) in the CFD models where k is the thermal conductivity of the solid materials in the models.

3.7.4 Equations of State

The motion of a fluid in three dimensions is described by a system of five partial differential equations i.e. mass conservation, x, y and z momentum equations and energy equation. Among the unknowns are four thermodynamic variables i.e. density, pressure, temperature and internal energy. Relationships between the thermodynamic variables can be obtained through the assumption of thermodynamic equilibrium.

The fluid velocities may be large, but they are usually small enough that, even though properties of a fluid particle change rapidly from place to place, the fluid can thermodynamically adjust itself to new conditions so quickly that the changes are effectively instantaneous. Thus, the fluid always remains in thermodynamic equilibrium. The only exceptions are certain flows with strong shockwaves, but even some of those are often well enough approximated by equilibrium assumptions. The state of a substance in thermodynamic equilibrium can be described by means of just two state variables. Equations of state relates the other variables to the two state variables i.e. density and temperature [74]. The equations of state are:

$$p=p(\rho,T) \quad (3.15)$$

And;

$$i=i\,(\rho,T) \quad (3.16)$$

In case of perfect gas, the equations of state are written as follows,

$$p = \rho RT \tag{3.17}$$

And;

$$i = C_v T \tag{3.18}$$

where C_v denotes as the heat capacity at constant volume.

Liquids and gases flowing at low speeds behave as incompressible fluids. Without density variations, there is no linkage between the energy equation, mass conservation equation and momentum equations. The flow field can often be solved by considering mass conservation and momentum conservation equations only. The energy equation only needs to be solved alongside the others if the problem involves heat transfer.

3.7.5 Navier-Stokes equations

The shear stresses are proportional to shear strains rate for a Newtonian fluid [76] . Navier-Stokes equations for incompressible flows can be written as:

$$\rho g_x - \frac{\partial p}{\partial x} + \mu\left(\frac{\partial^2 u}{\partial x^2} + \frac{\partial^2 u}{\partial y^2} + \frac{\partial^2 u}{\partial z^2}\right) = \rho\left(\frac{\partial u}{\partial t} + u\frac{\partial u}{\partial x} + v\frac{\partial u}{\partial y} + w\frac{\partial u}{\partial z}\right) \tag{3.19}$$

$$\rho g_y - \frac{\partial p}{\partial y} + \mu\left(\frac{\partial^2 v}{\partial x^2} + \frac{\partial^2 v}{\partial y^2} + \frac{\partial^2 v}{\partial z^2}\right) = \rho\left(\frac{\partial v}{\partial t} + u\frac{\partial v}{\partial x} + v\frac{\partial v}{\partial y} + w\frac{\partial v}{\partial z}\right) \tag{3.20}$$

$$\rho g_z - \frac{\partial p}{\partial z} + \mu\left(\frac{\partial^2 w}{\partial x^2} + \frac{\partial^2 w}{\partial y^2} + \frac{\partial^2 w}{\partial z^2}\right) = \rho\left(\frac{\partial w}{\partial t} + u\frac{\partial w}{\partial x} + v\frac{\partial w}{\partial y} + w\frac{\partial w}{\partial z}\right) \tag{3.21}$$

3.8 Pre- Processing

The pre-processing in CFD is subdivided into two main categories; creation of the geometry and the meshing of the flow domain. This section provides details of the geometric modelling and the meshing of the multi-tubes and fins heat exchanger.

3.8.1 Geometry

In this section, a novel CFD model which include a full 3D geometry of the heat exchanger with plain fin is presented. The geometry of the heat exchanger has been created using ANSYS design modeler as shown in Figure 3.13. The heat exchanger model has the same geometry as described in section 3.2.5.

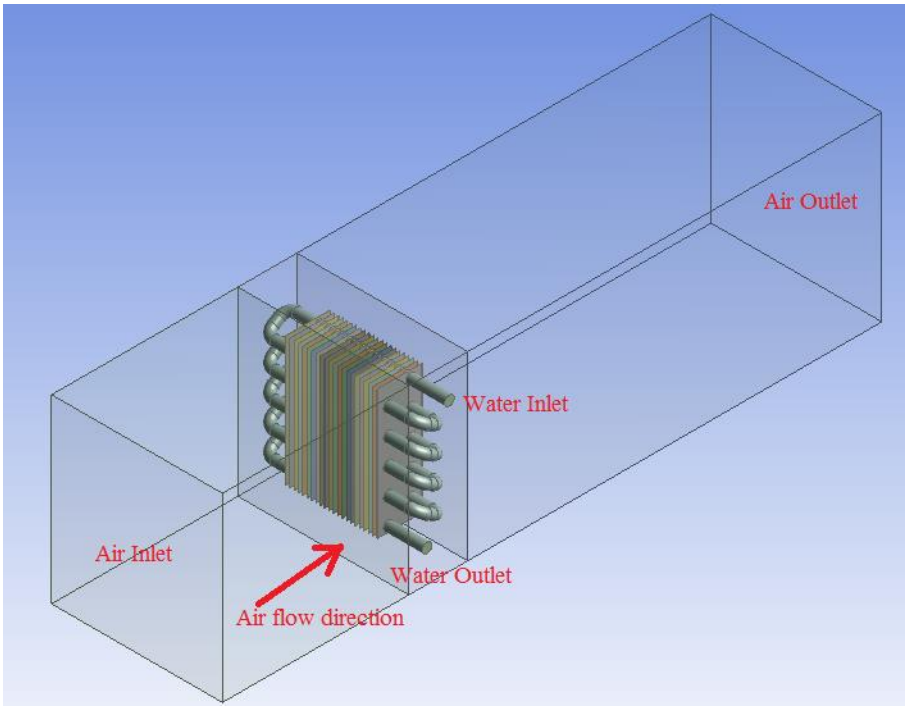

Figure 3.13 CFD Model for Multi-tube and Fin Heat Exchanger with Plain Fins

The numerical model also consists of 21 fins made up from Aluminium. The thickness of each fin is 0.12 mm. The fins are placed 4.23mm apart from each other (6 fins per inch). The detail of the plain fins shape is shown in Figure 3.14.

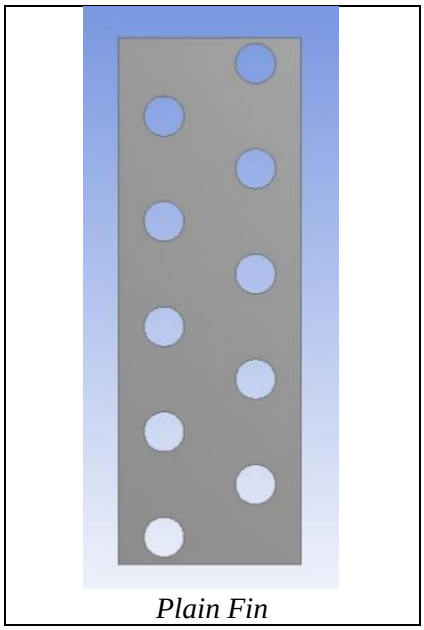

Figure 3.14 Plain Fins Shape

3.8.2 Meshing of the Flow Domain

In order to analyse the heat exchanger model in the FLUENT® solver, it is required to create a mesh structure [78]. The hybrid meshing concept was incorporated for the flow domain. The concept based on using more than one type of meshing. The test section was meshed with

tetrahedral elements and it is divided into three sections to allow more mesh elements around the heat exchanger. The sweep method was used to mesh the tubes with quad elements in the critical inflation layer region. The mesh structure specifies the resolution at which FLUENT® analyses the model. Therefore, a grid independence study was carried out to ensure the results accuracy, the results of this test are shown in chapter 4. Figure 3.15 shows the model meshing.

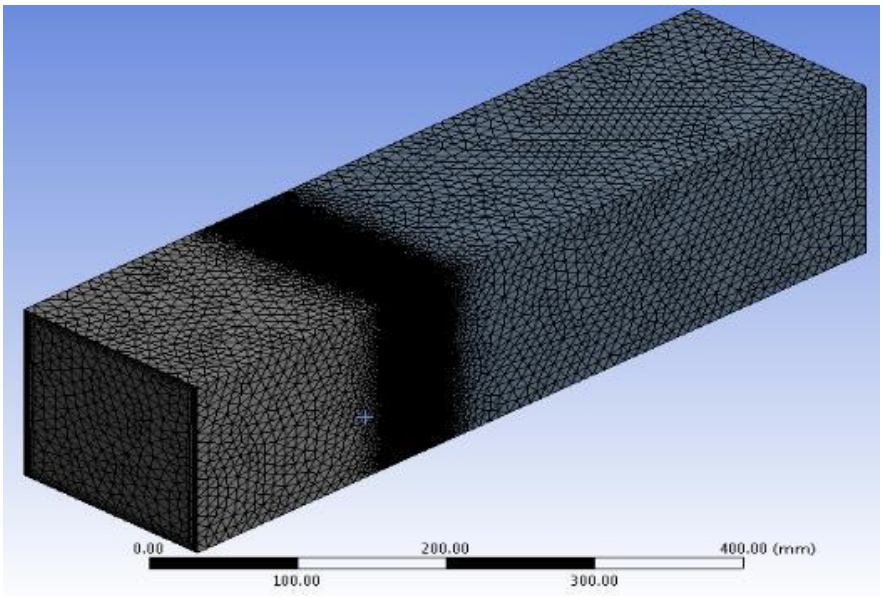

Figure 3.15 Model Meshing

3.8.3 (y+) Consideration

The parameter y^+ is defined as a non-dimensional distance from the wall. This term refers to the size of the first cell height from the wall. A higher y^+ value prevents to predict the flow characteristics close to the wall in good accuracy. Therefore, a lower y^+ is required for better results. Furthermore, the SST $k-\omega$ turbulence model, used in this study, does not involve the complex nonlinear functions required for the $k-\varepsilon$ model. the SST $k-\omega$ turbulence model involves a near wall resolution of ($y^+ < 0.2$) which is not easy to reach in industrial flows. However, the $k-\omega$ requires a minimum of ($y^+ < 2$). As the current study deals with heat transfer predictions, the automatic wall treatment in $k-\omega$ model permits for consistent refining of coarse mesh and insensitive y^+. Hence, a mesh with y^+ around 1 is recommended [79].

This section provides the detailed steps to calculate the first layer height in the viscous sublayer of the boundary layer (Δy) based on the above recommendation for y^+,

$$y^+ = \frac{U_T}{\nu}\Delta y \tag{3.22}$$

Or: $$\Delta y = \frac{\nu}{U_T} y^+ \quad (3.23)$$

where ν denotes as the kinematic viscosity (m^2/sec) and U_T denotes as the frictional velocity (m/sec).

$$U_T = \sqrt{\frac{\tau_w}{\rho}} \quad (3.24)$$

where τ_w is the wall shear stress and it can be calculated from,

$$\tau_w = C_f . \frac{1}{2} \rho U^2 \quad (3.25)$$

where C_f denotes as the skin friction coefficient, ρ denotes as the fluid density and U denotes as the freestream velocity.

C_f can be estimated as a function of Reynolds number (Re) using the Empirical equations as follows [80],

For internal flow,

$$C_f = 0.079 Re^{-0.25} \quad (3.26)$$

And for external flow,

$$C_f = 0.058 Re^{-0.2} \quad (3.27)$$

Following the previous steps, the estimated Δy for the water side was equal to 0.047 mm and for the air side was equal to 0.8 mm.

3.9 Boundary Conditions

The boundary conditions types that have been specified in this study are as follows

3.9.1 Water and Air Inlets

The inlets of the test section and the tube were considered as velocity inlets.

3.9.2 Water and Air Outlets

The outlets of the test section and the tube were considered as pressure outlets. The pressure of the water outlet has been kept at atmospheric pressure, i.e. 0 Pascal gauge.

3.9.3 Tubes and Fins Walls

In this study, the wall which forms the interface between the two regions, such as the interface liquid / solid, FLUENT® enables the two sides of the wall to be combined, prompting the solver to calculate heat transfer directly from the solution in the contiguous cells.

3.10 Solving Setting

The solver used in the present study is called FLUENT®, which is an integral part of CFD package ANSYS 17.2. In this study, the following solver setting has been used:

- Double Precision solver because it provides more precise results [81],
- Pressure-Based solver as the flow is subsonic and incompressible flow [78],
- The SST k-ω turbulence model is employed [82] because it recalls the properties of the k-ω model near the wall and gradually declines away from the wall in the k-ε model, to give more accurate results [83],
- Under-relaxation factors for pressure, density, body force, momentum and energy are 0.3, 1, 1, 0.7 and 1 respectively [78],
- Second Order Upwind discrimination has been used as it predicts more accurate results [78],
- Gravitational acceleration acting in the negative Y- direction was set as of 9.81 m/s^2,
- Coupled interfaces were used; the interface between the two regions, such as the interface liquid / solid, FLUENT® enables the two sides of the wall to be combined, prompting the solver to calculate heat transfer directly from the solution in the contiguous cells [78],
- Add the command (rpsetvar 'temperature/secondary-gradient? #f), which turns off the secondary gradient and helps to converge in case of bad quality mesh [78],
- The heat transfers by conduction through the walls; where the thermal conductivity of the Copper (tubes) has been set to 387.6 W/m K, whereas the thermal conductivity of the Aluminium (fins) has been set to 202.4 W/m K,
- Water and Air properties are shown in Table 3-8.

Table 3-8 Water and Air properties

Property	**Water**	**Air**
Density (kg/m^3)	998.2	incompressible ideal gas [58]
Viscosity (kg/m sec)	0.000471	0.00001789
Specific Heat (J/kg K)	4179	1005.684

Chapter 4 **PERFORMANCE CHARACTERISTICS OF THE BASELINE MODEL**

SUMMARY: In this chapter, quantitative and qualitative analysis of the data from the experiments and the numerical simulations are presented for the baseline model; multi-tube and fin heat exchanger with plain fins. The mesh independence and time independence study are carried out to validate a newly developed CFD model. This analysis is important in order to understand the forced convection and the complex flow structure happening within the heat exchanger. Furthermore, effects of geometric parameters on the heat transfer and pressure drop characteristics of the heat exchanger under steady state operating condition have been numerically investigated. The data from this study has been used to develop a novel semi-empirical prediction model which takes into consideration effects of these geometric parameters.

4.1 Experiments Results

The following sections show the results obtained experimentally for the baseline model; multi-tube and fin heat exchanger having plain fins. The geometry of this heat exchanger has been described in section 3.2.5. Tests were carried out at different operating conditions; steady state and transient operating conditions.

4.1.1 Steady State Tests Results

Steady state tests represent the simplest tests to perform and evaluate because the flow is independent of time. In general, steady state condition is used in the process of designing a heat exchanger. Boundary conditions for steady state tests that have been carried out on the baseline model of the heat exchanger are shown in Table 4-1. The data for each test have been recorded once every second and then averaged. The air velocity used in this study is in the range of 0.7 to 5 m/sec which represents the velocity arithmetic mean (velocity average) of the gross cross-sectional area for airflow (face area) which is computed using the ASHRAE standard 41.2 [84] and it was reported by [85], [16]. The method for measuring air flow velocity in the experiments is described in detail in APPENDIX B. Moreover, the range for water flow rate is from 2 L/min to 6 L/min which make the flow inside the tubes fully turbulent.

4.1.2 Data Analysis

In this study, the temperatures of both hot water and air at inlets and outlets were measured together with the pressure drop across water and air sides. Based on the ε-NTU method, the number of heat transfer units (NTU) can be written as:

$$\mathrm{NTU} = \frac{\mathrm{UA}}{\mathrm{C_{min}}} \tag{4.1}$$

where, $\mathrm{C_{min}}$ denotes to the product of mass and specific heat of the fluid which has lower thermal capacity rate (air side).

Table 4-1 Boundary Conditions of Steady State Tests for Plain Fins Heat Exchanger

Test Name	Water Side		Air Side	
	Water Flow rate (L/min)	Water Inlet Temperature (° C)	Air Velocity (m/sec)	Air Inlet Temperature (° C)
Test 1	2 ±0.03	60 ± 1	0.705	24 ± 1
Test 2			1.546	
Test 3			2.183	
Test 4			3.177	
Test 5			3.991	
Test 1	3±0.03	60 ± 1	0.705	24 ± 1
Test 2			1.546	
Test 3			2.183	
Test 4			3.177	
Test 5			3.991	
Test 1	4±0.03	60 ± 1	0.705	24 ± 1
Test 2			1.546	
Test 3			2.183	
Test 4			3.177	
Test 5			3.991	
Test 1	5±0.03	60 ± 1	0.705	24 ± 1
Test 2			1.546	
Test 3			2.183	
Test 4			3.177	
Test 5			3.991	
Test 1	6±0.03	60 ± 1	0.705	24 ± 1
Test 2			1.546	
Test 3			2.183	
Test 4			3.177	
Test 5			3.991	

The heat transfer rate for water side and air side can be calculated from,

$$\dot{Q}_w = \dot{m}_w Cp_w (T_{wi} - T_{wo}) \tag{4.2}$$

$$\dot{Q}_a = \dot{m}_a Cp_a (T_{ao} - T_{ai}) \tag{4.3}$$

In order to minimise the drop-off in Colburn j factor, the data should be reduced based on the average heat transfer rate ($\dot{Q}_{avg}$) [7], hence, ($\dot{Q}_{avg}$) can be calculated as follows,

$$\dot{Q}_{avg} = \frac{\dot{Q}_w + \dot{Q}_a}{2} \tag{4.4}$$

The heat exchanger effectiveness (ε) is defined as the ratio between the actual heat transfer rates to the maximum possible heat transfer rate, therefore ε can be written as: -

$$\varepsilon = \frac{\dot{Q}_{avg}}{C_{min}(T_{wi} - T_{ai})} \tag{4.5}$$

The maximum possible heat transfer rate occurs when the difference in inlet temperature and outlet temperature is maximum value.

The UA value (the overall conductance) is defined as [9],

$$UA = \frac{1}{\frac{1}{\eta_o h_a A_a} + R_{wall} + \frac{1}{h_w A_w}} \tag{4.6}$$

where h_w and h_a are the heat transfer coefficients for water and air, respectively, A_w and A_a are the heat transfer surface areas for water and air, respectively, and R_{wall} is the wall thermal resistance. For flat wall, this resistance equals to:

$$R_{wall} = \frac{\delta_{wall}}{k_{wall} A_{wall}} \tag{4.7}$$

where, δ_{wall} is the wall thickness, k_{wall} is the thermal conductivity of the wall material and A_{wall} is the heat transfer area of the wall.

The water side heat transfer coefficient (h_w) can be evaluated using Gnielinski semi-empirical correlation [86],

$$h_w = \left(\frac{k}{D}\right)_w \frac{(Re_{D_w} - 1000) P_r \left(f_i/2\right)}{1 + 12.7 \sqrt{\left(f_i/2\right)\left(P_r^{2/3} - 1\right)}} \tag{4.8}$$

where,

$$f_i = \left[1.58 \ln\left(Re_{D_w}\right) - 3.28\right]^{-2} \tag{4.9}$$

The surface efficiency (η_o) is defined as the ratio between the actual heat transfer for the fin and base and the heat transfer for the fin and base when the fin is at the same base temperature (T_b). Equation (5.10) expresses the surface efficiency as a function of fin efficiency (η_f),

$$\eta_o = 1 - {}^{A_f}/_{A_o}\,(1 - \eta_f) \tag{4.10}$$

where, $A_o = A_f + A_b$

A_o ,A_f and A_b are the total surface area, fin and base areas, respectively.

The Colburn j factor and the friction factor f can be calculated from Eq.s (4.11) and (4.12), respectively.

$$j = \frac{h_a}{\rho_a V_{a(max)} C_{pa}} P_r^{\frac{2}{3}} \tag{4.11}$$

$$f = \frac{A_c}{A_o}\frac{\rho_m}{\rho_1}\left[\frac{2\rho_1 \Delta P}{G_c^2} - (K_i + 1 - \sigma^2) - 2\left(\frac{\rho_1}{\rho_2} - 1\right) + (1 - \sigma^2 - K_e)\frac{\rho_1}{\rho_2}\right] \tag{4.12}$$

The equation (4.12) has been proposed by Kays and London [11] and the coefficients K_I and K_e are the abrupt contraction pressure-loss coefficient and the abrupt expansion pressure-loss coefficient, respectively. These coefficients are adapted from Figure 4.1[12].

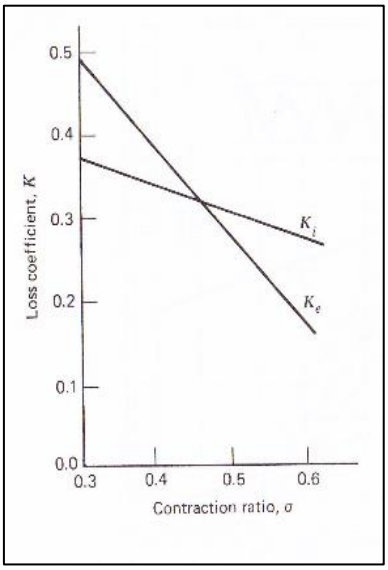

Figure 4.1Entrance and Exit Pressure Drop Coefficients for Plate-Fin Heat Exchanger [12]

A_c is the flow cross sectional area and σ represents the ratio of the minimum flow area to the frontal area. $P_1, \rho_2\ and\ \rho_m$ are the density of air inlet, air outlet and mean density, respectively.

Results of steady state tests carried out for plain fins heat exchanger have been presented in the form of surface characteristics; friction factor (f) and Colburn factor (j) against Reynolds number. Figure 4.2 depicts the variations of Colburn (j) factor and Fanning friction factor (f)

with Reynolds number for plain fins model. The calculated values of (j) and (f) are depending on the variations of the inputs. i.e. water and air inlet temperatures, water flow rate and air velocity as it has been shown in the analysis method in section 4.1.2. Therefore, an error bars have been set on the values of (j) and (f) factors plotted in Figure 4.2 to show the variability of these factors.

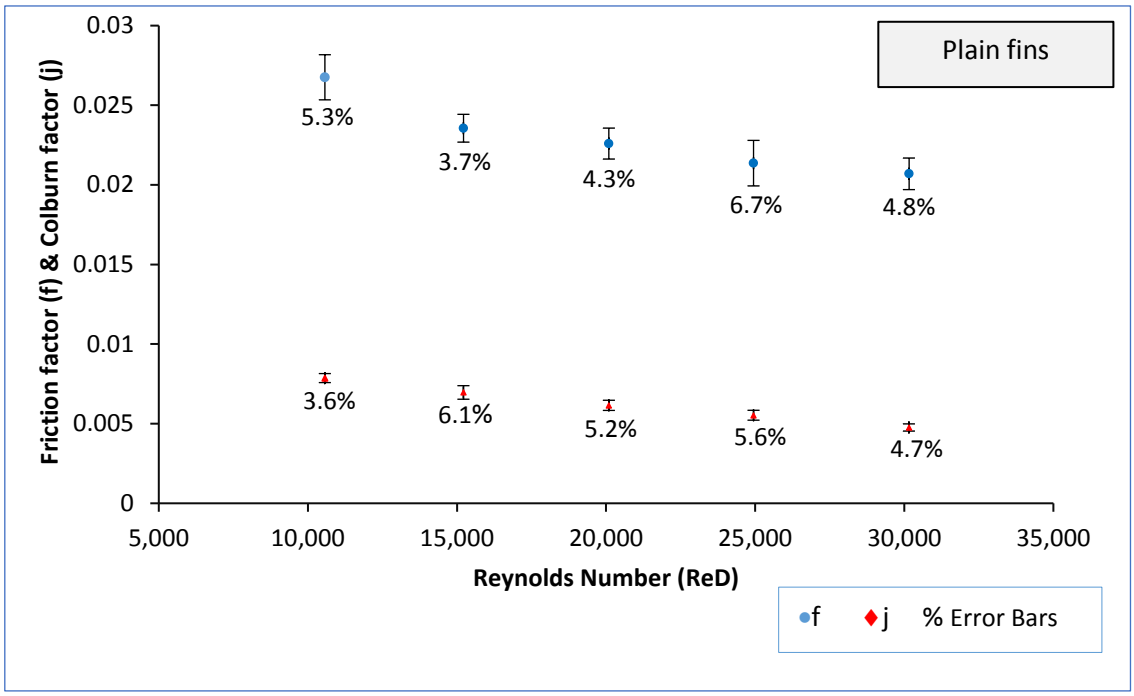

Figure 4.2 Variations of Colburn j Factor and Fanning Friction Factor *f* with Reynolds for Baseline Model

Figure 4.3 represents the variations of efficiency index (j/f) of the plain fins heat exchanger with Reynolds number (Re_D). In Figure 4.3 and in order to show the variability of this factor, an error bars have been set on the values of (j/f) factor. The calculated value of (j/f) factor depends on the values of (j) and (f) which are depending on the variations of the inputs. i.e. water and air inlet temperatures, water flow rate and air velocity as it has been shown in the analysis method in section 4.1.2.

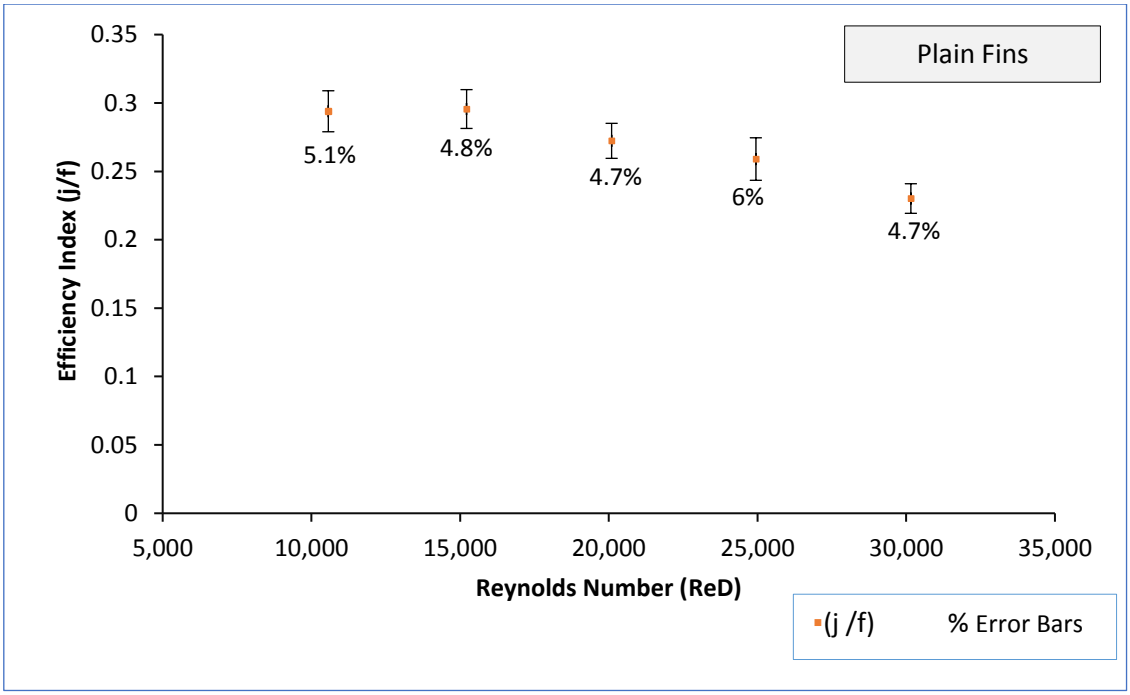

Figure 4.3 Variation of the Efficiency Index (j/f) for Baseline Model

As shown in Figure 4.2, both Colburn (j) factor and Fanning friction factor (f) tend to decrease with increasing Reynolds number and they are almost parallel to each other. Moreover, it can be noticed that at the same Reynolds number, friction factor is three times more than Colburn factor. Furthermore, the efficiency index (j/f) has the same trend as both Colburn (j) factor and Fanning friction factor (f) which show that the percentage decreases in the friction factor is more than the percentage decrease in the Colburn factor.

The relationship between heat exchanger thermal effectiveness with air velocity at different water flow rates, in a range from 2 L/min to 6 L/min, for plain fins heat exchanger is depicted in Figure 4.4. For all cases of different water flow rates, it can be realised that the heat exchanger thermal effectiveness decreases with increasing air velocity. In general, the effectiveness of the plain fins heat exchanger varies from as low as 10% to as high as 25%. Moreover, as the water flow rate increases the heat exchanger effectiveness increases. For example, at 0.7 m/sec air velocity the heat exchanger thermal effectiveness at 2 L/min water flow rate is 22% whereas the effectiveness is increased by 10% at 6 L/min water flow rate. In addition, at low air velocity, the baseline model is showing high thermal effectiveness where the amount of energy transferred would be high.

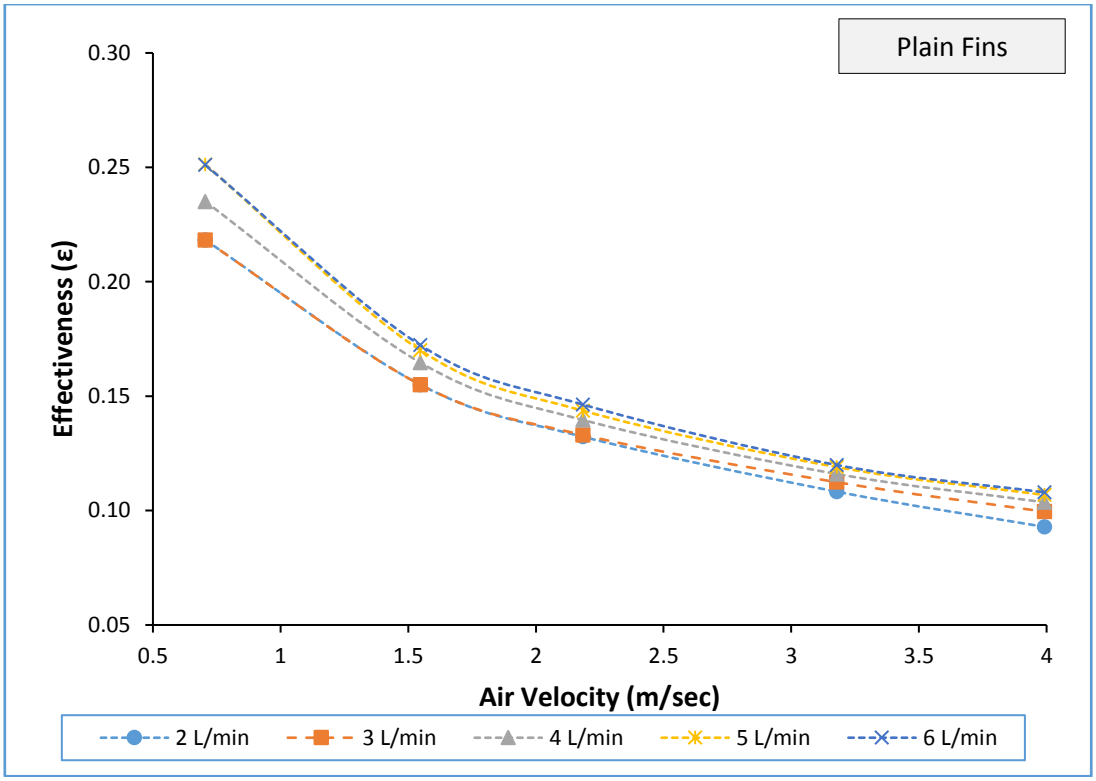

Figure 4.4 Variations of Heat Exchanger Thermal Effectiveness with Air Velocity at Different Water Flow Rates for Plain Fins Heat Exchanger

4.1.3 Transient Tests Results

Under practical conditions, steady testing is not feasible or practical because the inputs of the heat exchanger are timely dependent. Hence, it is very important to analysis the heat exchanger under transient conditions where the inputs and the outputs are dependent on time [17]. Transient tests can be used to investigate the response of the heat exchanger during some operating conditions such as transient behaviour between two steady conditions, step input test, or transient behaviour during start up and shutdown conditions. Although most of the analysis of the heat exchanger has been carried out for steady state operating condition. However, this section includes transient tests for validation purpose and to prove that the presented CFD is reliable and it can be used to predict heat transfer and pressure drop characteristics for multi-tube and fin heat exchanger with plain fins under different operating conditions. In this section, two different transient tests were carried out; starting up test and step input test.

I. Starting up Test

This test was carried out to establish the operating characteristics of the heat exchanger while starting up. In this test, the single blow transient testing technique, where the experiment uses

transient variation only on one fluid stream [87], was used to obtain the heat transfer characterises of the heat exchanger.

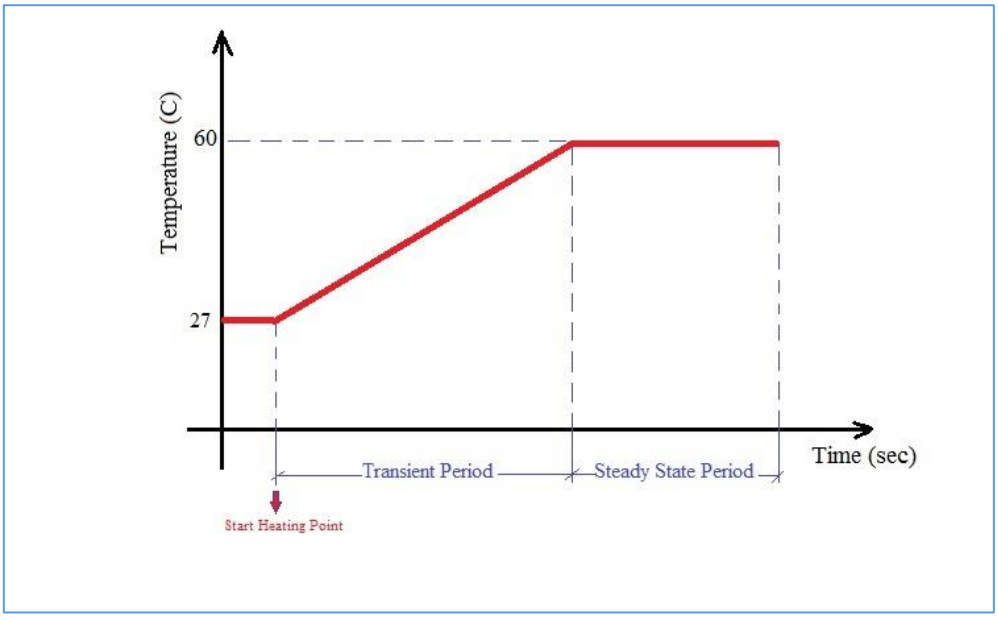

Figure 4.5 Staring Up Test Diagram

As shown in Figure 4.5, the water temperature was increased from 27° C to 60 ° C, during this test water flow rate (3 L/min) and air velocity (2.183 m/sec) were kept constant (single blow transient testing technique). Figure 4.6 illustrates variations of water inlet, water outlet, air inlet and air outlet temperatures with operating time for starting up test in experiments for the baseline model.

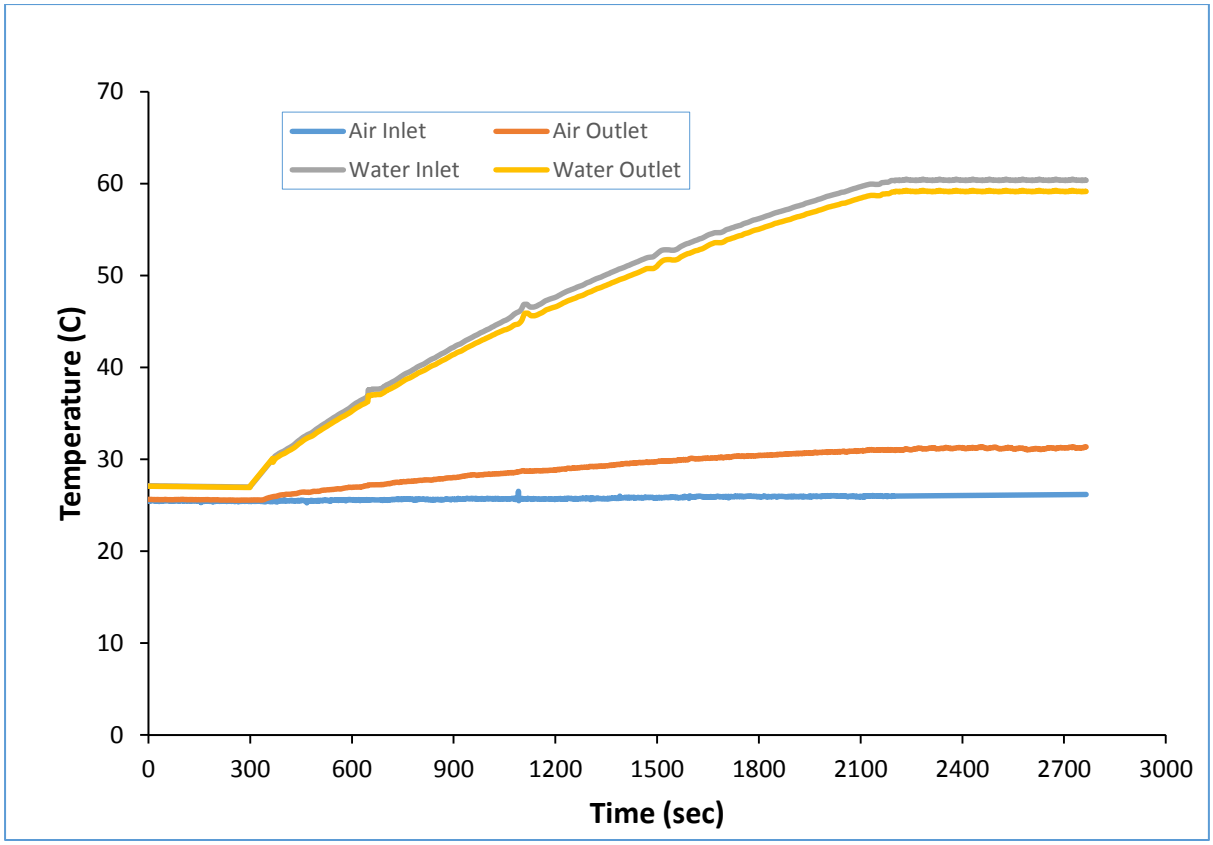

Figure 4.6Variations of Water Inlet, Water Outlet, Air Inlet and Air Outlet Temperatures with Operating Time for Starting Up Test

It can be seen from Figure 4.6 that after 300 seconds the water started heating and it took 1900 seconds to reach 60 ° C where the heat exchanger started operating at steady state condition.

II. Step Input Test

The step input test represents the characteristics in the heat exchanger due to a dynamic change in its inputs. This test was performed by suddenly changing the water inlet temperature from 25 °C to 60 °C at a constant water flow rate (3 L/min) and constant air velocity (2.183 m/sec). Figure 4.7 describes the test procedure.

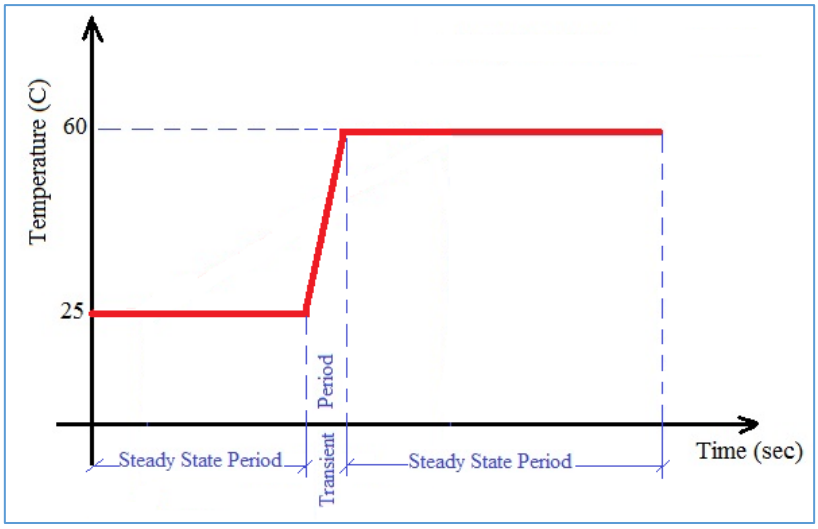

Figure 4.7 Step Input Test Diagram

Figure 4.8 depicts variations of water inlet, water outlet, air inlet and air outlet temperatures with operating time for step input test in experiments for the baseline model.

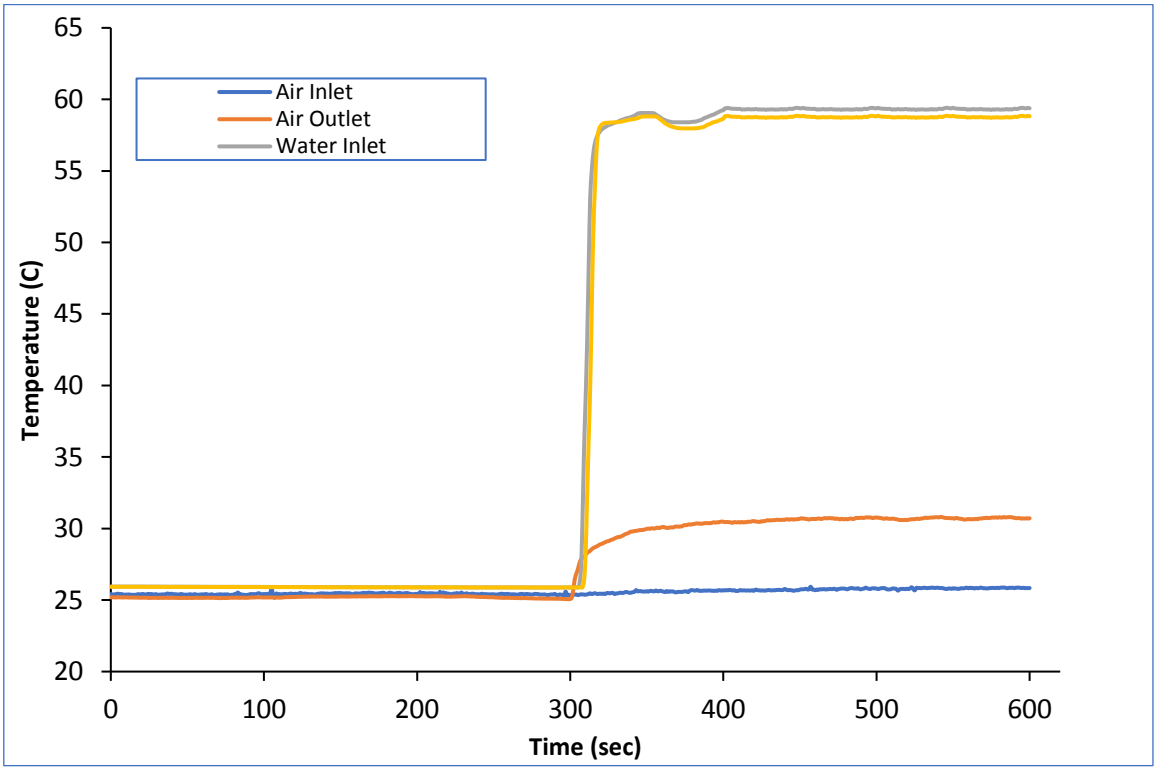

Figure 4.8 Variations of Water Inlet, Water Outlet, Air Inlet and Air Outlet Temperatures with Operating Time for Step Input Test

From Figure 4.8 it can be seen clearly that the water inlet temperature has suddenly increased from 25 °C to 60 °C and the heat exchanger took about 20 seconds to reach the steady state again.

4.2 Numerical Results

In this section, the numerically predicted results using the novel CFD model which include a full 3D geometry of the heat exchanger with plain fin (baseline model) are presented in order to validate them with the results for the baseline model computed experimentally.

4.2.1 Grid Independence

The mesh independence test is essential in order to demonstrate the improvement of results by using successively smaller cell sizes for the calculation with less computational time [78]. As discussed in chapter 3, three different meshes 4, 8 and 12 million mesh elements were chosen for this test for plain fins model, where a model with 4 million mesh elements is a coarse mesh and it has been gradually refined to reach a fine mesh. Furthermore, the air outlet temperature has been chosen as a parameter for comparing the test results because it represents the main output of the CFD model and indicates the performance of the system. The results of this test are shown in Table 4-2.

Table 4-2 Mesh Independence Test Results

Mesh Size (million)	*Air Outlet Temperature CFD (^{o} C)*	*Computation Time (Hours)*	*Percentage Difference (%)*	*Time Saving (Hours)*
4	*31.387*	*4.50*	---	---
8	*32.920*	*8.61*	*4.9*	*4.11*
12	*33.105*	*11.74*	*0.6*	*3.13*

The results of the mesh independence test reveal that a 4.9% difference in the air outlet temperature between 4 million mesh elements model and 8 million mesh elements model, whereas 0.6% difference between 8 million mesh elements model and 12 million mesh elements model. It can therefore be concluded that 8 million mesh elements model is can give a good accuracy to the work with a valuable time saving in computational time and hence it has been chosen for further numerical analysis of the heat exchanger with plain fins. Moreover, the mesh for other cases has been determined by using the similar methodology.

4.2.2 Temporal Discretisation

In transient tests, it is essential to carry out a time step independence test. Otherwise, it can lead to inaccurate results of CFD. Therefore, time-step independence test has been carried out with three different time steps (0.5, 1, and 2 seconds) for test 3 and water flow rate equal to 3 L/min as presented in Table 4-1. Table 4-3 summarises the result of the temporal discretisation.

Table 4-3 Temporal Discretisation Results

Time Step (second)	*Air Outlet Temperature CFD (^{o} C)*	*Percentage Difference (%)*
2	*30.745*	---
1	*31.313*	*1.84*
0.5	*31.451*	*0.45*

The temporal discretisation results depicted in Table 4-3 showed that the percentage difference in air outlet temperature is less than 1.85 % between the three-time steps considered in this test. Hence, it can be concluded that the time step with 1 second is capable of predicting the flow features accurately and therefore 1 second time step has been chosen for carrying out the simulations of the baseline model.

4.3 Benchmark Tests

In order to ensure the reliability of the numerical CFD model, a benchmark test has to be carried out. The process of comparing the numerical results against experimental findings is known as **Benchmarking**. In this section, the numerically predicted results using the novel CFD model which include a full 3D geometry of the heat exchanger with plain fin have been validated against experimental data in terms of water and air outlet temperatures and pressure drop obtained in both water and air sides and at different operating conditions. These variables are the main outputs of the numerical model. Therefore, these variables were plotted against each other at a constant water flow rate (3 L/min) and constant air velocity (2.183 m/sec) with the same boundary conditions as previously shown in Table 4-1.

4.3.1 Steady State Tests Results Validation

Figure 4.9 depicts a comparison between the numerically predicted results and the experimental data for water outlet temperature for plain fins heat exchanger.

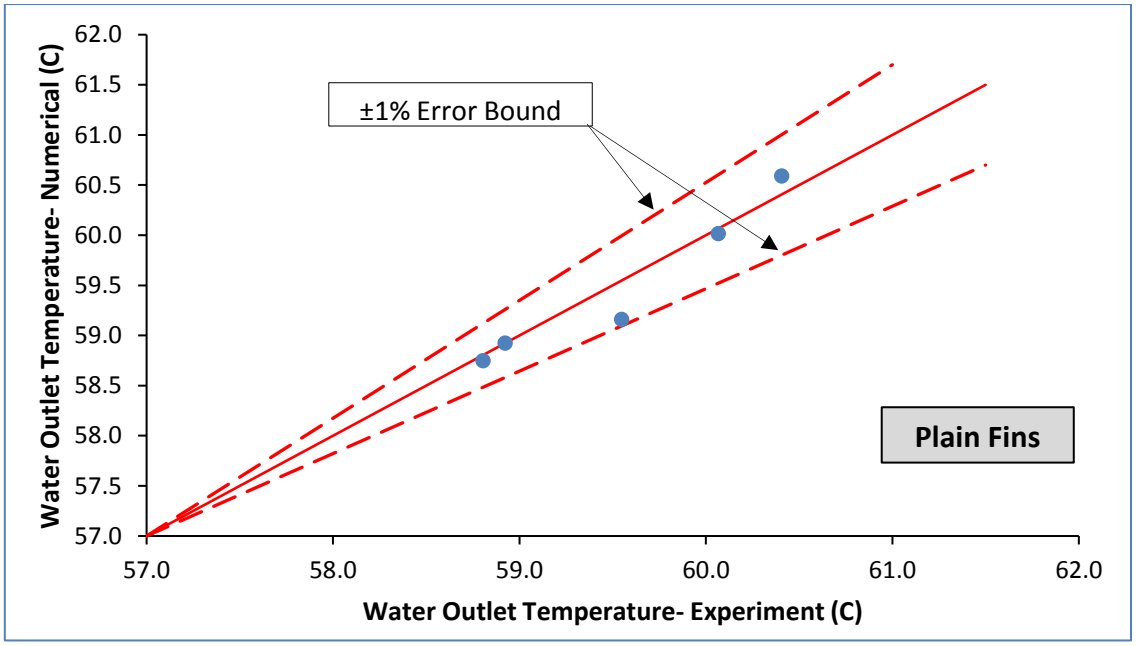

Figure 4.9 Comparison of Numerical and Experimental Results for Water Outlet Temperature Plain Fins Heat Exchanger

A comparison between the numerically predicted results and the experimental data for air outlet temperature for plain fins heat exchanger is depicted in Figure 4.10.

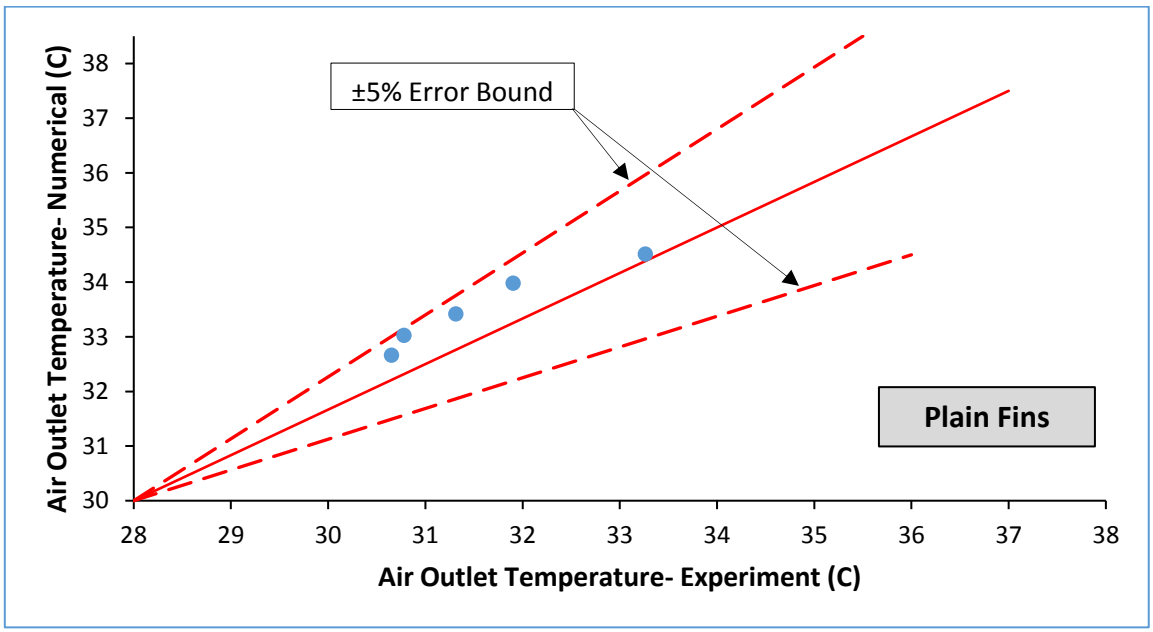

Figure 4.10 Comparison of Numerical and Experimental Results for Air Outlet Temperature Plain Fins Heat Exchanger

Based on the results plotted in Figure 4.8 and 4.9, it can be clearly seen that the differences between the numerically predicted results and the experimental data for water outlet and air outlet temperatures are very small and the numerical results agree well with the experimental

results for the baseline model. The percentage differences between theses results for the water outlet and the air outlet temperatures were observed to be less than 5%.

Figure 4.11 depicts a comparison between the numerically predicted results and the experimental data for water-side pressure drop for heat exchanger with plain fins.

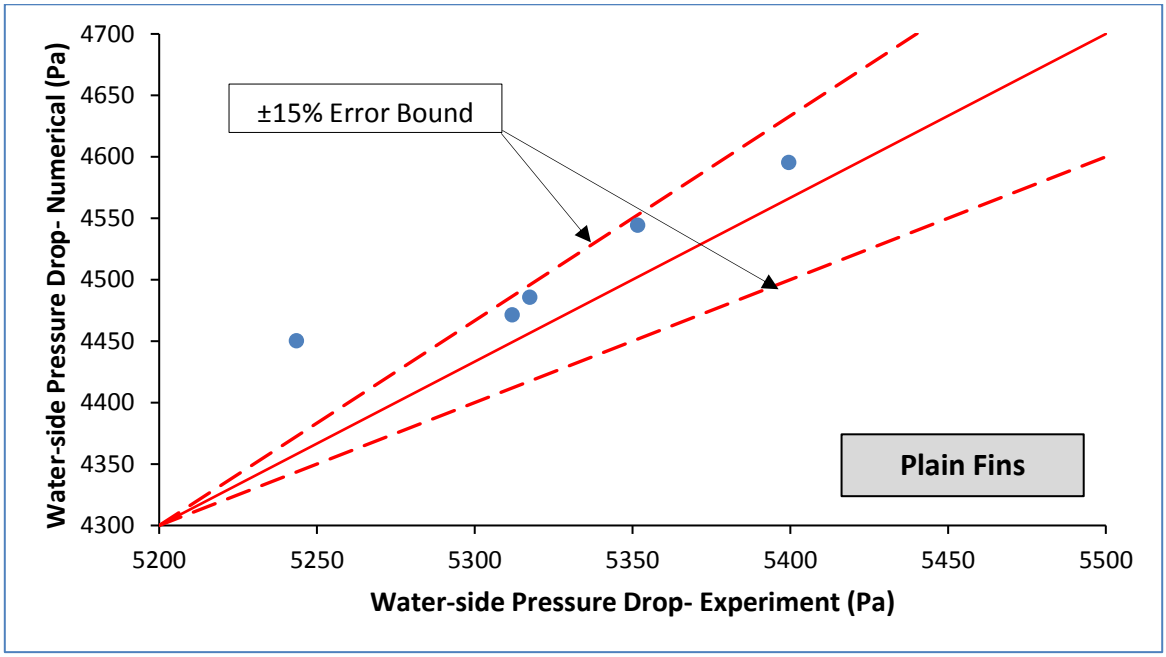

Figure 4.11Comparison of Numerical and Experimental Results for Water-side Pressure Drop Plain Fins Heat Exchanger

From Figure 4.11, a good agreement has been reached between numerically predicted results with the experiments for water-side pressure drop, where the percentage differences for the heat exchangers with plain fins were less than 15%.

A comparison between the numerically predicted results and the experimental data for air-side pressure drop for the heat exchanger with plain fins is depicted in Figure 4.12.

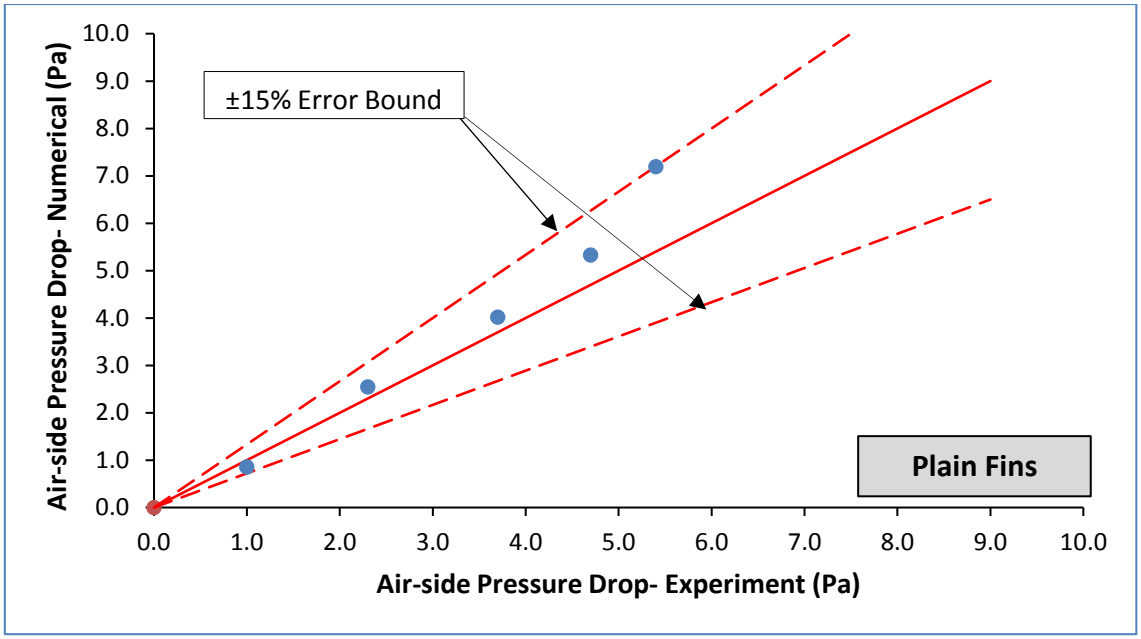

Figure 4.12Comparison of Numerical and Experimental Results for Air-side Pressure Drop Plain Fins Heat Exchanger

The results plotted in Figure 4.12 reveal that the percentage differences between the numerically predicted results and the experimental data for air-side pressure drop are observed to be less than 15%.

4.3.2 Transient Tests Results Validation

I. Starting Up Test

In order to simulate the starting up test in CFD, a user-defined function (UDF) has been adopted to express the inputs (water inlet temperature and air inlet temperature) of the CFD simulation as a function of time [80]. The C language program based on the data of the experiment for water inlet temperature and air inlet temperature used to define these inputs has been attached in the APPENDIX C1.

Figure 4.13 depicts the variations for air outlet and water outlet temperatures in both experiments and CFD results for starting up test.

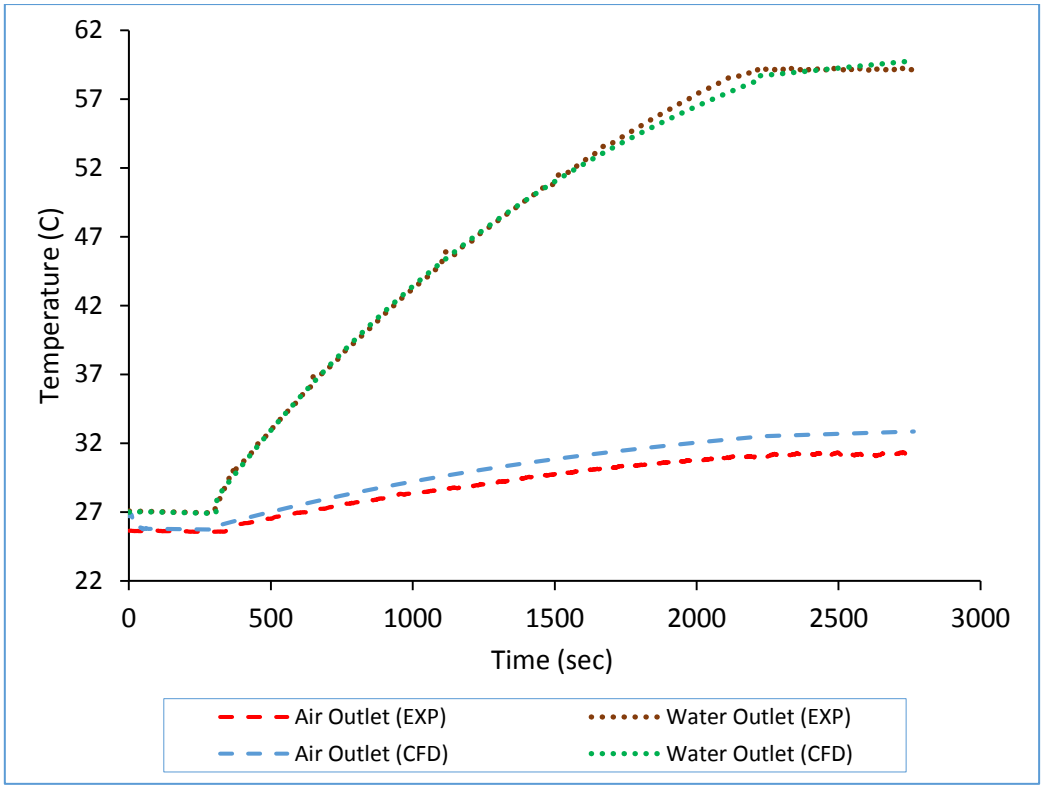

Figure 4.13Validation of the CFD results with respect to the experimental results for Air Outlet and Water Outlet Temperatures at Starting up Test

The graphs depicted in Figure 4.13 are shown a good agreement in both water outlet and air out temperatures for the results computed numerically using CFD with respect to the experimental results. The maximum difference between the CFD and experimental results is observed for both water outlet temperature was less than 2% and for air out temperature was to be less than 6 %.

II. Step Input Test

The same inputs in the experiments; water inlet and air inlet temperatures, have been used as inputs to simulate the CFD model for step input test. A user-defined function (UDF) has been adopted to define both water inlet and air inlet temperatures as a timely dependent function using C language program based on the data of the experiment. The UDF for step input test has been presented in the APPENDIX C2.

Figure 4.14 depicts the variations for air outlet and water outlet temperatures in both experiments and CFD results for step input test.

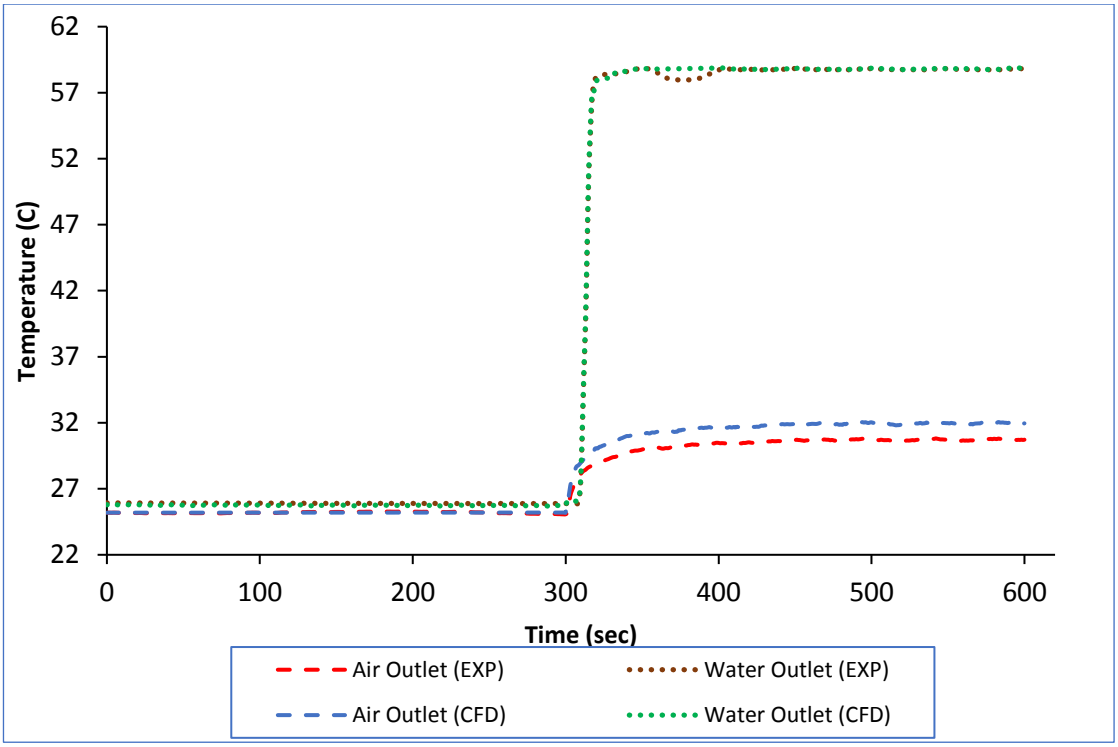

Figure 4.14 Validation of the CFD Results with Respect to Experimental Results for Air Outlet and Water Outlet Temperatures at Step Input Test

A very good agreement has been achieved in both water outlet and air outlet temperatures for the results computed using CFD with respect to the experimental results for step input test. The percentage difference for water outlet temperature was less than 1% while the percentage difference for air outlet temperature was less than 5%.

Based on the Benchmark tests carried out in sections 4.3.1 and 4.3.2, it can be concluded that the presented novel CFD model which include a full 3D geometry of the heat exchanger with plain fin is reliable and hence it can be used to predict heat transfer and pressure drop characteristics for multi-tube and fin heat exchanger with plain fins under different operating conditions with good accuracy.

4.4 Flow Field Analysis

The numerical analysis carried out on multi-tube and fin heat exchanger which has plain fins under steady state operating condition helps to understand the forced convection phenomena happened inside this system by knowing the distribution of temperature and velocity of working fluids within the system. In the next section, the analysis the thermal performance of the plain fins heat exchanger has been carried out for air-side, water-side and flow in tube bends.

4.4.1 Air-Side Flow Field Analysis

In order to analysis the flow field in the air-side the temperature contours at mid-section (X-axis) and mid-section (Y-axis) have been chosen. These planes were chosen because the flow in more streamlined at those sections and they are shown in Figure 4.15. CFD simulations were carried out at constant water velocity of 1 m/sec and five different air velocities; 1, 2, 3, 4 and 5 m/sec, respectively.

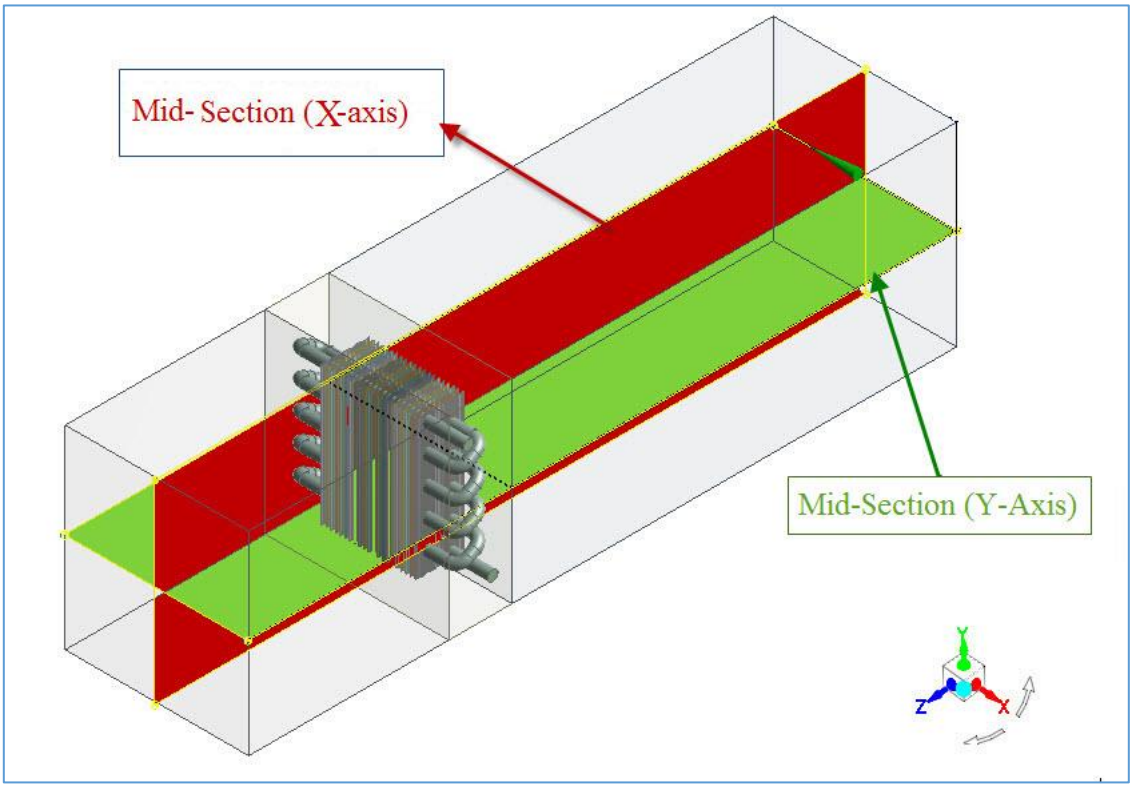

Figure 4.15 Locations of Analysed Planes in the Test Section

Figure 4.16 depicts the contours of the temperature variation in the test section at mid-section (X-Axis) and mid-section (Y-axis) under steady state operating condition. The contours describe the behaviour of the air-side due to a change in the air velocity and at constant water

velocity. It is clear from the figure as the air velocity increases the temperature of the air at the outlet section tends to decrease. For example, the difference between air inlet and outlet temperatures (ΔT_a) at 1 m/sec air velocity is equal to 8.7° C and this difference decreased by about 40% to reach 5.23° C at 4 m/sec. This can be explained as, at low air velocity there is a large amount of heat transferred from the hot fluid (water) to the cold fluid (air) and as the air velocity increase the air fluid particles have less chance to pick up more thermal energy. Moreover, the backflow phenomenon can be seen for the airflow at low velocity due to a negative pressure difference in the back-side of the heat exchanger. This phenomenon becomes less effective at high air velocity and the flow in more streamlined.

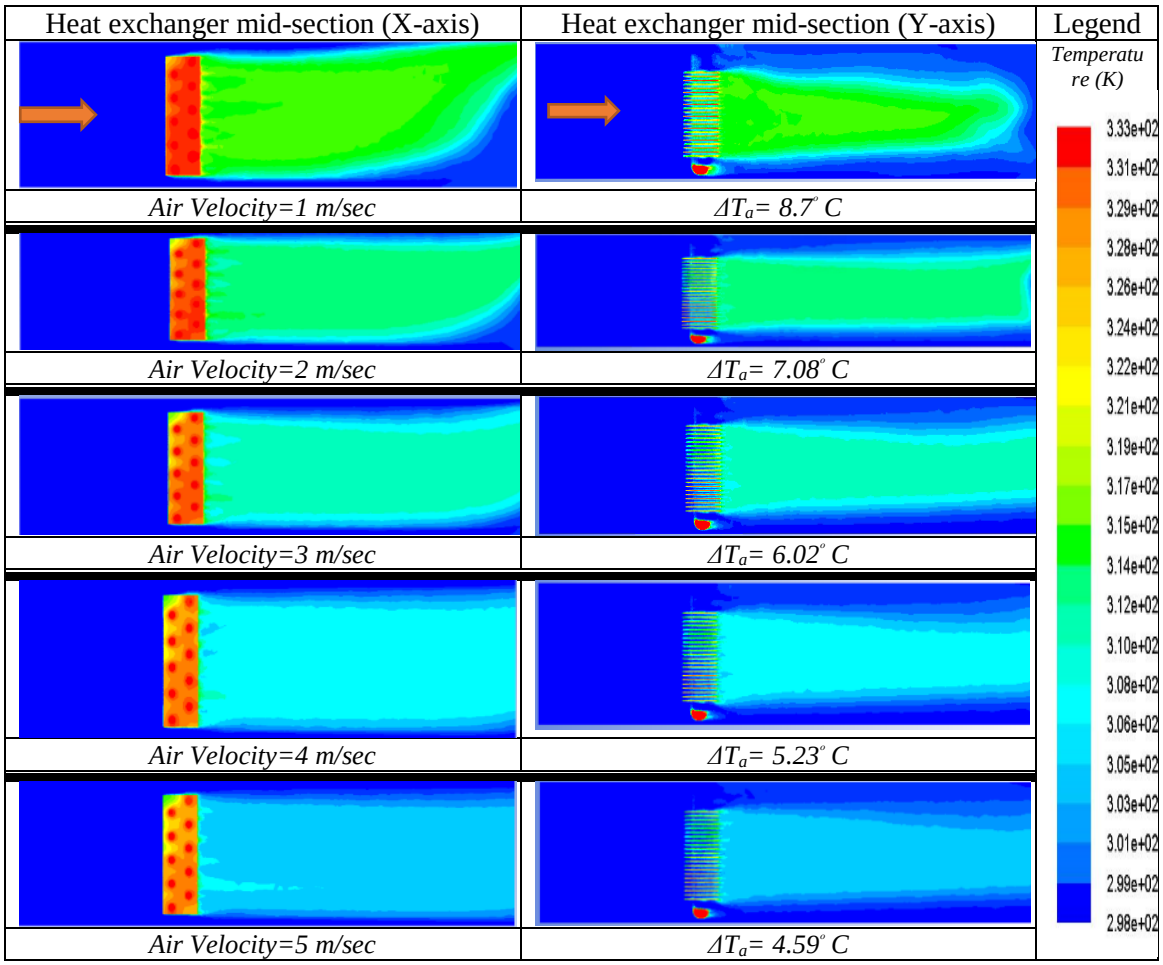

Figure 4.16 Contours of Temperature Variation at mid-section (X-axis) and mid-section (Y-axis) of the Heat Exchanger Due to Change in Air Velocity under Steady State Operating Condition

In order to understand the behaviour of the local flow characteristics; velocity magnitude, static pressure and static temperature of the air inside the test section (housing), the local flow characteristics have been computed at different cross-sections along the test section and for 5 different points; middle (M), right (R), left (L), top (T) and bottom (B) in each cross-section.

The locations of these points in each cross-section is shown in Figure 4.17. In addition, the points have been selected away from the test section walls to avoid the effect of the boundary layer.

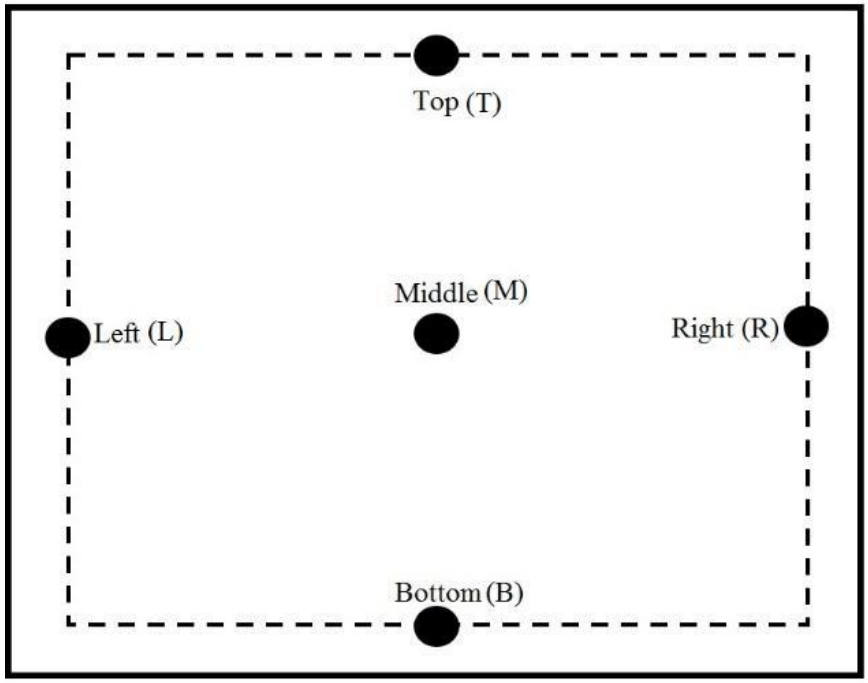

Figure 4.17 Locations of the Analysed Points in Each Cross-Section along the Test Section

Figure 4.18 depicts the variations of the velocity magnitude ratio between middle point and right, left, top and bottom, respectively for the analysed points in each cross-section along the test section.

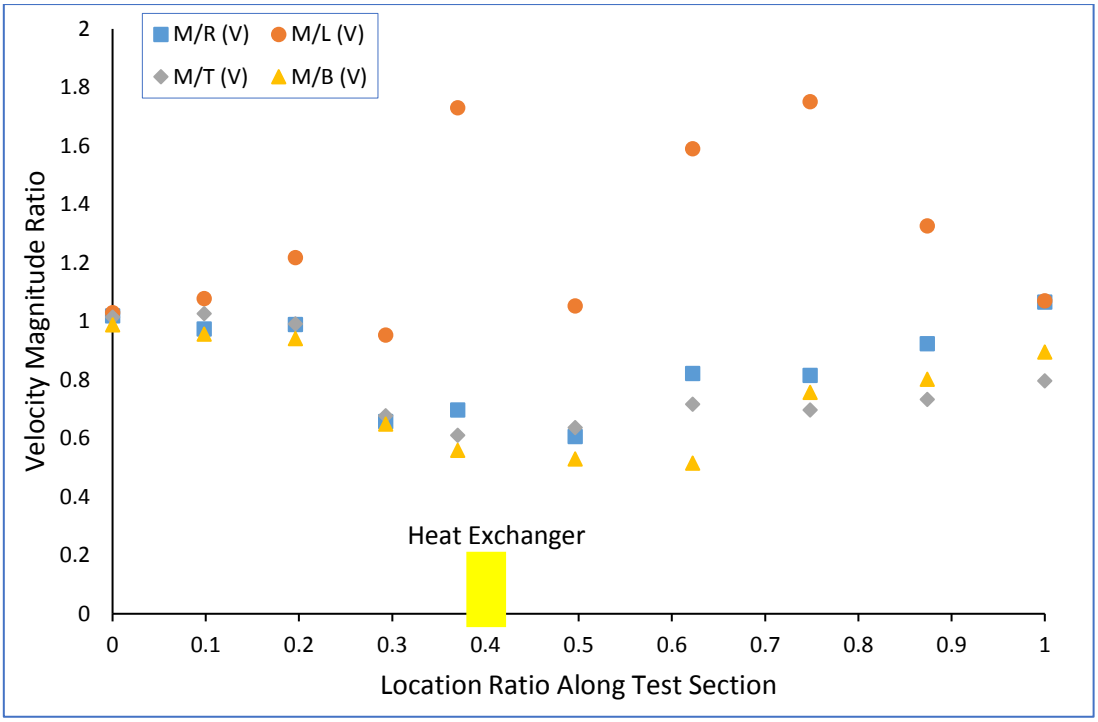

Figure 4.18 Variations of the Velocity Magnitude Ratio for the Analysed Points in each Cross-Section Along the Test Section

The velocity ratio variations depicted in Figure 4.18 showed a uniform distribution for the velocity magnitude along the test section for the selected points middle and right, top and bottom. However, nonuniform flow distribution is observed at the left points where the velocity is always higher than the velocity magnitude at the middle point. This non-uniform flow distribution of the velocity magnitude is affecting the thermal performance of the air flow coming out of the test section by creating high velocity regions.

The variations of the static pressure ratio between middle point and right, left, top and bottom, respectively for the analysed points in each 6 different cross-sections along the test section is shown in Figure 4.19.

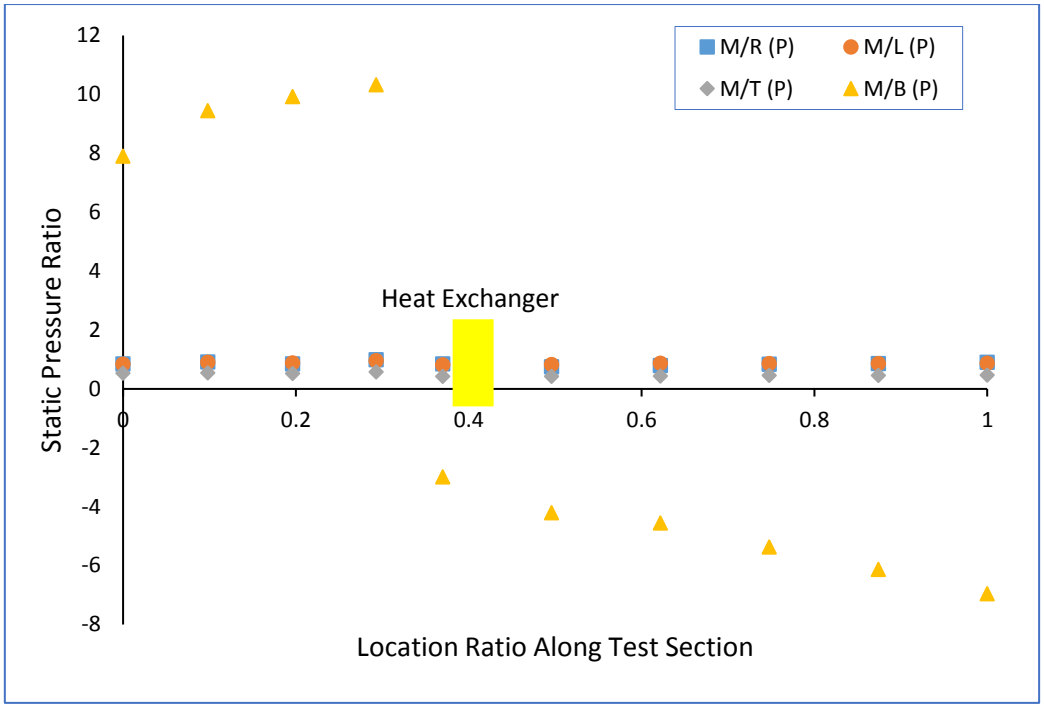

Figure 4.19 Variations of the Static Pressure Ratio for the Analysed Points in each Cross-Section Along the Test Section

Due to backflow phenomenon occurred in the test section at low air velocity, the static pressure has a negative value for the points in bottom side, this can be seen clearly as for the points after the heat exchangers. Furthermore, a uniform static pressure distribution has been observed for the other points. The backflow phenomenon may affect the overall performance of the heat exchanger by increasing the amount of power required to run the fan.

Figure 4.20 illustrates the variations of the static temperature ratio between middle point and right, left, top and bottom, respectively for the analysed points in each cross-section along the test section.

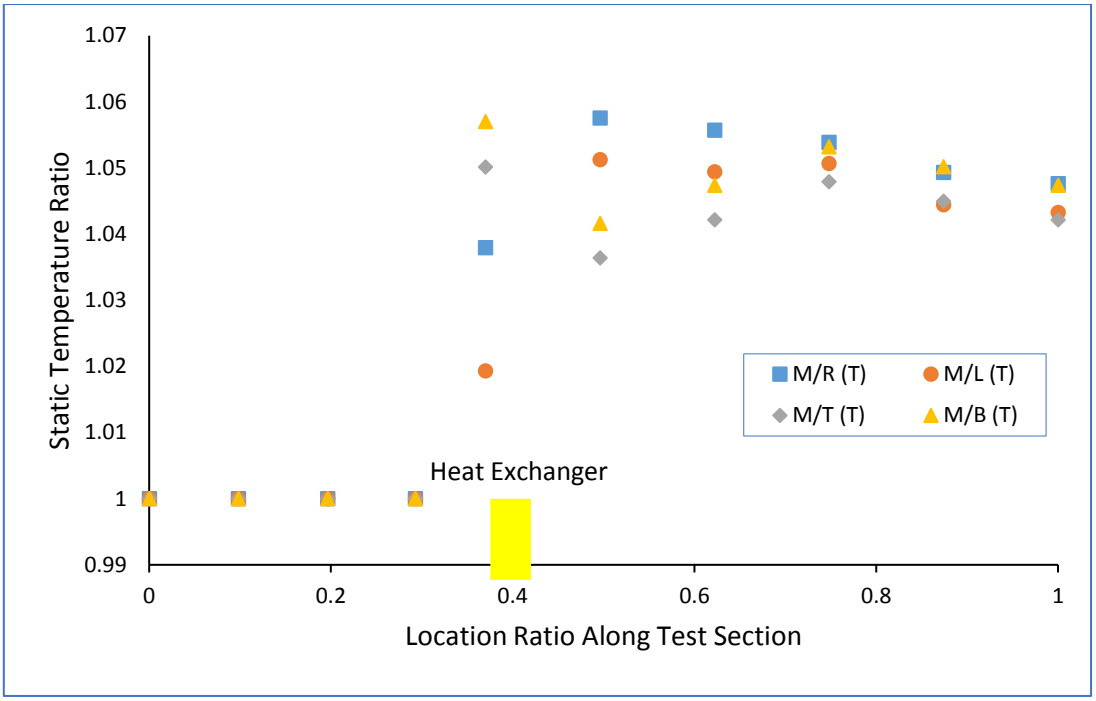

Figure 4.20 Variations of the Static Temperature Ratio for the Analysed Points in each Cross-Section Along the Test Section

The static temperature variations depicted in Figure 4.20 reveal that as the air flow passed through the heat exchanger, the static temperature of the air is increased for all the points. Furthermore, the points on the right and bottom of the test section have a relatively high temperature because they are in the hot water feeding side. Moreover, the static temperature variations were mostly small. In general, non-uniform flow distribution badly affects the thermal performance of the heat exchanger and also could produce high-velocity regions. Thus, to obtain maximum thermal performance, the flow should be uniform across the entire frontal area of the core. However, the flow may not be uniform due to nonuniform fin spacing, deformation of the fin shape and non-uniform flow coming out from the fan. [74]

4.4.2 Water-Side Flow Field Analysis

Figure 4.21 illustrates the contours of the temperature variation in the heat exchanger at water inlet section and water outlet section under steady state operating condition. CFD simulations were carried out at constant water velocity of 1 m/sec and five different air velocities; 1, 2, 3, 4 and 5 m/sec, respectively.

Water Inlet Section	*Water Outlet Section*	Legend
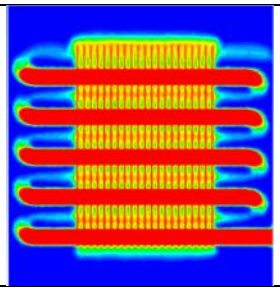	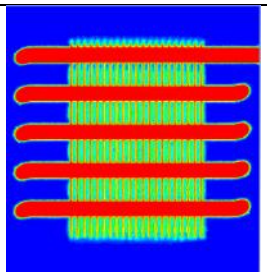	*Temperature (K)* 
Air Velocity=1 m/sec	*ΔT_w= 0.85° C*	
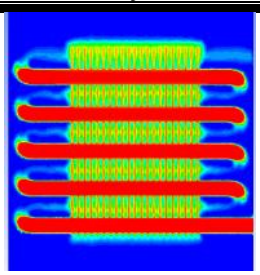	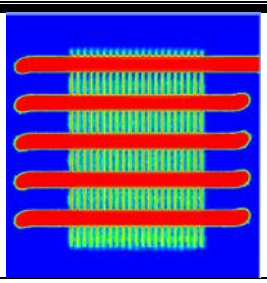	
Air Velocity=2 m/sec	*ΔT_w= 1.3° C*	
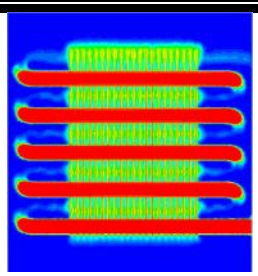	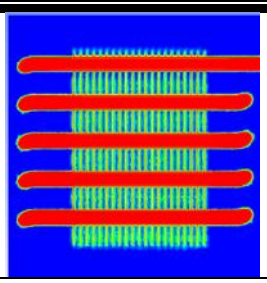	
Air Velocity=3 m/sec	*ΔT_w= 1.65° C*	
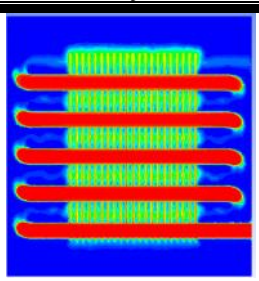	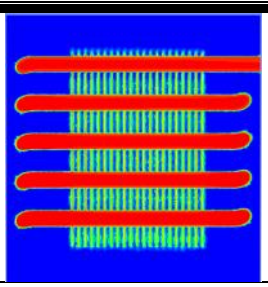	
Air Velocity=4 m/sec	*ΔT_w= 1.91° C*	
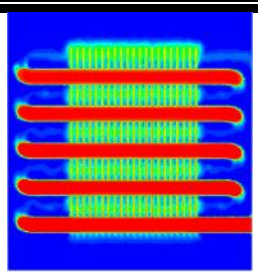	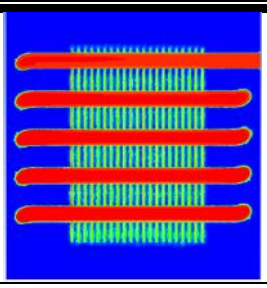	
Air Velocity=5 m/sec	*ΔT_w= 2.11° C*	

Figure 4.21 Contours of Temperature Variation Water Inlet Section and Water Outlet Section of the Heat Exchanger Due to Change in Air Velocity under Steady State Operating Condition

The temperature contours depicted in Figure 4.21 describe the behaviour of the water-side due to a change in the air velocity and at constant water velocity. It is evident from the figure the temperature of the water inside tubes, in both inlet and outlet sections of the water, is decreasing due to an increase in the heat transfer rate which is a consequence of increasing the air flow velocity. For example, as the air velocity increases from 1 m/sec to 5 m/sec, the difference between the inlet and outlet temperature of the water (ΔT_w) has increased from 0.85° C to 2.11° C. In addition, the water inlet section is less heated than the outlet section because it is facing the airflow.

4.4.3 Tube Bends Flow Field Analysis

A bend in a tube represents a means to enhance the heat transfer compared with a straight tube due to creation of secondary flows and curvature affects the flow's turbulence structure. These two effects not only affecting the pressure drop, but also the heat transfer characteristics [88], [89]. However, separation of flow after the bend cause a significant increase in the water pressure drop. This increase is due to both friction and momentum exchanges resulting from a change in the direction of flow.

Figure 4.22 depicts variations of water velocity magnitude contours at 6 different cross-sections (P1 to P6) through a tube bend in the water-side of the heat exchanger when the inlet water velocity is 1 m/sec and water inlet temperature is equal to 60° C.

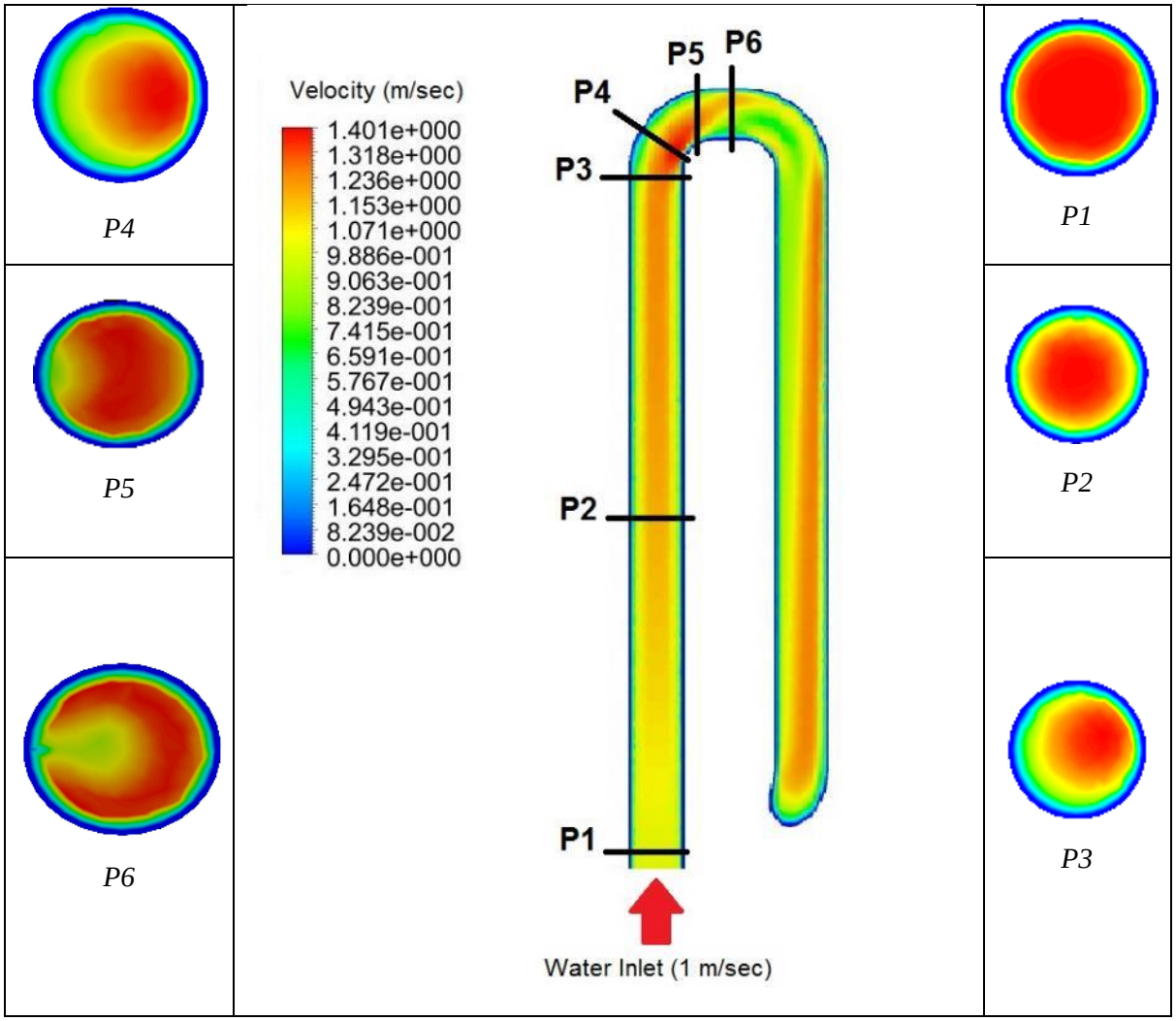

Figure 4.22 Variations of Water Velocity Magnitude Contours at 6 Different Cross-Sections Through a Tube Bend in the Water-Side of the Heat Exchanger

The variations of water static pressure contours at 6 different cross-sections (P1 to P6) through a tube bend in the water-side of the heat exchanger when the inlet water velocity is 1 m/sec is illustrated in Figure 4.23.

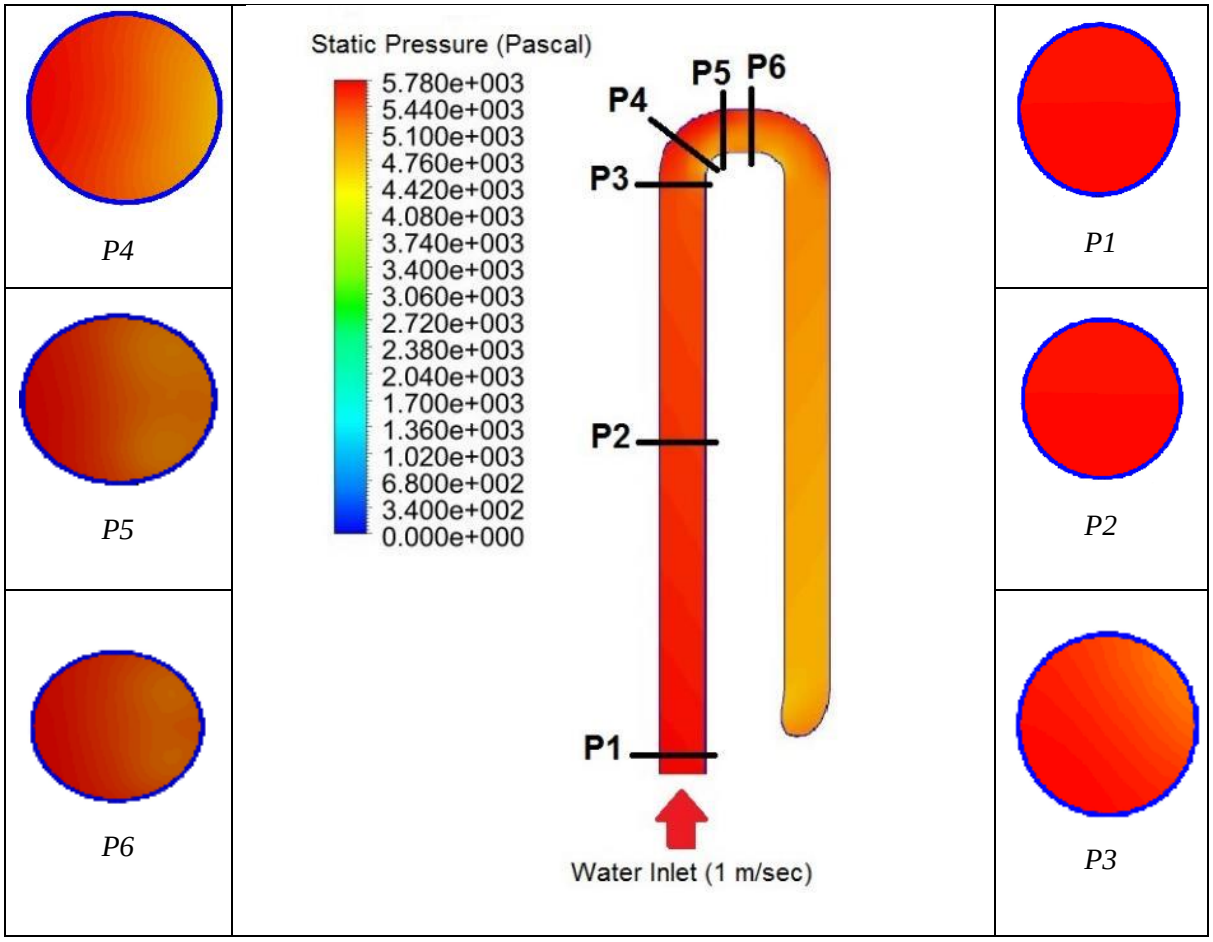

Figure 4.23 Variations of Water Static Pressure Contours at 6 Different Cross-Sections Through a Tube Bend in the Water-Side of the Heat Exchanger

Figure 4.24 depicts variations of water static temperature contours at 6 different cross-sections (P1 to P6) through a tube bend in the water-side of the heat exchanger when the inlet water velocity is 1 m/sec and water inlet temperature is equal to 60° C.

From the contours depicted in Figure 4.22, 4.23 and 4.24, the water velocity varies from a maximum at the centre of the tube to zero at the tube walls due to the effect of the boundary layer (P1 and P2). As the water flow approaches a tube bend (P3), the water velocity decreases from the inside to outside of the bend in order to keep the total pressure constant through the tube (P4). However, the static pressure of the water increases with the radius of the bend which enhances the heat transfer through the bend. This increase has to balance the centrifugal force caused by passing of the water in the bend. In addition, the flow is generally unstable in both cross-sections (P5 and P6) due to the small length of the tube after the bend. It was found that the process described above keeps repeating till the flow reaches the outlet. In general, the temperature variations were identical to the static pressure variations for the different cross-

sections (P1 to P6) and it is noticed a high temperature distribution at the outer surface of the bend due to high static pressure in this area.

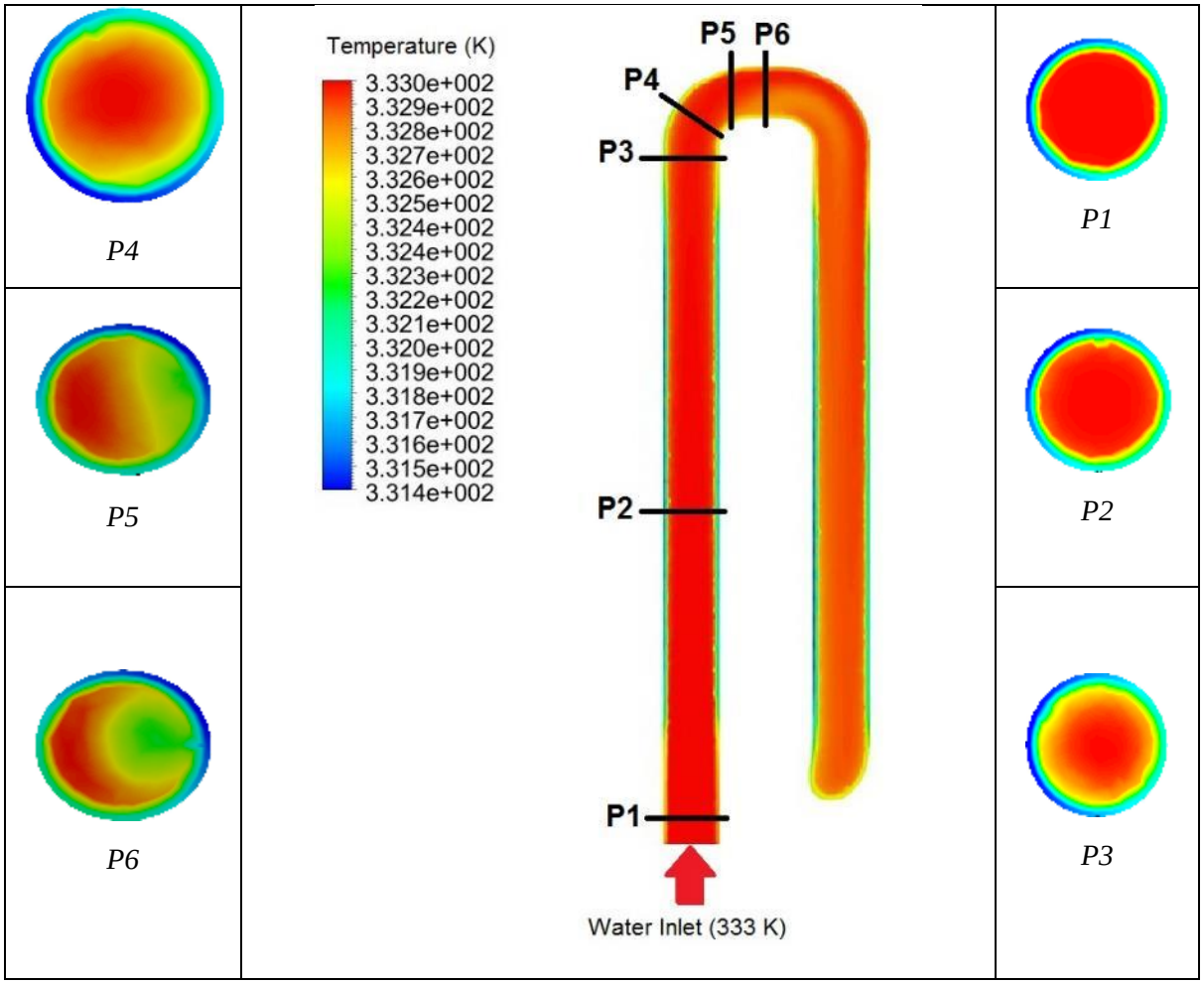

Figure 4.24 Variations of Water Static Temperature Contours at 6 Different Cross-Sections Through a Tube Bend in the Water-Side of the Heat Exchanger

In order to achieve a deep analysis of the flow through a bend, a local velocity magnitude, static pressure and static temperature ratios has been plotted at the 6 different cross-sections through a tube bend, described in the previous section. These ratios represent the ratio between the local flow characteristics; velocity magnitude, static pressure and static temperature at a point in the top of the tube divided by the local flow characteristics at a point in the bottom of the tube. And another ratio which take into consideration the local flow characteristics at a point in the right of the tube divided by the local flow characteristics at a point in the left of the tube. Figure 4.25 shows the locations of these points in the cross-section of the tube. In addition, the points have been selected away from the tube walls to avoid the effect of the boundary layer.

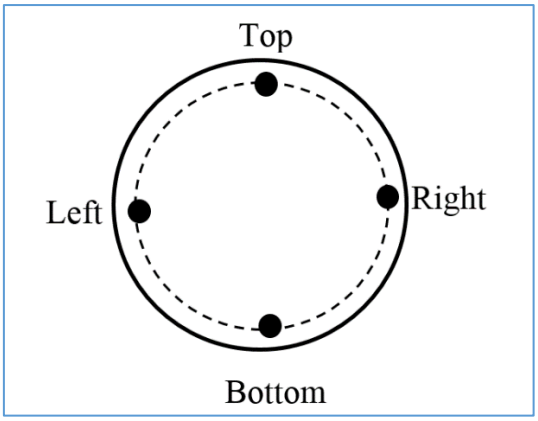

Figure 4.25 Locations of the Analysed Points in the Cross-Section of the Tube

Figure 4.26 depicts the variations of the velocity magnitude ratio for the analysed points at 6 different cross-sections through a tube bend.

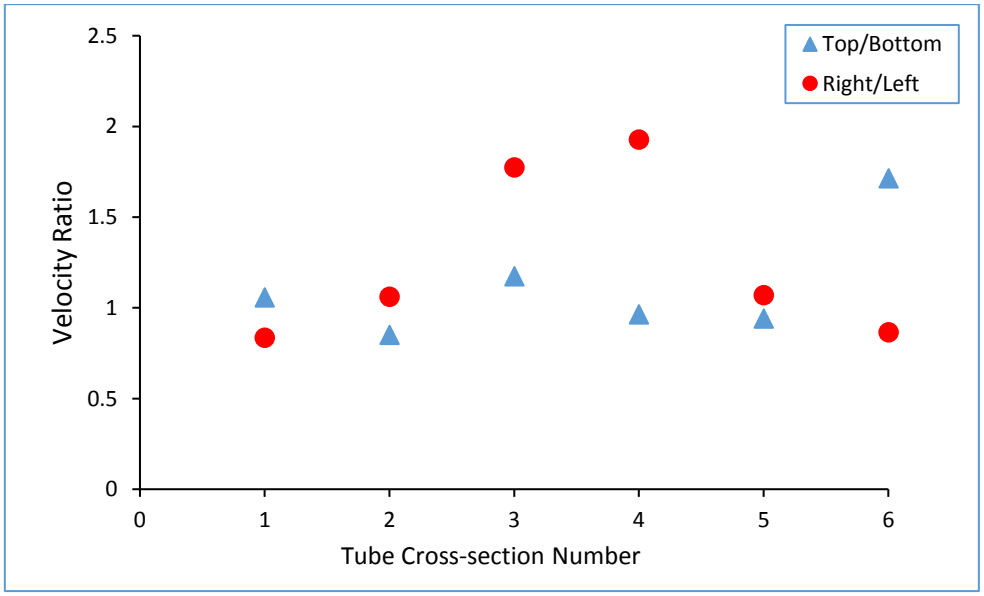

Figure 4.26 Variations of the Velocity Magnitude Ratio for the Analysed Points at 6 Different Cross-Sections Through a Tube Bend

From Figure 4.26 it can be seen that the velocity magnitude for the right points (the inner side of the bend) are higher than those is the left side. This agrees with the idea presented previously where it has been detected a high velocity region at the inner side of the bend. However, the no any notable change in the velocity magnitude between the right and left points.

The variations of the static pressure ratio for the analysed points at 6 different cross-sections through a tube bend is shown in Figure 4.27.

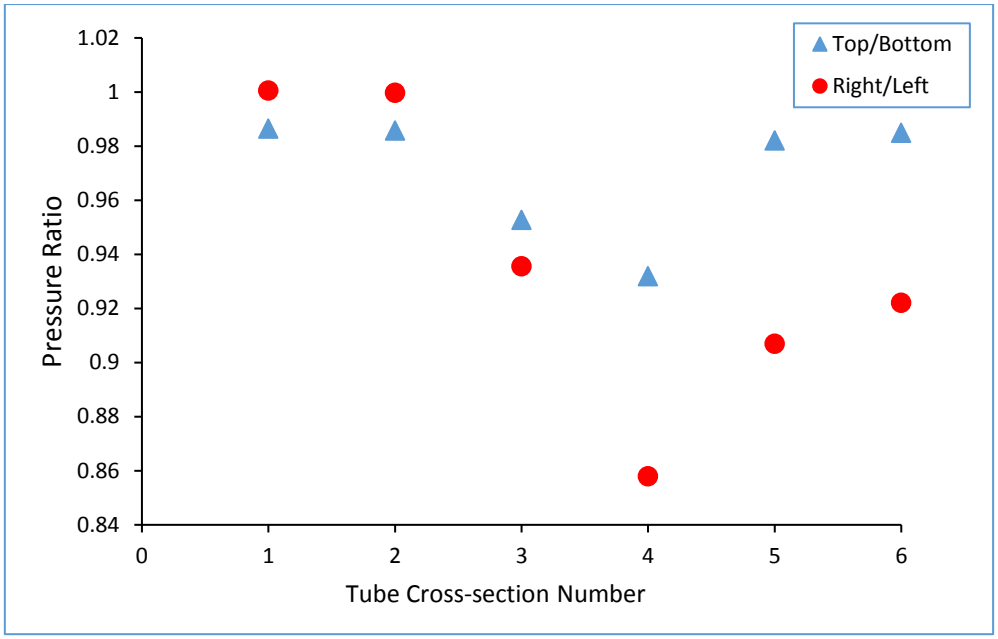

Figure 4.27 Variations of the Static Pressure Ratio for the Analysed Points at 6 Different Cross-Sections Through a Tube Bend

As it has been described before, the static pressure was higher at the outer side of the bend. Therefore, the static pressure at the top point in section 4 was higher than the bottom point. Furthermore, it can be observed that the water pressure decreases in general due to the frictional forces.

Figure 4.28 illustrates the variations of the static temperature ratio for the analysed points at 6 different cross-sections through a tube bend.

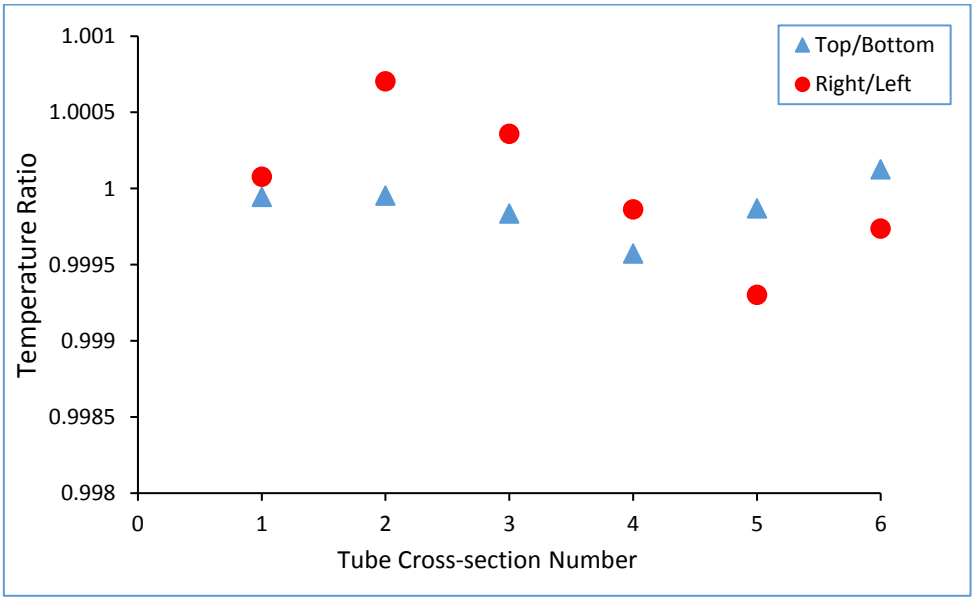

Figure 4.28 Variations of the Static Temperature Ratio for the Analysed Points at 6 Different Cross-Sections Through a Tube Bend

Based on the data plotted in Figure 4.28, the variations in the static temperature for 6 different cross-sections through a tube bend are small. Moreover, points on the right of tube (inner side of the bend) are having higher temperature comparing with the left points. This is happened because of the left side of the tube is facing the air flow. The situation has changed as the water reached section 5. The same behaviour can be observed for the points in top and bottom of the tube.

4.5 Incorporating the novel CFD model to Predict Heat Transfer Coefficients and Local Fin Efficiency for Multi-tube and Fin Heat Exchanger

The main purpose of using fins is to increase the surface area and therefore to enhance the total heat transfer rate. The heat transfers through fins in two methods; conduction through fins and convection from their surface area to the air. Hence, an accurate model is required to predict the heat transfer characteristics of the heat exchanger as the fin efficiency is one of the main parameters affecting heat transfer on the air-side [90].

In the next section, the novel CFD model, presented in chapter 3, was incorporated to predict heat transfer coefficients and local fin efficiency for the baseline model; multi-tube and fin heat exchanger with plain fins.

The fin efficiency (η_f) can be described as the ratio of the actual heat transferred through the fin to ideal case where the whole fin would be at the base temperature [16]. Schmidt empirical method [91] is used to determine fins efficiency of the multi-tube and fin heat exchanger having plain fins. Based on this method, the fin efficiency can be calculated from [12],[16]:

$$\eta_f = \frac{\tanh(m r_o \phi)}{(m r_o \phi)} \tag{4.13}$$

where m is defined as,

$$m = \sqrt{\frac{2\, h_a}{k_a f_t}} \tag{4.14}$$

where, h_a is the air side heat transfer coefficient for the fin (W /m^2 K) which can be predicted from the novel CFD model

K_a is the thermal conductivity of the fin material (W/m K)

f_t is the fin thickness (m)

r_o is the outer radius of the tube (m)

$$\phi = (\frac{R}{r_o} - 1)\left[1 + 0.35\ln(R/r_o)\right] \quad (4.15)$$

Based on this method, R is the radius of a circular fin which has the same efficiency as the rectangular fin (m). The ratio (R/r_o) for staggered fin configuration (hexagonal tube array), as shown in Figure 4.29, can be calculated from,

$$\frac{R}{r_o} = 1.27\psi\sqrt{\beta - 0.3} \quad (4.16)$$

where, $$\psi = \frac{M}{r_o} \text{ and } \beta = \frac{L}{M} \quad (4.17)$$

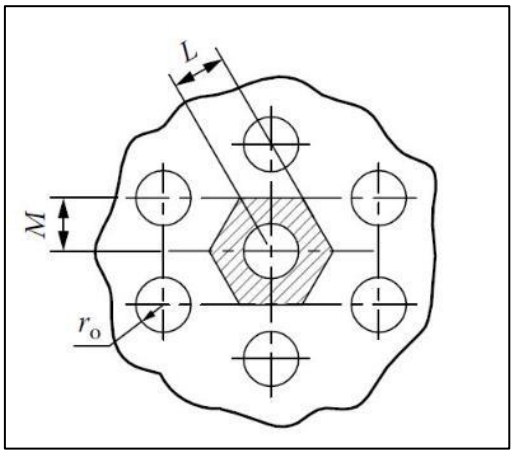

Figure 4.29 Geometrical Details of Staggered Fin Configuration [16]

4.5.1 Sample Calculation of Local fin efficiency (η_f)

As described in the previous section, steps to calculate the fin efficiency are summarised below,

1. Calculate ψ and β

   For M=0.0125 m, r_o=0.00476 m, and L= 0.0125 m, then from Eq. (4.17),

$$\psi = \frac{0.00125}{0.00476} = 2.626$$

$$\beta = \frac{0.0125}{0.0125} = 1.0$$

2. Calculate the ratio (R/r_o) from Eq. (4.16)

$$\frac{R}{r_o} = 1.27 * 2.626 * \sqrt{1.0 - 0.3}$$

$$\frac{R}{r_o} = 2.79$$

3. Calculate ϕ from Eq. (4.15)

$$\phi = (2.97 - 1)[1 + 0.35\ln(2.97)]$$

$$\phi = 2.433$$

4. Calculate m from Eq. (4.14), where K_a (Aluminum) = 202.4 W/m.K [92], f_t =0.00012 m and the value of h_a is computed from FLUENT and after considering the following reference values:
   - Area= 1 m^2 (per unit area)
   - Density= 1.184 Kg/m3 (Air density at T_∞ =25° C) [92]
   - Length= 0.043 m (fin width)
   - Temperature $T_{ref} = \frac{T_{wall}+T_\infty}{2}$ [93] and [94]

     T_{wall} is the area-weighted average temperature of the fin (computed from FLUENT). T_{wall} for the fin 1 of the baseline model for test 3 and water flow rate 3 L/min with the boundary condition shown in Table 4-1 is equal to 53.85° C

     $T_{ref} = \frac{53.85+25}{2}$ = 39.42 ° C
   - Air Velocity= 3 m/sec
   - Viscosity= 1.8364e-05 Kg/m.sec (Air Dynamic Viscosity at T_∞ =25° C)[92]
   - Ratio of air specific heat= 1.4
5. The air side heat transfer coefficient (h_a) for fin 1 in the heat exchanger used in this study is equal to 98.116 W /m^2.K

$$m = \sqrt{\frac{2 * 98.116}{202.4 * 0.00012}}$$

$$m = 89.885$$

6. The last step is to calculate the fin efficiency (η_f) from Eq. (4.1)

$$\eta_f(1) = \frac{\tanh(89.885 * 0.00476 * 2.433)}{(89.885 * 0.00476 * 2.433)}$$

$$\eta_f(1) = 0.748$$

The same steps were repeated in order to calculate the local fin efficiency of each fin in the heat exchanger under study based on computing the local heat transfer coefficient using the

novel CFD model. The results of this calculations are shown in Figure 4.30 and 4.31, respectively.

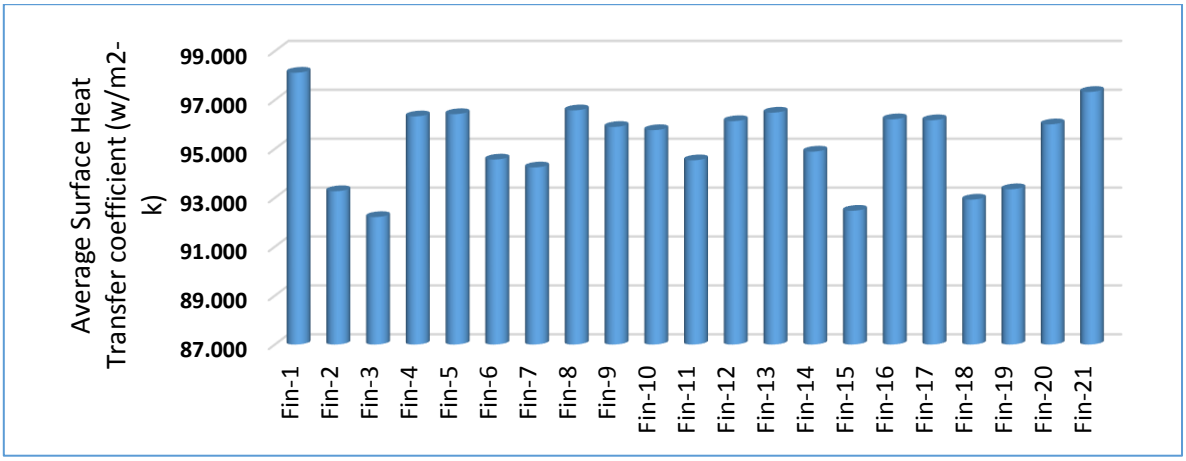

Figure 4.30 Local Heat Transfer Coefficient for Every Fin in the Heat Exchanger Computed from CFD- FLUENT

The vertical bars presented in both Figure 4.30 and 4.31 indicate that the local values for heat transfer coefficient and fin efficiency are not identical for all fins. A difference is observed and it can be clearly seen that in fin 1 and fin 21. As a result of this difference, values for the local heat transfer coefficient for both fin 1 and fin 21 were higher than the average value of other fins with 3.02 % and 2.2 %, respectively. Accordingly, the local values of fin efficiency for fin 1 and fin 21 were lower than the average value of other fins with 0.7 % and 0.5 %, respectively.

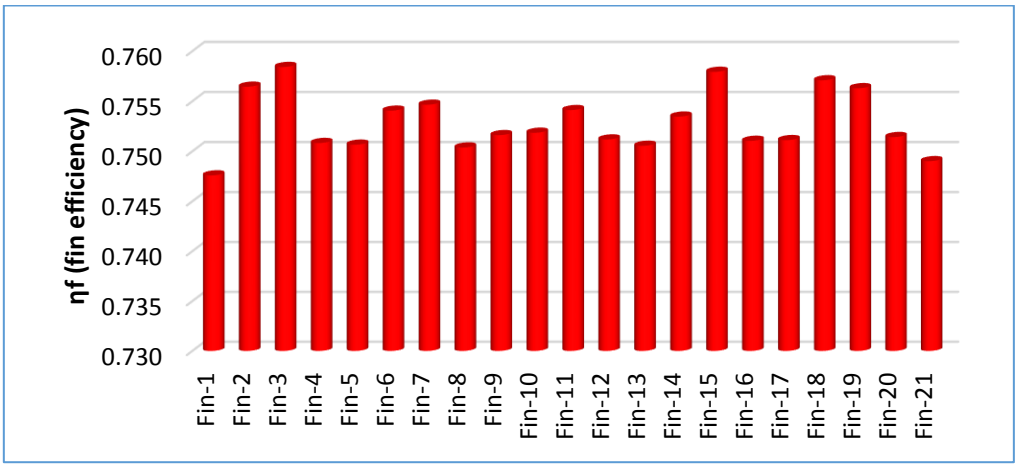

Figure 4.31 Local Fin Efficiency for Every Fin in the Heat Exchanger Computed from CFD-FLUENT

Figure 4.32 depicts the static temperature contours for the heat exchanger together with local values of air heat transfer coefficient and the local fin efficiency of fins 1, 5, 9, 13, 17 and 21.

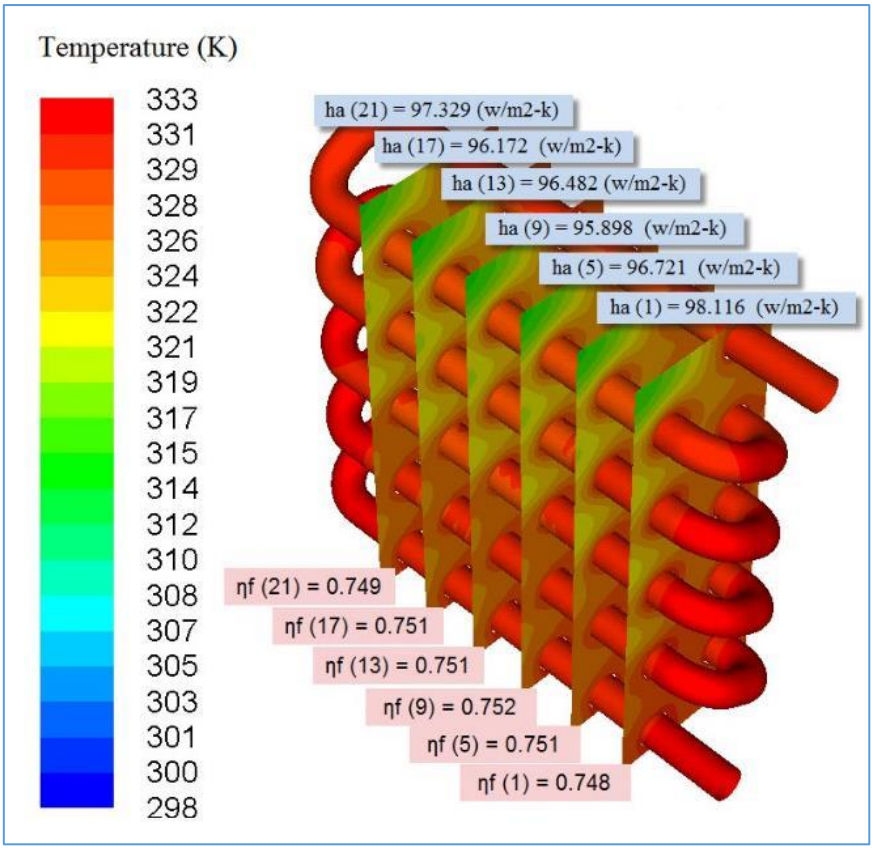

Figure 4.32 Static Temperature Contour for Some Fins in The Heat Exchanger

Table 4-4 illustrates in detail static temperature contours for fins 1, 5, 9, 13, 17 and 21 in both front and back sides.

Table 4-4 Static Temperature Contours for Fins 1, 5, 9, 13, 17 And 21 in both Front and Back Sides

Fin no.	*1*	*5*	*9*	*13*	*17*	*21*	*Legend*
Front-side						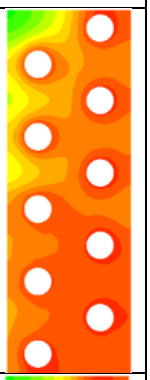	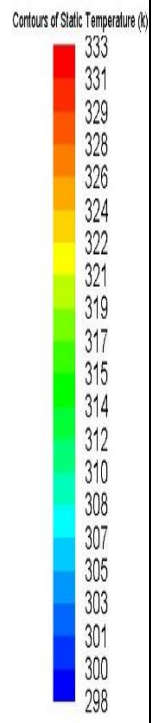
Back-side							

From both Figure 4.32 and Table 4-4, it can be seen that static temperature distribution on the fins is not alike. However, an identical temperature distribution is observed for both sides of the same fin. Moreover, local values of heat transfer coefficient and the fin efficiency for fins number 5, 9, 13, and 17 are in the same range.

By using this method to calculate the local fin efficiency of some fins in the baseline model of the heat exchanger it can be conclude that, due to the dissimilarity of thermal behaviour of the fins of the heat exchanger so the condition in one fin cannot be applied to the other one; hence it is vital to analysis the whole heat exchanger under this condition. This idea agreed with the idea presented in [95], where it has been reported that the heat transfer coefficient is not constant throughout its flow length and it is varying with location, the entrance length effect (due to the boundary layer development), surface temperature, maldistribution, fouling, manufacturing imperfections, fluid physical properties, etc.

4.6 Effect of Geometrical Parameters on the Thermal Performance of the Baseline Model

The main objective of this study (objective 2.2) is to understand the hydrodynamics of the flow, the heat transfer and pressure drop characterises as a function of geometrical parameters of the heat exchanger. The multi-tube and fin heat exchanger which has plain fins has been numerically investigated for the effects of fin spacings (F_p), longitudinal pitches (L_p) and transverse pitches (T_p) on the heat transfer and pressure drop characteristics of the heat exchanger under steady state operating condition. In this parametric study, three different cases have been considered for specific geometric parameters; F_p, L_p and T_p. These cases considered in this parametric study are tabulated in Table 4-5where case II represents the geometry of the baseline model. The effects of the geometrical parameters previously mentioned were investigated using Fanning friction factor (f) which symbolised the pressure drop characteristics, Colburn factor (j) which symbolised the heat transfer characteristics and the ratio between Colburn factor (j) and Fanning friction factor (f) them which is efficiency index (j/f). In addition, Fanning friction factor (f) and Colburn factor (j) were computed using the method previously described in section 4.1.2.

Table 4-5 Cases Considered in the Parametric Study

Parameter	Case I	Case II	Case III
Fin Spacing (F_p) *mm*	3.7	4.2	4.7
Longitudinal Tube Pitch (L_p) *mm*	20	22	24
Transverse Tube Pitch (T_p) *mm*	23.5	25	26.5

The boundary conditions of the present study are shown in Table 4-6. For each geometrical parameter, CFD simulations were carried out for steady state operating condition. The air velocity was varying from 1 to 5 m/sec, whereas the water velocity was varying from 0.3 to 1.5 m/sec.

Table 4-6 Boundary Conditions of Steady State Tests for Parametric Study

Test Name	*Water Side*		*Air Side*	
	Water Velocity (m/sec)	*Water Inlet Temperature (° C)*	*Air Velocity (m/sec)*	*Air Inlet Temperature (° C)*
Test 1	*1*	*60*	*1*	*25*
Test 2			*2*	
Test 3			*3*	
Test 4			*4*	
Test 5			*5*	
Test 1	*0.3*	*60*	*3*	*25*
Test 2	*0.6*			
Test 3	*0.9*			
Test 4	*1.2*			
Test 5	*1.5*			

4.6.1 Effect of Fin Spacings

This section is focusing on the impact of the spacing between the fins on the heat transfer and pressure drop characteristics of the heat exchanger. This effect controls the number of fins which can be installed in a given space along the tubes. The effects of three different fin spacings; 3.7 mm, 4.2 mm and 4.7 mm have been investigated.

Figure 4.33 depicts the variations of Colburn factor (j) of heat exchangers used in the present study with Reynolds number (Re_D) computed based on the hydraulic diameter of the tube and for three different fin spacings (F_p); 3.7 mm, 4.2 mm and 4.7 mm, respectively.

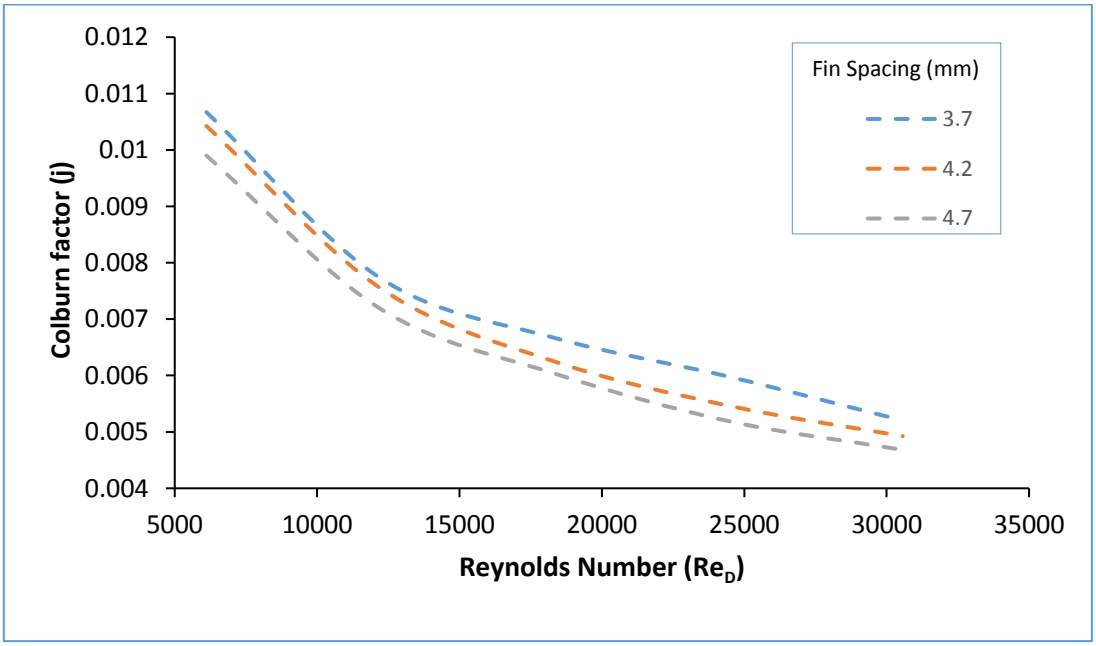

Figure 4.33 Effect of the Variation of Different Fin Spacing on Colburn Factor (j)

From Figure 4.33, Colburn factor (j) of heat exchangers used in the present study decreases as the Reynolds number goes higher. Furthermore, at a constant Reynolds number equal to 18,000

and when the fin spacing (F_p) is decreasing from 4.7 mm to 4.2 mm and from 4.2 mm to 3.7 mm, the Colburn factor (j) increase 3.53% and 6.7%, respectively. Therefore, a higher heat transfer is observed for the heat exchanger model with 3.7 mm fin spacing, i.e. at low fin spacing. This behaviour of the heat exchanger can be explained as the fin spacing (F_p) is decreasing, the flow becomes more turbulent and it can interrupt the development of the boundary layer.

Variations of Fanning friction factor (f) with Reynolds number (Re_D) for three different fin spacings (F_p); 3.7 mm, 4.2 mm and 4.7 mm, respectively is illustrated in Figure 4.34.

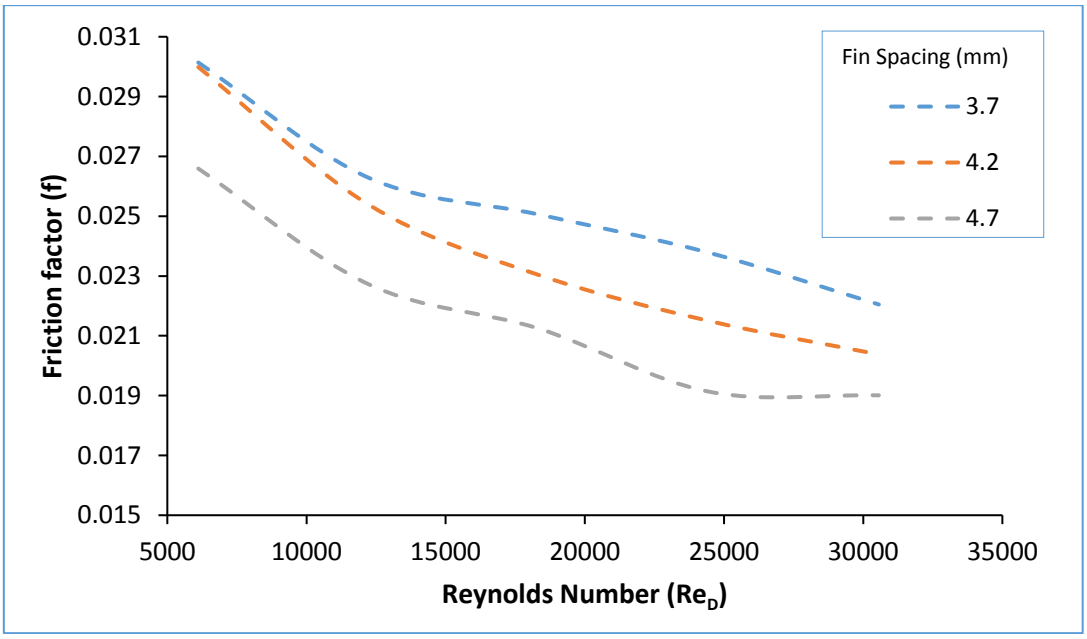

Figure 4.34 Effect of the Variation of Different Fin Spacings on Fanning Friction Factor (f)

It can be clearly seen from Figure 4.34 that, a significant effect of fin spacing on Fanning friction factor (f) has observed. Moreover, by decreasing the fin spacing, the tube surface area is reduced which affects the pressure drop performance. In other words, a higher-pressure drop has detected at 3.7mm fin spacing which represent a disadvantage of high heat transfer rate reached in the previous figure. The friction factor (f) increases 8.44% and 8.78% when the fin spacing is changed from 4.7 mm to 4.2 mm and 4.2 mm to 3.7 mm and at a constant Reynolds number of 18,000.

Figure 4.35 represents the variations of efficiency index (j/f) of heat exchangers used in the present study with Reynolds number (Re_D) for different fin spacings (F_p); 3.7mm, 4.2mm and 4.7mm, respectively.

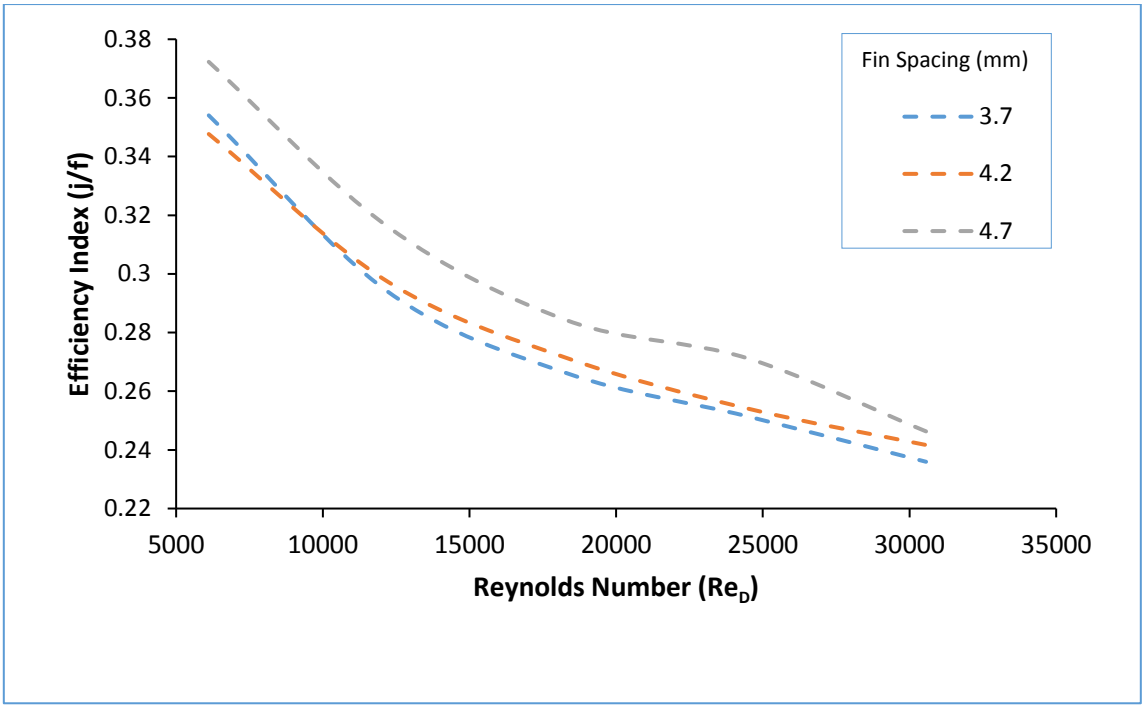

Figure 4.35 Effect of the Variation of Different Fin Spacings on Efficiency Index (j/f)

The data plotted in Figure 4.35 reveals that the efficiency index (j/f) decreases as the Reynolds number is increased. Moreover, a higher efficiency index is observed at high fin spacing, i.e. at 4.7 mm fin spacing.

The reason for an increase in heat transfer with low value of fin spacing can be generally explained by the fact that, as the fin spacing decreased the boundary layer thickness decreased which result an enhancement in the heat transfer characteristics of the heat exchanger. However, this enhancement has a disadvantage of higher pressure drop.

4.6.2 Effect of Longitudinal Pitches

The effect of longitudinal pitches (L_p) on the heat transfer and pressure drop characteristics of the heat exchanger presented in this study is discussed in this section. This effect is evaluated by varying the longitudinal pitches (L_p) for three different values; 20 mm, 22 mm and 24 mm.

Variations of Colburn factor (j) of heat exchangers used in the present study with Reynolds number (Re_D) for three different longitudinal pitches (L_p); 20 mm, 22 mm and 24 mm, respectively is illustrated in Figure 4.36.

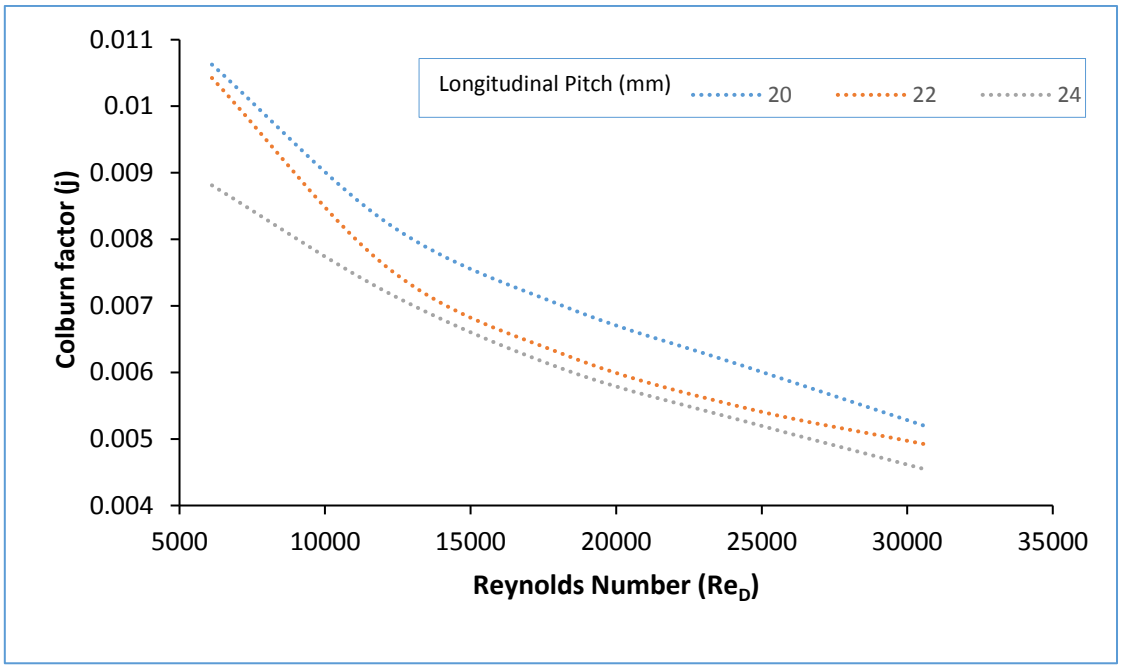

Figure 4.36 Effect of the Variation of Different Longitudinal Pitches on Colburn Factor (j)

It has found that as the longitudinal pitch (L_p) increases Colburn factor (j) decrease. For example, Colburn factor (j) declines by 10.22% and 3.71% when the longitudinal pitch (L_p) is varied from 20 mm to 22 mm and 22 mm to 24 mm, respectively for a constant Reynolds number of 25,000. This response of the heat exchanger can be clarified by increasing of tube surface area by an increase in longitudinal pitch (L_p) which however results a decrease in the heat transfer rate. This response of the heat exchanger contradicts with of the phenomenon which states that as the heat transfer area increases the heat transfer rate would increase.

Figure 4.37 depicts the variations of Fanning friction factor (f) of heat exchangers used in the present study with Reynolds number (Re_D) for different longitudinal pitches (L_p); 20 mm, 22 mm and 24 mm, respectively.

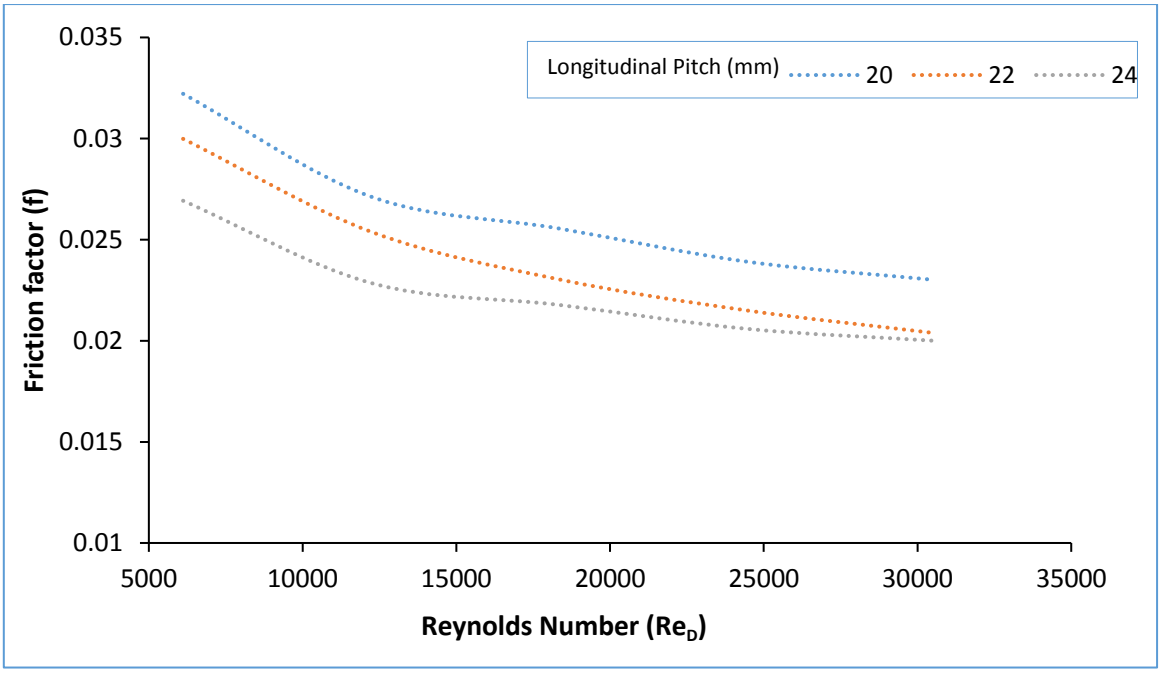

Figure 4.37 Effect of the Variation of Different Longitudinal Pitches on Fanning Friction Factor (f)

It can be seen clearly from Figure 4.37 that, friction factor (f) has the same behaviour as Colburn factor (j), i.e. as the Reynolds number (Re_D) increases the friction factor (f) decreases. Moreover, a higher friction factor (f) is observed at the lowest longitudinal pitch (L_p= 20 mm). At a constant Reynolds number of 25,000, friction factor (f) decrease by 10.1% and 4.23% when the longitudinal pitch (L_p) is changed from 20 mm to 22 mm and 22 mm to 24 mm, respectively

Figure 4.38 illustrates the variations of efficiency index (j/f) of heat exchangers used in the present study with Reynolds number (Re_D) for different longitudinal pitches (L_p); 20 mm, 22 mm and 24 mm, respectively.

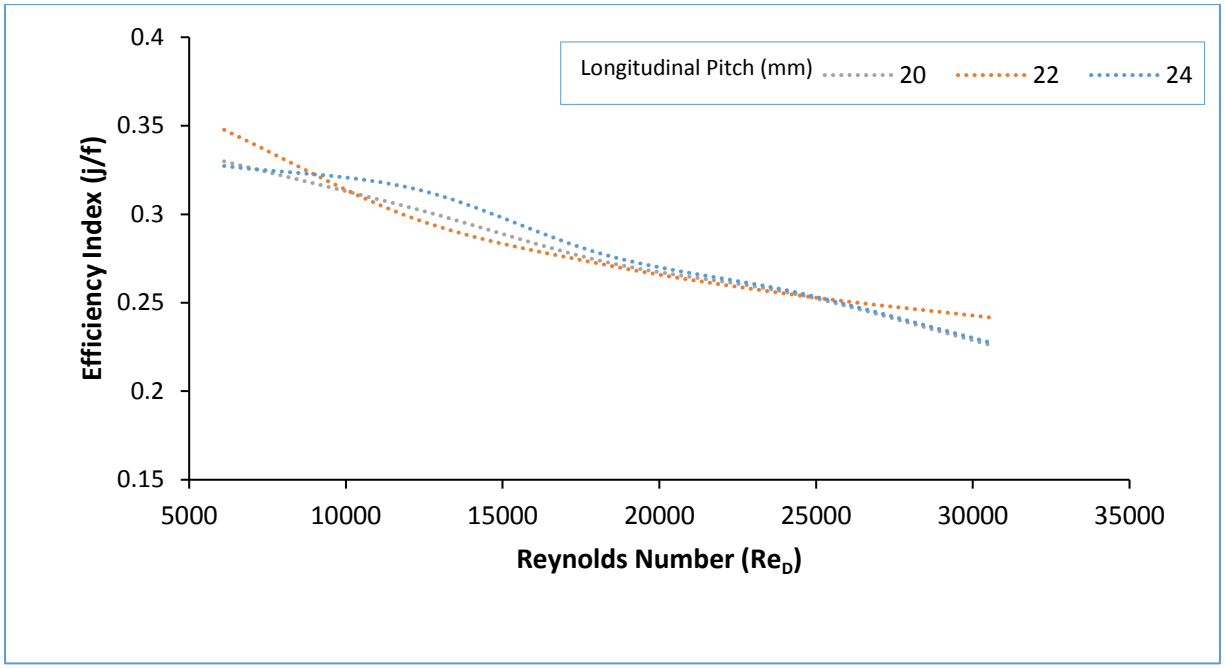

Figure 4.38 Effect of the Variation of Different Longitudinal Pitches on Efficiency Index (j/f)

The data plotted in Figure 4.38 reveals that, the efficiency index (j/f) decreases as Reynolds number (Re_D) increases. In contrast to the behaviour of friction factor (f) and Colburn factor (j), the efficiency index (j/f) is observed to be slightly higher for high longitudinal pitches (L_p). This can be explained as the rate of increase in Colburn factor (j) is lower than the friction factor (f).

4.6.3 Effect of Transverse Pitches

In this section, the effect of transverse pitches has been investigated. The numerical investigation has been carried out for three different transverse pitches (T_p); 23.5 mm, 25 mm and 26.5 mm, respectively.

Figure 4.39 depicts the variations of Colburn factor (j) of heat exchangers used in the present study with Reynolds number (Re_D) for different transverse pitches (T_p); 23.5 mm, 25 mm and 26.5 mm, respectively.

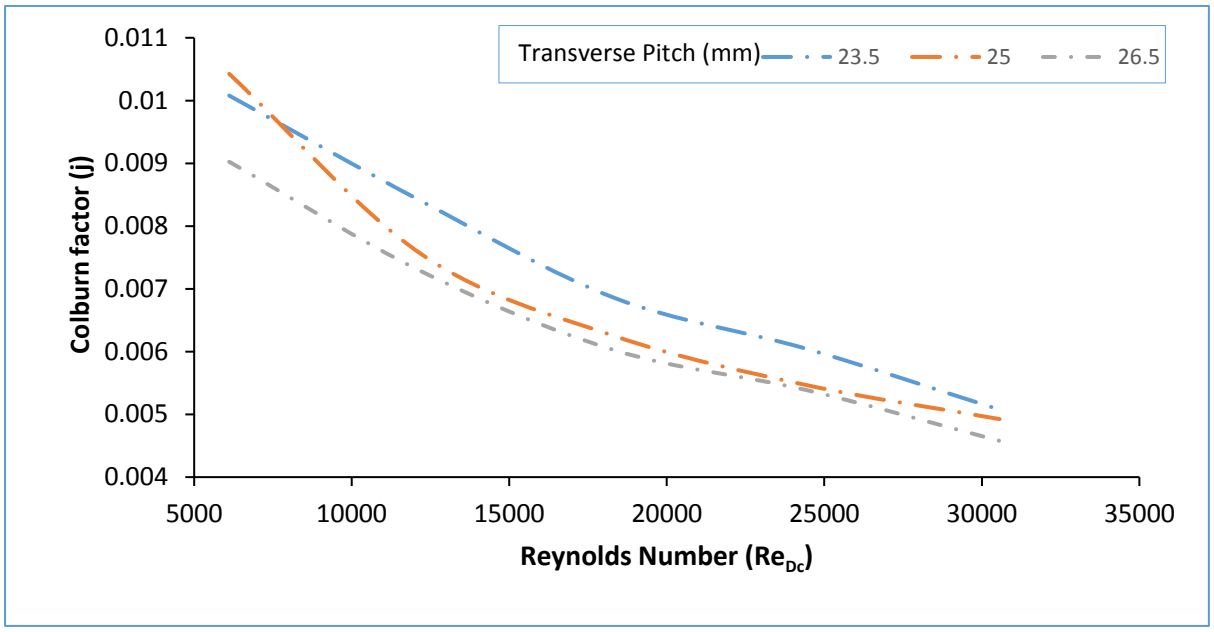

Figure 4.39 Effect of the Variation of Different Transverse Pitch on Colburn Factor (j)

It can be clearly seen from Figure 4.39 that the value of transverse pitch is affecting Colburn factor (j) and therefore affecting the heat transfer rate in the heat exchanger. In general, Colburn factor (j) of heat exchangers used in the present study decreases as the Reynolds number increases. Furthermore, at a constant Reynolds number equal to 30,000 and when the transverse pitch (T_p) is decreasing from 26.5 mm to 25 mm and 25 mm to 23.5 mm, the Colburn factor (j) increase by 7.58% and 3.05%, respectively. Therefore, a higher heat transfer is observed for the heat exchanger model with 23.5 mm transverse pitch, i.e. at low transverse pitch. This behaviour of the heat exchanger is similar to that of longitudinal pitch.

Variations of Fanning friction factor (f) of heat exchangers used in the present study with Reynolds number (Re_D) for different transverse pitches (T_p); 23.5 mm, 25 mm and 26.5 mm, respectively is illustrated in Figure 4.40.

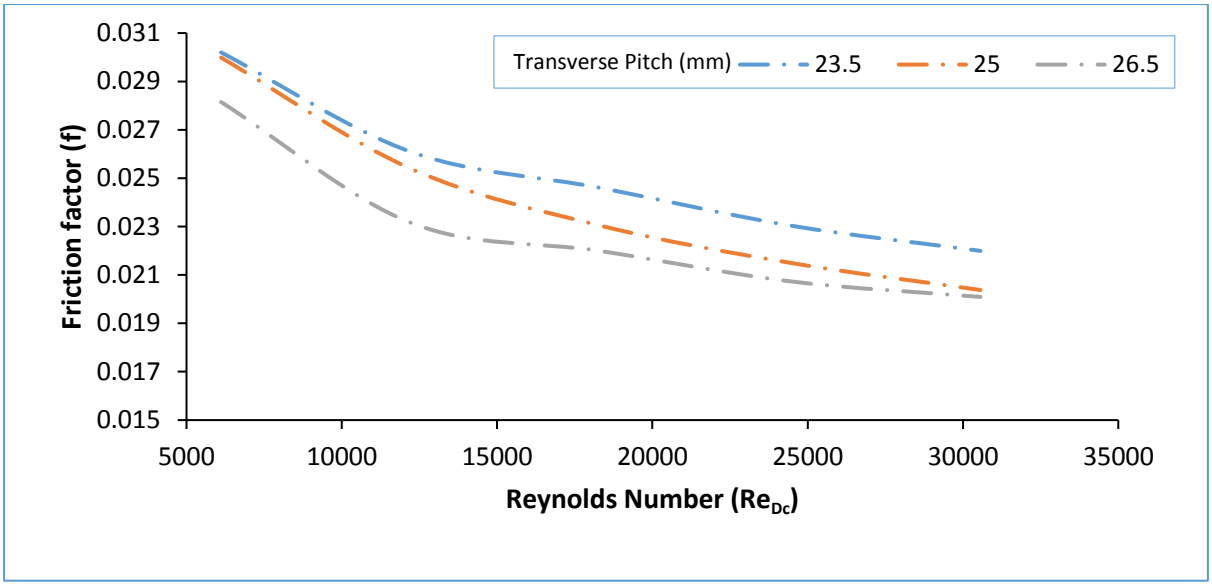

Figure 4.40 Effect of the Variation of Different Transverse Pitch on Fanning Friction Factor (f)

The results plotted in Figure 4.40 depict that, as Reynolds number (Re_D) increases the friction factor (f) tend to decrease for all the cases studied. A higher friction factor (f) is observed at a low transverse pitch (23.5 mm). This behaviour of the heat exchanger can be explained that, as the transverse pitch increased, the surface of tubes area is increased, which result an expanding in flow area and hence lower pressure drop.

Figure 4.41 represents the variations of efficiency index (j/f) of heat exchangers used in the present study with Reynolds number (Re_D) for three different transverse pitches (T_p); 23.5 mm, 25 mm and 26.5 mm, respectively. It can be seen that the efficiency index decreases as the Reynolds number is increased. Moreover, a higher efficiency index is observed at high transverse pitch, i.e. at 26.5 mm transverse pitch, which represents a difference for respective cases comparing with the behaviour of friction factor (f) and Colburn factor (j).

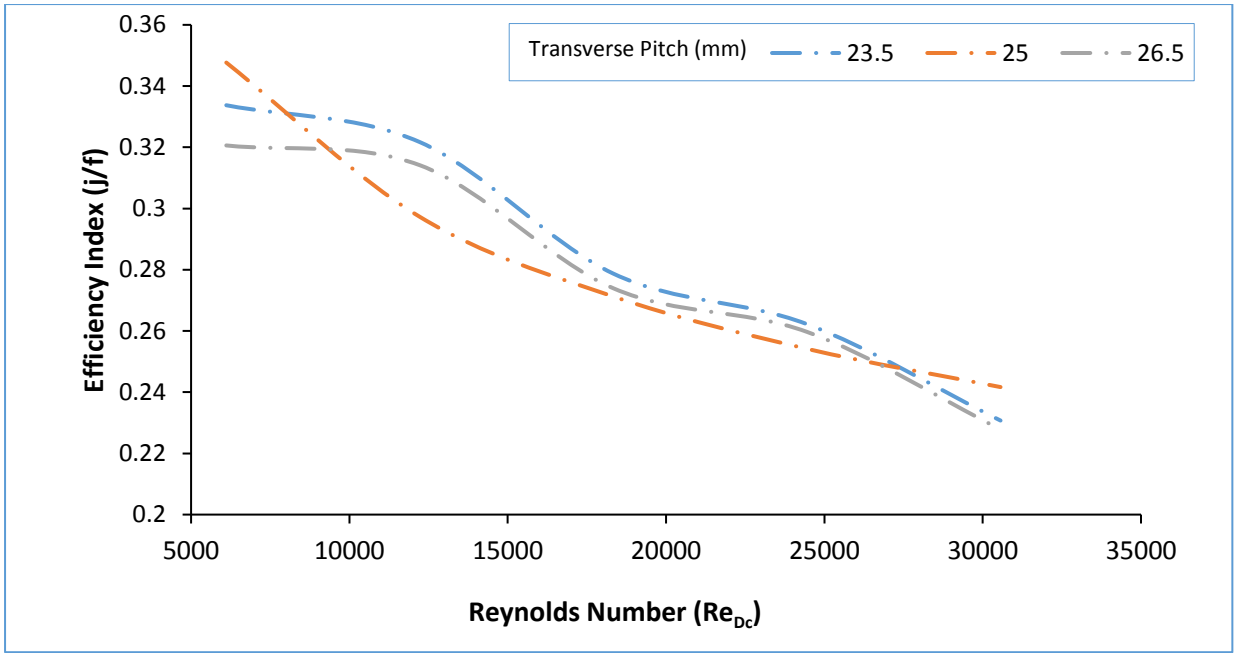

Figure 4.41 Effect of the Variation of Different Transverse Pitch on Efficiency Index (j/f)

4.7 Development of Novel Semi-Empirical Prediction Model

The results which have been obtained in the previous study which has quantified the effect of geometrical parameters; fin spacings (F_p), longitudinal pitches (L_p) and transverse pitches (T_p) on the thermal performance of multi-tube and fin heat exchanger having plain fins (baseline model) have been implemented to develop a novel semi-empirical prediction model for Fanning friction factor (f) and Colburn factor (j). As it has been stated before, Fanning friction factor (f) and Colburn factor (j) are representing the pressure drop heat transfer characteristics, respectively. Therefore, it is vital to develop a prediction model to correlate them. In addition, In the design of a plain fin heat exchanger, the geometric parameters are fin spacings (F_p), longitudinal pitches (L_p), transverse pitches (T_p), fin collar outside diameter (D_c), fin width (F_w), fin height (F_H) and Reynolds number computed based on the hydraulic diameter (Re_D). Theses parameters are affecting the thermal performance of the heat exchanger. Hence, the dimensionless geometric parameters used to develop the prediction model are Re_D, F_p/D_c, L_p/F_w and T_p/F_H.

The correlation has been carried out using multiple variable regression analysis. These novel equations are shown below.

$$j = 0.0468\ Re_D^{-0.439} \left(F_p/D_c\right)^{-0.413} \left(L_p/F_w\right)^{-0.819} \left(T_p/F_H\right)^{-1.001} \quad (4.18)$$

$$f = 0.0175\ Re_D^{-0.212} \left(F_p/D_c\right)^{-0.659} \left(L_p/F_w\right)^{-0.884} \left(T_p/F_H\right)^{-0.829} \quad (4.19)$$

where,

j is Colburn factor

f is Fanning friction factor

Re_D is Reynolds number computed based on the hydraulic diameter

F_p is fin spacing (m)

D_c is fin collar outside diameter (m)

L_p is longitudinal pitch (m)

T_p is transverse pitch (m)

F_w is fin width (m)

F_H is fin height (m)

The limitations of using the equations above are:

- These equations are applicable only to multi-tube and fin heat exchanger with plain fins
- These equations have been developed based on heating condition
- These equations are applicable only to forced convection heat transfer analysis

The correlation coefficient values between calculated and predicted data for Eqs. (4.6) and (4.7) are 0.987 and 0.977, respectively. Based on the above information it can be concluded that the developed prediction model shows no significant difference to the available data and they have the same trend. Therefore, this prediction model developed can be used during the design process of multi-tube and fin heat exchanger having plain fins.

4.7.1 The Accuracy of the Developed Equations for Predicting Colburn factor (j) and fanning friction factor (f)

This section illustrates the accuracy of the developed equations for predicting Colburn factor (j) and Fanning friction factor (f). Figure 4.42 and 4.43 depict the relation between the calculated values and the predicted values of Colburn factor (j) and Fanning friction factor (f), respectively.

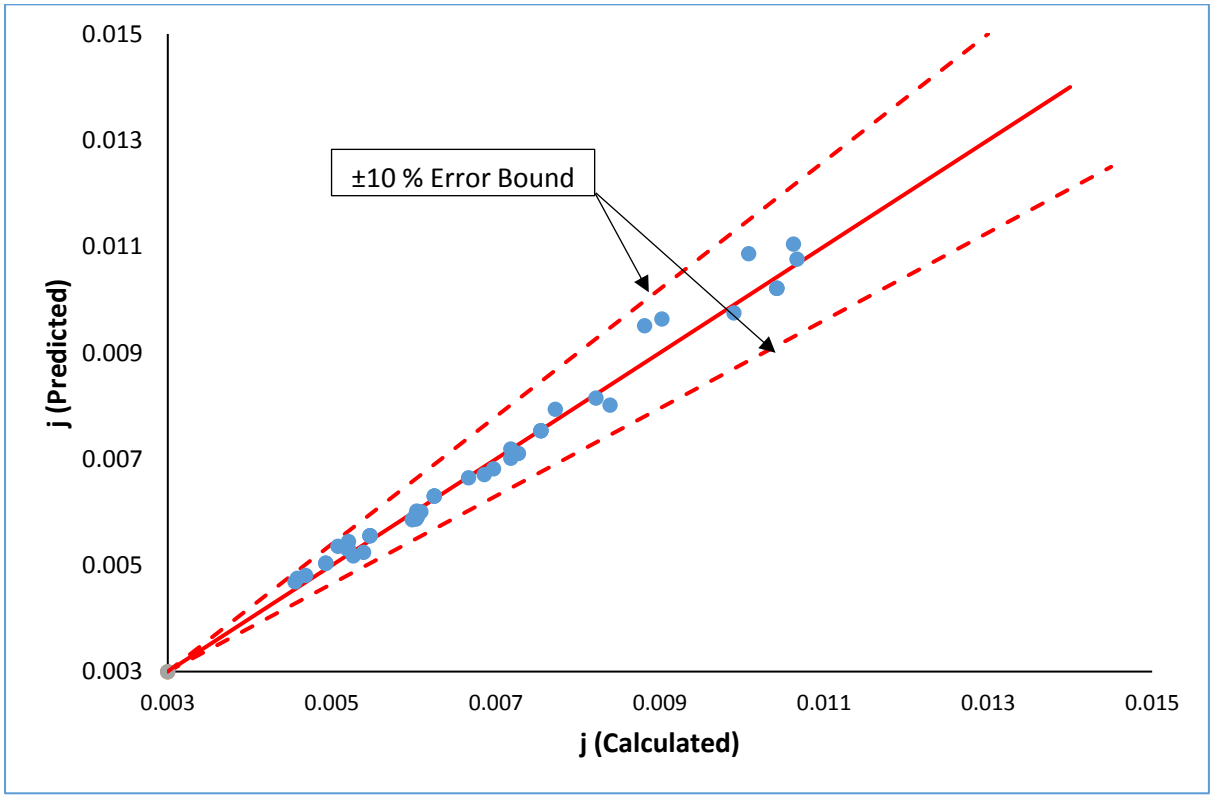

Figure 4.42 Calculated Against Predicted Values of Colburn Factor (j)

it can be seen that percentage differences between the calculated and predicted values of Colburn factor (j) and Fanning friction factor (f) are in range of less than 10%. Therefore, it can be concluded that, the developed equation (prediction model) is well capable of predicting Colburn factor (j) and Fanning friction factor (f) with a good accuracy.

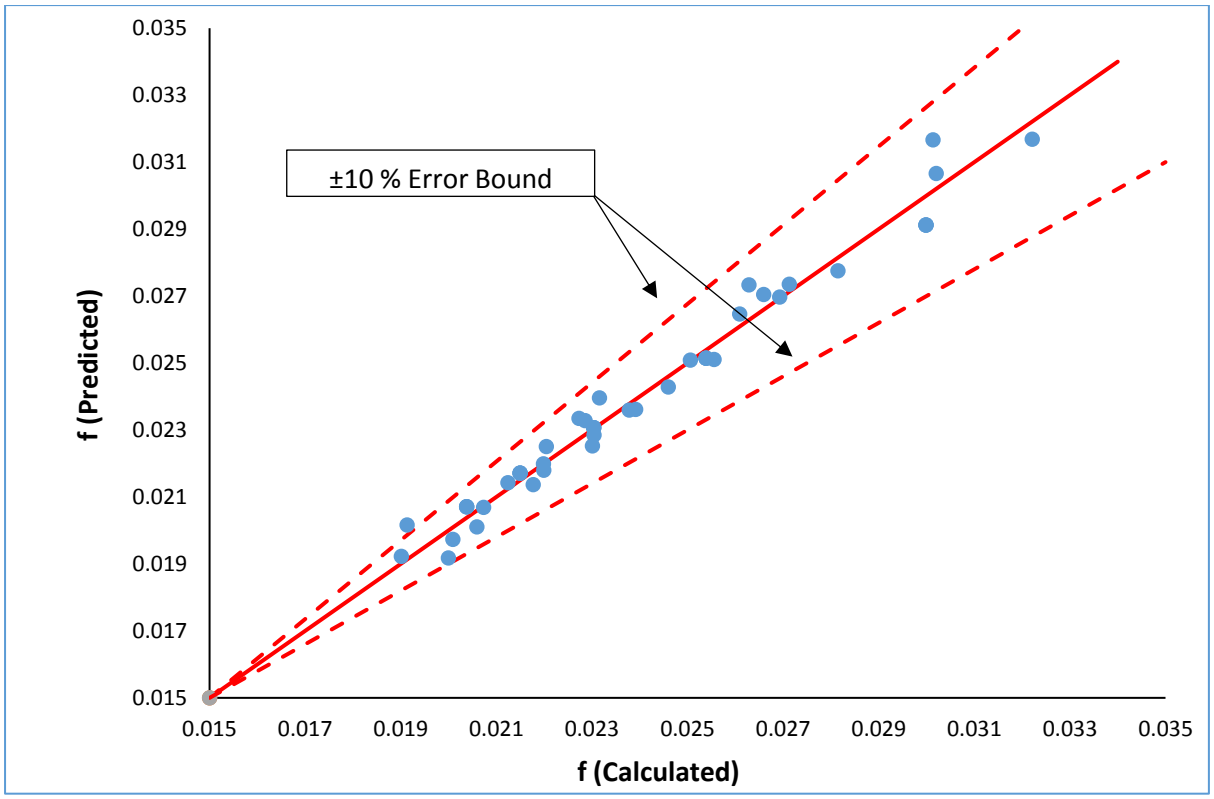

Figure 4.43 Calculated Against Predicted Values of Fanning friction factor (f)

4.8 Summary of the Analysis Carried Out on the Baseline Model

Detailed flow behaviour of working fluids within the multi-tube and fin heat exchanger having plain fins have been revealed in the following results:

- A novel CFD model for multi-tube and fin heat exchanger with a full geometry has been presented and verified against the experimental results at different operating conditions. Therefore, the numerical model can be used for further investigation with different design modifications.
- A flow field qualitative analysis has been carried out which helps to understand the forced convection phenomena happened inside this system.
- CFD has been incorporated to compute heat transfer coefficients and local fin efficiency for multi-tube and fin heat exchanger with plain fins.
- Fin spacing, longitudinal pitch and transverse pitch have a significant impact on the heat transfer and pressure drop characteristics of the heat exchanger under steady state operating condition.
- Minimising the fin spacing would enhance the heat transfer characteristics of the heat exchanger. However, it would increase the pressure drop across the heat exchanger.
- Plain fins provide the lowest possible air-side pressure drop and lowest fan power.
- A Prediction model to estimate Fanning friction factor (f) and Colburn factor (j) has been developed by taking in consideration the effects of heat exchanger geometrical parameters; fin spacing, longitudinal pitch and transverse pitch.

This chapter provides in detail information about the forced convection phenomena and behaviour of working fluids within the multi-tube and fin heat exchanger. Design modifications will be considered in the next chapter in order to enhance the heat transfer and pressure drop characteristics of the heat exchanger. This process will be carried out experimentally and numerically.

Chapter 5 **EXPERIMENTAL AND NUMERICAL INVESTIGATIONS OF DIFFERENT DESIGN CONFIGURATIONS OF HEAT EXCHANGER**

SUMMARY: In the previous chapter, validation and analysis of the baseline model for multi-tube and fin heat exchanger having plain fins under different operating conditions were carried out. This chapter focus on improving the thermal performance of the heat exchanger by employing different fin configurations. An experimental investigation has been carried out by comparing the heat transfer and pressure drop characteristics of a novel fin design (perforated plain fin) with plain and louvre fins. Moreover, a comparative numerical study of the airside thermal performance of the multi-tube and fin heat exchanger having perforated plain, louvre and perforated louvre fin has been carried out. The best thermal performance was found to be for perforated louvre fins.

5.1 Introduction

The baseline model which has been analysed in the previous chapter has plain fins. Thermal performance of the plain fins can be enhanced by using passive techniques which does not require application of any additional external power. This technique can be in form of surface or geometrical modifications of fin surfaces. This chapter deals with performance improvement of the heat exchanger used in the FCU by having different design configurations of the fins. This includes louvre and perforated fins.

The louvre fins have a surface area larger than plain fins and they are commonly used in auto industry because of their mass production manufacturability and high j and f factors compared with plain fins. In addition, proposed here perforation in the fin surfaces enhance turbulence around fins which cause an increase in the local heat transfer coefficient compared with plain fins as well as a reduction in the total weight of the heat exchanger.

In this chapter, when possible an experimental investigation has been carried out and in other cases numerical investigation, in order to evaluate the thermal performance of new fin arrangements. These investigations include:

- An experimental study to compare the thermal characteristics of multi-tube and fin heat exchanger with plain, louvre and perforated plain fins,
- A comparative numerical study of the airside performance of multi-tube and fin heat exchanger having perforated plain, louvre and perforated louvre fins,
- A numerical investigation to determine effects of the hole diameter (h_D) and hole spacing (h_S) on the heat transfer and pressure drop characteristics of the air side of the heat exchanger which has perforated louvre fins.

The results of those investigations have been used to develop the optimisation model which will discussed in the next chapter.

5.2 A Comparison of Thermal Characteristics of Multi-tube and Fin Heat Exchanger with Different Fin Arrangements

This study experimentally examines the thermal performance of a multi-tube and fin heat exchanger under steady state operating condition. The investigation has been carried out by comparing a heat exchanger having perforated plain fin, novel fin design, with plain and louvre fins heat exchangers. This study shows how the thermal performance of the baseline model can be improved by having perforations on the plain fins or using louvre fins instead of plain fins.

Moreover, this study aims to correct the novel predictions model developed in section 4.7 that can be applied on the perforated and louvre fins.

5.2.1 Heat Exchanger Model Description and Boundary Conditions

The test setup, described in chapter three, has been used in order to study the heat transfer and pressure drop characteristics of these heat exchangers. The model for heat exchanger having perforated plain fin was manufactured by punching 12 holes with 3 mm diameter in each plain fin material. Figure 5.1 depicts the heat exchanger having perforated plain fin and the distribution of the perforated holes in fin geometry.

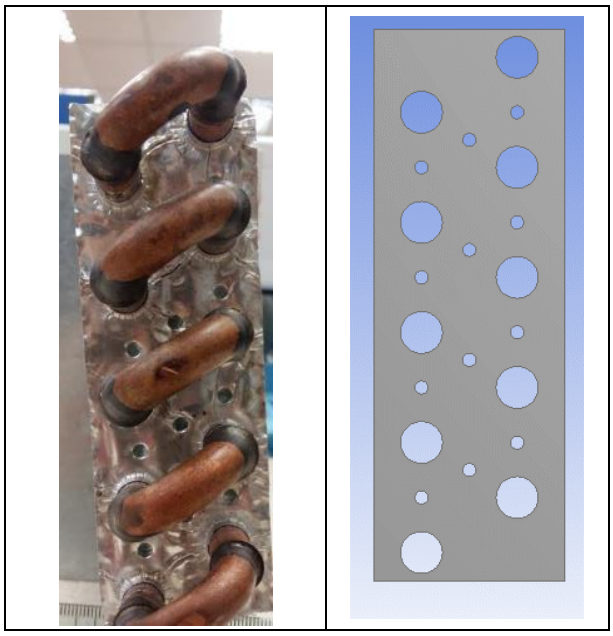

Figure 5.1 Perforated Plain Fin Heat Exchanger and Perforated Holes' Distribution in Fin Geometry

The air velocity used in this study is in the range of 0.7 to 4 m/sec which represents the velocity arithmetic mean (velocity average) of the gross cross-sectional area for airflow (face area) which is computed using the ASHRAE standard 41.2 [84] and it was reported by [85], [16]. The method for measuring air flow velocity in the experiments is described in detail in APPENDIX B. Moreover, the range for water flow rate is from 2 L/min to 6 L/min which make the flow inside the tubes fully turbulent. The detailed boundary conditions of this study are presented in Table 5-1.

Table 5-1 Boundary Conditions of Steady State Tests for the Comparative Experiential Study

Test Name	Water Side		Air Side	
	Water Flow rate (L/min)	Water Inlet Temperature (° C)	Air Velocity (m/sec)	Air Inlet Temperature (° C)
Test 1	2±0.03	60 ± 1	0.705	24 ± 1
Test 2			1.546	
Test 3			2.183	
Test 4			3.177	
Test 5			3.991	
Test 1	3±0.03	60 ± 1	0.705	24 ± 1
Test 2			1.546	
Test 3			2.183	
Test 4			3.177	
Test 5			3.991	
Test 1	4±0.03	60 ± 1	0.705	24 ± 1
Test 2			1.546	
Test 3			2.183	
Test 4			3.177	
Test 5			3.991	
Test 1	5±0.03	60 ± 1	0.705	24 ± 1
Test 2			1.546	
Test 3			2.183	
Test 4			3.177	
Test 5			3.991	
Test 1	6±0.03	60 ± 1	0.705	24 ± 1
Test 2			1.546	
Test 3			2.183	
Test 4			3.177	
Test 5			3.991	

5.2.2 Data Analysis

In this study, the temperatures of both hot water and air at inlets and outlets were measured experimentally together with the pressure drop across water and air sides. The average heat transfer rate ($\dot{Q}_{avg}$) has been computed using Eq. (4.4). Furthermore, the comparison has been carried out using Fanning friction factor (f) which symbolised the pressure drop characteristics, Colburn factor (j) which symbolised the heat transfer characteristics and the ratio between Colburn factor (j) and Fanning friction factor (f) them which is efficiency index (j/f). In addition, Fanning friction factor (f) and Colburn factor (j) were computed using the method previously described in section 4.1.2.

5.2.3 Comparison Results

Figure 5.2 depicts variations of the average heat transfer rate ($\dot{Q}_{avg}$) against air velocity for the three heat exchangers having different fin arrangements; perforated plain, plain and louvre fins at different water flow rates from 2 to 6 L/min.

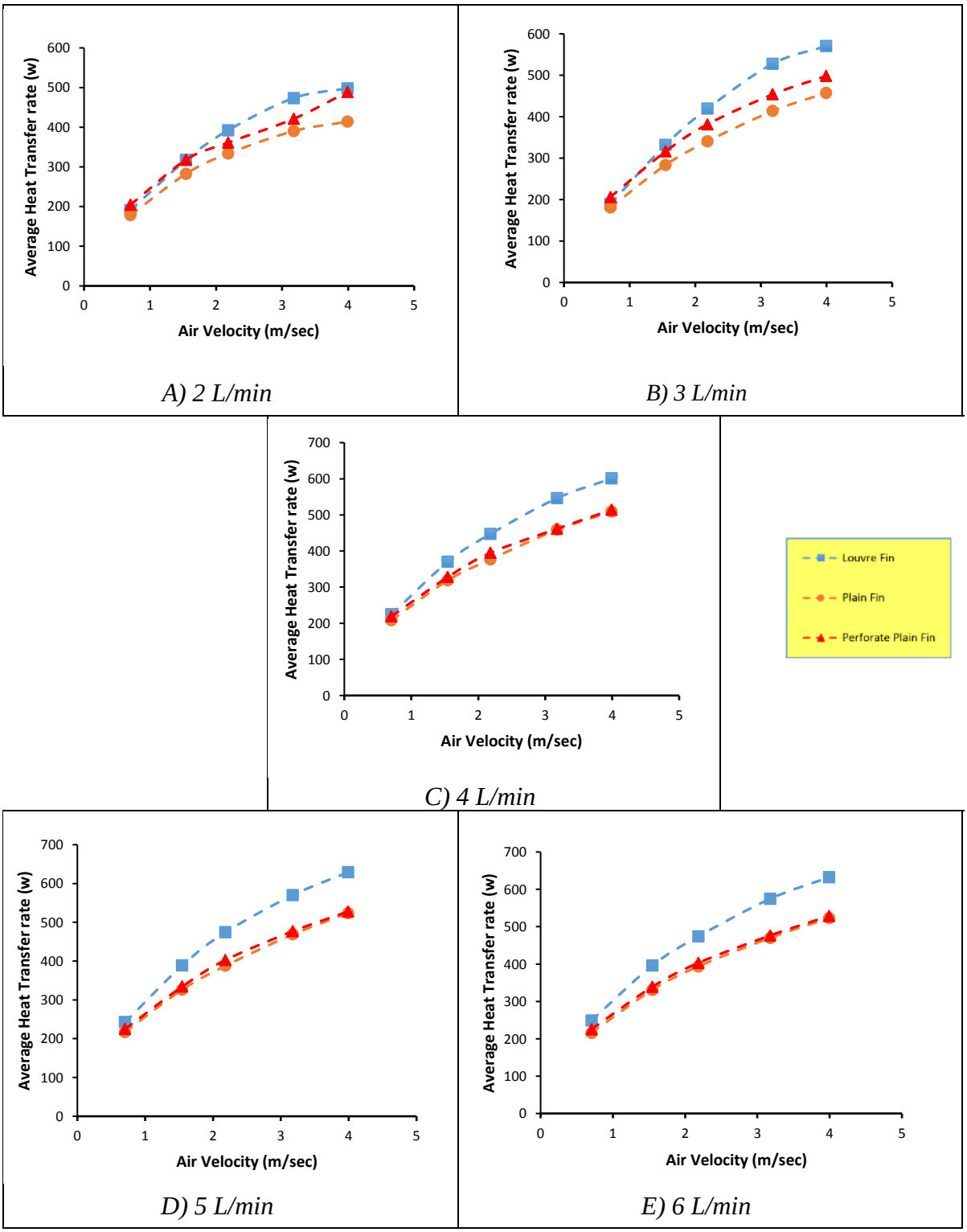

Figure 5.2 Variations of Average Heat Transfer Rate Against Air Velocity for Three Heat Exchanger with Different Fin Arrangements at Different Water Flow Rates; A) 2 L/min, B) 3 L/min, C) 4 L/min, D) 5 L/min and E) 6 L/min

Figure 5.3 illustrates variations of pressure drop per unit length across the air side against air velocity for three heat exchangers having different fin arrangements; perforated plain, plain and louvre fins at different water flow rates from 2 to 6 L/min.

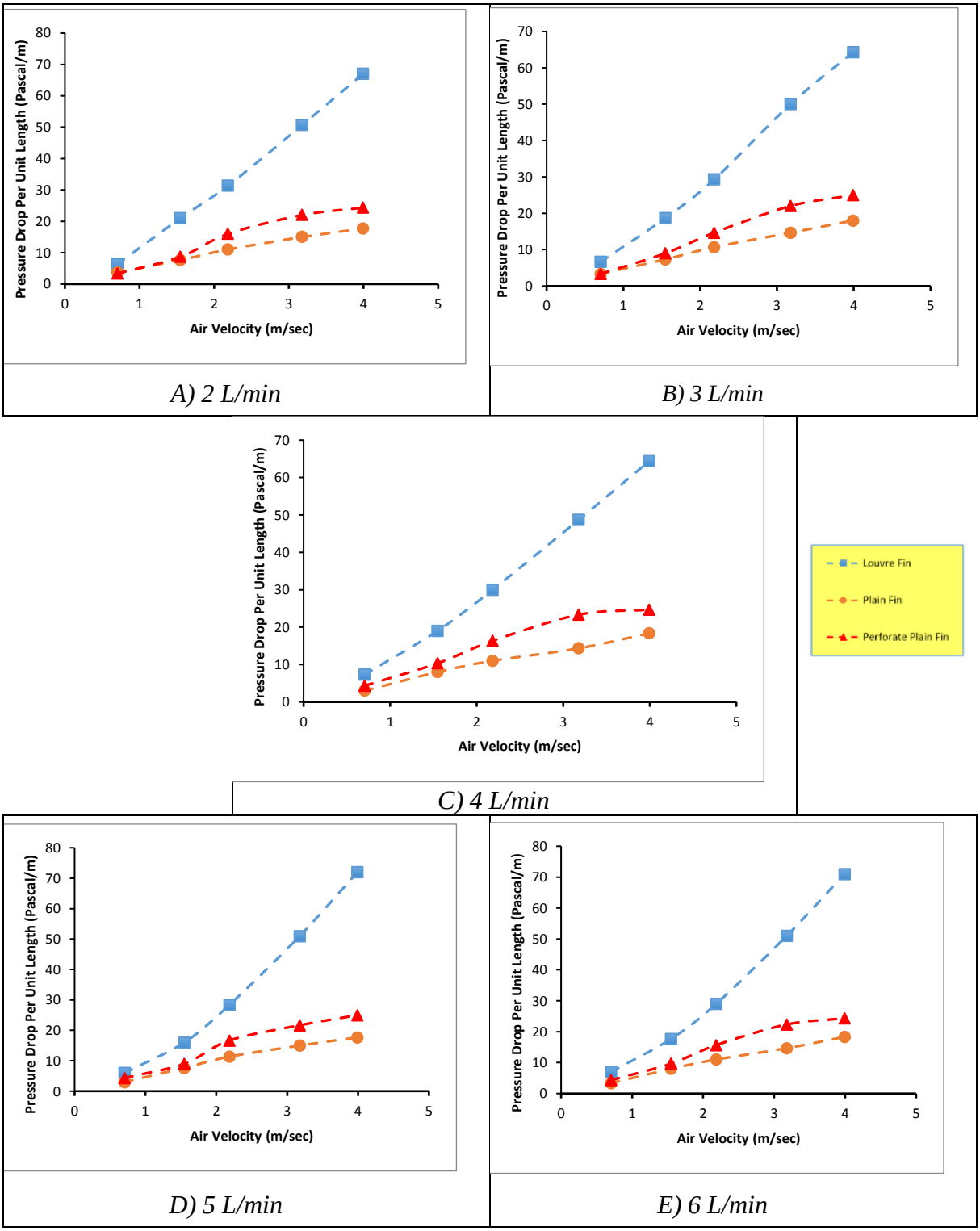

Figure 5.3 Variations of Pressure Drop Per Unit Length of the Air Side Against Air Velocity for Three Heat Exchanger with Different Fin Arrangements at Different Water Flow Rates; A) 2 L/min, B) 3 L/min, C) 4 L/min, D) 5 L/min and E) 6 L/min

From Figure 5.2 and 5.3 it can be seen that the louvre fins heat exchanger has the higher average heat transfer rate comparing with perforated plain fins and plain fins heat exchangers. The average heat transfer rate increases as the water flow rate increases. At 4 L/min water flow rate, the average increase in the average heat transfer rate for louvre fins heat exchanger is 16.95%

and 14.15% comparing with plain fins and perforated plain fins heat exchangers, respectively. However, this enhancement in the heat transfer is accompanied by a high pressure drop across the air side. Furthermore, due to the vortex generated by the holes, the perforated plain fins heat exchanger has achieved an enhancement in heat transfer characteristics when it is compared with the plain fins heat exchanger. This enhancement is small at high water flow rate and it has the disadvantage of an increase in the pressure drop. For example, at 3 L/min water flow rate, the average increase in the average heat transfer rate for perforated plain fins heat exchanger is 10.5%, this increase drop to 3.65% at 5 L/min water flow rate.

Figure 5.4 depicts the variations of friction factor (f) for three heat exchangers having different fin arrangements; perforated plain, plain and louvre fins due to a change in Reynolds number.

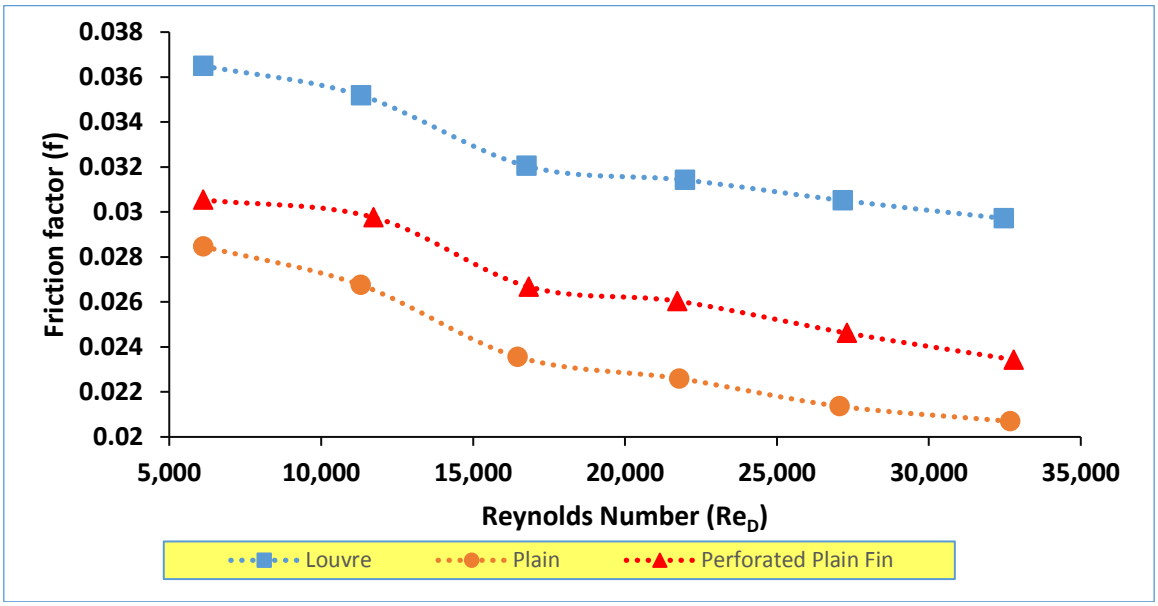

Figure 5.4 Variations of Friction Factor (f) for Different Fin Arrangements Due to a Change in Reynolds Number

Figure 5.5 depicts the variations of Colburn factor (j) for three heat exchangers having different fin arrangements; perforated plain, plain and louvre fins due to a change in Reynolds number.

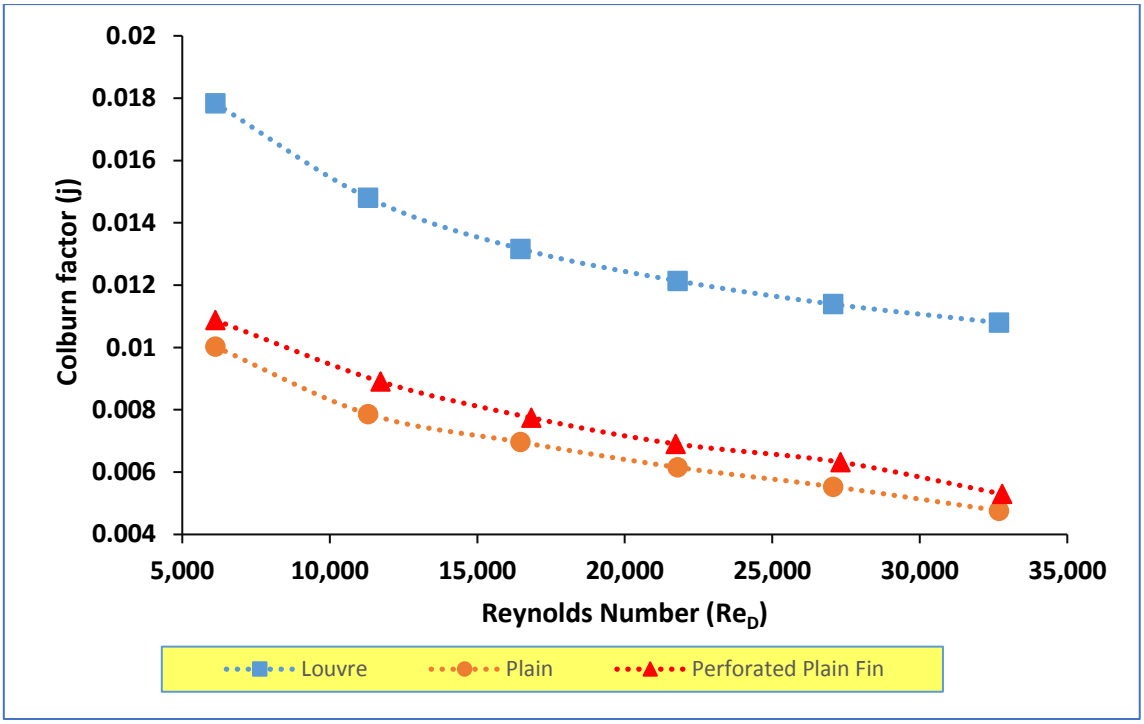

Figure 5.5 Variations of Colburn Factor (j) for Different Fin Arrangements Due to a Change in Reynolds Number

Figure 5.6 illustrates the variations of efficiency index (j/f) for three heat exchangers having different fin arrangements; perforated plain, plain and louvre fins due to a change in Reynolds number.

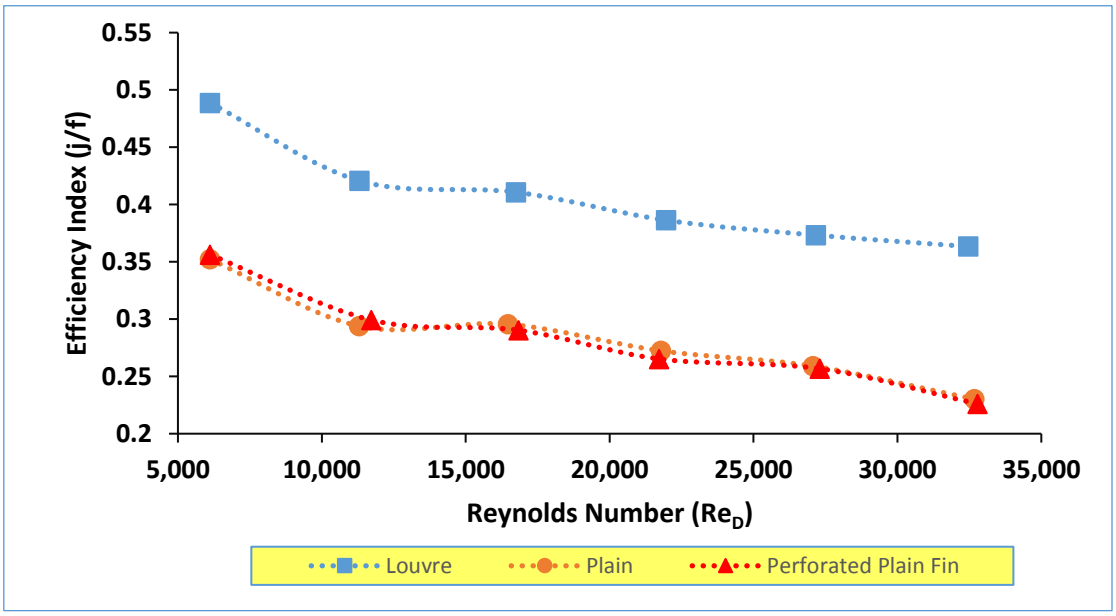

Figure 5.6 Variations of Efficiency Index (j/f) for Different Fin Arrangements Due to a Change in Reynolds Number

The plotted data in Figure 5.4, 5.5 and 5.6 reveal that, as Reynolds number is increased, friction factor (f), Colburn factor (j) and efficiency index (j/f) tend to decrease for all the three heat exchangers. Moreover, high Colburn factor (j) and friction factor (f) for the louvre fins heat exchanger are observed comparing with perforated plain fins and plain fins heat exchangers. This can be explained by, as the surface area of louvre fin is larger than the plain fin and perforated plain, this fact results an increase in the heat transfer coefficient which lead to high Colburn factor (j). Nevertheless, the friction factor (f) of the heat exchanger with louvre fins has increased due to louvre arrangement in the louvre fin shape.

The results of this study showed that an average improvement in the average heat transfer rate ($\dot{Q}_{avg}$) by 8% and 18% for the perforated plain fins and louvre fins heat exchanger, respectively when they were compared with the plain fins heat exchanger. However, this improvement was accompanied with an increase in the pressure drop across the air-side by 35% and 180%, respectively. The data for this study has been used to develop a novel semi-empirical prediction model for Fanning friction factor (f) and Colburn factor (j) as a function of Reynolds number, fins total surface area and total heat transfer surface area of the heat exchanger.

5.2.4 Development of Novel Semi-Empirical Prediction Model for computing Fanning friction factor (f) and Colburn factor (j)

The results which have been obtained in the previous experimental study were implemented to develop a novel semi-empirical prediction model for Fanning friction factor (f) and Colburn factor (j). As it has been stated before, Fanning friction factor (f) and Colburn factor (j) are representing the pressure drop heat transfer characteristics, respectively. Therefore, it is important to develop a prediction model to correlate them. The correlation has been carried out using multiple variable regression analysis. In addition, Fanning friction factor (f) and Colburn factor (j) were computed using the method previously described in section 4.1.2. the dimensionless geometric parameters used to develop the prediction model are (Re_D) Reynolds number and the ratio between fins total surface area and total heat transfer surface area of the heat exchanger $\left({A_f}/{A_t}\right)$

These novel equations are shown below,

$$j = 10^{4.595}\left({A_f}/{A_t}\right)^{29.918} {Re_D}^{-0.374} \quad (5.1)$$

$$f = 10^{1.203} \left({A_f}/{A_t}\right)^{12.811} {Re_D}^{-0.139} \quad (5.2)$$

where,

j is Colburn factor

f is Fanning friction factor

Re_D is Reynolds number

D_c is fin collar outside diameter (m)

A_f is the fins total surface area (m^2)

A_t is the total heat transfer surface area of the heat exchanger (m^2)

These equations for predicting both Fanning friction factor (f) and Colburn factor (j) are applicable only to multi-tube and fin heat exchanger with different fin arrangements in a heating condition and for forced convection heat transfer.

The correlation coefficient values between calculated and predicted data for Eqs. (5.1) and (5.2) are 0.853 and 0.811, respectively. Based on the above information it can be concluded that the developed prediction model shows no significant difference to the available. Therefore, this prediction models developed can be used during the design process of multi-tube and fin heat exchanger having louvre and perforated fins.

Figure 5.7 and 5.8 depict the relation between the calculated values and the predicted values of Colburn factor (j) and Fanning friction factor (f), respectively.

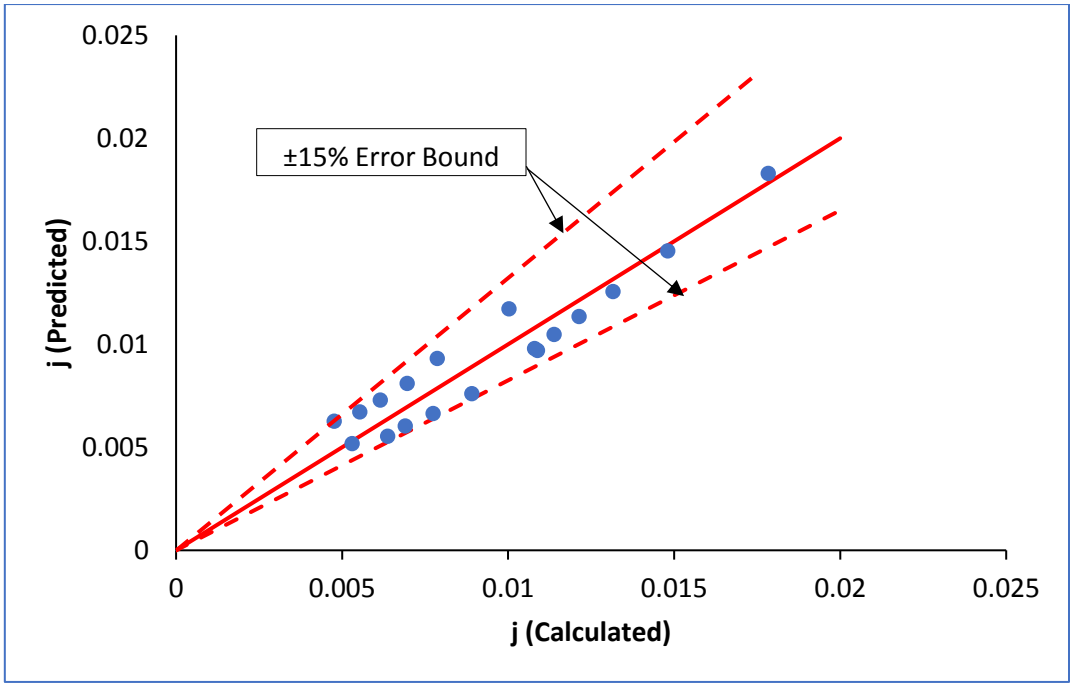

Figure 5.7 Calculated Against Predicted Values of Colburn Factor (j)

it can be seen that the percentage difference between the calculated and predicted values of Colburn factor (j) and Fanning friction factor (f) are in range of less than 15%. Therefore, it can be concluded that, the developed equation is well capable of predicting Colburn factor (j) with a good accuracy.

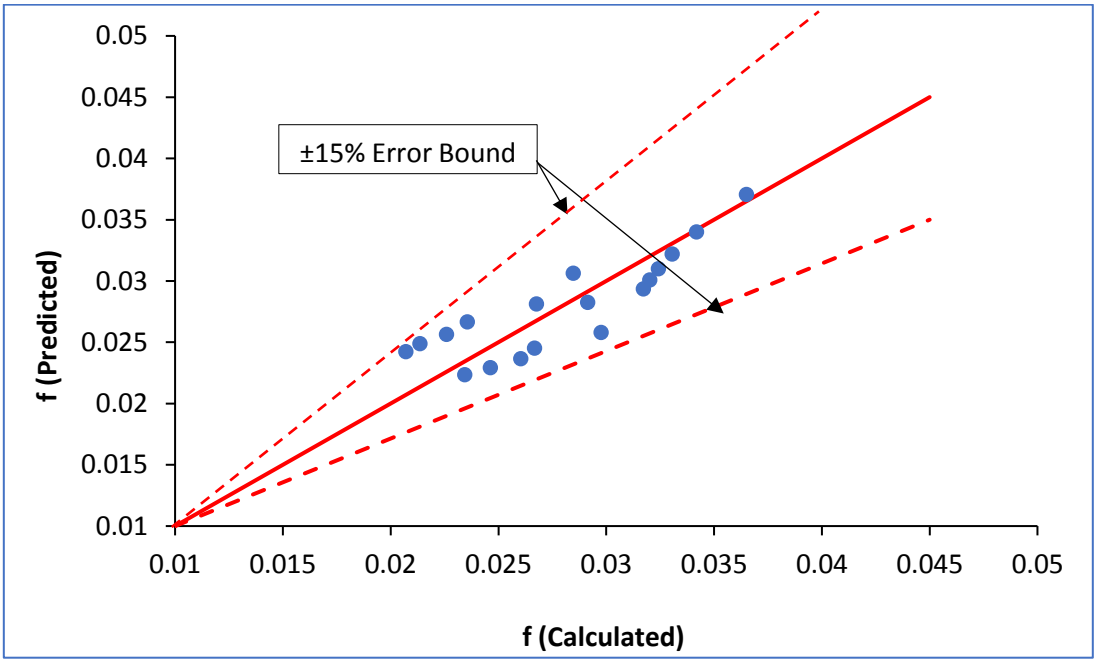

Figure 5.8 Calculated Against Predicted Values of Fanning friction factor (f)

5.2.5 Combined Prediction Models

The prediction model previously developed in section 4.7 has a limited use because it is developed based on the baseline model geometry. i.e. heat exchanger with plain fins. Therefore, a correction factors have been presented in this section in order to correct the predicted values of Fanning friction factor (f) and Colburn factor (j) by combining the values computed using the Prediction model developed in section 4.7 with the Prediction model developed in section 5.2.4. By doing this combination, the new prediction models can be used to predict Fanning friction factor (f) and Colburn factor (j) for a heat exchanger with either louvre or perforated fins. Corrections factors for Fanning friction factor (f) and Colburn factor (j) for perforated plain heat exchanger are 1.06 and 1.03, respectively. Hence, the corrected prediction model equations for a heat exchanger with perforated plain fins are:

$$f = 0.0186\ Re_D^{-0.212} \left(F_p/D_c\right)^{-0.659} \left(L_p/F_w\right)^{-0.884} \left(T_p/F_H\right)^{-0.829} \tag{5.3}$$

$$j = 0.0482\ Re_D^{-0.439} \left(F_p/D_c\right)^{-0.413} \left(L_p/F_w\right)^{-0.819} \left(T_p/F_H\right)^{-1.001} \tag{5.4}$$

Similarly, corrections factors for Fanning friction factor (f) and Colburn factor (j) for louvre fins heat exchanger are 1.21 and 1.56, respectively. Hence, the corrected prediction model equations for a heat exchanger with louvre fins are:

$$f = 0.0212\ Re_D^{-0.212} \left(F_p/D_c\right)^{-0.659} \left(L_p/F_w\right)^{-0.884} \left(T_p/F_H\right)^{-0.829} \tag{5.5}$$

$$j = 0.073\ Re_D^{-0.439} \left(F_p/D_c\right)^{-0.413} \left(L_p/F_w\right)^{-0.819} \left(T_p/F_H\right)^{-1.001} \tag{5.6}$$

The novel combined prediction models can be used to predict Fanning friction factor (f) and Colburn factor (j) for different fin configurations. Thus, it can be used as a prediction tool in the design process of multi-tube and fin heat exchanger as they contain wide range of geometrical parameters.

5.3 Comparative Numerical Study of the Airside Performance

In this section, a comparative numerical study of the airside performance of multi-tube and fin heat exchanger under steady operating condition having perforated plain, louvre and perforated louvre fins has been carried out. All the heat exchangers used in this study have the same fin

geometry, i.e. 125 mm height, 43 mm width and 0.12 mm thickness. Figure 5.9 depicts fins shapes used in this study.

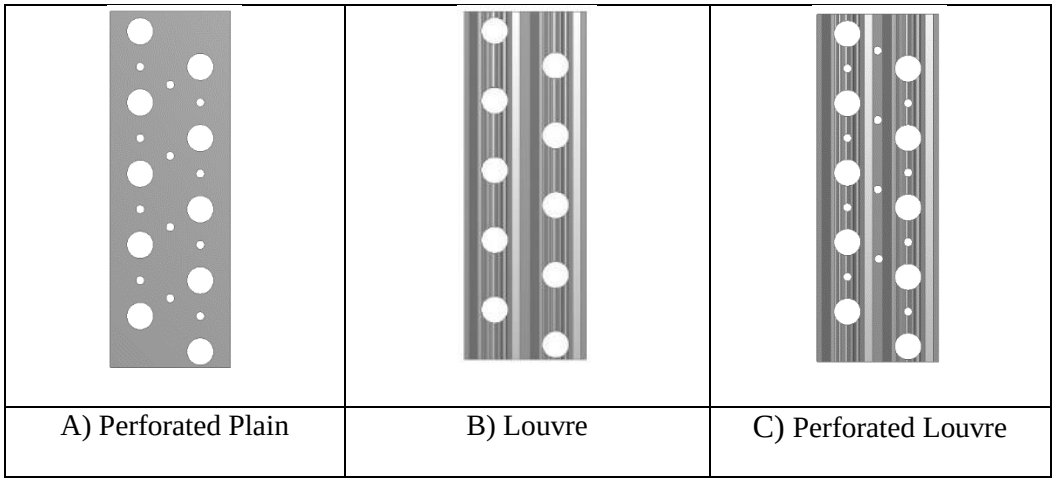

A) Perforated Plain	B) Louvre	C) Perforated Louvre

Figure 5.9 Type of fins A) Perforated Plain, B) Louvre and C) Perforated Louvre

CFD simulations have been run for different air velocity in range between 1 and 5 m/sec, whereas the water velocity was kept constant at 1 m/sec. The detailed boundary conditions of this study are shown in Table 5-2. Moreover, the simulations have been carried out for two different fin spacings of 3.7 mm and 4.2 mm.

Table 5-2 Boundary Conditions of Steady State Tests for the Comparative Numerical Study

Test Name	**Water Side**		**Air Side**	
	Water Velocity (m/sec)	Water Inlet Temperature (° C)	Air Velocity (m/sec)	Air Inlet Temperature (° C)
Test 1	1	60	1	25
Test 2			2	
Test 3			3	
Test 4			4	
Test 5			5	

The method developed in section 4.5; incorporate the novel CFD model to predict heat transfer coefficients and local fin efficiency, has been implemented to compare the air side thermal performance of the heat exchangers used in this study. The comparison has been carried out in terms of air side average heat transfer coefficient, average fins efficiency and air side pressure drop per unit length.

Figure 5.10 and 5.11 depict the variations of the air side average heat transfer coefficient with air velocity for different fin arrangements at 3.7 mm and 4.2 mm fin spacing, respectively.

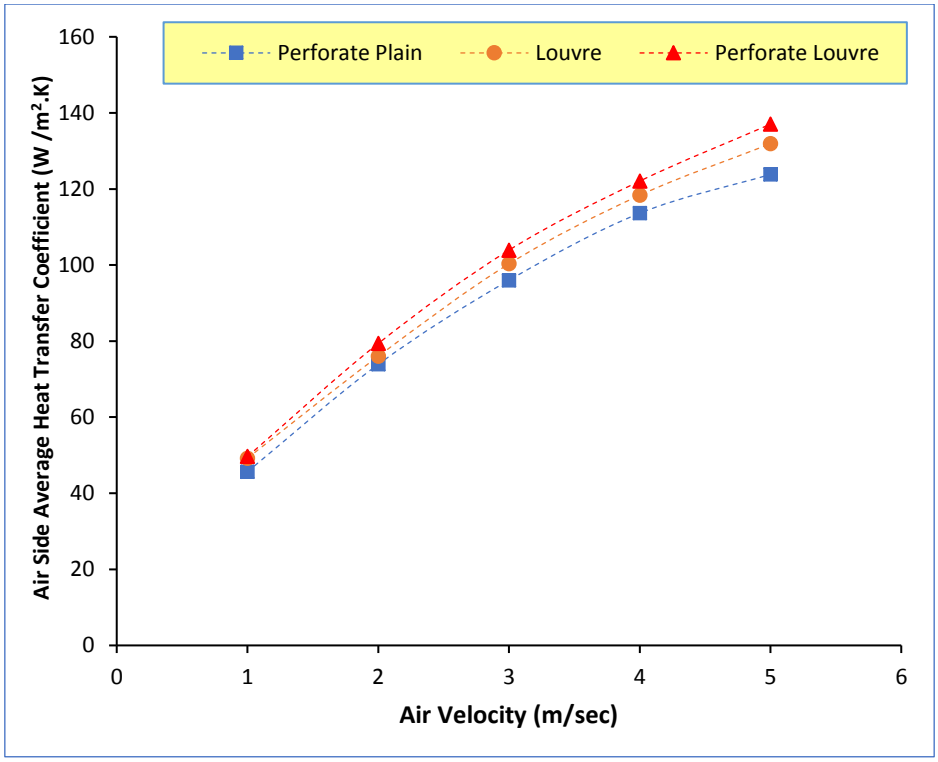

Figure 5.10 Variations of the Air Side Average Heat Transfer Coefficient with Air Velocity for Different Fin Arrangements at 3.7 mm Fin Spacing

Figure 5.10 and 5.11 showed that the air side average heat transfer coefficient for perforated louvre fin geometry is higher than those of perforated plain and louvre fin geometry for both fin spacings. Moreover, the values of air side average heat transfer coefficient of 3.7 mm fin spacing are higher than those at 4.2 mm, for all fin types. This is due to a decrease in fin spacing which result an enhancement in heat transfer characteristics as it was discussed in section 4.6.1.

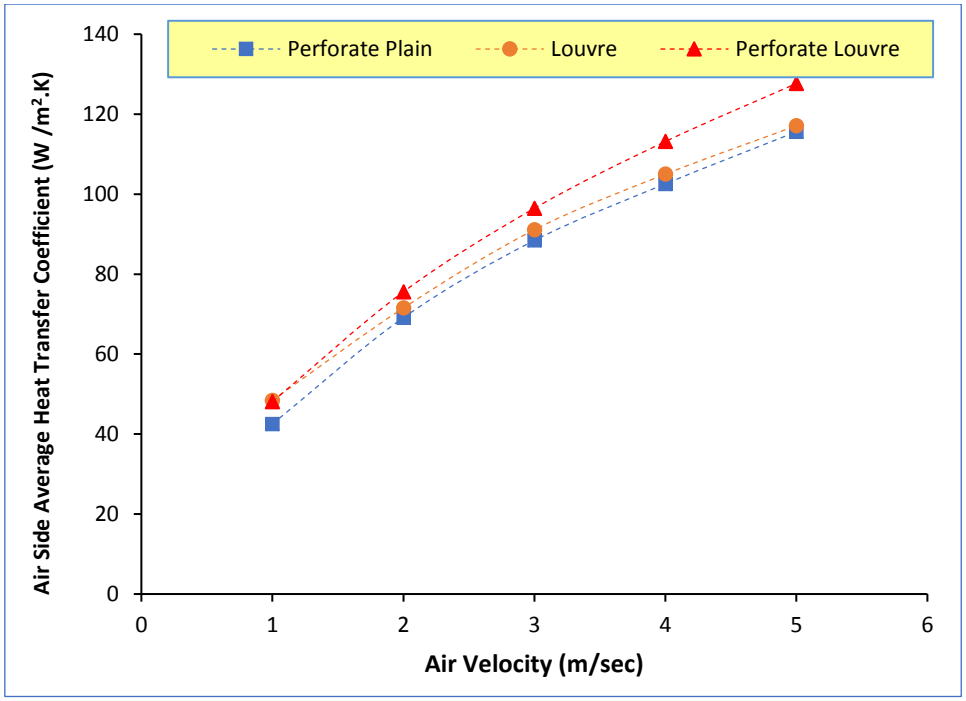

Figure 5.11 Variations of the Air Side Average Heat Transfer Coefficient with Air Velocity for Different Fin Arrangements at 4.2 mm Fin Spacing

Figure 5.12 and 5.13 illustrate the variations of the average fins efficiency with air velocity for different fin arrangements at 3.7 mm and 4.2 mm fin spacing, respectively.

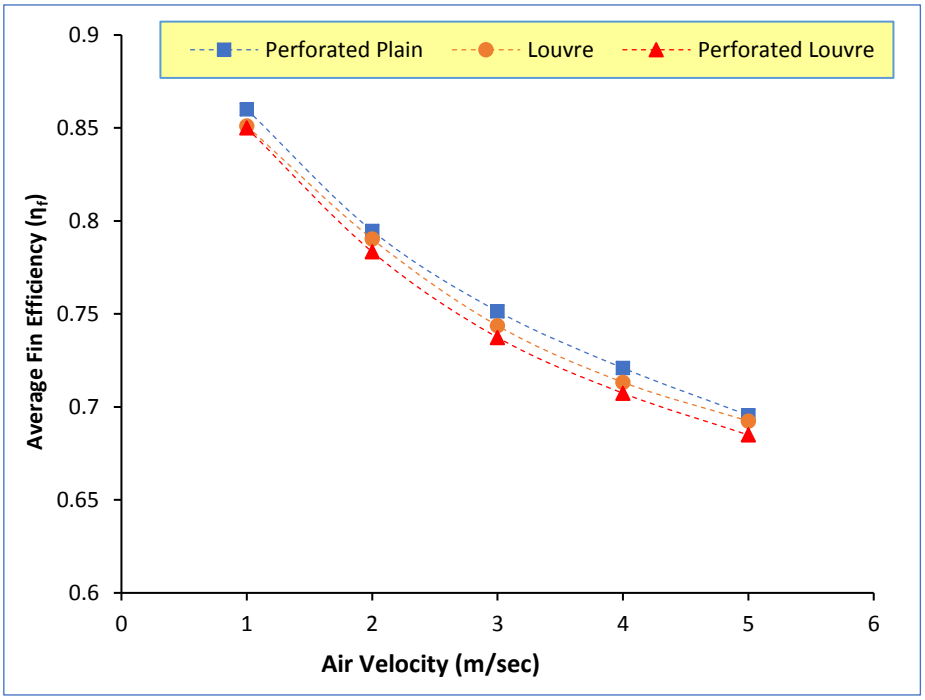

Figure 5.12 Variation of the Average Fins Efficiency with Air Velocity for Different Fin Arrangements at 3.7 mm Fin Spacing

The results in Figure 5.12 and 5.13 depict that the average fins efficiency decreases with the increase in fin pitch. In addition, the average fins efficiency is higher for plain fin geometry

than those of louvre and perforated louvre fin geometry for both fin pitch. This is due to low air side average heat transfer coefficient for plain fins which result high average fins efficiency.

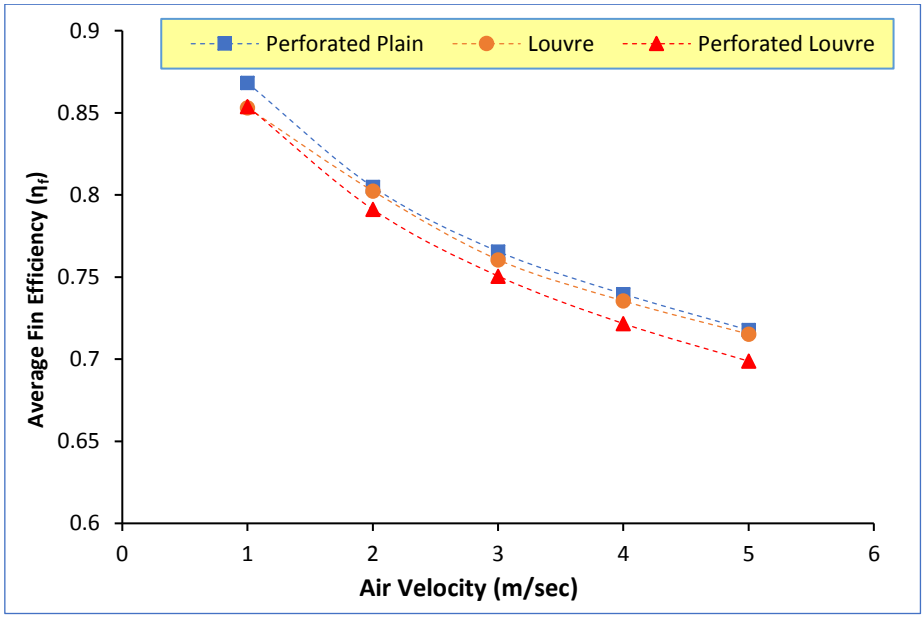

Figure 5.13 Variation of the Average Fin Efficiency with Air Velocity for Different Fin Arrangements at 4.2 mm Fin Spacing

The variations of the air side pressure drop per unit length with air velocity for different fin arrangements at 3.7 mm and 4.2 mm fin spacing are depicted in Figure 5.14 and 5.15, respectively.

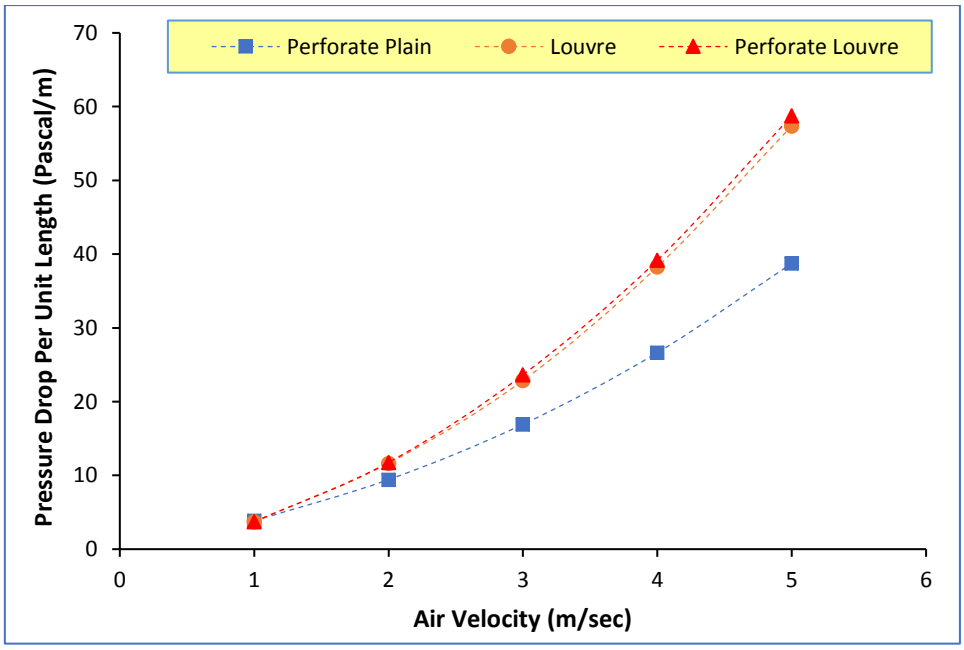

Figure 5.14 Variation of the Average Fin Efficiency with Reynolds Number for Different Fin Arrangements at 4.2 mm Fin Spacing

From both figures, the pressure drop per unit length across the airside is lowest for plain fin geometry than those of louvre and perforated louvre generator fin geometry for both fin pitch.

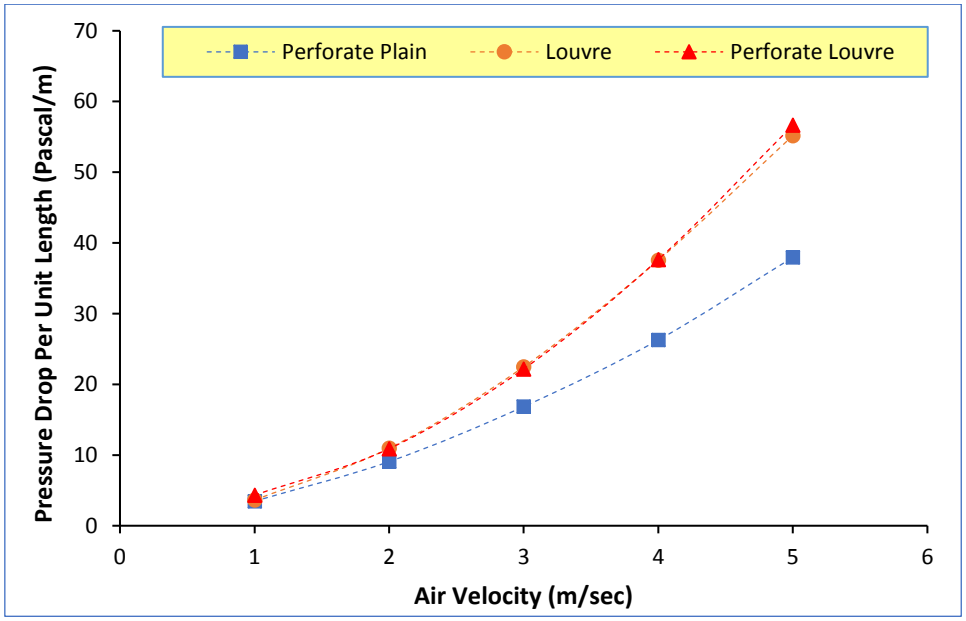

Figure 5.15 Variations of the Air Side Pressure Drop Per Unit Length with Air Velocity for Different Fin Arrangements at 4.2 mm Fin Spacing

Generally, the pressure drop decreases with the increase of fin pitch. The results obtained in this section have a good agreement with the experimental investigation carried out by [37] where authors carried out an experimental study of the air side performance of fin and tube heat exchangers having plain, louver, and semi-dimple vortex generator configuration to investigate the effect of fin spacing on the thermal performance of the heat exchanger.

5.4 Effect of Geometrical Parameters of Perforated Louvre Fins

As it was shown in the earlier section, the thermal performance of perforated louvre fins heat exchanger has improved comparing with plain and louvre fins heat exchanger. In this study, the multi-tube and fin heat exchanger which has perforated louvre fins has been numerically investigated for the effects of hole diameter (h_D) and hole spacing (h_S) on the heat transfer and pressure drop characteristics of the air side of the heat exchanger under steady state operating condition. Figure 5.16 depicts the geometrical details of the perforated louvre fin and the geometrical parameters which will be investigated in this study where D, F_H and F_W are tube outside diameter, fin height and fin width, respectively.

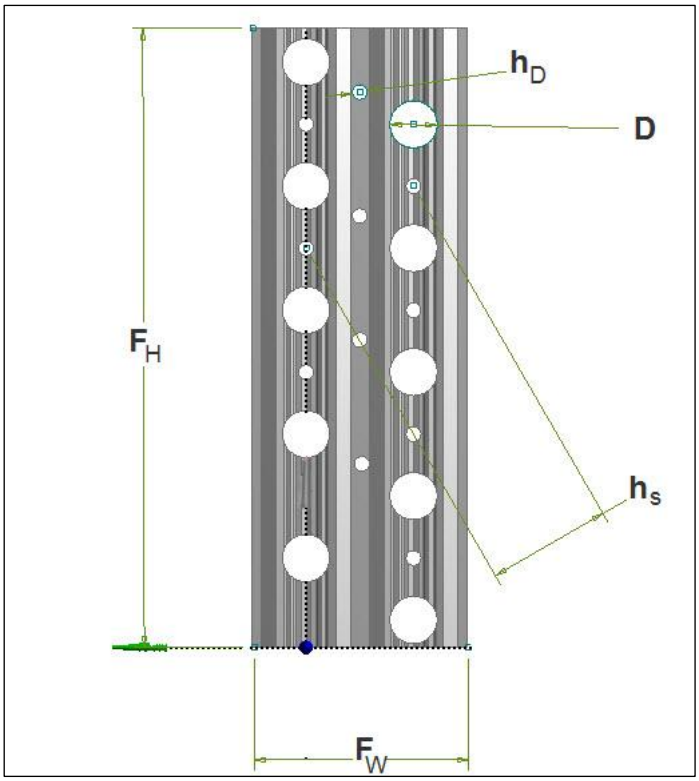

Figure 5.16 Geometrical Details of the Perforated Louvre Fin

In this parametric study, three different cases are considered for specific geometric parameters; h_D and h_S. These cases considered in this parametric study are tabulated in Table 5-3 where case II represents the baseline model.

Table 5-3 Cases Considered in the Parametric Study

Parameter	**Case I**	**Case II**	**Case III**
Hole Diameter (h_D) *mm*	4.5 (D/2)	3 (D/3)	2.25 (D/4)
Hole Spacing (h_S) *mm*	15	25	35

The boundary conditions of the present study are shown in Table 5-4. For each geometrical parameter, CFD simulations were carried out to show the response of the heat exchanger as the air velocity is varying.

Table 5-4 Boundary Conditions of Steady State Tests for Parametric Study

Test Name	*Water Side*		*Air Side*	
	Water Velocity (m/sec)	*Water Inlet Temperature (^{o} C)*	*Air Velocity (m/sec)*	*Air Inlet Temperature (^{o} C)*
Test 1	*1*	*60*	*1*	*25*
Test 2			*2*	
Test 3			*3*	
Test 4			*4*	
Test 5			*5*	

5.4.1 Effect of Hole Diameter (h_D)

As described in the previous section, three different hole diameters were chosen to carry out this study; D/2=4.5 mm, D/3=3 mm and D/4=2.25 mm. Table 5-5 illustrations the different fins used to build the CFD models to carry out this study.

Table 5-5 Different Hole Diameter Fins

4.5 mm (D/2)	*3 mm (D/3)*	*2.25 mm (D/4)*
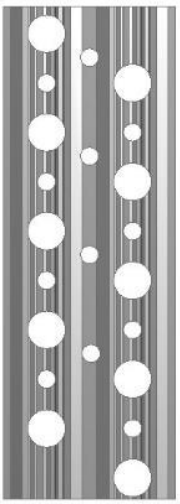	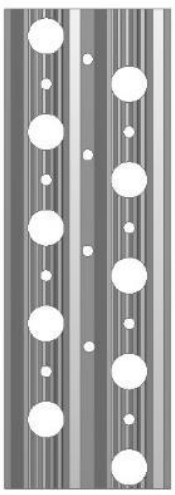	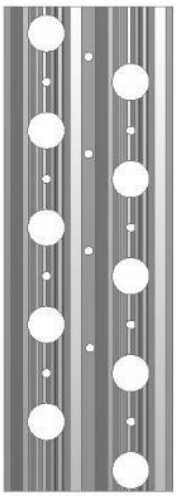

Figure 5.17 and 5.18 depict variations of average heat transfer rate and pressure drop per unit length across the air side due to a change in air velocity and at different hole diameter D/2, D/3 and D/4, respectively.

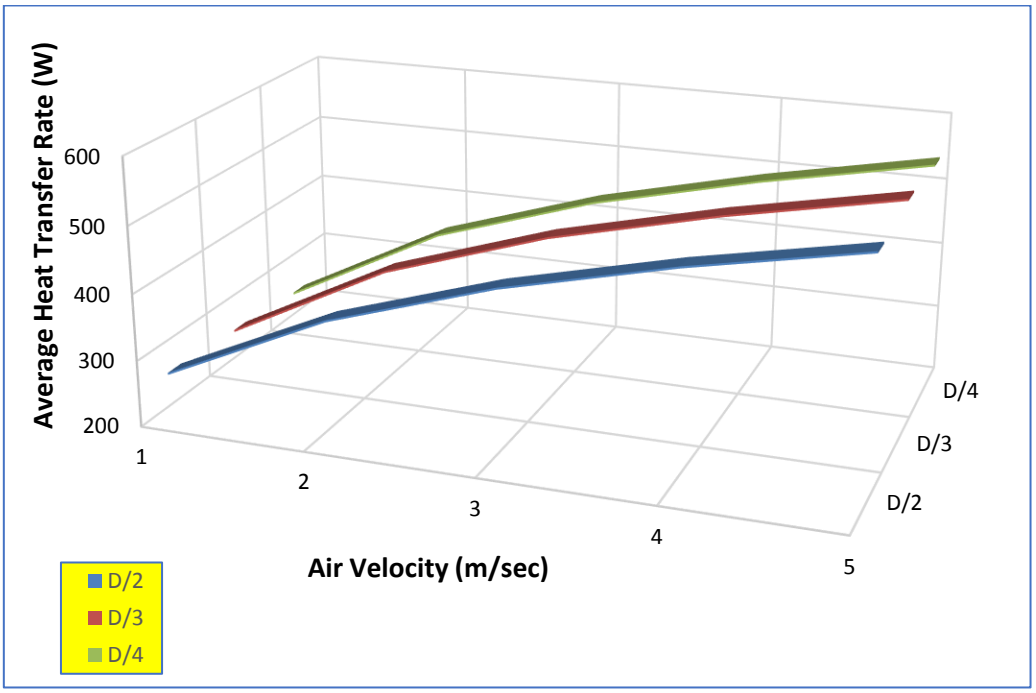

Figure 5.17 Average Heat Transfer Rate Versus Air Velocity at Different Hole Diameter

In Figure 5.17, the average heat transfer rate of heat exchangers varies between 240 and 560 Watts. As a general response, the average heat transfer rate of heat exchangers of the heat exchanger increases as the air velocity increases. Additionally, an increase of the average heat transfer rate of heat exchangers can be observed for model with D/3-hole diameter especially at low air velocity; 3% and 6.5% comparing with D/2 and D/4-hole diameter models, respectively.

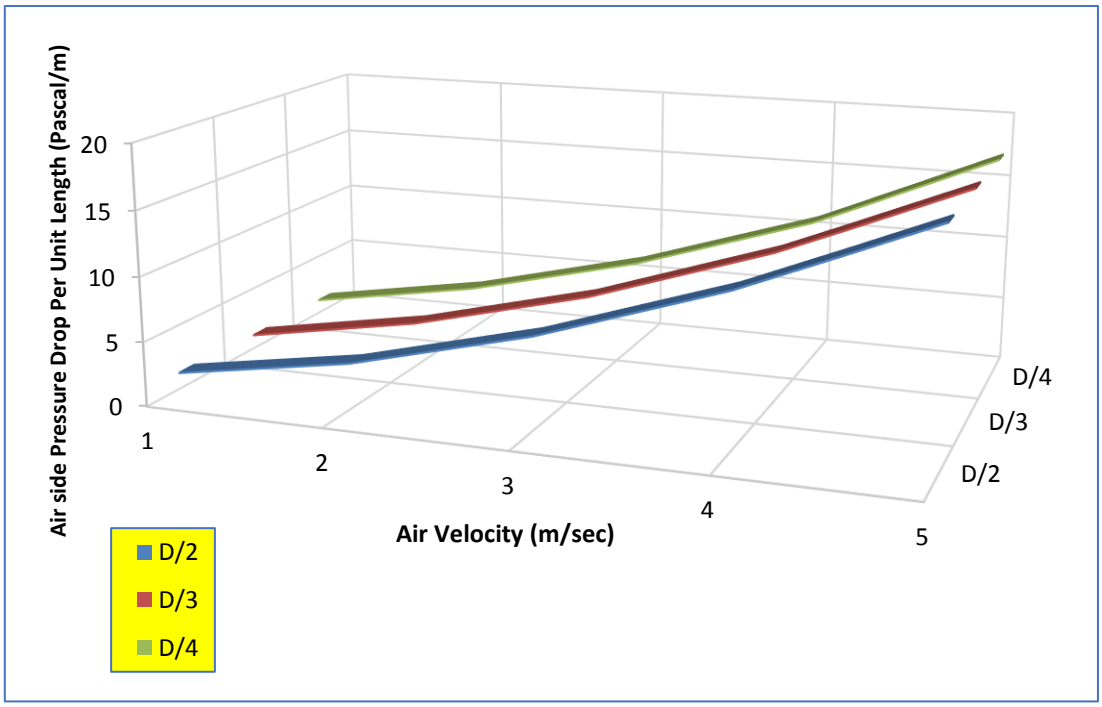

Figure 5.18 Air side Pressure Drop Per Unit Length Versus Air Velocity at Different Hole Diameter

As it can be seen from Figure 5.18, the pressure drop per unit length for D/3-hole diameter model is higher comparing with D/2 and D/4-hole diameter models. For example, at air velocity equal to 5 m/sec, the pressure drop per unit length for D/3-hole diameter has increased 0.5% and 1% comparing with D/2 and D/4-hole diameter models.

Contours of temperature variation in mid-section (x-axis) of the heat exchanger due to change in air velocity under steady state operating condition at different hole diameter are shown in Table 5-6. For effective comparison purposes, the scale of the contours has been kept constant. The air side temperature differences (ΔT_a) for the D/3-hole diameter model are higher comparing with D/2 and D/4-hole diameter models, the average of increase in temperature differences (ΔT_a) for the D/2-hole diameter model are 1.46% and 5.12%, respectively.

Table 5-6 Contours of Temperature Variation in mid-section (X-axis) of the Heat Exchanger Due to Change in Air Velocity under Steady State Operating Condition at Different Hole Diameter

Hole Diameter	*4.5 mm (D/2)*	*3 mm (D/3)*	*2.25 mm (D/4)*	*Legend*
	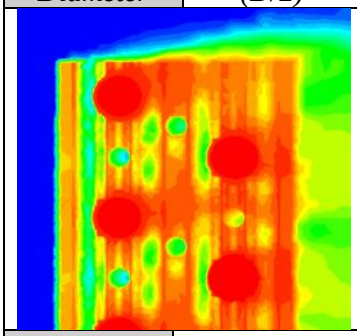	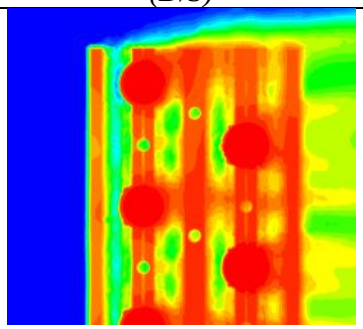	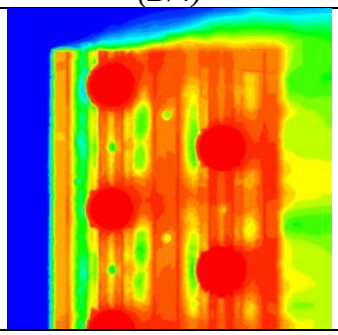	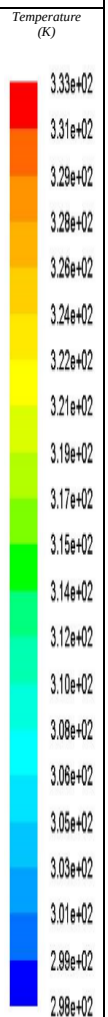
V_a=1 m/sec	ΔT_a=8.01° C	ΔT_a=8.1° C	ΔT_a=7.5° C	
	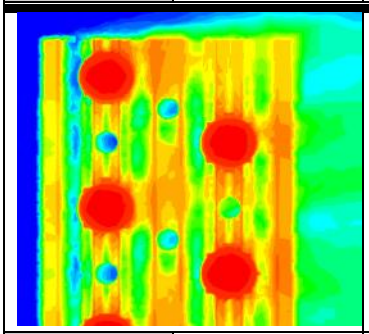	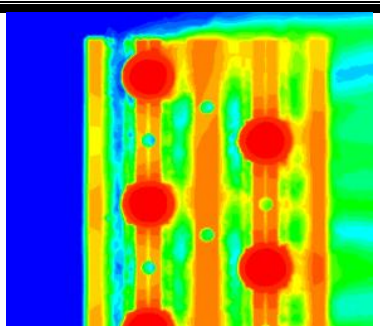	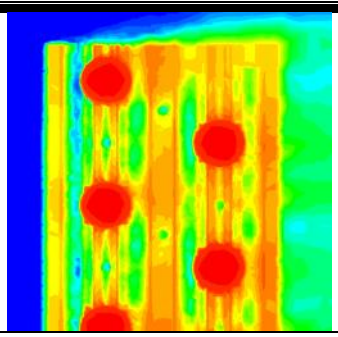	
V_a=3 m/sec	ΔT_a=4.84° C	ΔT_a=5.0° C	ΔT_a=4.8° C	
	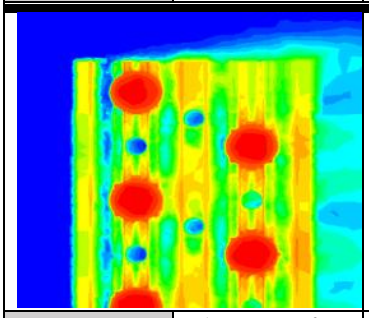	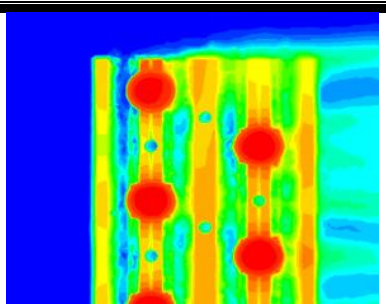	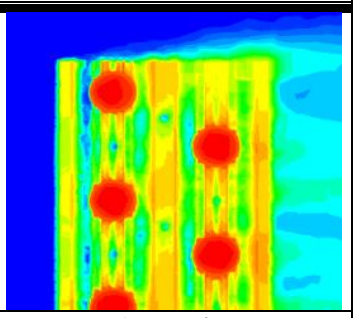	
V_a=5 m/sec	ΔT_a= 3.62 ° C	ΔT_a=3.7°C	ΔT_a=3.6° C	

5.4.2 Effect of Hole Spacing (hs)

The following section of this chapter will illustrate the effect of hole spacing on the thermal performance of the air side of the multi-tube and fin heat exchanger which has perforated louvre fins. Three different hole spacings were chosen to carry out this study; 15 mm, 25 mm and 35 mm. Details of the different fins used to build up the CFD models to carry out this study are shown in Table 5-7.

Table 5-7 Different Hole Spacing Fins

15 mm	*25 mm*	*35 mm*
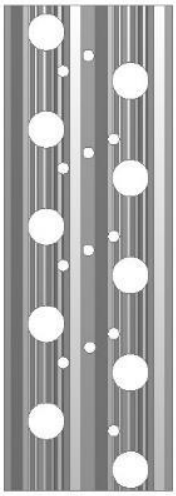	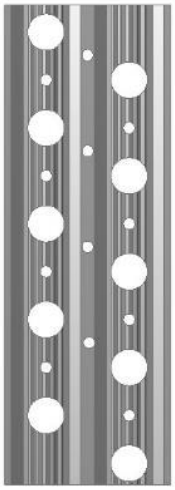	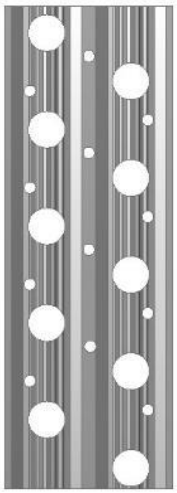

Variations of the average heat transfer rate due to a change in air velocity and at different hole spacings; 15mm, 25mm and 35mm, respectively is depicted in Figure 5.19.

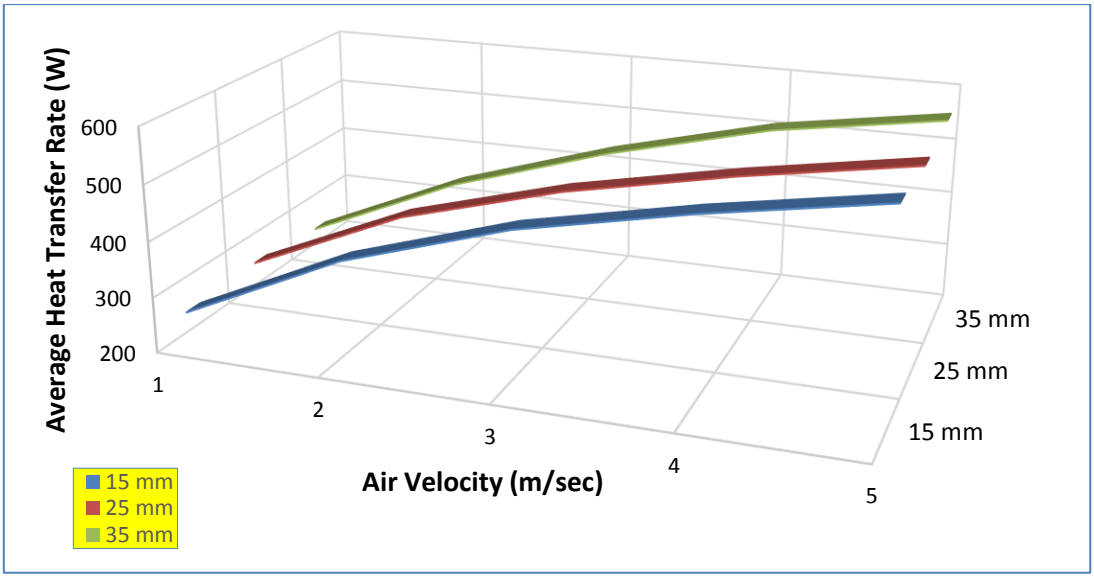

Figure 5.19 Average Heat Transfer Rate Versus Air Velocity at Different Hole Spacings

From Figure 5.19, the average heat transfer rate for the air side used in the present study increases as the air velocity goes higher. Additionally, at a constant air velocity of 3 m/sec, and when the hole spacing is changing from 25 mm to 15 mm and 25 mm to 35 mm, the average heat transfer rate for the air side decrease 2.52% and 2.84%, respectively. Therefore, a higher heat transfer rate is observed for the heat exchanger model with 25 mm hole spacing.

Figure 5.20 illustrates the variation of pressure drop across the air side of the heat exchanger at different hole spacings; 15mm, 25mm and 35mm, respectively. It can be seen that the pressure drop per unit length increases as the air velocity is increased. Moreover, it can be observed that at 25 mm hole spacing has a higher pressure drop per unit length which is a disadvantage of high heat transfer rate.

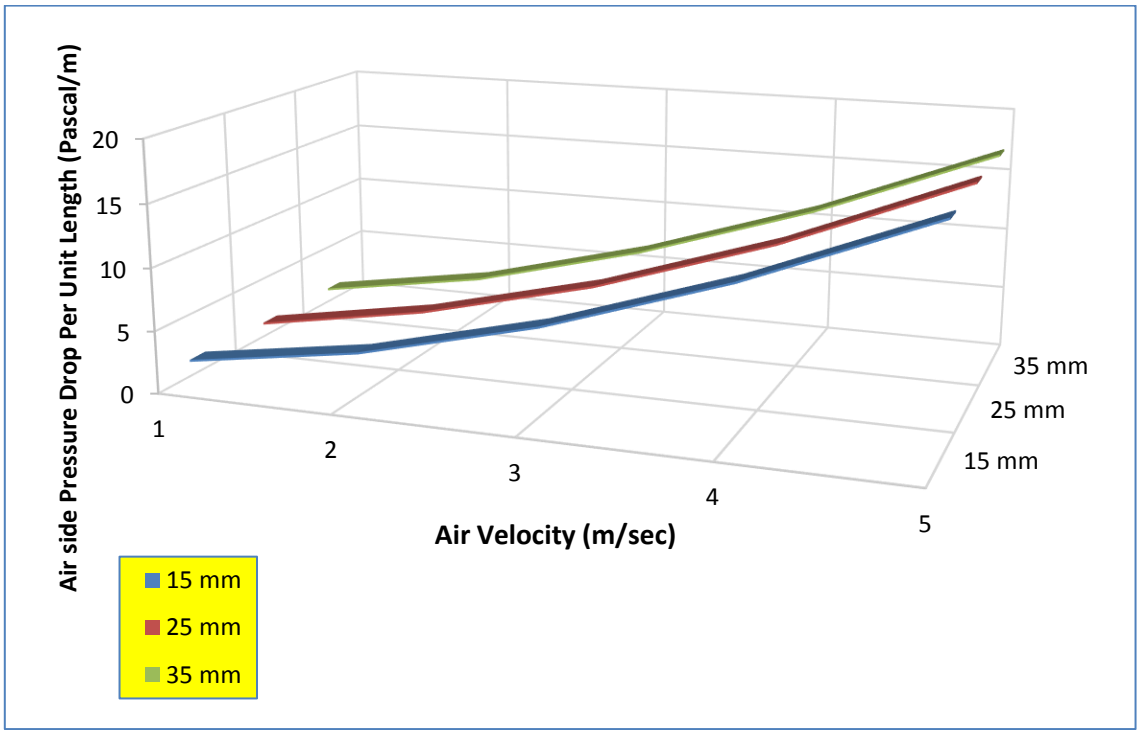

Figure 5.20 Air side Pressure Drop Per Unit Length Versus Air Velocity at Different Hole Spacings

Table 5-8 depicts contours of temperature variation in mid-section (x-axis) of the heat exchanger due to change in air velocity under steady state operating condition at different hole spacing. For effective comparison purposes, the scale of the contours has been kept constant. The air side temperature differences (ΔT_a) for with 25 mm hole spacing model are higher comparing with 15 mm and 35 mm hole spacings models, the average of increase in temperature differences (ΔT_a) for the 25 mm hole spacing model are 3.73% and 5.52%, respectively.

Table 5-8 Contours of Temperature Variation in mid-section (X-axis) of the Heat Exchanger Due to Change in Air Velocity under Steady State Operating Condition at Different Hole Spacings

Hole Spacing	*15 mm*	*25 mm*	*35 mm*	*Legend*
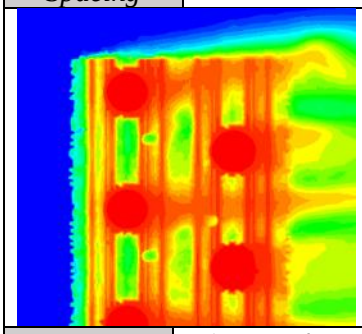		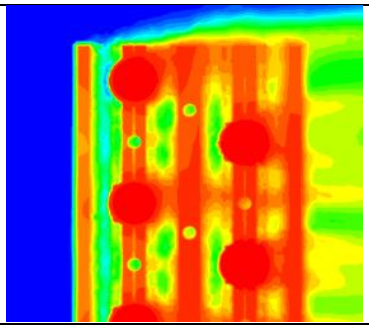	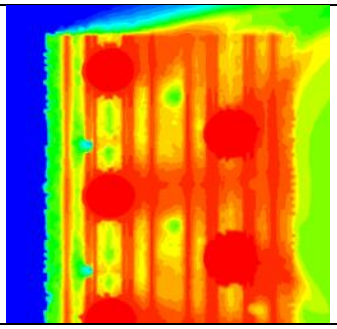	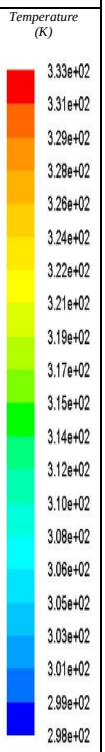
V_a=1 m/sec	ΔT_a=7.79° C	ΔT_a=8.03° C	ΔT_a=7.59° C	
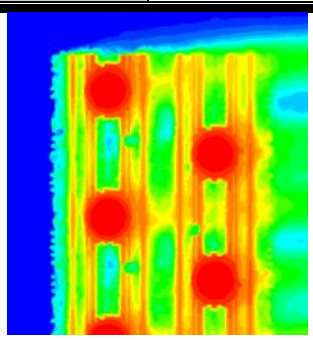		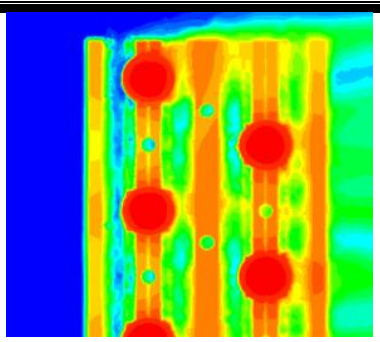	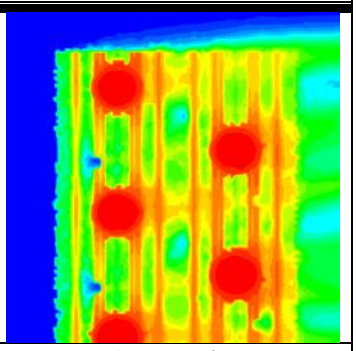	
V_a=3 m/sec	ΔT_a=4.91° C	ΔT_a=5.12° C	ΔT_a=4.87° C	
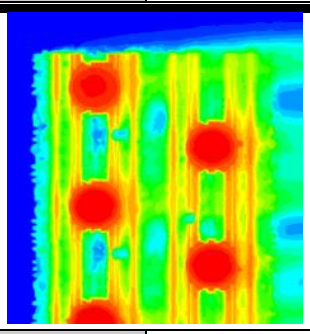		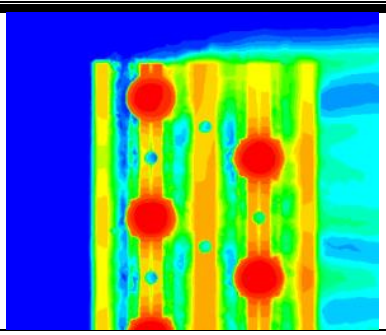	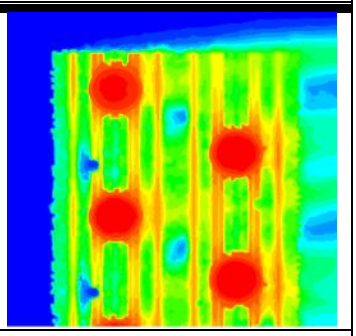	
V_a=5 m/sec	ΔT_a=3.81° C	ΔT_a=3.90° C	ΔT_a=3.77° C	

The results presented in this chapter have a good agreement with the results presented by Liu et al. in [49] where the two studies focused on the enhancement of the heat exchanger performance by adopting a perforation in fins surfaces and compare the results with plain fins. However, the numerical model used in [49] was limited by taken only half of the three tube rows of the heat exchanger as a calculation element. This consideration may affect the results by [49] as it has been proved in section 4.5.1 of this study, where it has been stated that the thermal behaviour of the fins of the heat exchanger is not the same and the condition in one fin cannot be applied to the other one; hence it is vital to analysis the whole heat exchanger under this condition.

5.5 Summary of the Design Modification of the Multi-tube and Fin Heat Exchanger

This chapter has presented novel geometric configurations for multi-tube and fin heat exchanger. These novel geometric configurations were arrived at after carrying out a careful experimental and numerical investigations of a variety of models with different heat transfer enhancement methods. Some important observations that have been made during the numerical and experimental investigations are listed below.

- Due to the vortex generated by the holes, the perforate plain fins heat exchanger model has achieved an enhancement in heat transfer characteristics when it is compared with the plain fins heat exchanger model. This enhancement is relatively high at small water flow rate and it has the disadvantage of an increase in the pressure drop. Hence, the perforate plain fins heat exchanger model has been considered for further investigations,
- The surface area of the louvre fins is larger comparing with plain fins. This fact results an increase in the heat transfer characteristics as well as increase in the pressure drop across the air side of the heat exchanger,
- By using a surface modification in the form of perforations in the louvre fins the thermal performance of the heat exchanger has improved. Hence, the model with perforate louvre fins can be considered as the best thermal performance model,
- Hole diameter and hole spacing have shown some effect on the thermal performance of perforate louvre fins heat exchanger model, whereas larger hole diameter (D/3-hole diameter) and 25 mm hole spacing are the optimum values of theses parameters,
- A novel Set of design equations have been developed based on the prediction models developed in this chapter and the previous chapter.

In this chapter, the effectiveness of the heat enhancement device used within the multi-tube and fins heat exchanger has been discussed. The new enhanced models flow behaviour has been analysed for various geometrical parameters. Based on this analysis, in next chapter a user friendly and reliable methodology for designing an optimised model with least-cost principle will be proposed.

Chapter 6 **MULTI-OBJECTIVE OPTIMISATION OF THE NEW DESIGN AND COST ANALYSIS**

SUMMARY: This chapter proposes a multi-objective optimisation procedure for four different models of multi-tube and fin heat exchangers, with different fin spacing, namely; plain fins, perforated plain fins, louvre fins and perforated louvre fins. The proposed optimisation procedure has been carried out with two main constraints; optimisation for maximising JF and optimisation for minimising total cost. In addition, a detailed method to estimate the total cost of the FCU integrated with multi-tube and fin heat exchanger has been included. The results of this chapter reveal that the heat exchanger with perforated louvre fins is the optimal model.

6.1 Optimisation Strategy

The process of developing a new design of heat exchanger and therefore a new design of FCU is complicated process due to the high cost and long development period involved. Nowadays, using computer in this design process has enabled engineers to accurately analyse parts with complex geometry at low cost and timely efficient. The previous chapter focused on enhancing the thermal performance of the heat exchanger by using a surface modification in the form of surface or geometrical modifications in fin surfaces. This design modification increases the heat transfer rates as well as reduces the weight of the heat exchanger. In this chapter, a time efficient optimisation strategy will be proposed. The optimisation strategy takes into consideration limited experimental inputs, CFD modelling and optimisation by using a new framework. The output of this framework is a prototype of the new design of FCU which will be validated with the experiments on the same model in order to achieve a new optimised design of the FCU. The flow chart of this optimisation strategy is depicted in Figure 6.1. furthermore, a detailed method to estimate the total cost of the FCU integrated with multi-tube and fin heat exchanger will be presented.

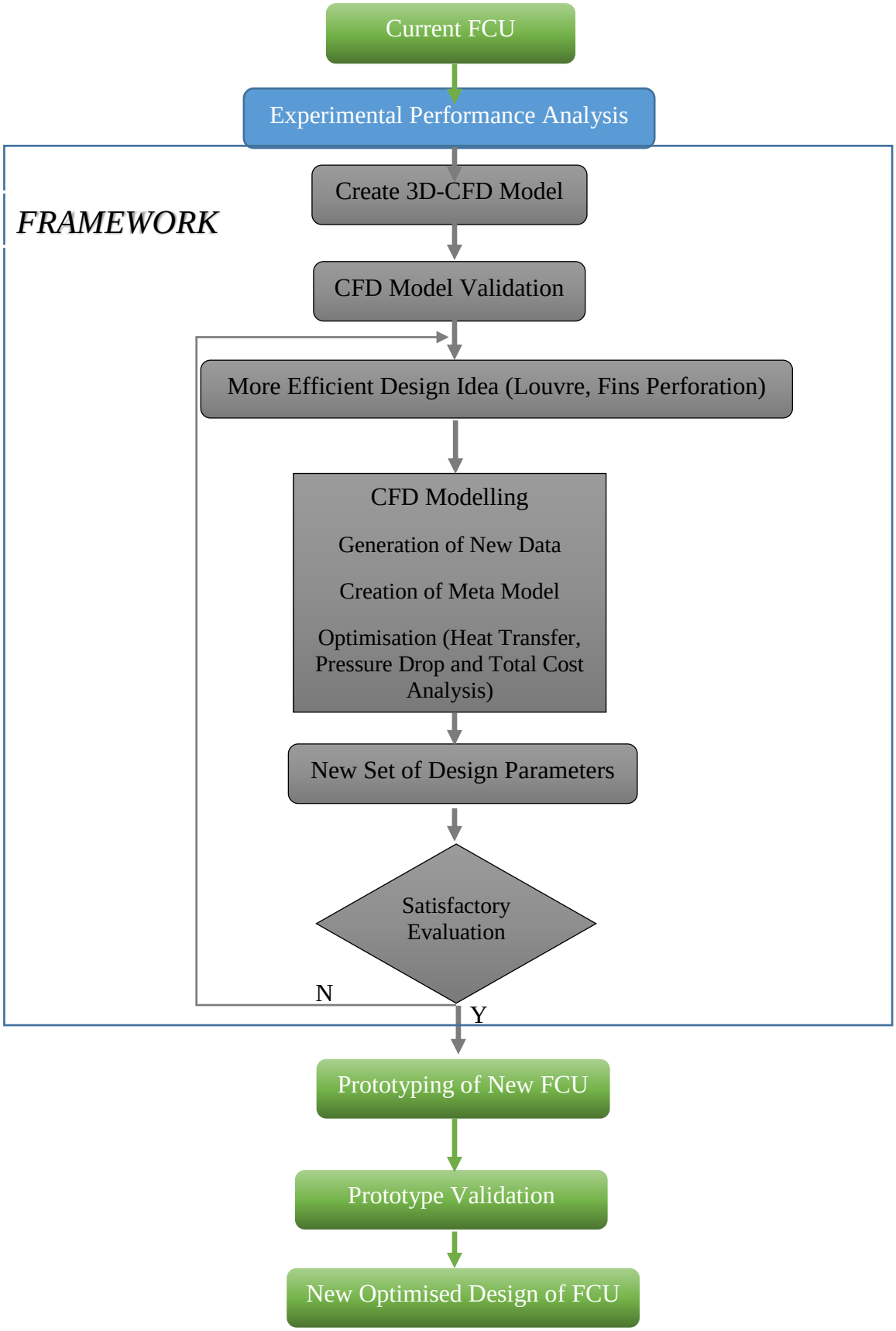

Figure 6.1 Flow Chart of the Optimisation Strategy

6.2 The Cost Estimation of FCU Integrated with Multi-tube and Fin Heat Exchanger

As it has been discussed in the previous chapter, each design configuration of the heat exchanger has some advantages, these advantages may affect the size of this heat exchanger and therefore the economics of the heat exchanger. In the next section, a method to estimate the total cost of the FCU integrated with multi-tube and fin heat exchanger has been described.

In general, there are two types of cost related with FCU; capital and operating costs [96].

$$C_{Total} = C_{Capital} + C_{Operating} \tag{6.1}$$

Where all costs are expressed in GBP (£).

6.2.1 Capital Cost

The capital cost of FCU includes the cost of material and manufacturing and installation cost.

$$C_{Capital} = C_{Material} + C_{Manufacturing} \tag{6.2}$$

The material cost consists of the cost of the tubes, fins and working fluids. The FCU is operating with water as a hot fluid and air as a cold fluid. Both of these fluids are widely available and inexpensive. Therefore, their cost can be considered negligible. Hence, the equation of the material cost can be written as:

$$C_{Material} = C_{Tubes} + C_{fins} + C_{Housing} \tag{6.3}$$

I. Cost of Tubes

As it has been described in section 3.2.5, heat exchanger tubes are made up from Copper with 0.26 mm thickness. Tubes cost can be estimated using the equation given by [97] and [98]. This equation uses the geometry of the tube to estimate its cost.

$$C_{Tubes} = C_1 * \rho * \pi * t_{Tube} * L_{Tube} * (D_{out} - t_{Tube}) \tag{6.4}$$

where, C_1 is the cost of tubes material (£/Kg), ρ is the material density (kg/m^3), t_{Tube} is the tube thickness (m), L_{Tube} is the total length of the tubes (m) and D_{out} is the outer diameter of the tube (m).

II. Cost of Fins

The heat exchanger has 22 staggered configuration fins made up from Aluminium with 0.12 mm thickness. Fins are 44 mm wide and 125 mm high. Eq. (6.5) has been provided by [99] and it can be implemented to estimate the cost of the fins (C_{Fins}).

$$C_{Fins} = C_2 * F_t * A_f \quad (6.5)$$

where, C_2 is the cost of Aluminium per unit volume (£/mm^3), F_t is the fin thickness (mm) and A_f is the total fins surface area (mm^2)

III. Cost of Housing

The housing of FCU is made up using galvanised steel sheet with 2 mm thickness riveted together to form the test section which holds the heat exchanger and fan assembly, as it has been described in section 3.2.5. The test section is 650 mm long, 165 mm wide and 175 mm high. The material cost of the test section ($C_{Housing}$) can be calculated using the following equation [100],

$$C_{Housing} = C_3 * V_{Housing} \quad (6.6)$$

where, C_3 is the cost for steel sheet per unit volume (£/mm^3) and $V_{Housing}$ is the volume of the steel sheet used to create the housing (mm^3)

Table 6-1 lists the prices of the materials used to manufacture the FCU. The prices are estimated based on the current market in the UK.

Table 6-1 Various Costs of The Materials Used to Manufacture the FCU

Material	*Price*
Copper	*6.3 £/Kg*
Aluminium	*2.303×10^{-4} £/mm^3*
Steel Sheet	*3×10^{-5} £/mm^3*

IV. Manufacturing Cost

The manufacturing cost represents the fabrication and assembly costs. It has been reported by [101] that the fabrication and assembly costs are 3 times the material cost. Thus,

$$C_{Manufacturing} = 3 * C_{Material} \quad (6.7)$$

6.2.2 Operating Cost

The power required to draw the air in the air side and the power required to circulate the water in the water side are the main components of the operating cost. Hence,

$$C_{Operating} = C_{KWhr} * t_{op} * (P_{Water\ side} + P_{Air\ side}) \quad (6.8)$$

where, $P_{Water-side}$ and $P_{Air-side}$ are the pumping powers in Watts required to operate the water-side and the air-side, respectively, C_{KWhr} is the power cost for 1 KWhr (kilowatt hour) which is assumed to be £ 0.20 and t_{op} is operational hours per year (hr/yr)

The pumping power (P_p) can be calculated from Eq. (6.9). This equation formulates the pumping power for moving devices such as pumps, fans, and blowers as a function of pressure drop [102].

$$P_p = \frac{\dot{m}\Delta P}{\rho \eta_p} \quad (6.9)$$

where, $\dot{m}$ is the working fluid flow rate (kg/sec), ΔP is the pressure drop (pascal), ρ is the working fluid density (kg/m^3) and fluid η_p is the efficiency of the fan or pump.

6.3 Estimating Total Cost Example:

In this section, the total cost for FCU which contain multi-tube and fin heat exchanger with perforated louvre fins will be estimated for comparison purpose.

To estimate the cost of the tubes, total length of the tubes should be calculated first.

$$L_{Tube} = (2 \times 150) + (8 \times 130) + (9 \times 25) = 1565\ mm = 1.565\ m$$

Then using Eq. 6.4,

$$C_{Tubes} = 6.3 \times 8978 \times \pi \times 0.00026 \times 1.565 \times \frac{(9.52 - 0.26)}{1000} = £\ 6.691$$

The cost of fins can be calculated from Eq.6.5

$$C_{Fins} = 2.3 \times 10^{-4} \times 0.12 \times (22 \times 9796) = £\ 5.955$$

The cost of the housing can be calculated from Eq.6.6

$$C_{Housing} = 3 \times 10^{-5} \times (650 \times 680 \times 2) = £\ 26.52$$

Then, the total material cost is,

$$C_{Material} = 6.691 + 5.955 + 26.52 = £\,39.167$$

The manufacturing cost can be calculated using Eq. 6.7

$$C_{Manufacturing} = 3 \times 39.167 = £\,117.501$$

Therefore, the capital cost is,

$$C_{Capital} = 39.167 + 117.501 = £\,156.668$$

As it has been mentioned previously, the operating cost is dependent on the pressure drop for both water-side and air-side. Therefore, assuming the efficiency of the pumping units (water pump and air fan) η = 60% and both of them would be used 7000 hours per year. Hence, a 15-year lifetime of the FCU will be used in the further calculations. Figure 6.2 depicts the variations of the operating cost with variations of water and air velocities for 15-year lifetime of the FCU.

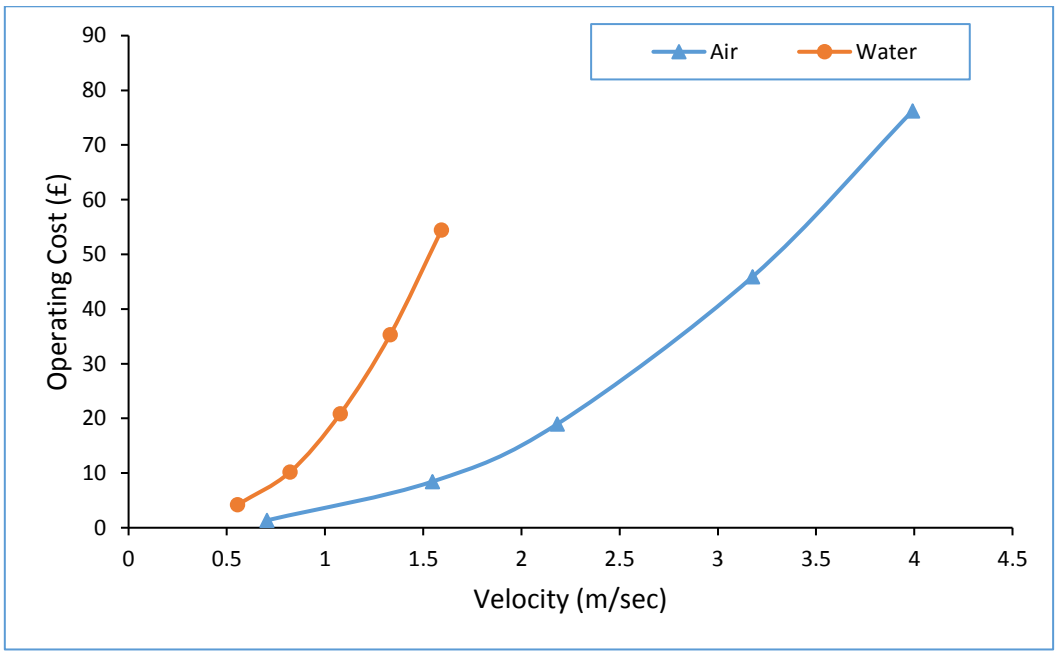

Figure 6.2 Variations of the Operating Cost with Variations of Water and Air Velocities for 15-Year Lifetime of the FCU

6.4 The Optimisation Model

Heat exchanger optimisation is an important field in order to design an economical and efficient system. The main aims of this process are to save materials or energy as well as saving in the total cost of this system. On the other hand, the complex design procedure of the heat exchanger includes selection of geometrical parameters and operating parameters for the design, cost

estimation and optimisation. This section provides in detail a multi-objective optimum design procedure of multi-tube and fin heat exchanger based on using CFD simulations as a main tool to achieve an optimum condition of maximum heat transfer, low pressure drop and least total cost. The multi-objective optimum design procedure has been carried out for four different models of multi-tube and fin heat exchangers namely; plain fins, perforated plain fins, louvre fins and perforated louvre fins. Each heat exchanger has three different configurations with three fin spacings; 4.2mm, 4.7mm and 5.2mm. The fin spacing has been chosen as an objective function in this optimum design procedure because of its significant effect on the thermal performance of the heat exchanger as it has been discussed in section 4.6.1. In addition, due to the design of the fins, it was not possible to decrease the fin spacing less than 4.2mm due to the fillet which is used to eliminate sharp edges created by fitting the fins on the tubes, as it can be seen in Figure 6.3.

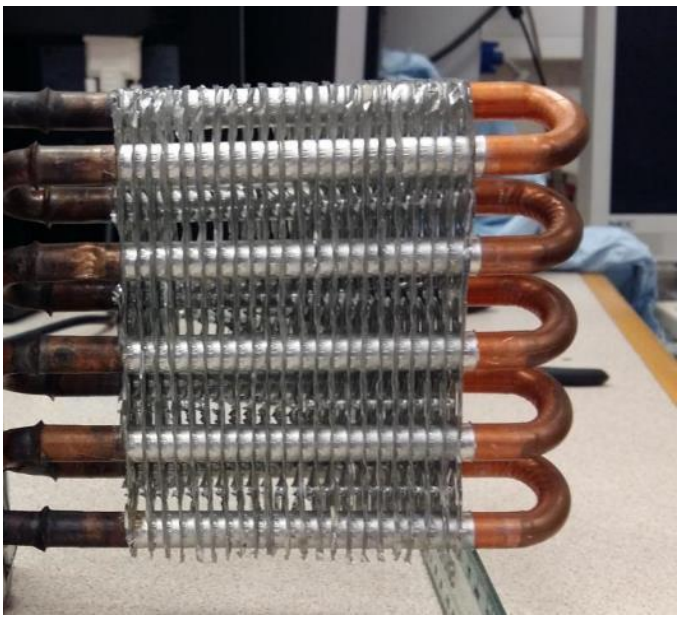

Figure 6.3 Fin Spacing in the Heat Exchanger

As it has been previously mentioned, Colburn factor (j) and friction factor (f) are generally adopted to symbolise the pressure drop characteristics and the heat transfer characteristics, respectively. However, it is not useful to use a direct comparison of them to evaluate the thermal performance of heat exchanger in order to select an optimum configuration, because as j increases, f increases as well. Therefore, a JF factor which is a nondimensionalised parameter has been proposed by [59] and it can be expressed as,

$$JF = \frac{{}^{j}/_{j_{Ref}}}{({}^{f}/_{f_{Ref}})^{1/3}} \tag{6.1}$$

where, j is Colburn factor f is friction factor of the evaluated heat exchanger. j_{Ref} and f_{Ref} are the values of j and f for the reference heat exchanger (in this study the baseline model has been selected as a reference heat exchanger). From Eq. (6.1) it can be noted that the higher value of JF factor is, the better performance of the heat exchanger. Thus, optimisation for maximizing JF factor has been employed as another objective function in this optimum design procedure.

The total cost of each heat exchanger can be normalised by dividing the its total cost by the baseline model total cost. Therefore, optimisation for minimum total cost is the last objective function in this optimum design procedure.

The steps to obtain the optimised design are as follows:

1. Input the heat exchanger geometrical parameters (fin spacing, fin collar outside diameter, longitudinal pitch, transverse pitch, fin width and fin height)
2. Input the water and air boundary conditions (velocity and temperature)
3. Choose the reference model (baseline model)
4. Calculate Fanning friction factor (f) and Colburn factor (j) of heat exchanger using the novel semi-empirical prediction models developed in sections 4.7, 5.2.4 and 5.2.5
5. Calculate JF factor from Eq. (6.1)
6. The first output of this optimum design procedure is optimised model based on JF as a single-objective function
7. Estimate the total cost of operating the heat exchanger using the method described in the previous section, i.e. section 6.1
8. Normalise the total cost by dividing the total cost of each heat exchanger by the baseline model total cost
9. Combine the two objectives of this optimum design procedure; optimisation for maximising JF and optimisation for minimising total cost
10. Repeat steps 1 to 9 for different Reynolds number and for different fin spacing in order to achieve the optimum case where maximum heat transfer, low pressure drop and least total cost

Figure 6.4 depict the flow chart for the optimisation methodology.

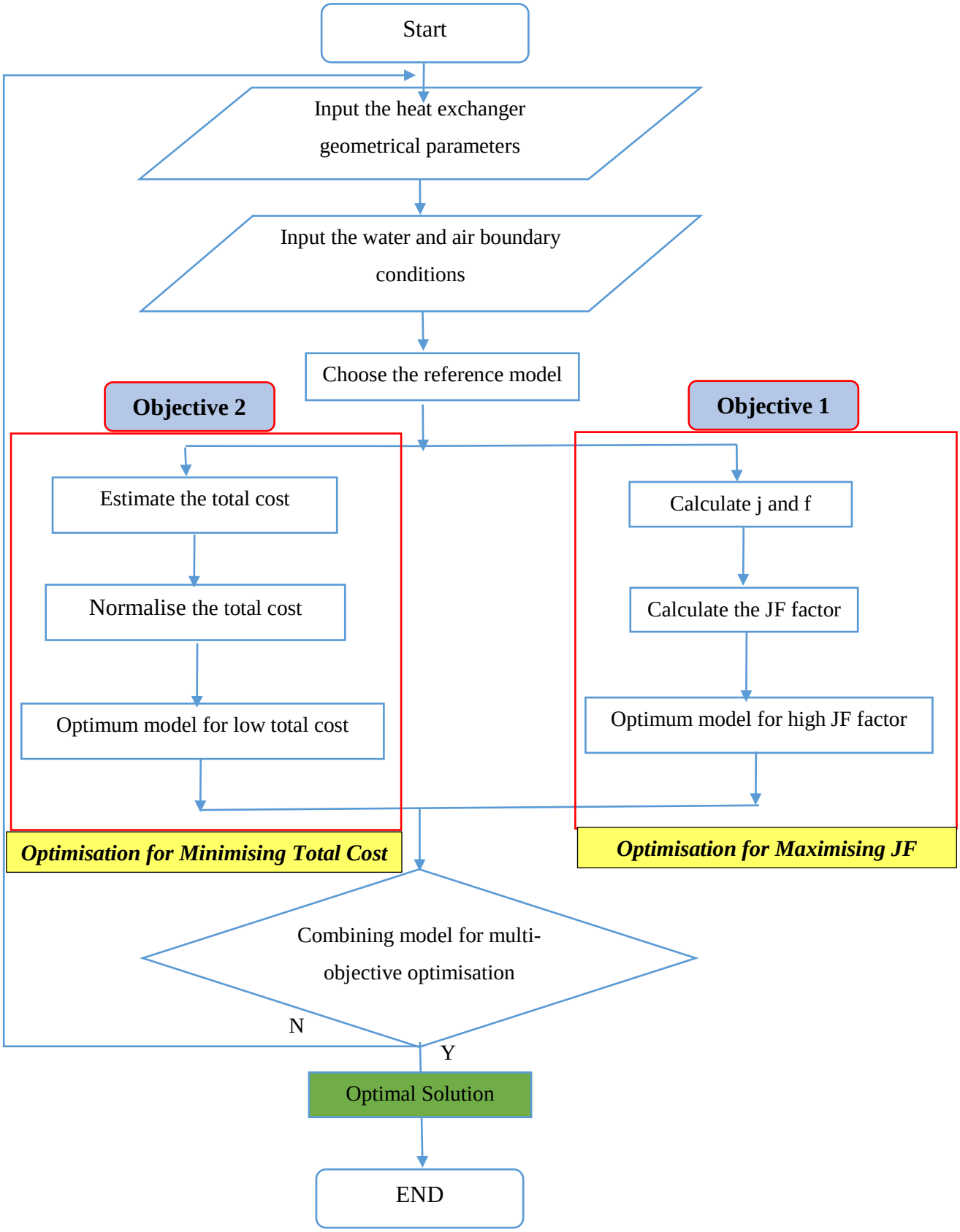

Figure 6.4 Flow Chart of the Optimisation Methodology

6.5 Optimisations Procedure for Multi-tube and Fin Heat Exchanger results

This section will show the results computed using the multi-objective optimum design procedure described in the previous section. The results will be shown for two different cases; optimisation for maximising JF and multi-objective optimisation.

6.4.1 Optimisation for Maximising JF

In this case, the JF factor is considered as a single-objective function for the optimisation process. Figure 6.5 depicts the variation of the JF factor for the four models of heat exchanger used in this study and for different fin spacing.

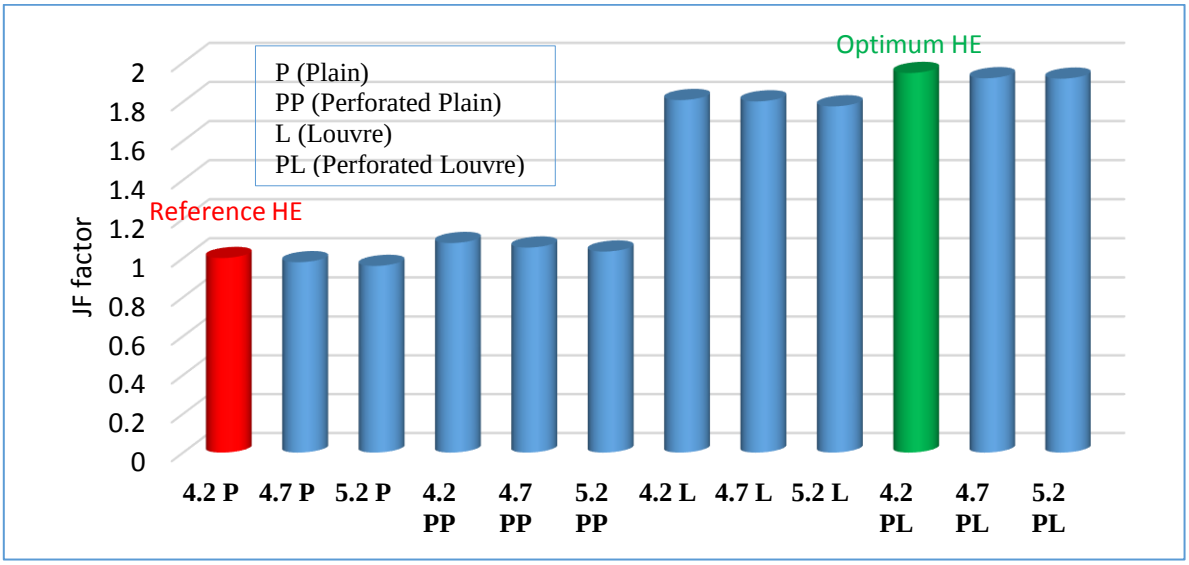

Figure 6.5 Variation of JF Factor for Different Heat Exchanger Configurations

The vertical bars presented in Figure 6.5 indicate that heat exchangers with perforated louvre fins have the highest values of JF factor, whereas heat exchanger with plain fins have the lowest values. For the same fin spacing (4.2 mm), when the fins of the model have been changed from plain to perforated plain, louvre and perforated louvre, the value for JF factor has increased 7%, 80% and 94%, respectively. Furthermore, a higher JF factor is observed for the heat exchanger model with perforated louvre fins at 4.2 mm fin spacing. Hence, this model can be considered as the optimum model when JF is employed as a single-objective function for the optimisation process.

6.4.2 Multi-Objective Optimisation

In this case, the optimisation carried out in the previous section has been combined with another optimisation objective which is optimisation for minimising total cost. This process is very important in order to achieve the optimal solution of the optimisation process. i.e. optimised model with high heat transfer, low pressure drop and lowest total cost.

Figure 6.6 illustrates the variation between Colburn factor (j) and normalised total cost calculated over 15 years for the heat exchangers presented in this study at different fin spacings.

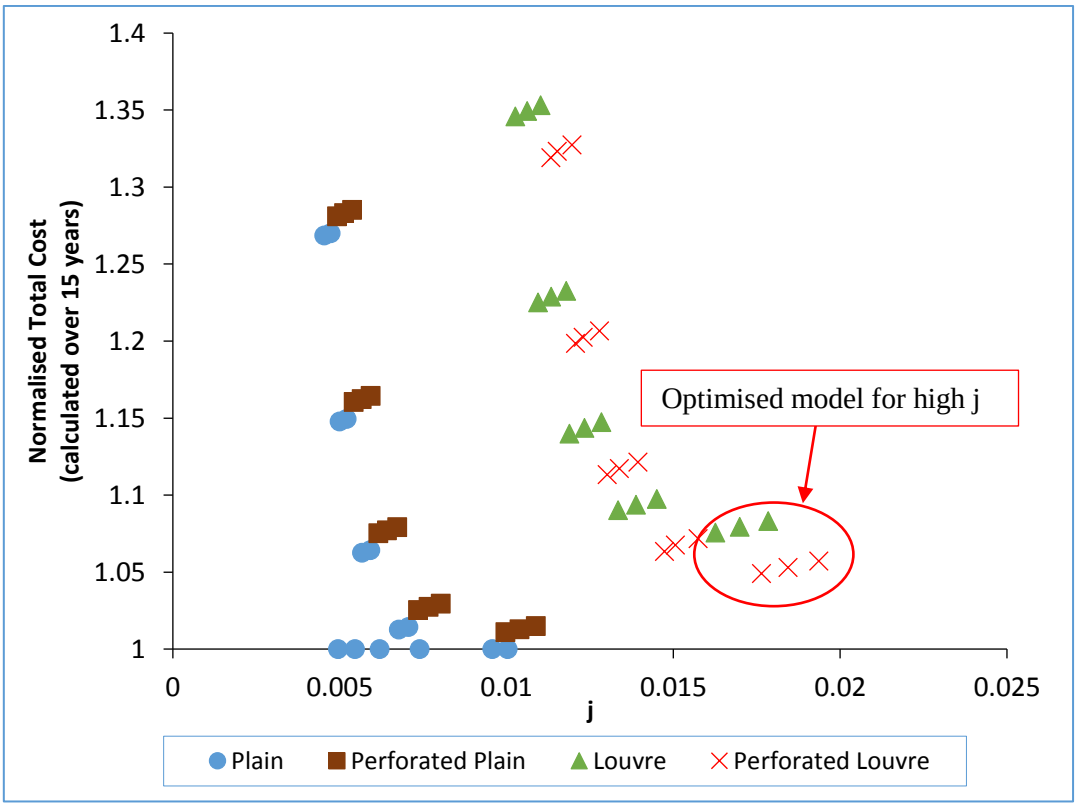

Figure 6.6 Optimised Model for High Colburn Factor (j)

The variation between Fanning friction factor (f) and normalised total cost calculated over 15 years for the heat exchangers presented in this study at different fin spacings is depicted in Figure 6.7.

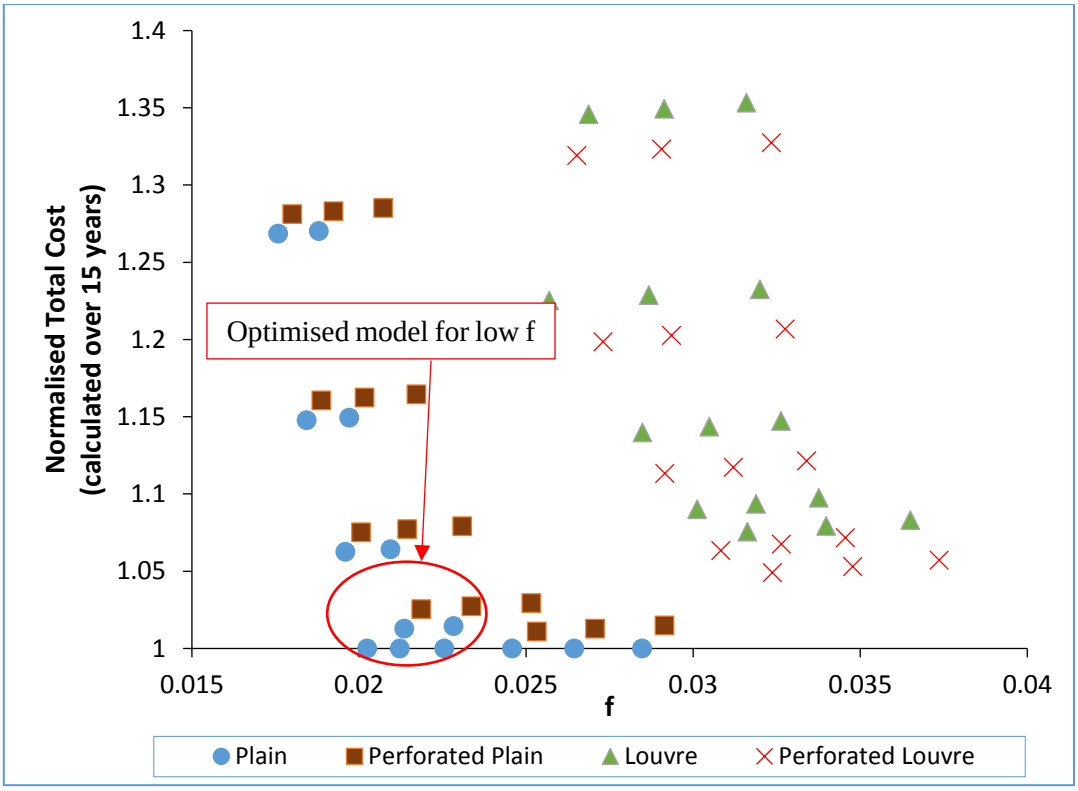

Figure 6.7 Optimised Model for Low Friction Factor (f)

The Pareto optimal fronts plotted in both Figure 6.6 and 6.6 help to select a final solution among the points plotted in these graphs. For the case of high Colburn factor (j), high heat transfer, the optimised model was found to be the perforated louvre fins model (JF= 0.0193) with 4.2 mm fin spacing operating at low Reynolds number. The second choice was the louvre fins model (JF= 0.0178) with 4.2 mm fin spacing and also operating at low Reynolds number. These results agreed with the results obtained in section 4.6.1 where it has stated that the highest heat transfer rate can be obtained at low fin spacing because as the fin spacing decreases the flow becomes more streamlined which result a better flow mixing. For the case of low friction factor (f), the plain fins model with 5.2 mm fin spacing operating at Reynolds number (12,000) has proven low pressure drop which result a low total cost. The second choice was the perforated plain fins model with 5.2 mm fin spacing operating at Reynolds number (12,000).

Figure 6.8 depicts the relation between JF factor and normalised total cost calculated over 15 years for the heat exchangers presented in this study at different fin spacings.

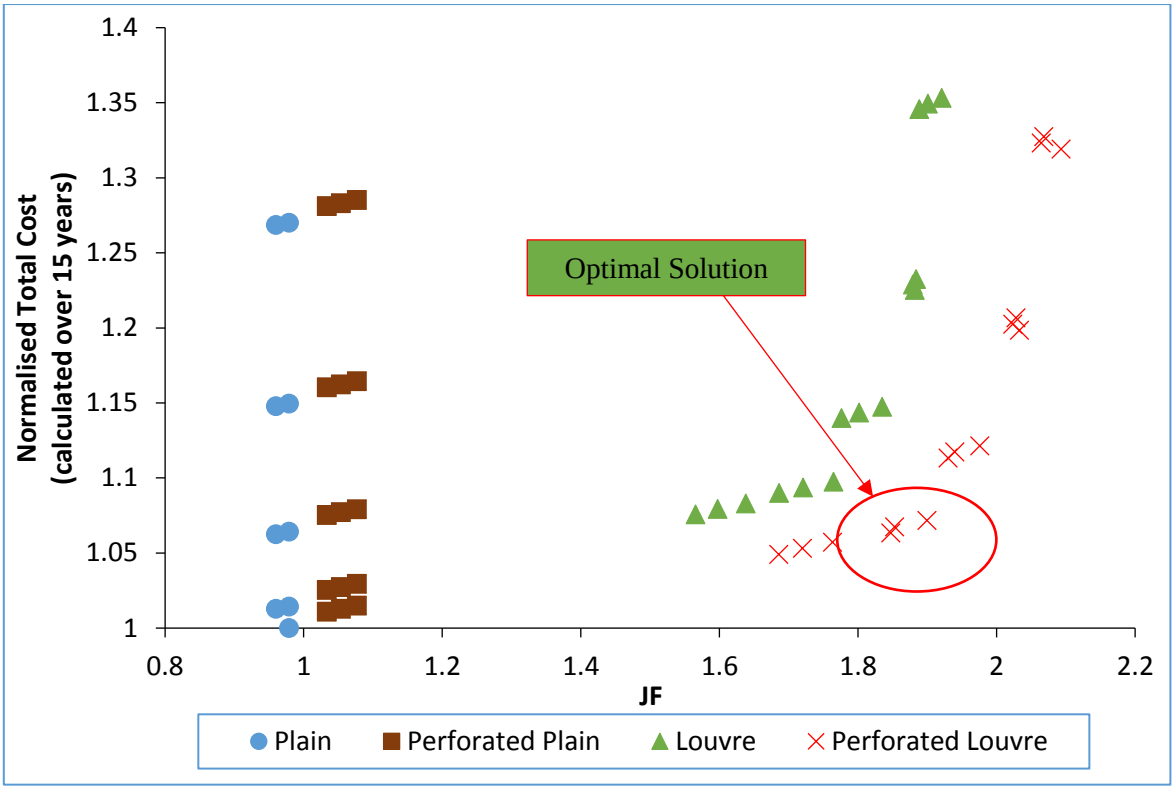

Figure 6.8 Optimised Solution for the Multi-Objective Optimisation

The Pareto front plotted in Figure 6.8 reveals that, the perforated louvre fin models operating at 12,000 Reynolds number are the optimal solutions of this optimum design process. This result comes after combining the two main objectives of this process; optimisation for maximising JF and optimisation for minimising total cost. The JF factors for the optimal solutions were in range from 1.847 to 1.899, whereas the normalised total costs calculated over 15 years were in range from 1.063 to 1.071. Hence, these values can be used to design and operate the enhanced heat exchanger with optimum thermal performance and at lowest total cost. In addition, it should be clear that the optimal solutions selected are independent of fin spacing. However, the optimal design model is the heat exchanger with perforated louvre fins with 4.2 mm fin spacing.

6.6 Validate the numerical predicted results with experimental data for the optimal design model

In order to ensure the reliability of the numerical model, a benchmark test has to be carried out on the optimised design model; perforated louvre fins with 4.2 mm fin spacing. In this section, the numerically predicted results have been validated against experimental data for heat exchangers with perforated louvre fin in terms of water and air outlet temperatures and pressure drop obtained in both water and air sides. These variables were plotted against each other at a

constant water flow rate (3 L/min). Boundary conditions for steady state tests that have been carried out on the optimised model are shown in Table 6-2.

Table 6-2 Boundary Conditions of Steady State Tests for Optimised Model

Test Name	Water Side		Air Side	
	Water Flow rate (L/min)	Water Inlet Temperature (° C)	Air Velocity (m/sec)	Air Inlet Temperature (° C)
Test 1	3	60 ± 1	0.705	25 ± 1
Test 2			1.546	
Test 3			2.183	
Test 4			3.177	
Test 5			3.991	

Figure 6.9 depicts a comparison between the numerically predicted results and the experimental data for water outlet temperature for the optimised model.

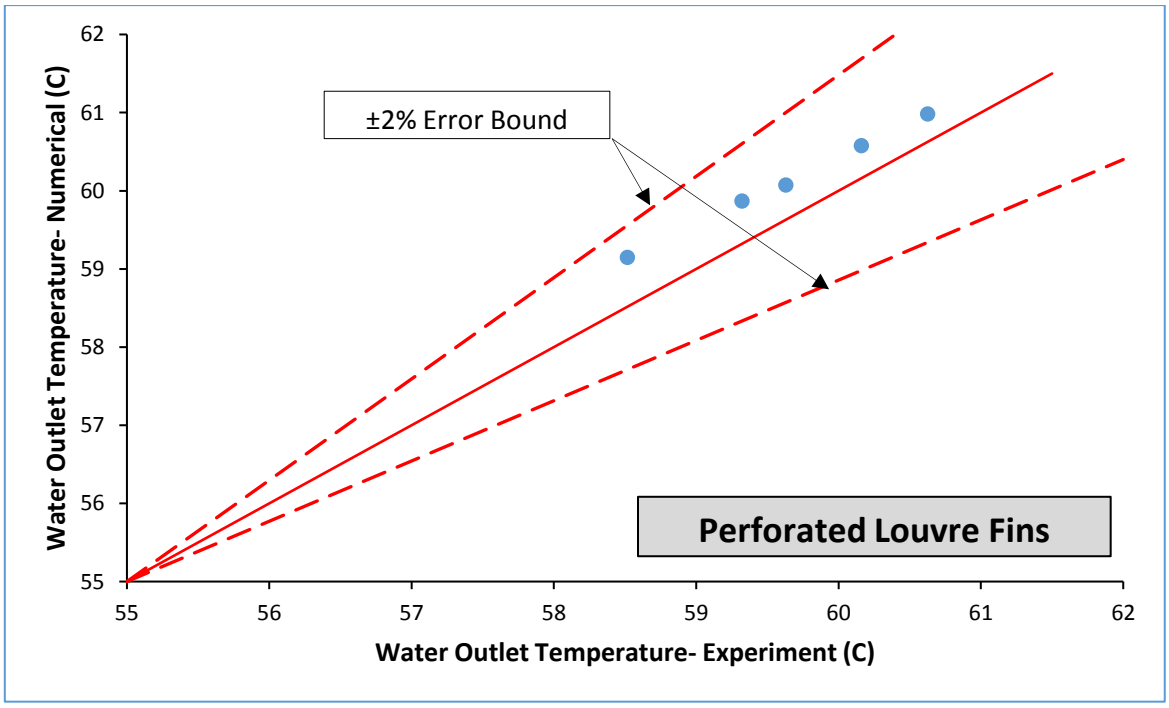

Figure 6.9 Comparison of Numerical and Experimental Results for Water Outlet Temperature Perforated Louvre Fins Heat Exchanger

Figure 6.10 illustrates a comparison between the numerically predicted results and the experimental data for air outlet temperature.

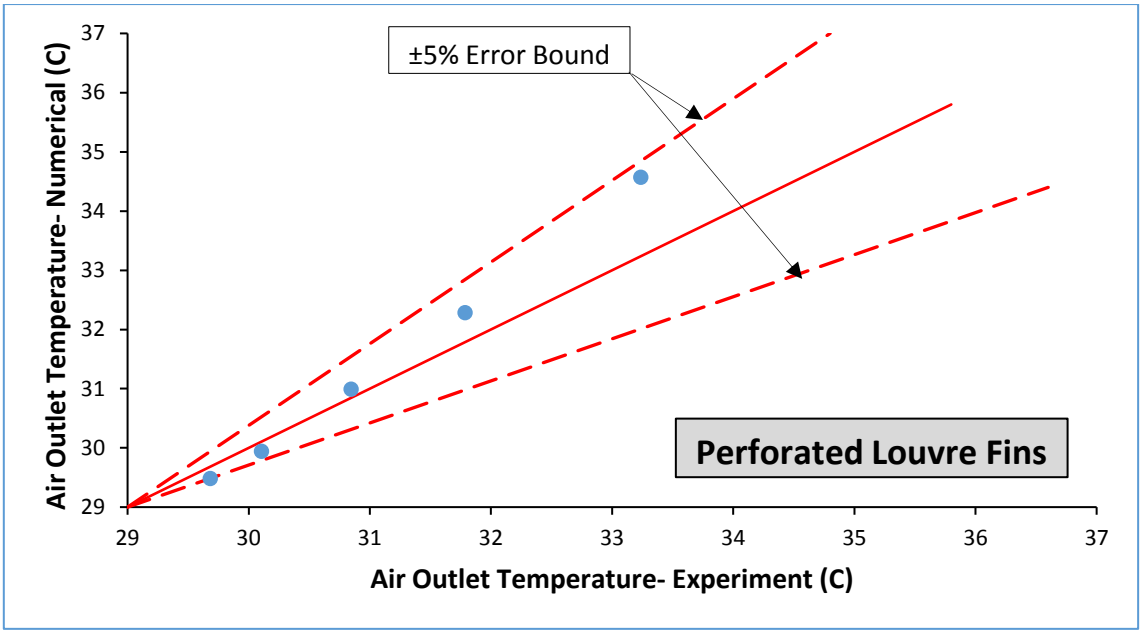

Figure 6.10 Comparison of Numerical and Experimental Results for Air Outlet Temperature Perforated Louvre Fins Heat Exchanger

Figure 6.11 depicts a comparison between the numerically predicted results and the experimental data for waterside pressure drop for heat exchangers with perforated louvre fins.

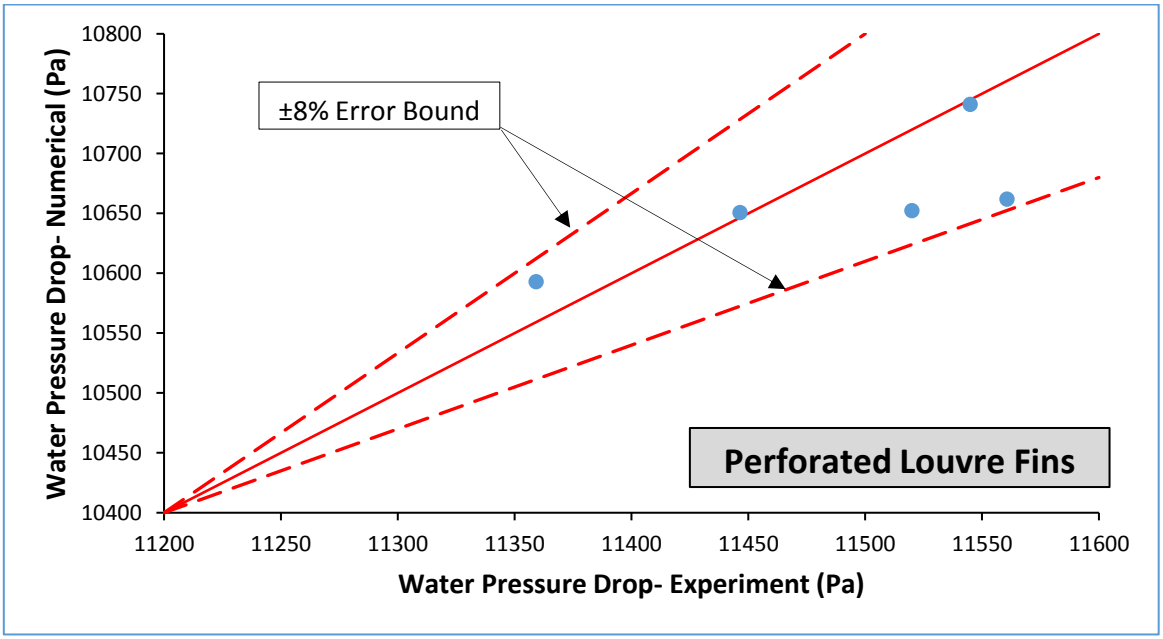

Figure 6.11 Comparison of Numerical and Experimental Results for Waterside Pressure Drop Perforated Louvre Fins Heat Exchanger

A comparison between the numerically predicted results and the experimental data for airside pressure drop for heat exchangers with perforated louvre fins is depicted in Figure 6.12.

Based on the results depicted in figures 6.8, 6.9, 6.10 and 6.11, it can be clearly seen that the differences between the numerically predicted results and the experimental data for water outlet and air outlet temperatures are very small and the numerical results agree well with the experimental results for the perforated louvre fins heat exchanger. The percentage differences between theses results for the water outlet and the air outlet temperatures were less than 2% and 5%, respectively. Furthermore, the percentage differences between the numerically computed results and the experimental data for water-side pressure drop were observed to be less than 8%, while the percentage differences between the numerically computed results and the experimental data for air-side pressure drop were detected to be less than 15%.

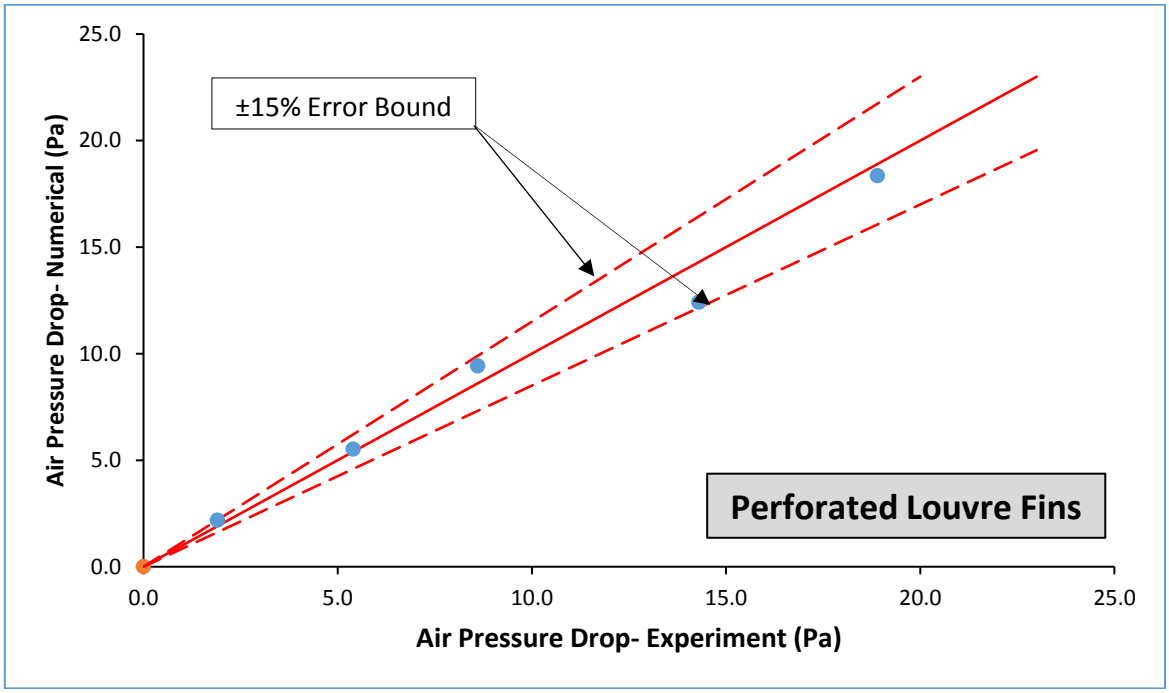

Figure 6.12 Comparison of Numerical and Experimental Results for Airside Pressure Drop Perforated Louvre Fins Heat Exchanger

6.7 Summary of the Multi-Objective Optimisation of the New Design and Cost Analysis

This chapter has presented a multi-objective optimisation procedure for different models of multi-tube and fin heat exchanger based on two main objectives; optimisation for maximising JF and optimisation for minimising total cost. This procedure comes after presenting a method to estimate the total cost of the FCU integrated with multi-tube and fin heat exchanger. Some important observations that have been made during this chapter are listed below.

- The operating cost of the FCU is dependent on the cost of operating the water pump and the fan,
- Fin spacing is a key factor in designing the heat exchanger because by reducing the fin spacing a high heat transfer performance can be achieved. However, reducing the fin spacing may case a significant increase in the total cost,
- The derivation of an optimised model for the FCU design based on the heat exchanger performance with different fin arrangements helps to design and operate a better performance FCU with optimum thermal performance and at lowest total cost,
- Perforated louvre fins have proven better thermal performance with reasonable total cost. Nevertheless, plain fins can provide the lowest operating cost.

Chapter 7 **CONCLUSIONS**

SUMMARY: This chapter concludes the thesis by summarising the achievements of this research. This thesis includes an experimental and numerical investigations of the design and optimisation based on the best performance and lowest cost of multi-tube and fin heat exchanger used in the Fan Coil Unit (FCU).

7.1 Context and Importance of Research Question

Fan Coil Units (FCU) are commonly used in central air conditioning systems, especially in office buildings and hotels. They are playing a very important role in the heating, ventilation and air conditioning (HVAC) systems which are designed to control thermal comfort in the buildings. Consumption of energy required to run such a device will directly influence the overall energy requirements for such buildings and therefore its CO_2 footprint. Therefore, it is important to optimise the design of the FCU in order to improve its thermal performance and minimise the total cost.

FCU consists of a heating or cooling coil (heat exchanger) and a fan. Heat exchangers have a significant impact on the energy efficiency, cost, size, and weight of this system. In recent years, there have been numerous methods and new technologies reported worldwide to enhance the heat transfer and pressure drop characteristics of the heat exchanger to improve performance envelop of such devices in a cost-effective manner. However, a majority of these studies did not consider overall energy efficiency and overall costs analysis. In this thesis, a novel approach based on time efficient multi-objective optimisation strategy with limited experimental inputs at development stage, results of CFD modelling based on a full 3D representation of the FCU which also include local heat transfer approach and the total costs analysis has been developed.

The main outcome of this study is to improve the thermal performance of the current FCU based on high heat transfer rate, low pressure drop and lowest total cost.

In order to formulate the research objectives, an extensive literature review has been carried out in chapter two. The major achievements and contributions from this study have been presented in a summarised form in the following sections of this chapter.

7.2 Research Aims and Major Achievements

This section is summarising the work done to achieve the research aims together with the major achievements of this study.

Research Aim # 1: Development of novel approach to analysis of thermal performance of a multi-tube and fin heat exchanger used in the current FCU unit experimentally and numerically under steady state operating condition.

Achievement # 1: A novel CFD model with full 3D geometry for multi-tube and fin heat exchanger has been presented and verified against the experimental results at different operating conditions. This model has been used for an additional investigation with different design modifications. Furthermore, qualitative analysis of flow field has been carried out in order to quantify the complex and non-uniform flow phenomena on both water and air sides. numerically simulated data has been employed to develop a Prediction model to estimate Fanning friction factor (f) and Colburn factor (j) has been developed by taking in consideration the effects of heat exchanger geometrical parameters.

Research Aim # 2: Development of more efficient design for multi-tube and fin heat exchanger geometry to improve FCU thermal performance.

Achievement # 2: A passive heat transfer enhancement technique has been adopted to develop more efficient design for multi-tube and fin heat exchanger geometry to improve FCU thermal performance. This includes having louvre fins or by creating perforation on the fin surface. The technique has proven to provide enhancement in the heat transfer of about 10%. However, it has the disadvantage of an increase in the pressure drop. This enhancement is due by the large surface area of louvre fins and by the vortex generated by the holes. Moreover, it has been demonstrated that by reducing the fin spacing the heat transfer characteristics of the heat exchanger could be further improved.

Research Aim # 3: To develop a novel performance optimisation model and to apply it to develop more efficient design of fins configuration for the multi-tube heat exchanger used in the current FCU based on multi-objective optimisation and total cost analysis.

Achievement # 3: A time efficient optimisation strategy which takes into consideration limited experimental inputs, CFD modelling and optimisation has been proposed. The outcome from this strategy is an optimised model developed based on two main optimisation objectives; optimisation for maximising JF and optimisation for minimising total cost. Furthermore, detailed method to estimate the total cost of the FCU integrated with multi-tube and fin heat exchanger has been discussed.

7.3 Thesis Conclusions

An inclusive study has been carried out to extend the existing literature regarding the design and performance of the multi-tube and fin heat exchanger used in the FCU and to provide novel techniques to improve the current understanding of the design process, operational

characteristics and geometry related effects. The major conclusions for each objective of this research study are summarized as follows:

1.1 To carry out a qualitative and quantitative analyses of the results achieved experimentally and numerically using a novel 3D CFD model for the baseline model,

A novel CFD model with full 3D geometry for multi-tube and fin heat exchanger with different fin configurations (i.e. plain, louvre and perforated) has been developed. In addition, qualitative and quantitative analyses have been carried out on the baseline model. This analysis suggests that full 3D modelling is required to achieve more accurate results. Very good agreement with experimental results was observed for temperature distribution. However, pressure drop results were within 15% of error margin. This indicates that often used in a literature much simpler 3D single fin simulation may not be sufficiently accurate to estimate an overall thermal performance and pressure drop of the FCU. Therefore, developed full 3D CFD model can be valuable contribution to the research field in this area.

1.2 To use CFD to predict heat transfer coefficients and local fin efficiency for multi tube and fin heat exchanger,

The CFD model has been used to compute heat transfer coefficients and local fin efficiency for a heat exchanger. Obtained results indicate significant variations of the air flow across different sections of the heat exchanger. Moreover, heat transfer coefficient is higher at external fins (i.e 1^{st} and 21^{st}) and its distribution is not uniform across other fins.

1.3 To determine the effect of longitudinal pitch, transvers pitch and fin spacing on the thermal performance of multi tubes and fins heat exchanger,

Fin spacing, longitudinal pitch and transverse pitch have a significant impact on the heat transfer and pressure drop characteristics of the heat exchanger under steady state operating condition. Lower fin spacing will enhance the heat transfer characteristics of the heat exchanger. However, it will also raise the pressure drop across the heat exchanger. For example, change of fin spacing from 5.2mm to 4.2mm will increase operating cost of 1% but will enhance thermal performance (JF factor) of 3%.

1.4 To develop a novel semi-empirical prediction model for the Colburn (j) factor and Fanning friction factor (f) for the multi-tube and fin heat exchanger with plain fins.

A prediction model to estimate Fanning friction factor (f) and Colburn factor (j) has been developed by taking into consideration the effects of heat exchanger geometrical parameters; fin spacing, longitudinal pitch and transverse pitch. The prediction model and its modifications have been used to optimise thermal performance of new FCU design.

2.1 To present a novel fin configuration (perforated plain fin) and compare its thermal performance with plain and louvre fins configurations,

Due to the vortex generated by the holes, the perforated plain fins heat exchanger model has achieved an enhancement in heat transfer characteristics when it is compared with the plain fins heat exchanger model. This enhancement is relatively high at small water flow rate but it has disadvantage of an increase in the pressure drop. Hence, the perforated plain fins heat exchanger model has been considered for further investigations.

2.2 To carry out a comparative numerical study of the airside performance of multi-tube and fin heat exchanger under steady state operating conditions having plain, louvre and perforated louvre fins,

By using a surface modification in the form of perforations in the louvre fins the thermal performance of the heat exchanger has been improved. Hence, the model with perforated louvre fins can be considered as the optimal model. Furthermore, the surface area of the louvre fins is larger comparing with plain fins. This fact results in an increase of the heat transfer characteristics as well as an increase in the pressure drop across the air-side of the heat exchanger.

2.3 To develop a combined semi-empirical prediction model for Colburn (j) factor and Fanning friction factor (f) which can be used for different fin configurations,

The prediction model developed in chapter 4 was only applicable to predict Fanning friction factor (f) and Colburn factor (j) for plain fins heat exchanger based on its geometrical parameters. Therefore, a novel set of design equations have been developed based on propose correction factors to account for the predicted values of Fanning friction factor (f) and Colburn factor (j) computed using the prediction model for the baseline model. Hence, these set of novel equations are applicable for louvre and perforated fins heat exchangers.

2.4 To formulate the effect of hole diameter and hole spacing of the perforations on the thermal performance of the multi-tube and fin heat exchanger.

The holes diameter and holes spacing have shown some effect on the thermal performance of perforate louvre fins heat exchanger model especially at low air velocity, whereas larger hole diameter (D/3-hole diameter) and 25 mm holes spacing are the optimum values for theses parameters.

3.1 To propose a time efficient optimisation strategy which take into consideration limited experimental inputs, CFD modelling and optimisation

The optimisation approach for more efficient design which require only limited experimental inputs and is based on analytical analysis of thermal performance prediction, CFD modelling and costs analysis has been proposed. This strategy is used for multi-objective optimisation developed in chapter 6.

3.2 To employ the new optimisation strategy to evaluate the thermal performance of the heat exchanger used in the FCU with combination of plain, perforated and louvre fins arrangements,

The optimisation strategy has been employed to evaluate the thermal performance of the heat exchanger used in the FCU with combination of plain, perforated and louvre fins arrangements by using when possible an experimental technique and in other cases numerical technique. The perforated louvre fins heat exchanger has been considered the best performance heat exchanger.

3.3 To derive an optimised model for the FCU design based on the heat exchanger performance with the following inputs: fins geometry, fins arrangements and total cost

Developed in this thesis optimisation strategy was used to design new heat exchanger with the following parameters: type of fins are louvre perforated, fins spacing 4.2mm, surface area of a single fin 9796 mm^2, number of fins 21 and operating at Reynolds number equal to12,000 with total manufacturing and operating costs only 6% higher than for plain fins, when calculated over 15 years of intended use. Increase of the costs is mainly attributed to much higher air pressure drop of up to 40% higher than for plain fins. However, thermal efficiency (JF factor) of this configuration is 80% better than for plain fins and 10% better than for unperforated louvre fins.

3.4 To assess the effectiveness of the proposed optimisation strategy by prototyping and validating the new optimised design

A prototype of the optimised model has been manufactured. A benchmark test has been carried out to validate the numerically predicted results against experimental data in order to evaluate the effectiveness of the proposed optimisation strategy.

7.4 Main Conclusions

The main conclusions from the carried-out research can be summarised as follows:

- New optimisation strategy for designing the FCU has been developed, which is based on the combination of initial experimental input, CFD modelling and analytical thermal performance calculations and cost analysis.
- New and more efficient FCU optimised design has been created which include geometrical modification to the fins in term of perforation of louvre fins and its spacing 4.2mm. Comparing to a plain fins design, thermal performance of newly proposed design improved 80% and comparing to unperforated louvre fins improved 10%.
- Having perforations in the fin surface improve its thermal performance and therefore improve the thermal performance of the heat exchanger. The holes on the fin surface enhance turbulence, which increases the local heat transfer coefficient compared to unperforated fins. Moreover, having a perforation on the fin helps to create secondary flows due to disturbance effect in the flow inside the boundary layer. For louvre fins perforation is increasing heat transfer (Q_{avg}) of 5% and thermal performance (JF factor) of 10% at a cost of very moderate increase of the pressure drop of about 2%.
- A local thermal analysis has been introduced by incorporating CFD modelling to predict heat transfer coefficients and local fin efficiency for multi-tube and fin heat exchanger.
- Using a combination of different tools developed in this study, the cost and time of the design process can be significantly reduced.

7.5 Thesis Contributions

The major contributions of this research study are summarised below in which novelties of this research are described.

Contribution # 1:

A novel local flow field analysis using CFD model with full 3D geometry for multi-tube and fin heat exchanger as numerical model has been carried out. This analysis includes the local behaviour of both working fluids, the change in the local flow characteristics as the flow pass through a tube bend. The local flow analysis has been extended to incorporate the heat transfer coefficients and local fin efficiency corresponding to local flow field around a fin placed within the heat exchanger. Evaluation of local heat transfer performance of individual fins is a major step forward in performance analysis of heat exchangers. The available literature use of part or whole fin to simulate the flow in a heat exchanger and hence provide only simplified view of heat transfer process within heat exchangers. It has been observed that depending on the fin location within the heat exchanger both the heat transfer coefficient and hence the heat transfer efficiency of fins can vary substantially.

Contribution # 2:

The realistic CFD model has been implemented to study the effect of fin spacing, longitudinal pitches and transverse pitches on the heat transfer and pressure drop characteristics of the heat exchanger under a number of steady state operating conditions. Based on the numerical results of this parametric study, a novel mathematical model has been suggested. This model can predict the heat transfer and pressure drop characteristics of the plain fins heat exchanger as a function of its geometrical parameters. Therefore, it can be used to design a heat exchanger. Furthermore, correction factors have been presented for this model in order to make it more applicable for the design modification carried out on the heat exchanger. i.e. louvre and perforated configurations. All the equations developed are novel as these are not based on the assumption of single fin efficiency parameter but take actual variations in fin efficiency into account.

Contribution # 3:

A novel optimisation procedure for designing the FCU integrated with multi-tube and fin heat exchanger has been developed. The optimisation procedure combined two optimisation objectives; optimisation for maximising the thermal performance and for minimising total cost. In addition, this work has been carried out based on a unique optimisation strategy which is based on the combination of initial experimental input, CFD modelling and analytical thermal performance calculations and cost analysis.

7.6 Recommendations for Future Work

After carrying out this study on improving the thermal performance of the FCU with mainly focus on the heat exchanger, it has become obvious that there is a huge potential for further research and studies in this field. Suggestions for future works are as follows:

Recommendation # 1: To study the improving of the thermal performance of the FCU by increasing the surface area of the water-side to enhance the amount of heat transfer. This can be done by redesigning the water-side by having different tube shapes such as helical, wavy and spiral.

Recommendation # 2: Analysing energy consumption without affecting the duty in FCU by finding an environmentally friendly source of heating the water such as a closed loop thermo-syphon system. This can reduce the total cost of operating the FCU and improve the thermal performance as well.

Recommendation # 3: To further evaluate the noise level in FCU with design modifications. This can be carried out by studying the electromagnetic, mechanical and aerodynamic performance of the fan and by applying an acoustic insulation.

REFERENCES

[1]. Davison, D., the Redesign of the Amethyst Fan Coil Unit, in Engineering and Technology. 2013, University of Huddersfield: Huddersfield.

[2]. Naphon, P. and S. Wongwises, A review of flow and heat transfer characteristics in curved tubes. Renewable and Sustainable Energy Reviews, 2006. **10**(5): p. 463-490.

[3]. Markowitz, M. and D. Fischer, Heat exchanger for an air conditioning system. 2015, Google Patents.

[4]. Torii, K., K. Kwak, and K. Nishino, Heat transfer enhancement accompanying pressure-loss reduction with winglet-type vortex generators for fin-tube heat exchangers. International Journal of Heat and Mass Transfer, 2002. **45**(18): p. 3795-3801.

[5]. Joardar, A. and A. Jacobi, Heat transfer enhancement by winglet-type vortex generator arrays in compact plain-fin-and-tube heat exchangers. International Journal of refrigeration, 2008. **31**(1): p. 87-97.

[6]. Sobhan, C., et al., Experimental investigations on a 1–2 heat exchanger with wire-wound tubes. Wärme-und Stoffübertragung, 1994. **29**(4): p. 211-217.

[7]. Shah, R.K. and D.P. Sekulic, Fundamentals of heat exchanger design. 2003: John Wiley & Sons.

[8]. McDonald, A.G. and H.L. Magande, Introduction to thermo-fluids systems design. 2012: Wiley-Blackwell.

[9]. Lee, H.S., Thermal Design : Heat Sinks, Thermoelectrics, Heat Pipes, Compact Heat Exchangers, and Solar Cells. 2010, Hoboken, NJ, USA: Wiley.

[10]. Lee, H.S., Thermal design: heat sinks, thermoelectrics, heat pipes, compact heat exchangers, and solar cells. 2010: John Wiley & Sons.

[11]. Kays, W.M. and A.L. London, Compact heat exchangers. 1984.

[12]. McQuiston, F.C. and J.D. Parker, Heating, ventilating, and air conditioning: analysis and design. 1982.

[13]. Shah, R.K. and D.P. Sekulić, Classification of heat exchangers. Fundamentals of Heat Exchanger Design, 2007: p. 1-77.

[14]. Thulukkanam, K., Heat Exchanger Design Handbook. 2013: CRC Press.

[15]. London, A. and R. Seban, A generalization of the methods of heat exchanger analysis. International Journal of Heat and Mass Transfer, 1980. **23**(1): p. 5-16.

[16]. Thulukkanam, K., Heat Exchanger Design Handbook, Second Edition ed. S. Edition. 2013 Taylor and Francis.

[17]. Bunce, D., The Transient response of heat exchangers. 1995.

[18]. Spiga, G. and M. Spiga, Two-dimensional transient solutions for crossflow heat exchangers with neither gas mixed. Journal of heat transfer, 1987. **109**(2): p. 281-286.

[19]. Chen, H.-T. and K.-C. Chen, Simple method for transient response of gas-to-gas cross-flow heat exchangers with neither gas mixed. International journal of heat and mass transfer, 1991. **34**(11): p. 2891-2898.

[20]. Mishra, M., P. Das, and S. Sarangi, Transient behavior of crossflow heat exchangers with longitudinal conduction and axial dispersion. Journal of heat transfer, 2004. **126**(3): p. 425-433.
[21]. Kays, W.M. and A.L. London, Compact heat exchangers. 1964.
[22]. Gvozdenac, D., Analytical Solution of Dynamic Response of Heat Exchanger. 2012.
[23]. Pucci, P., C. Howard, and C. Piersall, The single-blow transient testing technique for compact heat exchanger surfaces. Journal of Engineering for Gas Turbines and Power, 1967. **89**(1): p. 29-38.
[24]. Wilson, E.E., A basis for rational design of heat transfer apparatus. Trans. ASME, 1915. **37**(47): p. 47-82.
[25]. Fernandez-Seara, J., et al., A general review of the Wilson plot method and its modifications to determine convection coefficients in heat exchange devices. Applied Thermal Engineering, 2007. **27**(17): p. 2745-2757.
[26]. Sieder, E.N. and G.E. Tate, Heat transfer and pressure drop of liquids in tubes. Industrial & Engineering Chemistry, 1936. **28**(12): p. 1429-1435.
[27]. Colburn, A.P., A method of correlating forced convection heat-transfer data and a comparison with fluid friction. International Journal of Heat and Mass Transfer, 1964. **7**(12): p. 1359-1384.
[28]. Dittus, F. and L. Boelter, Heat transfer in automobile radiators of the tubular type. International Communications in Heat and Mass Transfer, 1985. **12**(1): p. 3-22.
[29]. Wang, C.-C., et al., Sensible heat and friction characteristics of plate fin-and-tube heat exchangers having plane fins. International Journal of Refrigeration, 1996. **19**(4): p. 223-230.
[30]. Abu Madi, M., R. Johns, and M. Heikal, Performance characteristics correlation for round tube and plate finned heat exchangers: Equations relatives aux performances d'échangeurs de chaleur constitués de tubes ronds et de plaques à ailettes. International journal of refrigeration, 1998. **21**(7): p. 507-517.
[31]. Wang, C.-c. and K.-Y. Chi, Heat transfer and friction characteristics of plain fin-and-tube heat exchangers, part I: new experimental data. International Journal of Heat and Mass Transfer, 2000. **43**(15): p. 2681-2691.
[32]. Halıcı, F., I. Taymaz, and M. Gündüz, The effect of the number of tube rows on heat, mass and momentum transfer in flat-plate finned tube heat exchangers. Energy, 2001. **26**(11): p. 963-972.
[33]. Wang, C.-C. On the heat and mass analogy of fin-and-tube heat exchangers. in International Heat Transfer Conference 13. 2006. Begel House Inc.
[34]. Taler, D., Experimental and numerical predictions of the heat transfer correlations in the cross-flow plate fin and tube heat exchangers. Archives of Thermodynamics, 2007. **28**: p. 3-18.
[35]. Chaudhari, J.M., D. Subhedar, and N. Patel, Experimental Investigation of Finned Tube Heat Exchanger. 2014.
[36]. Taler, D. and P. Ocłoń, Thermal contact resistance in plate fin-and-tube heat exchangers, determined by experimental data and CFD simulations. International Journal of Thermal Sciences, 2014. **84**: p. 309-322.

[37]. Wang, C.-C., et al., An experimental study of the air-side performance of fin-and-tube heat exchangers having plain, louver, and semi-dimple vortex generator configuration. International Journal of Heat and Mass Transfer, 2015. **80**: p. 281-287.
[38]. Song, K., et al., Effect of geometric size of curved delta winglet vortex generators and tube pitch on heat transfer characteristics of fin-tube heat exchanger. Experimental Thermal and Fluid Science, 2017. **82**: p. 8-18.
[39]. Varun Singh, V.A., Reinhard Radermacher, Numerical approach for modeling air-to-refrigerant fin-and-tube heat exchanger with tube-to-tube heat transfer. International Journal of Refrigeration, 2008. Volume 31**,** (Issue 8): p. 1414-1425.
[40]. Borrajo-Peláez, R., J. Ortega-Casanova, and J. Cejudo-López, A three-dimensional numerical study and comparison between the air side model and the air/water side model of a plain fin-and-tube heat exchanger. Applied Thermal Engineering, 2010. **30**(13): p. 1608-1615.
[41]. Dong, J., et al., Experimental and numerical investigation of thermal-hydraulic performance in wavy fin-and-flat tube heat exchangers. Applied Thermal Engineering, 2010. **30**(11): p. 1377-1386.
[42]. Lu, C.-W., et al., A numerical investigation of the geometric effects on the performance of plate finned-tube heat exchanger. Energy Conversion and Management, 2011. **52**(3): p. 1638-1643.
[43]. Čarija, Z., et al., Heat transfer analysis of fin-and-tube heat exchangers with flat and louvered fin geometries. International journal of refrigeration-revue internationale du froid, 2014. **140**: p. 7007.
[44]. Altwieb, M.O. and R. Mishra, Experimental and Numerical Investigations on the Response of a Multi Tubes and Fins Heat Exchanger under Steady State Operating Conditions. 2016.
[45]. Wang, C.-C., W.-S. Lee, and W.-J. Sheu, A comparative study of compact enhanced fin-and-tube heat exchangers. International Journal of Heat and Mass Transfer, 2001. **44**(18): p. 3565-3573.
[46]. Webb, R.L. and N.-H. Kim, Advances in air-cooled heat exchanger technology. Journal of Enhanced Heat Transfer, 2007. **14**(1).
[47]. WANG, C.-C., A survey of recent patents of fin-and-tube heat exchangers from 2001 to 2009. International Journal of Air-Conditioning and Refrigeration, 2010. **18**(01): p. 1-13.
[48]. Erek, A., et al., Effect of geometrical parameters on heat transfer and pressure drop characteristics of plate fin and tube heat exchangers. Applied Thermal Engineering, 2005. **25**(14): p. 2421-2431.
[49]. Liu, X., J. Yu, and G. Yan, A numerical study on the air-side heat transfer of perforated finned-tube heat exchangers with large fin pitches. International Journal of Heat and Mass Transfer, 2016. **100**: p. 199-207.
[50]. Fax, D. and R. Mills, Generalized optimal heat exchanger design. Trans. ASME, 1957. **79**: p. 653-661.
[51]. Queipo, N., R. Devarakonda, and J. Humphrey, Genetic algorithms for thermosciences research: application to the optimized cooling of electronic components. International Journal of Heat and Mass Transfer, 1994. **37**(6): p. 893-908.

[52]. Guessous, L. and S. Maddipatla. Improving radiator design through shape optimization. in ASME 2002 International Mechanical Engineering Congress and Exposition. 2002. American Society of Mechanical Engineers.
[53]. Suram, S., D. Ashlock, and K. Bryden. Graph based evolutionary algorithms for heat exchanger fin shape optimization. in 11th AIAA/ISSMO Multidisciplinary Analysis and Optimization Conference. 2006.
[54]. Mishra, M., P. Das, and S. Sarangi, Second law based optimisation of crossflow plate-fin heat exchanger design using genetic algorithm. Applied thermal engineering, 2009. **29**(14): p. 2983-2989.
[55]. Xie, G., B. Sunden, and Q. Wang, Optimization of compact heat exchangers by a genetic algorithm. Applied Thermal Engineering, 2008. **28**(8): p. 895-906.
[56]. Rao, R. and V. Patel, Thermodynamic optimization of cross flow plate-fin heat exchanger using a particle swarm optimization algorithm. International Journal of Thermal Sciences, 2010. **49**(9): p. 1712-1721.
[57]. Juan, D. and Q.Z. Qin, Multi-objective optimization of a plain fin-and-tube heat exchanger using genetic algorithm. Thermal Engineering, 2016. **61**(4): p. 309-317.
[58]. Myhren, J.A. and S. Holmberg, Improving the thermal performance of ventilation radiators–The role of internal convection fins. International journal of thermal sciences, 2011. **50**(2): p. 115-123.
[59]. Yun, J.-Y. and K.-S. Lee, Influence of design parameters on the heat transfer and flow friction characteristics of the heat exchanger with slit fins. International Journal of Heat and Mass Transfer, 2000. **43**(14): p. 2529-2539.
[60]. Kim, M.-S., et al., Correlations and optimization of a heat exchanger with offset-strip fins. International Journal of Heat and Mass Transfer, 2011. **54**(9): p. 2073-2079.
[61]. Lee, J. and K.-S. Lee, Correlations and shape optimization in a channel with aligned dimples and protrusions. International Journal of Heat and Mass Transfer, 2013. **64**: p. 444-451.
[62]. Singh, S., et al., Implications of fin profiles on overall performance and weight reduction of a fin and tube heat exchanger. Applied Thermal Engineering, 2017. **115**: p. 962-976.
[63]. Ebmpapst. 2010; Available from: http://www.ebmpapst.fi/fi/tuotteet/Varaosavalikoima/Kaavulliset-yhdelt%C3%A4-puolelta-imev%C3%A4t-keskipakopuhaltimet/G3G146AB5401.
[64]. Wang, C.-C., K.-Y. Chen, and Y.-T. Lin, Investigation of the semi-dimple vortex generator applicable to fin-and-tube heat exchangers. Applied Thermal Engineering, 2015. **88**: p. 192-197.
[65]. Ltd, R.C. RS Pro T Type Thermocouple 2m Cable -75°C → +250°C. 2010; Available from: http://uk.rs-online.com/web/p/thermocouples/8479687/?searchTerm=8479687&relevancy-data=636F3D3126696E3D4931384E525353746F636B4E756D6265724D504E266C753D656E266D6D3D6D61746368616C6C26706D3D5E5C647B367D247C5E5C647B377D247C5E5C647B31307D2426706F3D313426736E3D592673743D52535F53544F434B5F4E554D4245522677633D4E4F4E45267573743D38343739363837267374613D3834373936383726.

[66]. Technology, P. Temperature Probe, PT100. 2010; Available from: http://docs-europe.electrocomponents.com/webdocs/0097/0900766b80097a2f.pdf.
[67]. Ltd, I.S.S. 2012; Available from: http://www.impress-sensors.co.uk/images/products/Datasheets/Impress/D-IMP-Industrial-pressure%20transmitter-ceramic-sensor.pdf.
[68]. Limited, P.T., Thermocouple Data Logger. 2012.
[69]. Technology, P. PT-104 Platinum Resistance Data Logger. 2012; Available from: https://www.picotech.com/download/datasheets/usb-pt-104-data-sheet.pdf.
[70]. Moffat, R.J., Describing the uncertainties in experimental results. Experimental thermal and fluid science, 1988. **1**(1): p. 3-17.
[71]. Kline, S.J. and F. McClintock, Describing uncertainties in single-sample experiments. Mechanical engineering, 1953. **75**(1): p. 3-8.
[72]. Administration, N.A.a.S., Measurement Uncertainty Analysis Principles and Methods July 2010 NASA-HDBK-8739.19-3: Washington DC. p. 275.
[73]. Bell, S., A beginner's guide to uncertainty of measurement. 2001: National Physical Laboratory Teddington, Middlesex.
[74]. Versteeg, H.K. and W. Malalasekera, An introduction to computational fluid dynamics: the finite volume method. 2007: Pearson Education.
[75]. Cebeci, T., et al., Computational fluid dynamics for engineers. 2005: Springer Berlin Heidelberg.
[76]. Blazek, J., Computational fluid dynamics: principles and applications. 2001: Butterworth-Heinemann.
[77]. Fluent, A., ANSYS Fluent UDF Manual.[Online](Updated February 2015). Avaliable at: http://orange. engr. ucdavis. edu/Documentation12. 0/1, 2015. **20**.
[78]. Guide, A.F.U.s., ANSYS Fluent User's Guide. ANSYS, Inc, 2010.
[79]. Craft, T.J., Wall Function. 2011: Manchester-UK.
[80]. Schlichting, H., Boundary Layer Theory. 7th Edition ed. 1979.
[81]. Inc, F., Single-Precision and Double-Precision Solvers. 2006.
[82]. Ardila Marín, J.G., D.A. Hincapié Zuluaga, and J.A. Casas Monroy, Comparison and validation of turbulence models in the numerical study of heat exchangers. Tecciencia, 2015. **10**(19): p. 49-60.
[83]. Neopane, H.P., Sediment erosion in hydro turbines. 2010.
[84]. Standard, A., Standard 41.2-1987, Standard methods for laboratory air-flow measurement. American Society of Heating, Refrigerating and Air-Conditioning Engineers, Inc., Atlanta, 1987.
[85]. Saunders, E.A.D., Heat exchangers. 1988.
[86]. Gnielinski, V., New equations for heat and mass-transfer in turbulent pipe and channel flow. International chemical engineering, 1976. **16**(2): p. 359-368.
[87]. Luo, X. and W. Roetzel, The single-blow transient testing technique for plate–fin heat exchangers. International journal of heat and mass transfer, 2001. **44**(19): p. 3745-3753.
[88]. Miller, D.S., Internal flow system. 1990: BHRA.
[89]. Carlsson, C., Heat Transfer in Curved Pipes. Lunds Universitet, Lund, Sweden, 2014.
[90]. Schwentker, R.A., Advances to a computer model used in the simulation and optimization of heat exchangers. 2005.

[91]. Schmidt, T.E., Heat transfer calculations for extended surfaces. Refrig. Eng, 1949. **57**(4): p. 351-357.
[92]. Holman, J., Heat transfer, 1986. McGraw–Hill Book Company, Southern Methodist University, 1986.
[93]. Neale, A., et al., CFD calculation of convective heat transfer coefficients and validation–Part 2: Turbulent flow. 2006, Annex.
[94]. Zhang, T.T., H. Zhou, and S. Wang, An adjustment to the standard temperature wall function for CFD modeling of indoor convective heat transfer. Building and environment, 2013. **68**: p. 159-169.
[95]. Shah, R.K. and A.L. London, Laminar flow forced convection in ducts: a source book for compact heat exchanger analytical data. 2014: Academic press.
[96]. Book, S.A., Estimating probable system cost. Crosslink, 2001. **2**(1): p. 12-21.
[97]. Menon, E.S., Gas pipeline hydraulics. 2005: CRC Press.
Clark, R.M., et al., Cost models for water supply distribution systems. Journal of Water Resources Planning and Management, 2002. **128**(5): p. 312-321.
[98]. Castagne, S., et al., A generic tool for cost estimating in aircraft design. Research in engineering design, 2008. **18**(4): p. 149-162.
[99]. Trew, M.S. and V.A. Bird, Sheet-metal work. 1923: The Manual arts press.
[100]. Hazell, D.D., Modeling and Optimization of Condensing Heat Exchangers for Cooling Boiler Flue Gas. 2011.
[101]. Alamu, O., O. Adigun, and M. Durowoju, Computer–aided Optimum Pipe Size Selection for Non Viscous Flow. Annals of Engineering Analysis, 2002. **1**(4): p. 30-39.
[102]. Standard, A., Standard 41.1-1986, 1986,"Standard Method for Temperature Measurement,". American Society of Heating, Refrigerating and Air-Conditioning Engineers, Inc., Atlanta, GA.
[103]. TFI. Cobra Probe User Guide. 2012; Available from: http://www.turbulentflow.com.au/Downloads/Getting%20Started%20-%20Cobra%20Probe.pdf.
[104]. Hozo, S.P., B. Djulbegovic, and I. Hozo, Estimating the mean and variance from the median, range, and the size of a sample. BMC medical research methodology, 2005. **5**(1): p. 1.

APPENDIX A - CALIBRATION PROCEDURE

A.1 RTD Sensors Calibration

To ensure that the water temperature readings stayed accurate, both RTD sensors (Temperature Probe- PT100) used in this experiment were carefully calibrated. The calibration was performed using an open surface water bath which has a thermometer indicator with 0.1 (°C) divisions [103]. PT-104 Platinum resistance data logger and water bath are the main equipment used to carry out this calibration, as shown in figure A.1.

Figure A.1 RTD Sensors Calibration Equipment

The procedure of calibrating the RTD sensors can be summarised in the following steps:

1. Connect RTD sensors to PT-104 data logger. The data logger should be connected the computer
2. Place both RTD sensors into the water bath
3. Heat water in the water bath until it reaches 60 ±0.2°C. Ensure the equilibrium of the water temperature by allowing some time before starting recording the readings
4. Record the data form both RTD sensors and the water bath thermometer at constant intervals
5. Take the average value of data for both RTD sensors and thermometer
6. Lastly, compute the percentage difference by subtracting the average value of data for each RTD sensor from the average value of data for thermometer

Table A-1 summarise the results of this calibration.

Table A-1 RTD Sensors Calibration Results

	Water Bath Thermometer Reading (°C)	RTD Sensor Reading Water-IN (°C)	RTD Sensor Reading Water-OUT (°C)
	60.200	59.966	59.969
	60.100	59.794	59.763
	60.100	59.793	59.732
	60.000	59.594	59.660
	60.100	59.702	59.591
	60.000	59.544	59.686
	60.100	59.635	59.532
	60.100	59.603	59.544
	60.000	59.575	59.608
	60.100	59.556	59.625
Average Value (°C)	60.080	59.676	59.671
Difference (°C)	===	0.404	0.409
	59.900	59.558	59.523
	60.000	59.566	59.584
	60.100	59.566	59.549
	59.800	59.534	59.632
	60.000	59.603	59.620
	60.100	59.615	59.612

	60.000	59.563	59.689
	60.000	59.550	59.643
	60.100	59.575	59.709
	60.100	59.621	59.612
Average Value (°C)	60.010	59.575	59.617
Difference (°C)	===	0.435	0.393
Average Difference (°C)	===	0.419	0.401

A.2 Thermocouples Calibration

Calibrating thermocouples is essential in order to achieve accurate readings from theses thermocouples. A mercury in glass thermometer with 0.5 (°C) divisions and a TC-08 thermocouple data logger were used to perform the calibration for T-type exposed welded tip thermocouples [103], as shown in figure A.2 . The thermocouple data logger can convert the voltage coming through the thermocouples into temperature and using Pico log data logger software to record the data.

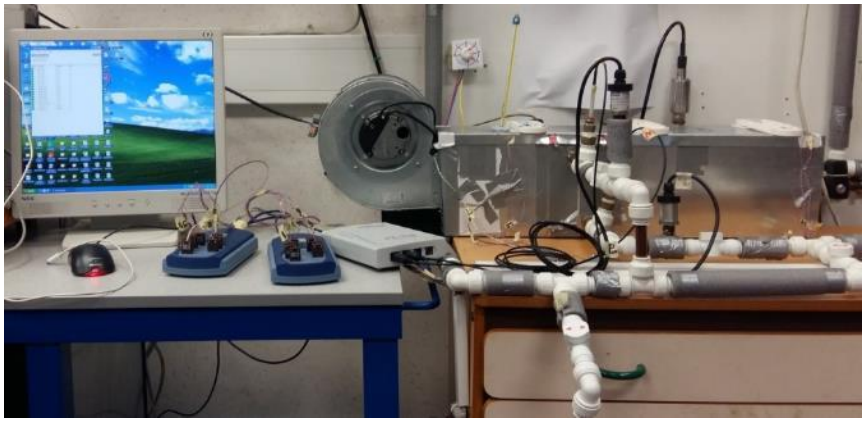

Figure A.2 Thermocouples Calibration Equipment

As discussed in chapter 3, two measuring stations were used to measure the air inlet and outlet temperatures; each measuring station contains of 7 T-type exposed welded tip thermocouples. The distribution of these thermocouples in the measuring station is shown in figure A.3.

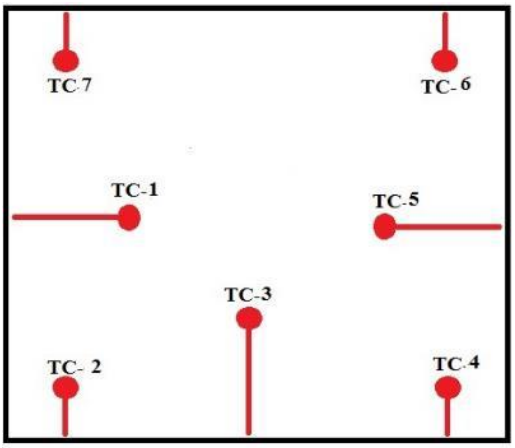

Figure A3 Thermocouples Distribution in the Measuring Station

The procedure of calibrating the thermocouples can be summarised in the following steps:

1. Plug the TC-08 into a USB port on a computer, plug in the thermocouples in to the data logger
2. Place the thermometer in the inlet measuring station as shown in figure A.4

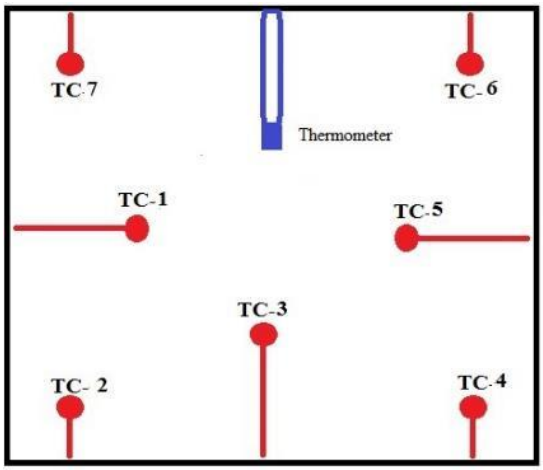

Figure A.4 Inserting the Thermometer in the Measuring Station

3. Turn on the centrifugal fan and record the measured temperature from both thermocouples and thermometer
4. Average value of recorded data from both thermocouples and thermometer
5. Compute the percentage difference by subtracting the average value of data for every thermocouple from the average value of data for thermometer
6. Table A-2 summarise the results of calibrating the thermocouples in the inlet measuring station

Table A-2 *Results of Calibrating the Thermocouples in the Inlet Measuring Station*

	Thermometer Reading (°C)	TC-1 (°C)	TC-2 (°C)	TC-3 (°C)	TC-4 (°C)	TC-5 (°C)	TC-6 (°C)	TC-7 (°C)
	22.700	23.176	23.443	23.100	23.400	23.063	23.490	23.450
	23.000	23.229	23.476	23.124	23.433	23.104	23.539	23.514
	23.000	23.229	23.480	23.127	23.437	23.116	23.536	23.518
	23.000	23.192	23.466	23.110	23.426	23.105	23.530	23.502
	23.000	23.191	23.470	23.108	23.444	23.115	23.526	23.504
	22.700	23.162	23.461	23.105	23.441	23.114	23.520	23.489
	22.700	23.134	23.446	23.093	23.439	23.121	23.548	23.506
	23.000	23.108	23.444	23.080	23.438	23.134	23.568	23.511
	23.000	23.122	23.445	23.068	23.428	23.139	23.571	23.526
	23.000	23.176	23.474	23.139	23.472	23.167	23.592	23.555
Average Value (°C)	22.910	23.172	23.461	23.105	23.436	23.118	23.542	23.508
Difference (°C)	===	0.262	0.551	0.195	0.526	0.208	0.632	0.598
	23.000	23.240	23.528	23.208	23.523	23.212	23.667	23.628
	23.000	23.211	23.524	23.151	23.501	23.210	23.686	23.612
	23.000	23.162	23.488	23.099	23.468	23.178	23.647	23.573
	23.300	23.210	23.509	23.150	23.467	23.222	23.691	23.675
	23.300	23.236	23.521	23.169	23.466	23.258	23.726	23.728
	23.300	23.223	23.522	23.165	23.468	23.261	23.729	23.726

	23.300	23.280	23.552	23.226	23.529	23.289	23.779	23.772
	23.300	23.263	23.551	23.172	23.493	23.278	23.780	23.770
	23.000	23.179	23.504	23.092	23.439	23.227	23.744	23.711
	23.000	23.160	23.484	23.091	23.440	23.215	23.730	23.693
Average Value (°C)	23.150	23.216	23.518	23.152	23.479	23.235	23.718	23.689
Difference (°C)	===	0.066	0.368	0.002	0.329	0.085	0.568	0.539
Average Difference (°C)	===	0.164	0.459	0.099	0.428	0.146	0.600	0.568

7. The same steps have been followed to calibrate thermocouples in the measuring outlet station
8. Table A-3 summarise the results of calibrating the thermocouples in the outlet measuring station

Table A-3 Results of Calibrating *the Thermocouples in the Outlet Measuring Station*

	Thermometer Reading (°C)	TC-1 (°C)	TC-2 (°C)	TC-3 (°C)	TC-4 (°C)	TC-5 (°C)	TC-6 (°C)	TC-7 (°C)
	28.500	28.621	27.619	29.232	29.531	31.176	26.465	28.146
	28.500	28.670	27.711	29.227	29.514	31.162	26.473	28.168
	28.000	28.561	27.593	29.176	29.504	31.070	26.402	28.127
	28.000	28.568	27.578	29.171	29.527	31.102	26.401	28.117
	28.500	28.502	27.578	29.054	29.510	30.985	26.388	28.075
	28.500	28.608	27.620	29.150	29.520	31.116	26.422	28.139

	28.500	28.667	27.668	29.168	29.549	31.120	26.447	28.164
	28.500	28.513	27.619	29.086	29.472	31.012	26.387	28.094
	28.500	28.609	27.599	29.144	29.654	31.117	26.435	28.157
	29.000	28.633	27.560	29.166	29.486	31.100	26.402	28.132
Average Value (°C)	28.450	28.595	27.614	29.157	29.526	31.096	26.422	28.132
Difference (°C)	===	0.145	0.836	0.707	1.076	2.646	2.028	0.318
	29.000	28.708	27.590	29.160	29.594	31.132	26.368	28.157
	28.500	28.648	27.578	29.151	29.528	31.041	26.377	28.119
	25.800	28.674	27.541	29.198	29.605	31.077	26.388	28.154
	28.500	28.670	27.629	29.178	29.632	31.112	26.391	28.165
	29.000	28.674	27.656	29.184	29.646	31.079	26.428	28.148
	29.000	28.721	27.677	29.234	29.699	31.132	26.440	28.186
	29.500	28.712	27.698	29.166	29.533	31.075	26.385	28.133
	29.500	28.800	27.673	29.282	29.759	31.175	26.448	28.220
	30.000	28.646	27.707	29.106	29.522	31.086	26.396	28.125
	30.000	28.578	27.592	29.167	29.550	30.985	26.420	28.058
Average Value (°C)	28.880	28.683	27.634	29.182	29.607	31.089	26.404	28.147
Difference (°C)	===	0.197	1.246	0.302	0.727	2.209	2.476	0.733

Average Difference (°C)	===	0.171	1.041	0.505	0.902	2.428	2.252	0.526

APPENDIX B- MEASURING AIR FLOW VELOCITY

In the experiments, the ASHRAE standard 41.2 [84] was adopted to measure the air flow velocity. Due to the consideration of density effects on accurate measurement of air, the TFI cobra probe was used to measure the air velocity at 25 points at the inlet section. Figure B.1 illustrations the location of measuring points at the test section using log-Tchebycheff method (The test section is 165 mm wide and 175 mm high).

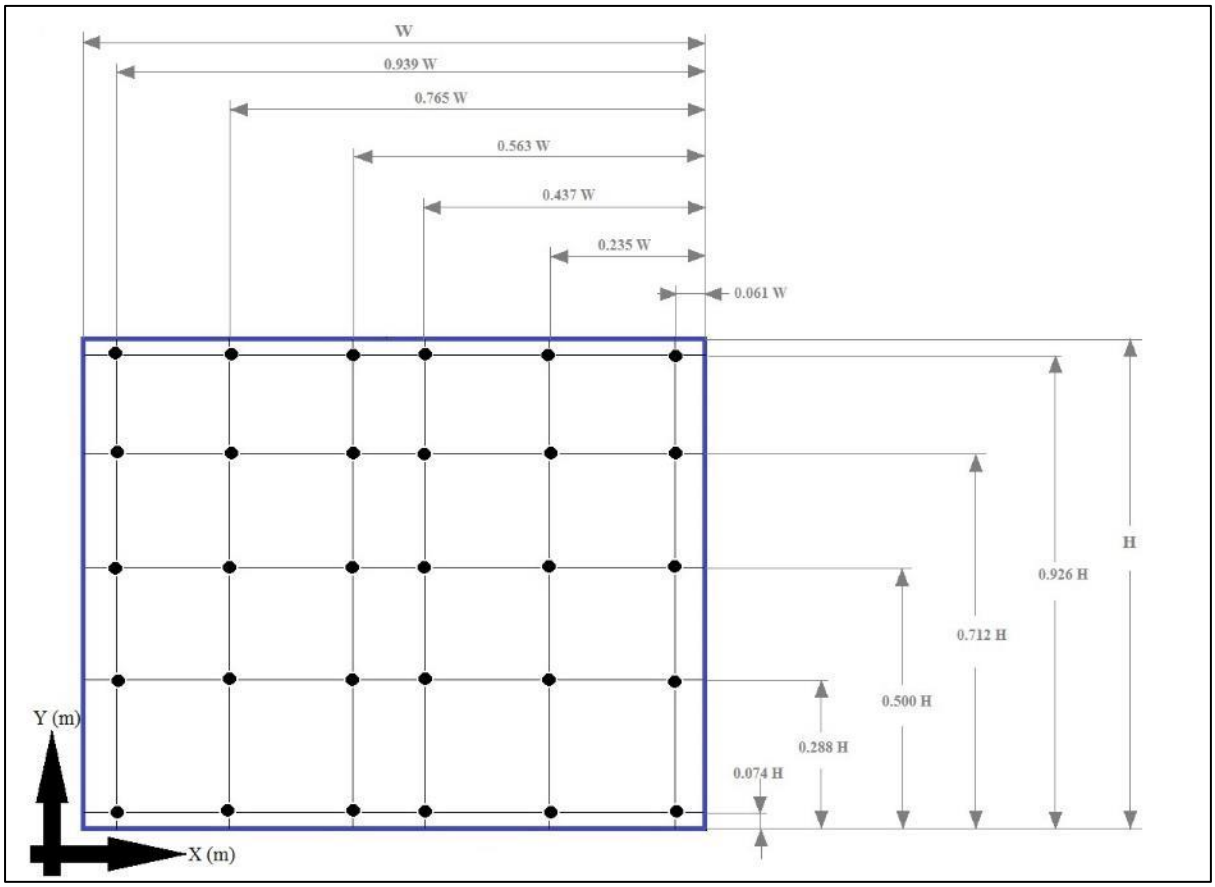

Figure B.1 Location of Measuring Points at Test Section Using Log-Tchebycheff Method

The Cobra probe is a multi-hole pressure probe able to determine 3-components of velocity and local static pressure in real time. The probe is manly composed of body, head, stem, connector socket and a reference pressure port. The schematic diagram of the series 100 TFI Cobra probe is shown in figure B.2.

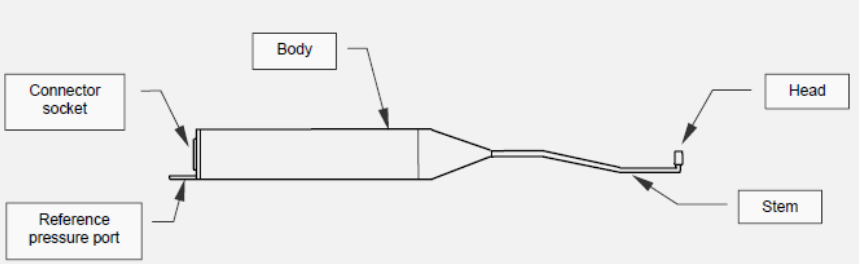

Figure B.2 Schematic Diagram of the Series 100 TFI Cobra Probe *[104]*

The probe measures the 3-component velocity and static pressure within a ±45° acceptance cone, figure B.3.

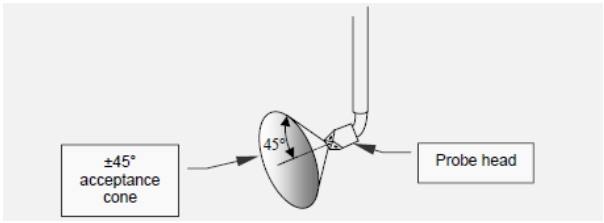

Figure B.3 Flow Directions for Cobra Probe *[104]*

For the purpose of measuring air flow velocity components these steps need to be followed:

Preparing Cobra Probes

1. Plug the cobra probe into its cable. Make sure that the two red signs match each other

2. Place the cobra probe inside its holder.

3. Insert the cobra probe in it is position where the probe head is facing the air flow direction.
4. Plug cobra probe into the DAQ port (2-input interface unit).

5. Plug the DAQ cable into PC.

Setting-up the Cobra Probe

1. In PC, open the software named ‘TFI Device Control’

TFI Device Control main interface

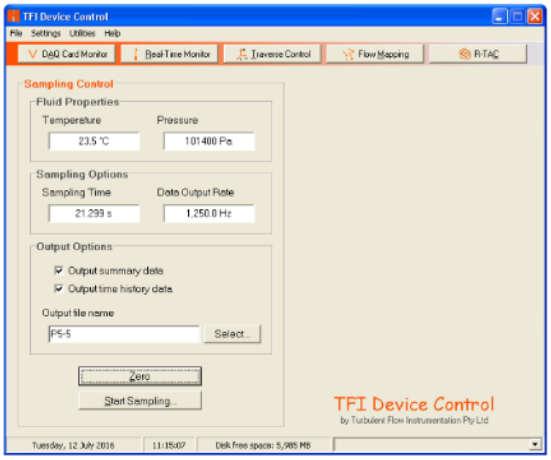

2. Set air properties (temperature and pressure) and sampling time

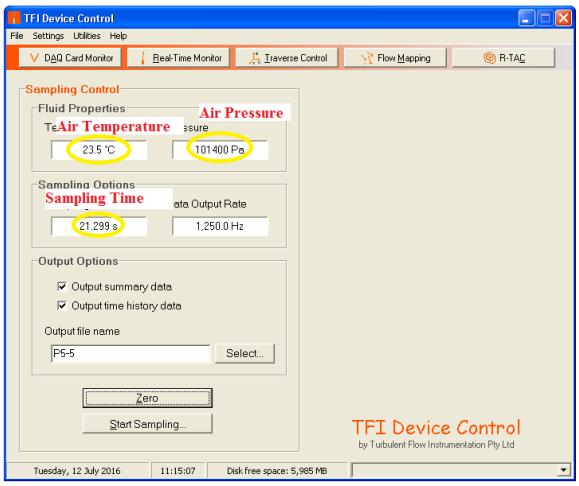

3. Go to setting/ devices

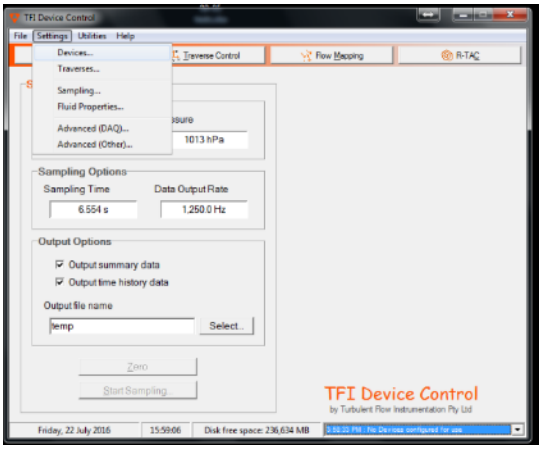

4. Calibrate the probe

Click on calibration

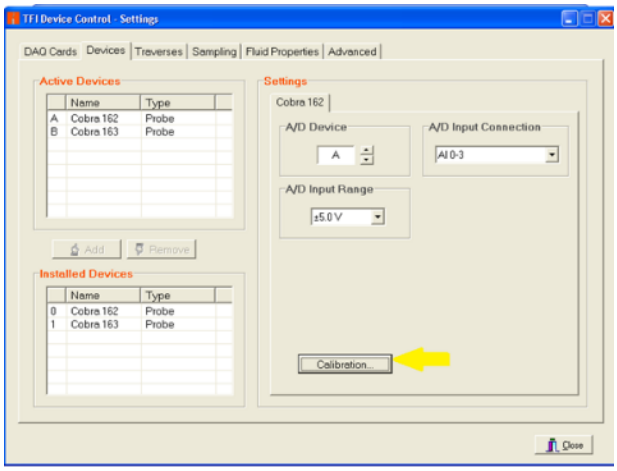

Click on calibrate

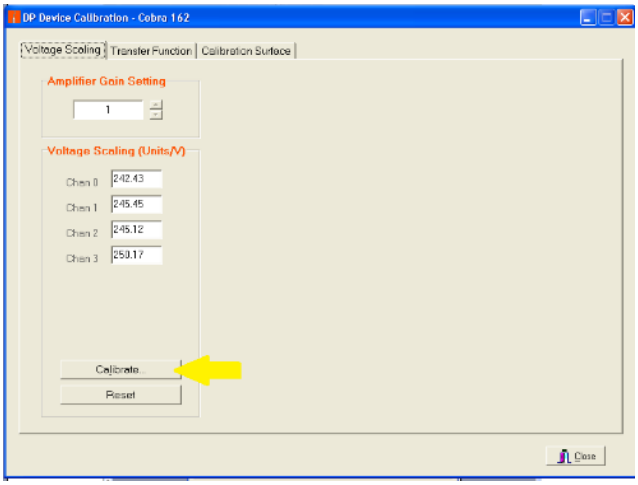

Input the reference pressure (atmospheric pressure) and click on sample

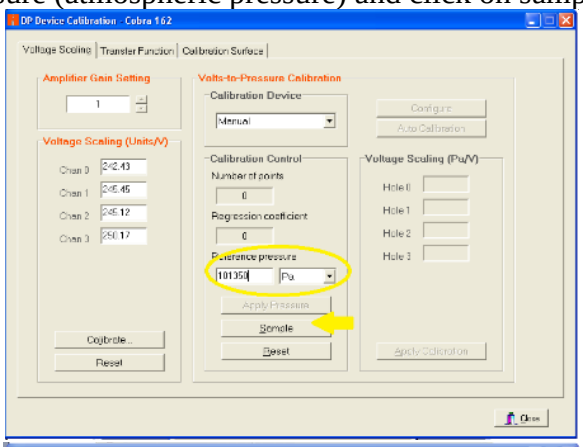

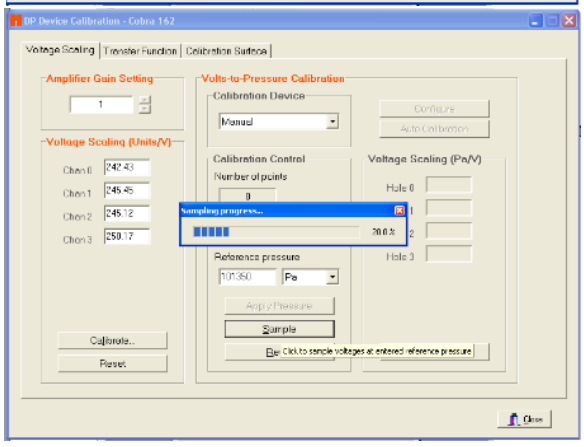

Now the probe is ready for use.

Measuring the Air Velocity Components

To measure the air velocity components, you need first to measure the air velocity when the fan is off, this can be named as “Zero-flow velocity”, then measure the air velocity at certain flow velocity. In order to get the exact value for the measured velocity, the zero-flow velocity should be subtracted from the measure the air velocity at certain flow velocity. The steps below show how to do that.

1. From the main interface in TFI Device Control, click on select

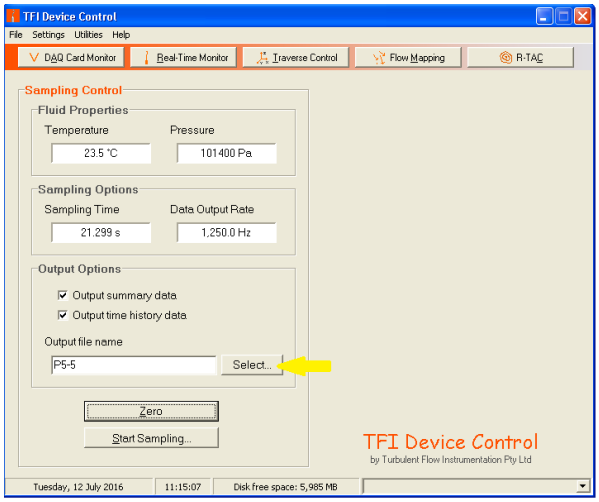

2. Name the file as Zero

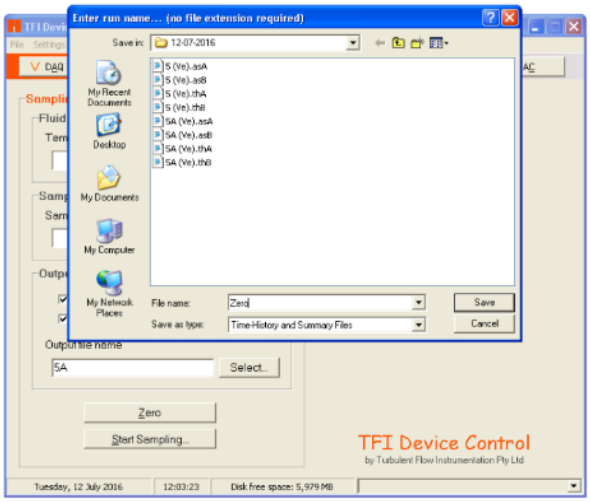

3. Click on Zero

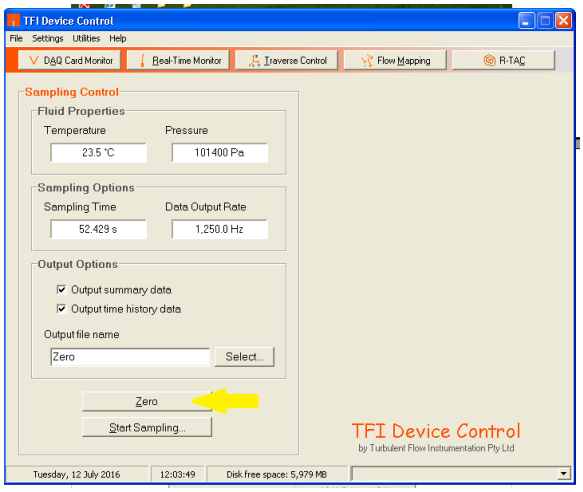

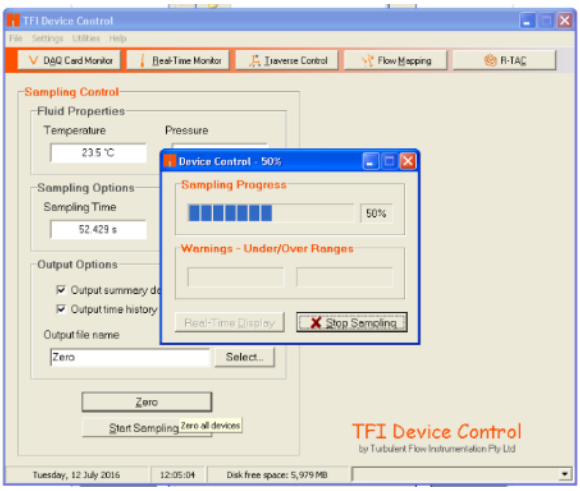

4. Click on Start Sampling

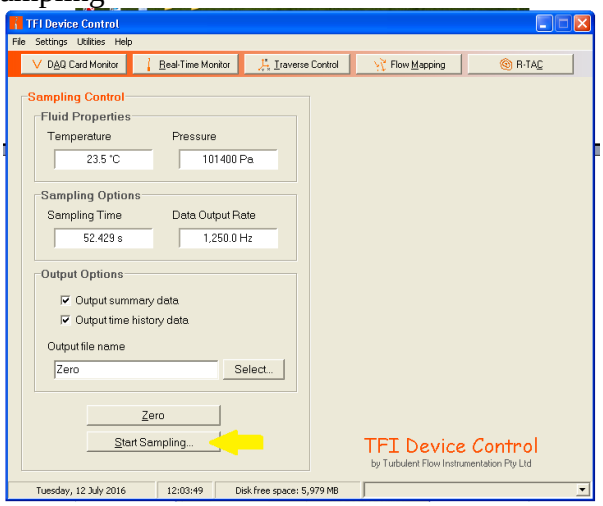

The software is recording data for the sampling time

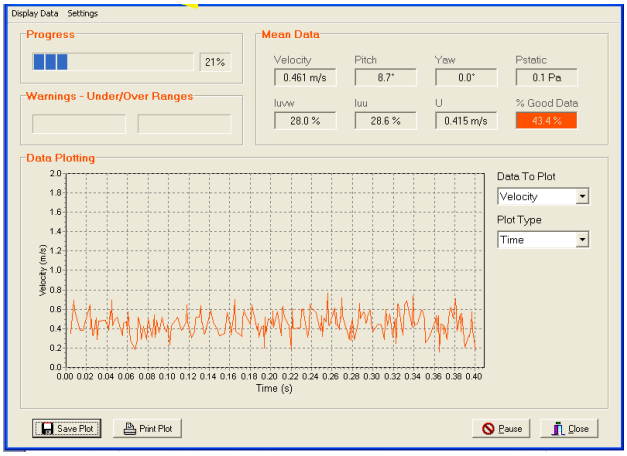

The recorded data is saved in two files (Zero (Ve).asA and Zero (Ve).thA)

The file (*.as*) contains the values for velocity components, as well as, the velocity magnitude.

file (Zero (Ve).asA)

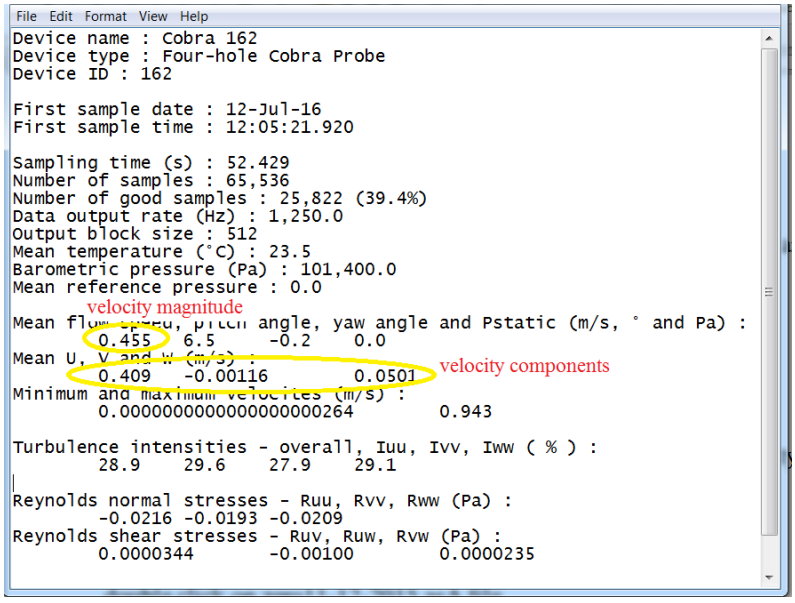

5. To measure the velocity components at certain flow velocity, turn on the air flow from the fan.
6. Follow the same steps as in measuring zero-flow velocity to measure the air velocity at certain flow velocity (the test is named 3).

The recorded data is saved in two files (3.asA and 3.thA)

The file (*.as*) contains the values for velocity components, as well as, the velocity magnitude.

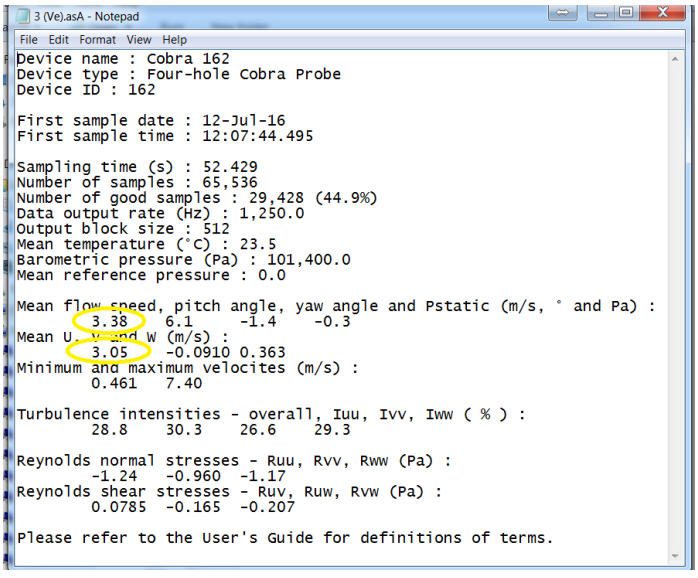

Calculations Example

Based on the results from test (3),

Upstream velocity (U-component) = 3.05 m/sec

Zero-flow velocity (U-component) = 0.409 m/sec

Then the exact measured velocity can be calculated as follows,

Exact measured velocity (U-component) = Upstream velocity (U-component) – zero-flow velocity (U-component)

= 3.05 – 0.409

Exact measured velocity (U-component) = 2.641 m/sec

Figure B.4 depicts the variations of measured velocity components upstream the test section. It can be seen clearly that the value of the measured velocity component almost zero near the test section walls and tends to increase near the centre.

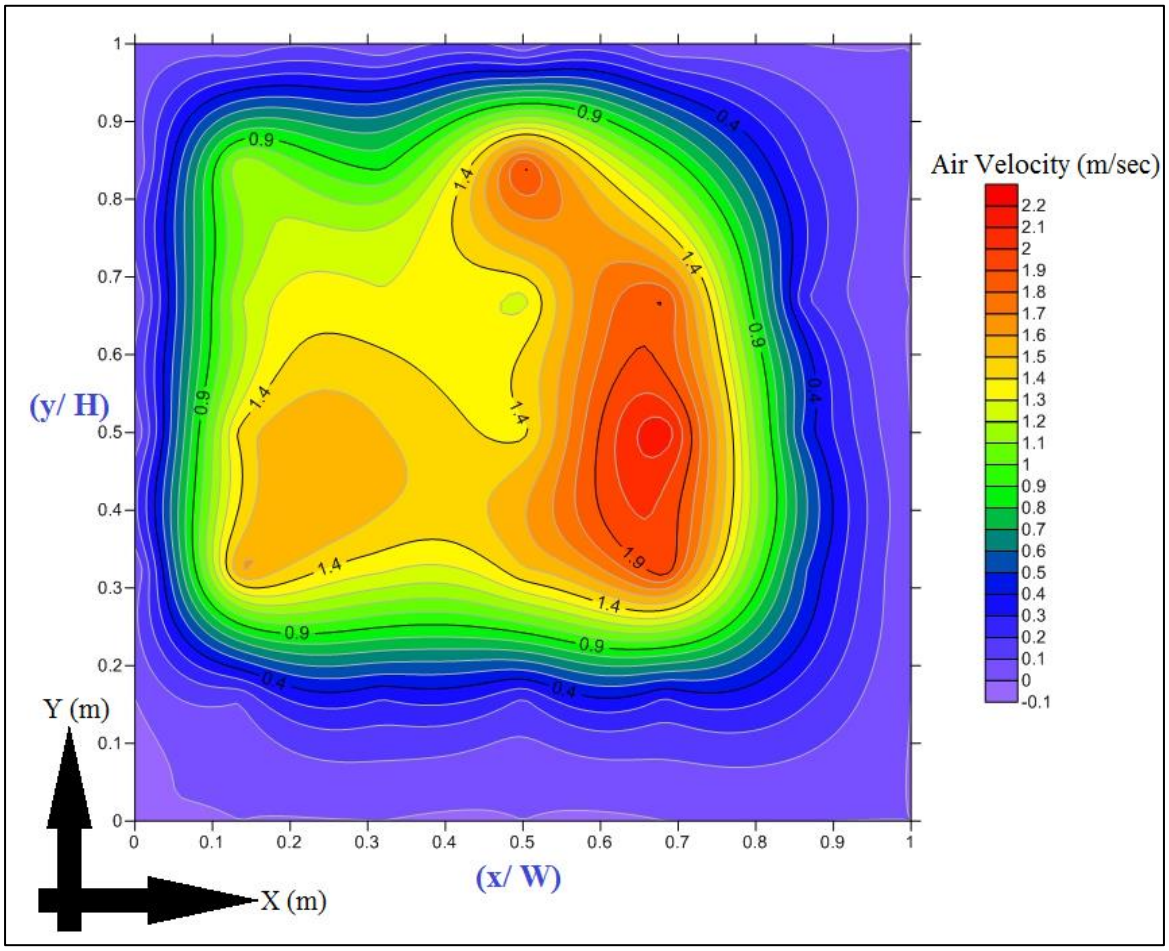

Figure B.4 Variations of Measured Velocity Components Upstream the Test Section

Using the measured data, the velocity arithmetic mean (velocity average) has been calculated by using the following formula [105]:

$$\overline{V} = \frac{\sum_{i=1}^{n} A_i V_i}{\sum_{i=1}^{n} A_i} \qquad \text{(B-1)}$$

Where,

$\overline{V}$ is the velocity mean value (m/sec)

V_i is the average of the measured velocities effective at the centre of the area A_i (m/sec)

A_i is the area each element (m^2)

The results of this process led to five different air velocities (0.705, 1.546, 2.183, 3.177 and 3.991 m/sec) which they were used to carry out the experiments.

APPENDIX C- USER-DEFINED FUNCTIONS (UDFS) FOR TRANSIENT TEST

C.1 Starting Up test UDF

```
#include "udf.h"

DEFINE_PROFILE(ramp_waterIN, thread, position)
{

  float t, water;
  face_t f;

   t = RP_Get_Real("flow-time");
  if (0 < t <= 300)
  {  water = (-0.0005*t)+300.13;
}
else if (300 < t <= 2200)
  {  water = (0.000000001*(t*t*t))-
(0.000009*(t*t))+(0.0337*t)+291.64;
}

else if (2200 < t <= 2767676765)
  {  water = (0.0021*t)+328.68;
}


  begin_f_loop(f, thread)
  {
   F_PROFILE(f, thread, position) = water;
  }
  end_f_loop(f, thread)

}


DEFINE_PROFILE(ramp_airIN, thread, position)
{

  float t, air;
  face_t f;

   t = RP_Get_Real("flow-time");
  if (0 < t <= 300)
  {  air = (-0.0002*t)+298.49;
}
else if (300 < t <= 2200)
  {  air = (0.0003*t)+298.37;
}
else f (2200 < t <= 2765)
  {  air = (0.0003*t)+298.33;
}
```

```
  begin_f_loop(f, thread)
  {
   F_PROFILE(f, thread, position) = air;
  }
  end_f_loop(f, thread)

}
```

C.2 Step Input test UDF

```
#include "udf.h"

DEFINE_PROFILE(ramp_waterIN, thread, position)
{

  float t, water;
  face_t f;

   t = RP_Get_Real("flow-time");
  if (0 < t <= 300)
  {  water = (-0.0002*t)+298.94;
}
else if (300 < t <= 318)
  {  water = (-0.002*(t*t*t*t))+(2.59*(t*t*t))-
(1191.2*(t*t))+(243057*t)-2E+07;
}
else if (318 < t <= 600)
  {  water = (0.0045*t)+330.15;
}



  begin_f_loop(f, thread)
  {
   F_PROFILE(f, thread, position) = water;
  }
  end_f_loop(f, thread)

}



DEFINE_PROFILE(ramp_airIN, thread, position)
{

  float t, air;
  face_t f;

   t = RP_Get_Real("flow-time");
```

```
  if (0 < t <= 300)
  {  air = (8E-05*t)+298.41;
}
else if (300 < t <= 318)
  {  air = (0.006*t)+296.53;
}
else if (318 < t <= 600)
  {  air = (0.0012*t)+298.15;
}



  begin_f_loop(f, thread)
  {
   F_PROFILE(f, thread, position) = air;
  }
  end_f_loop(f, thread)

}
```